THE UNIVERSITY *of* EDINBURGH

Macrocyclic pacman complexes for secondary coordination sphere control

James W. Leeland

University of Edinburgh

Submitted for the degree of Doctor of Philosophy
28th of April 2011

Declaration

The work described in this thesis is entirely my own, except where I have either acknowledged help from a named person or given reference to a published source. Text taken from another source will be enclosed in quotation marks and a reference given. This thesis has not been submitted, in whole or in part, for any other degree.

Signature: Date:

Acknowledgements

I would first like to thank Dr. Jason Love for his support and guidance throughout my PhD, without whom, this thesis would not be possible.

A big thank you also to Prof. Polly Arnold for her input during many group meetings during my PhD as well as to Prof. Hiroyuki Kawaguchi during my summer in Japan. I am very grateful to EaStCHEM school of chemistry for the funding as well as to the JSPS and the RSC.

Furthermore, I am indebted to the following people: Dr. Juraj Bella and Dr. Marika McCremoux for their NMR expertise, Prof. Simon Parsons, Prof. Alex Slawin, Dr. Anna Collins and Dr. Fraser White for all their help regarding crystal structures, Mr. Alan Taylor for mass spectrometry and Mr. Stephen Boyer for elemental analyses. A thanks also to Dr. Logan Mckay, Prof. Lee Cronin and Jennifer Mathieson for specialist mass spectrometry help. Further thanks go to all of the people in stores and workshops and all of the support staff here at Edinburgh.

I would like to express my gratitude to the post-docs who have helped me with my various questions and queries: Dr. Manuel Volpe, Dr. Chris Carmichael, Dr. Sergey Zlatogorsky, Dr. Emma Hollis and Dr. Stephen Mansell at Edinburgh and Dr. Yutaka Ishida at Tokyo.

All the project students that worked with me, Jane, Amy, Berengere and Colin, also receive my thanks for their hard work.

Thank you to everyone in the Love, Arnold and Bailey groups, past and present, who made my time in Edinburgh very enjoyable as well as bared the brunt of my anger resulting from the many and varied frustrations of research chemistry. I have particularly enjoyed tea breaks with the Metro, which has increased my knowledge of 6 letter words dramatically. I am also appreciative of the playing of UNO, the over-used biscuit fund and the close proximity of the fire blanket to the sink.

A huge thank you to family and friends for all their support both throughout my PhD and whilst a poor thesis-writing bore.

Finally I would like to thank Alex for all her help, support and fantastic food during, and after, this PhD. You almost single-handedly kept me sane at times and I could not have done it without you…

Abbreviations

General

°	degrees	EtOH	ethanol
°C	degrees Celsius	eq	equivalents
Å	Ångström	*exo*	exogenous
Ac	acetyl, -C(O)CH_3	IPA	*iso*-propylalcohol
Ar	generic aryl group	Fc	Ferrocene, Cp_2Fe
Boc	Di-*tert*-butyl dicarbonate	g	gram(s)
Btu	British Thermal Unit	h	hour(s)
Bu	butyl	IR	infrared
^{n}Bu	*n*-butyl	J	joule(s)
^{t}Bu	*tert*-butyl	K	Kelvin
ca.	*circa*, about	Me	methyl
Cp	cyclopentadienyl, C_5H_5	Mes	mesityl, 2,4,6-Me-C_6H_2
CV	cyclic voltammogram	mbar	millibar(s)
d	day(s)	MeOH	methanol
DABCO	1,4-diazabicyclo[2.2.2]octane	mins	minutes
Dipp	2,6-iPr-C_6H_3	mL	millilitre(s)
dm^3	cubic decimeter(s)	µL	microlitre(s)
DME	dimethoxyethane	M	mols dm^{-3}
DMF	dimethylformamide	mol	mole(s)
DFT	Density Functional Theory	mmol	millimole(s)
endo	endogenous	µmol	micromole(s)
Et	ethyl	MS	Mass Spectrometry
EtOAc	ethylacetate	ms	milliseconds
Et_2O	diethylether	mV	millivolt(s)

N_{im}	imine nitrogen	pyr	pyridine
N_{py}	pyrrolic nitrogen	RT	room temperature
N_{pyr}	pyridine nitrogen	R	generic alkyl group
Ph	phenyl	s	seconds(s)
pm	picometres	TFA	trifluoroacetic acid
^{i}Pr	*iso*-propyl	THF	tetrahydrofuran

Nuclear Magnetic Resonance spectroscopic data

δ	chemical shift in ppm	Hz	Hertz
Ar^{F}	fluorenyl	m	multiplet
br	broad	MHz	Megahertz
$^{13}C\{^{1}H\}$	proton decoupled ^{13}C NMR spectroscopy	NMR	Nuclear Magnetic Resonance
COSY	^{1}H-^{1}H 2-D correlation spectroscopy	NOESY/ nOe	Nuclear Overhauser effect
d	doublet	ppm	parts per million
dd	doublet of doublets	s	singlet
dt	doublet of triplets	t	triplet
J	coupling constant	td	triplet of doublets
HSQC	^{1}H-^{13}C 2-D correlation spectroscopy	tt	triplet of triplets

Mass spectroscopic data

amu	atomic mass units	*m/z*	mass to charge ratio
EI	electron impact	M^{+}	molecular ion
ESI	electrospray ionisation		

Infrared spectroscopic data

br	broad	m	medium
cm^{-1}	wavenumbers	s	strong
IR	Infrared	w	weak

Abstract

The work presented in this Thesis describes the design, synthesis and reactivity of a symmetric and various asymmetric Schiff-base macrocycles that are capable of forming a wedge-shaped "Pacman" conformation upon metal binding.

Chapter One introduces catalysts for small molecule transformation as well as transition metal complexes of pyrrole-containing macrocycles. Further to this, Pacman systems, including previous work from Love and co-workers, and complexes capable of secondary coordination-sphere control will be discussed.

Chapter Two details the design and synthesis of two asymmetric macrocycles that both contain one neutral and one N_4-donor imine-pyrrole binding pocket, H_2L^{P} and H_2L^{NMe}. The synthesis and characterisation of the series of complexes [M(L^{P})] and [M(L^{NMe})] (M = Pd, K_2, Co, VCl, TiCl, Mg, Fe and Mn) and their characteristics highlighted, including the formation of a supramolecular cyclic hexamer.

Chapter Three presents the modification of the above ligands at the meso-group, the N-substituent and the non-pyrrolic binding pocket to give H_2L^{FP} and H_2LF^{NMe}, H_2L^{NMes} and $H_2L^{(NH)NMe}$ respectively. Palladium and cobalt complexes of these macrocycles were prepared and characterised.

Chapter Four describes the design and synthesis of the ligand H_4L^{Et} as well as the synthesis and characterisation of tin-alkyl and mononuclear calcium complexes of L^{Et}, as well as the heterobimetallic complexes [$SnMe_2$(M)(THF)(L^{Et})] (M = Zn or Fe). The homobimetallic complexes [M_2(L^{Et})] (M = Co, Mg and NbCl) are also presented along with a magnesium-cubane structure of L^{Et} in which the cubane is encapsulated by two, bowl-shaped macrocycles.

Chapter Five provides a summary of the work presented in this thesis.

Chapter Six describes the full experimental details and analytical data for all compounds synthesised in this work.

Table of contents

Chapter 1: Introduction

In 2007 the world's total energy consumption was estimated to be 495 quadrillion Btu (5×10^{20} J), corresponding to an average consumption rate of 16.5 terawatts (16.5×10^{12} W). With increasing worldwide populations and the emergence of China and India as major industrial powers, this energy consumption is estimated to increase by a further 50 % over the next 25 years alone.[1] This poses many problems as currently the world's energy supply is reliant upon limited, non-renewable resources. Fossil fuels such as crude oil are escalating in price due to an increased demand as well as political instabilities in their source countries. In addition, the products of burning fossil fuels are a major contributor to global warming, which threatens to melt the icecaps, make numerous species extinct, displace millions of people and even destroy low-lying countries such as the Seychelles. It is for these reasons that over the coming decades, finding a carbon neutral alternative fuel source which can be used on a scale comparable to current energy supply is of paramount importance. One technology thought to able to meet part of this demand is the hydrogen fuel cell (Figure 1).

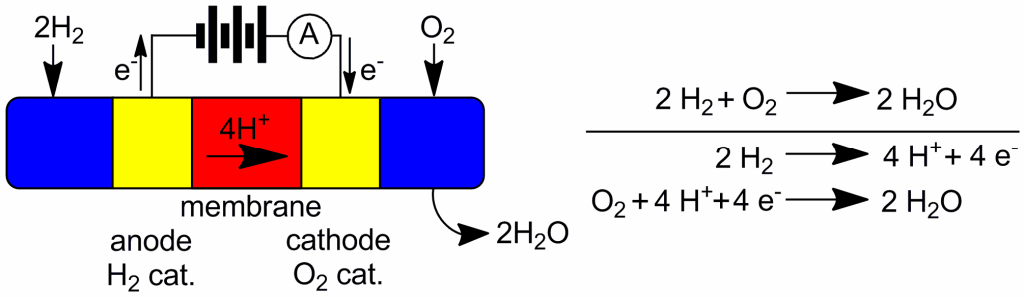

Figure 1: Left: A hydrogen fuel cell creates electricity from H_2. Right: Redox equations undergone in the fuel cell. Pictures modified from ref[2]

A fuel cell uses H_2 as its energy source, splitting the hydrogen into protons and electrons. The protons travel across a membrane with the electrons forced around a circuit to create electricity. Although the formation of water from dioxygen is thermodynamically favourable, large activation barriers require a catalyst to be employed.[3] Platinum is employed in current hydrogen fuel cells of this type due to its ability to split dihydrogen efficiently; however, its rarity and subsequent high cost prevent it from being a large-scale global solution. Furthermore, current industrial production of hydrogen occurs by steam reforming of methane and thus a hydrogen fuel cell is not a complete answer to the problem.

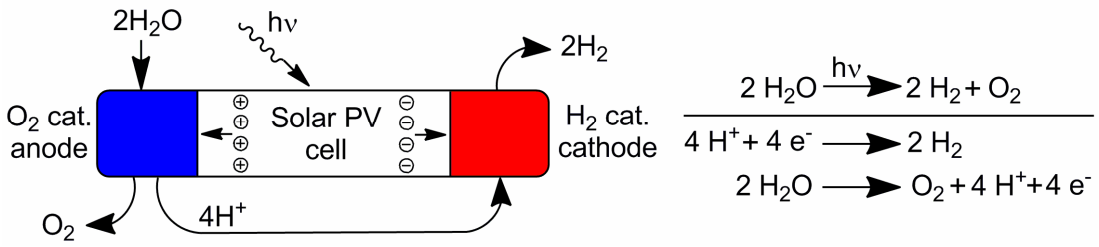

Figure 2: Left: Solar fuel cell for the splitting of water (PV = photovoltaic). Right: Redox equations undergone in the solar fuel cell. Picture modified from ref[2]

It is also hoped that fuel cells will be designed to catalyse the reverse reaction, splitting H_2O into O_2 and H_2 (Figure 2). This would ultimately make water a fuel source, with energy stored in the form of chemical bonds (in H_2 and O_2) which could later be used either in a fuel cell or in some sort of combustion engine. To make the cycle carbon neutral, an energy source such as sunlight would have to be utilised for the initial splitting of water.[2] Such a system would have many obvious advantages such as the low cost and plentiful supply of water. For each of the reactions shown in Figure 1 and Figure 2 however, catalysts are required to enable the processes to occur at a low enough potential to make them viable.[2-4] Closer investigation of the reactions required to harness energy in this manner reveal a number of problems such as photovoltaic cell design and hydrogen storage. One major challenge is that each reaction is a multi-electron, multi-proton process. Furthermore, the proton-coupled electron transfer (PCET) reduction of dioxygen can occur *via* two different routes, a two-electron, two-proton reduction to peroxide or a four-electron, four-proton reduction to water. To maximise energy output as well as preventing release of harmful peroxides into the atmosphere, the four-electron reduction path must be preferred to the two-electron path.

Biological catalysts provide systems capable of a catalysing a myriad of different PCET transformations under ambient conditions. The ability to understand and recreate transformations of various small molecules achieved by nature, including the interconversion of water and dioxygen, has been one of the ultimate goals of science for many decades. The ability to mimic the reactivity of enzymes could have far reaching consequences not only to the global energy industry but many other industries too. However, the ability to recreate these transformations in a laboratory environment has proven extremely challenging.

1.1 Small molecule activation catalysts

1.1.1 Biological catalysts

Despite the large size and immensely complex structure of enzymes, small molecule transformations generally occur at relatively small, well-defined active sites which are often inhabited by one or more metal centres. Furthermore these transformations, which are vital for life on this planet, occur under ambient conditions.

One such biological catalyst that exhibits these properties is cytochrome c oxidase, which catalyses the full four electron PCET reduction of dioxygen to water. A related protein, cytochrome P450, will be discussed in Section 1.3.1 with an emphasis on the involvement of secondary coordination sphere control. Cytochrome c oxidase maximises energy output by catalysing only the full four-electron reduction, as opposed to the two-electron reduction, as well as preventing the production of superoxides and peroxides which can be harmful to the body. The energy released in this reaction is used to convert ADP to ATP, the body's chemical energy store. The active site of this particular enzyme is inhabited by an iron (a_3-heme) bound in a porphyrin and a copper (Cu_B) centre coordinated to three histidine groups, with the Fe and Cu held near to each other (*ca*. 4.5 Å).[5] The key intermediate is the formation of a pre-organised oxo/hydroxo species bound by Fe(IV) and a Cu(II) centres (Scheme 1).[6, 7]

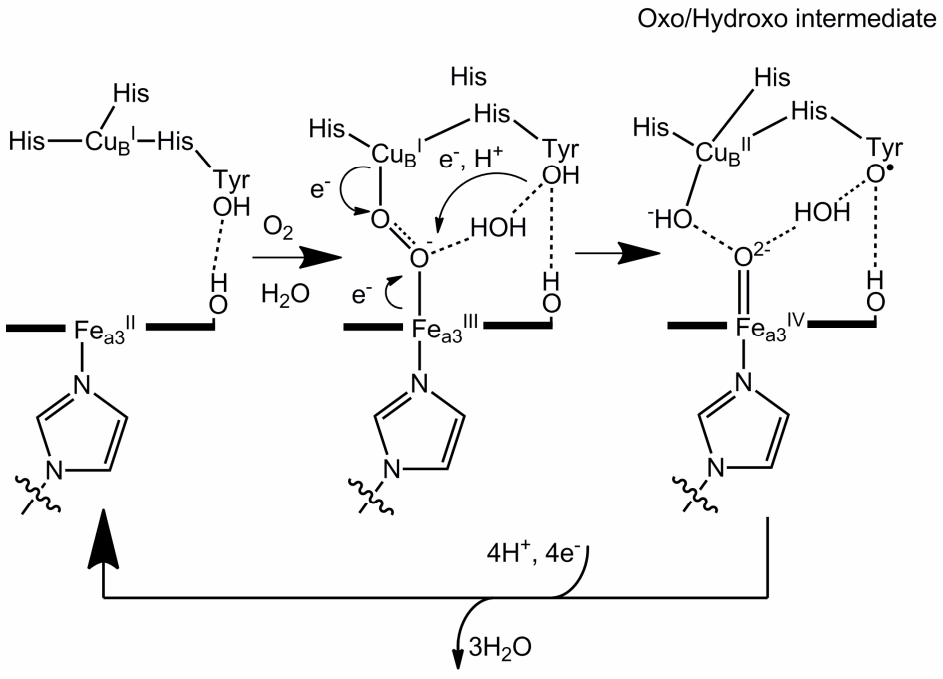

Scheme 1: Part of the catalytic cycle of the four electron reduction of dioxygen to water showing the oxo/hydroxo intermediate

To facilitate small molecule transformations, such as the reduction of dioxygen to water, protons and electrons are delivered to the active site in a controlled fashion and much research has been, and is being undertaken to attempt to understand the processes involved. Of great interest is the mechanism of the proton pump which various enzymes, including cytochrome c oxidase, employ to deliver protons to/from active sites (Figure 3).[7-9]

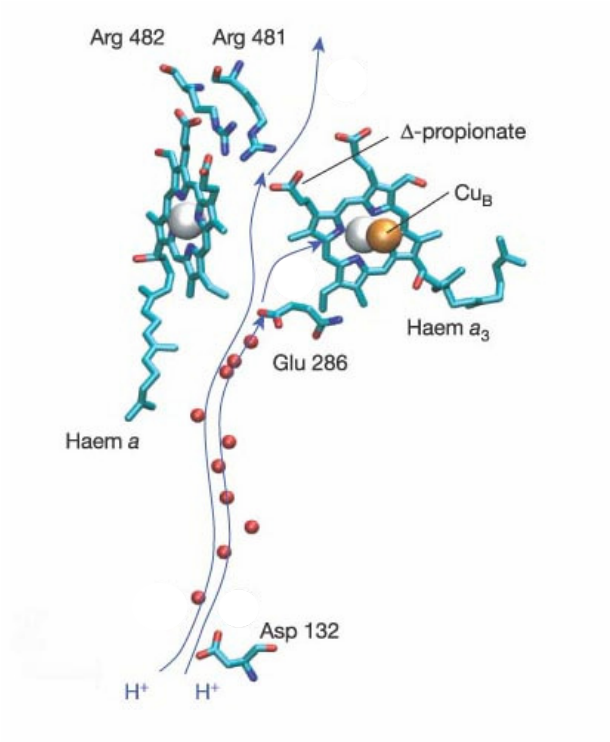

Figure 3: Proton pump of cytochrome c oxidase. Picture modified from ref[9]

Photosystem II (PSII), found in green plants, catalyses the microscopic reverse reaction of cytochrome c oxidase, the oxidation of water to oxygen. These reactions are very similar due to the oxo/hydroxo intermediates common to both processes.[10] Despite this similarity, the O-O bond coupling reaction is undoubtedly very complex and thermodynamically demanding. The core of PSII consists of a cubane-like Mn_3CaO_4 cluster, held together by bridging oxo groups (Figure 4).[11] At this cluster-centre, it is thought two water molecules are pre-assembled through secondary coordination interactions and then undergoes a series of PCET events *via* an oxo/hydroxo intermediate. The Ca^{2+} is thought to be responsible for producing a free hydroxide ion from water, resulting in the key oxo/hydroxo intermediate as a prelude to O-O bond formation. The nucleophilic attack of this hydroxide on the electrophilic oxo bound to the high valent manganese cation results in O-O bond formation.[3, 12] Electrons and

protons are removed from the active site by the protein environment with the proton output channel shown to be orthogonal to the electron output channel (Figure 4).[3, 11, 13] Due to damage caused by production of singlet oxygen however, the active site has to be replaced approximately every 30 minutes under ambient sunlight conditions.

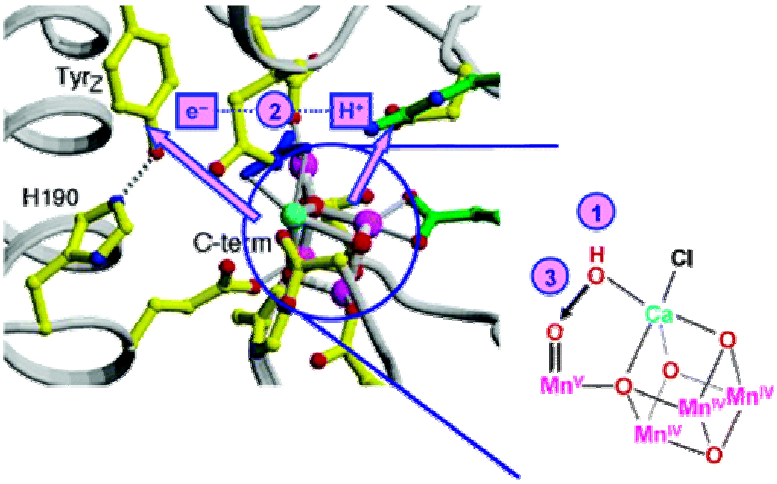

Figure 4: Active site of PSII. (1) Protein controls the primary and secondary coordination sphere to bring two water molecules within close proximity of each other. (2) Exit channels for protons and electron in the PCET reaction is in differing directions. (3) O-O bond forming reaction is far from a simple reaction. Picture from ref[3]

In conclusion, biological catalysts are capable of catalysing many reactions which are challenging to recreate in a laboratory environment. The addition and/or removal of protons and electrons are key to successful transformations, as well as the transportation of substrates, often through H-bonding interactions, to and from the active site.

1.1.2 Synthetic catalysts

Despite the challenges outlined above, much effort has been undertaken to attempt to recreate the transformations achieved by enzymes in a laboratory environment. In this section a few examples of synthetic small molecule activations will be discussed. Processes including the activation of small molecules such as O_2, H_2O, CO_2, CH_4, N_2 or H_2 all share similar basic problems regarding bond-making and breaking processes which involve multiple PCET events.

The ability to mimic photosynthesis in a laboratory environment could have huge applications in the energy industry.[2] The first major step with regards to water oxidation came with the now heavily studied[14] "blue-dimer" first investigated by the Meyer group (Scheme 2).[15, 16] This oxo-bridged bis-ruthenium bipyridyl-complex was found to be

capable of the four-electron oxidation of water to oxygen in the presence of strong acids and Ce(IV). It has been the subject of various studies by isotopic labelling as well as by electrochemistry, EPR and NMR spectroscopy and DFT calculations to elucidate the mechanism by which the oxidation occurs.[14, 16, 17]

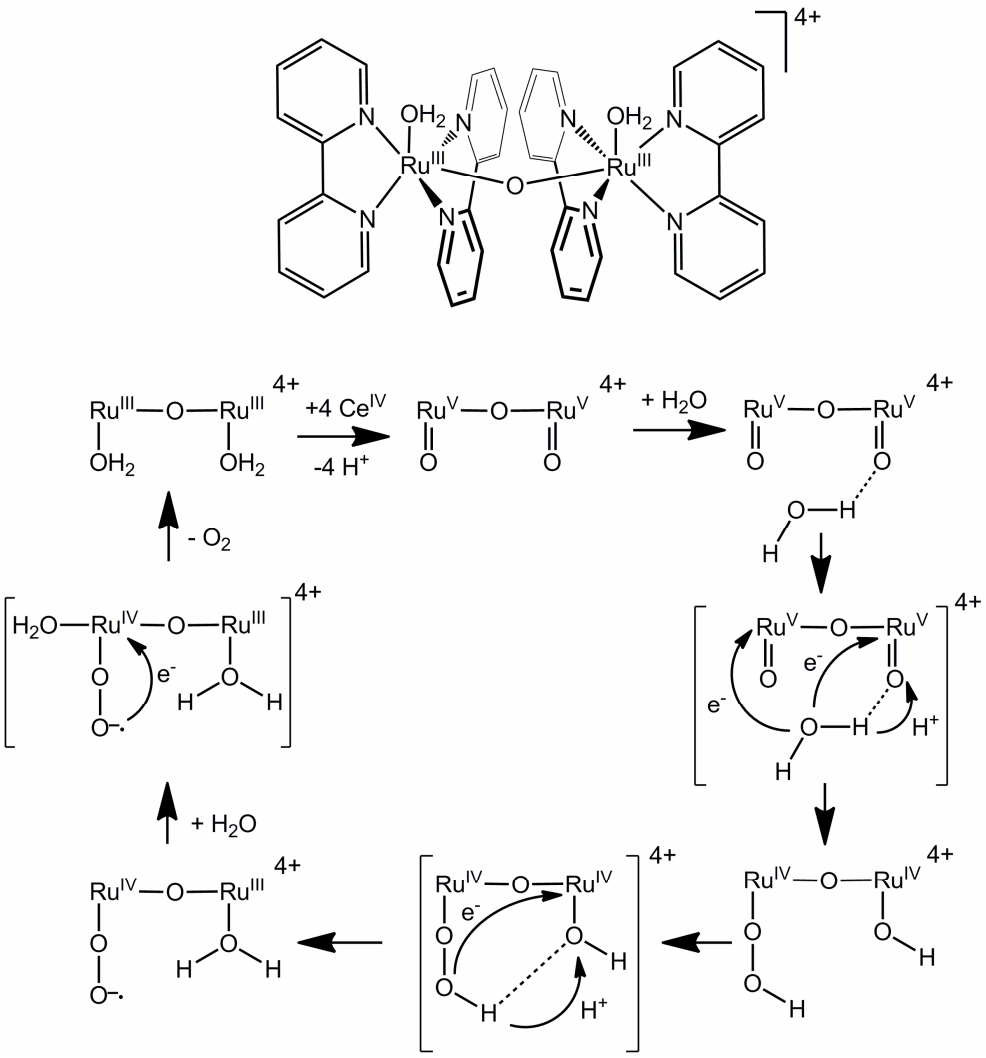

Scheme 2: Blue dimer (top) and proposed mechanism of water oxidation (brackets = transition states) (bottom). Diagrams modified from ref[14]

The process is thought to proceed through the formation of a Ru(V)-O-Ru(V) dioxo intermediate and subsequent proton-coupled electron transfers. Work by Baik and co-workers used DFT calculations, as well as experimental evidence, to propose a mechanism, which was subsequently modified by Meyer, shown above (Scheme 2).[14, 17] There is evidence however, for a slower route through a Ru(V)-Ru(IV) intermediate and so an overall definitive mechanism is yet to be reported. The key feature of the catalyst is the ability of each ruthenium to exist in the 3+ and 5+ oxidation states, *via* an

intermediate 4+ state, and for the oxidation to occur stepwise thus preventing the building up of charge. Further development of the process included the use of amine ligands[18, 19] as well as deposition of the catalyst on different electrode materials.[18, 20, 21] Many variations, containing either multiple[21-23] or single[23, 24] ruthenium centres have been investigated for their activity towards water. Though the majority of complexes based on the blue-dimer contain a bridging oxo group, Llobet and co-workers have shown activity is maintained when employing terpy/bpp ligands, preventing μ-oxo formation (Figure 5, left).[25] The highest oxidation state reached was Ru(IV)/Ru(IV); however, unlike the blue dimer a Ru(II)/Ru(II) complex could be accessed.

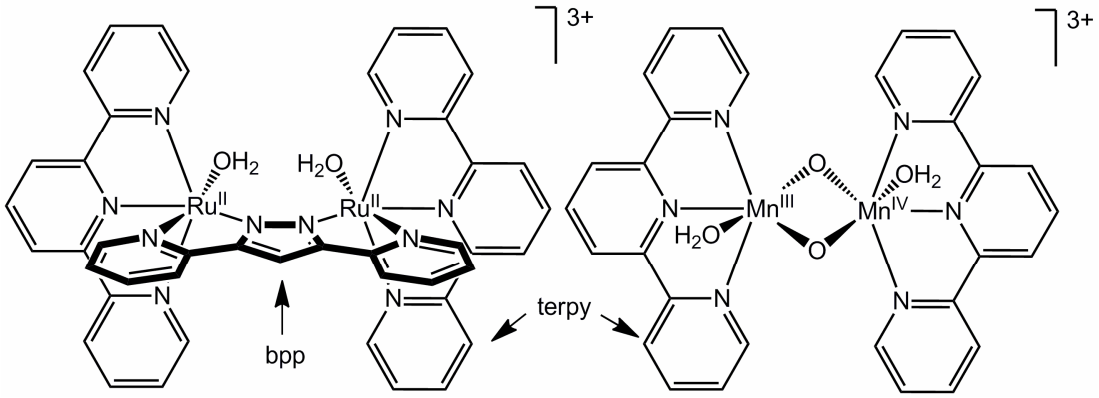

Figure 5: Complexes capable of water oxidation by Llobet and co-workers[25] (left) and the Crabtree group[26] (right) based on terpy ligands

Efforts have also been made to synthesise manganese-containing complexes akin to PSII, with Crabtree and co-workers synthesising binuclear manganese-terpy complexes which show activity towards water oxidation (Figure 5, right).[26] Other attempts at recreating the manganese-cubane structure which are also capable of water oxidation are yet to be reported[27] though there is some success in employing manganese oxide nanoparticles.[28]

Recently, a vastly different approach to catalytic water oxidation was employed by Nocera and co-workers, who found that using simple cobalt phosphate in an aqueous medium catalyses water oxidation to dioxygen.[29] The discovery has sparked a flurry of subsequent research due to the low cost of these materials and efficiency of this oxidation.[30, 31] Though the exact mechanism is still unknown, it is thought to proceed *via* a Co(IV) oxo intermediate.[30, 32] Importantly, these oxidation reactions can occur in both polluted and salt water. Furthermore, nickel borates have also shown similar activity in performing water oxidation reactions.[33]

1.2 Porphyrin, porphyrin-based and Schiff-base ligand complexes

1.2.1 Porphyrin complexes

One particular ligand-scaffold found extensively in nature is the porphyrin. This fully aromatic macrocycle containing 22 aromatic electrons and four pyrrolic nitrogens (Figure 6), is found in hemoglobins, myoglobin and cytochromes, as well as many other enzymes.

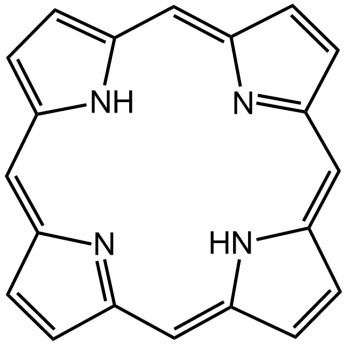

Figure 6: A basic porphyrin

Various substituents found on either the *meso*- or pyrrolic backbone positions create a wide variety of very complex structures. Though found in nature, porphyrins have been synthesised in the laboratory from the late 1920s and have since been studied extensively for their rich chemistry in a variety of applications and are still extensively studied today with entire journals and multiple-volume books devoted to the subject.[34] Certain specific types of porphyrins and porphyrin-related compounds will be discussed in this section and section 1.3.3. Importantly, porphyrins have been found to coordinate a wealth of metals, forming a variety of complexes, making them good candidates for a variety of catalytic applications. One such application, the reduction of dioxygen, will be highlighted below.

Cobalt complexes of porphyrins have been found to be active as catalysts for dioxygen reduction although in general, mono-metallated single porphyrin units are only capable of the two electron reduction to peroxide.[35] However, Anson and co-workers found that coordination of ruthenium or osmium cations *via* appendages at the periphery of the porphyrin resulted in compounds that catalyse the full four-electron reduction of dioxygen to water (Figure 7).[36]

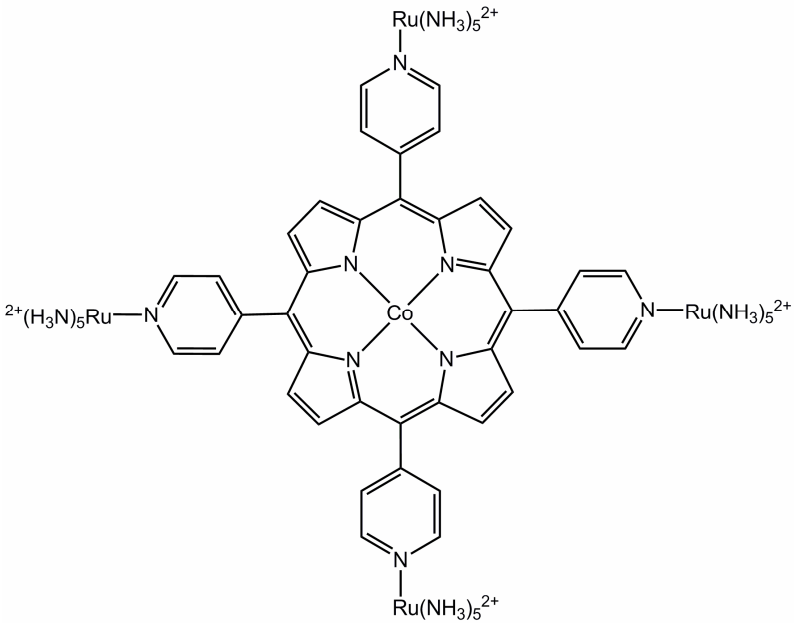

Figure 7: Single porphyrin capable of four electron reduction by Annan and co-workers

Certain iron porphyrin complexes have also been shown to undergo two, two-electron reduction steps from O_2 to H_2O, *via* H_2O_2.[37] Furthermore, dimers of iridium porphyrins are also capable of catalysing the four-electron reduction of dioxygen.[38]

1.2.2 Evolution of Pacman diporphrins

More success with regards to four-electron reduction of dioxygen came with the advent of cofacial diporphyrins, known as "pacman" diporphyrins. Initially, two porphyrin units were held in a cofacial arrangement by two or more flexible strapping groups (FTF4, Figure 8).[39, 40] These complexes were found to catalyse the four-electron reduction of dioxygen to water without the formation of any hydrogen peroxide.[40]

Due to the low yielding, multi-step synthesis of these strapped diporphyrins, Chang and co-workers employed a single rigid anthracene (DPA)- or biphenylene (DPB)-pillar to hold two porphyrins in a cofacial arrangement (Figure 8).[41] These were named "pacman" complexes due to their small amount of vertical flexibility enabling the cleft, or "mouth", to open and close akin the NAMCO computer game character.

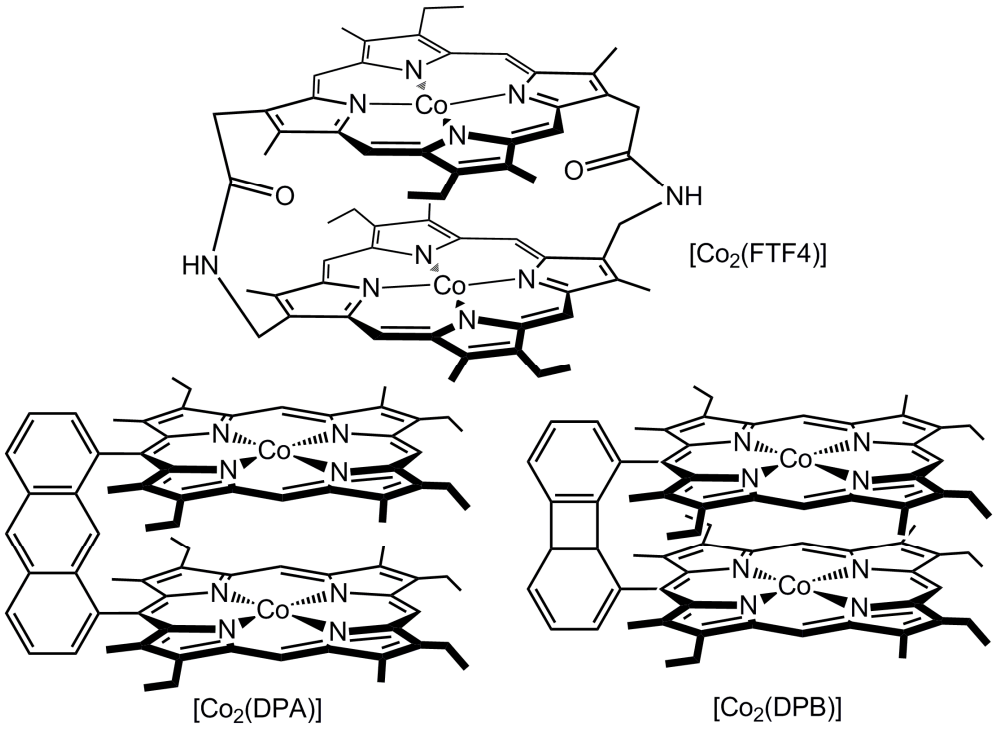

Figure 8: A doubly-strapped cofacial diporphyrin by Collman and co-workers[40] (top), first generation single pillared pacman diporphyrins by the Chang group[41] (bottom). All complexes catalyse the four electron reduction of dioxygen to water

Complexes of these ligands showed increased activity compared to the strapped counterparts, attributed to small vertical shifts allowing for a greater range of possible binding geometries in the cleft, thus enabling efficient PCET reactions without the need for large active site rearrangements.[42, 43] Cobalt complexes of DPA and DPB were found to be effective catalysts for O_2 reduction to water when coated on electrodes.[43, 44] Binding of the two cobalt centres *ca*. 5 Å apart enabled the binding and stepwise reduction of dioxygen *via* a Co(IV)=O and bridging superoxo intermediates.[45, 46] Further to this, ruthenium pacman complexes were found to be capable of proton reduction to H_2, albeit at relatively negative potentials. It was also hoped that such complexes would also be active towards dinitrogen reduction, although this was met with limited success.[43] The small degree of vertical flexibility present in the complexes enabled intermetallic distances to alter by *ca*. 1 Å, a feature which caused problems for earlier transition metals such as Fe and Mn due to the formation of stable μ-oxo compounds preventing the complexes from undergoing further participation in catalytic cycles. A number of mono- and mixed-metal complexes were also synthesised, some of which were also found to be capable of catalysing the four electron reduction of dioxygen to water.[47, 48]

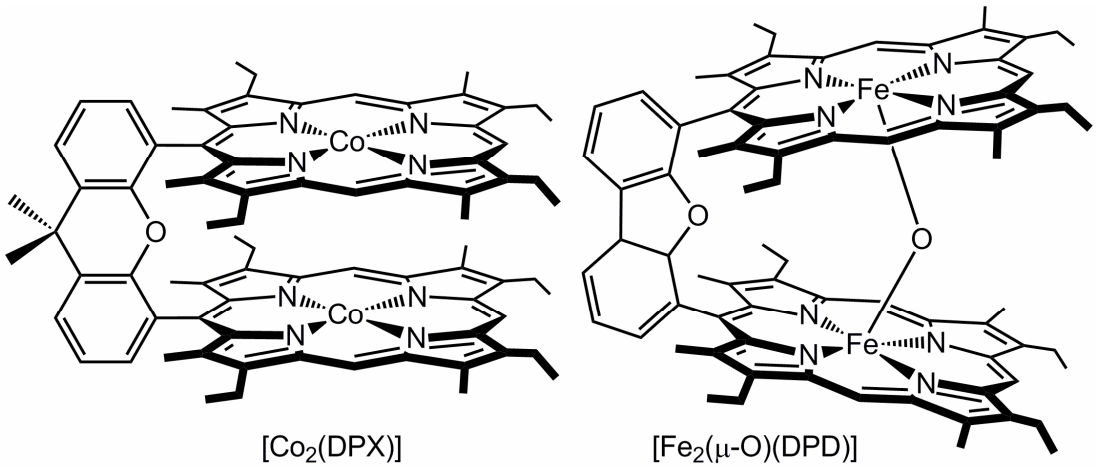

Figure 9: Second generation pacman porphyrins by the Chang and Nocera groups showing a binuclear cobalt DPX complex capable of the four electron reduction of dioxygen to water[49] (left) and an oxo-bridged DPX complex[50] (right)

In an effort to understand pacman complexes further a second generation of single-pillared pacman compounds based on xanthene (DPX)[42] and dibenzofuran (DPD)[51] backbones were synthesised by the Chang and Nocera groups (Figure 9). These second generation pacman molecules were designed to have very different metal-metal separation and also showed massively increased vertical flexibility compared to DPA and DPB with metal-metal distances varying from 3.504 to 7.775 Å.[52] Despite this increased flexibility however, activity towards dioxygen was comparable to that of DPA and DPB complexes, with binuclear cobalt complexes of these ligands catalysing the four electron reduction of dioxygen to water without formation of hydrogen peroxide.[49]

It was later found that when bulky aryl groups were introduced *trans* to the backbone of either DPX or DPD, this yielded cobalt complexes that showed preference for hydrogen peroxide formation.[53] It was thought that these bulky groups hindered proton delivery to the bound superoxo species, resulting in preferential electron transfer and subsequent hydrogen peroxide production. These observations were explained in mechanistic studies of dioxygen reduction by the Nocera group. It was suggested the four-electron reduction proceeded *via* a Co^{IV}=O intermediate in which the protonation of an initially-bound superoxo bypassed the two electron reduction route.[53] It was also noted that the second metal centre did not change its oxidation state throughout the catalytic cycle, a feature in agreement with observations from previous studies which

showed a redox active second metal centre was not required for reduction of dioxygen to water.[48, 54]

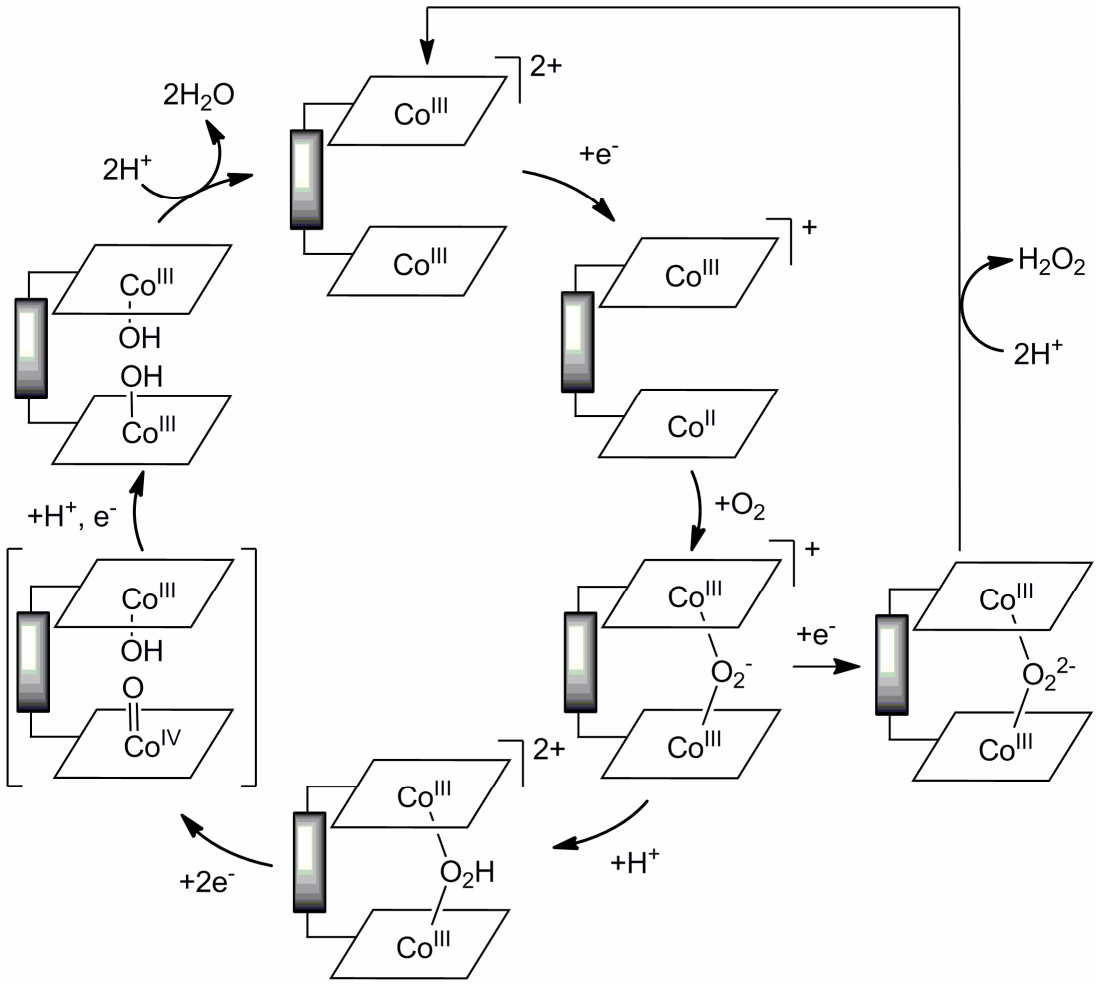

Scheme 3: Catalytic cycle of dioxygen reduction proposed by Nocera and co-workers. If bulky aryl substituents are placed in the *meso*-position opposite the backbone, proton delivery is hindered and two-electron reduction to hydrogen peroxide is favoured[53]

Once again however, formation of μ-oxo complexes were thought to hinder the catalytic activity in this dioxygen reduction cycle.

When studying the photooxidation reactions of phosphines catalysed by Fe_2(μ-O) pacman complexes, the highly flexible DPD-ligand complex showed a 10000-fold increase in activity over DPX.[52] This vastly improved reactivity was found to be due to the DPD binding pockets "springing" open allowing easier substrate transport to and from the cleft (Scheme 4).[46, 55] Binuclear Fe_2(DPD) complexes were also shown to catalyse the oxidation of sulfides,[50] olefins[56] and hydrocarbons[57] in photocatalytic reactions.

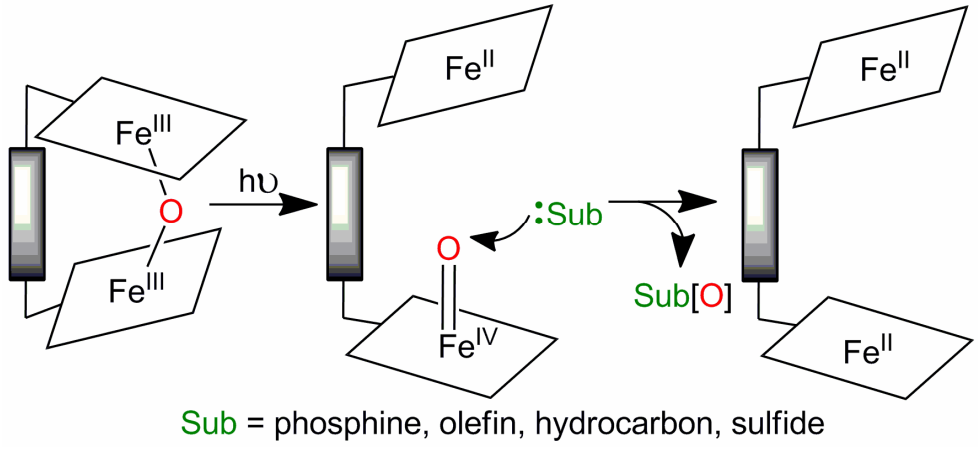

Scheme 4: Diagram of [(Fe_2(μ-O)DPD)] used as an oxidative photocatalyst[46]

To prevent μ-oxo formation in cobalt complexes, as well as gain secondary coordination sphere control, a further step in pacman-complex evolution led to "hangman" porphyrins, these will be discussed in Section 1.3.3.

1.2.3 Porphyrin-related macrocycles

Another macrocycle found in nature is corrole, related to the corrin ring found in vitamin B_{12}. It is an aromatic system similar to the porphyrin but with one less *meso*-carbon and three, rather than two, pyrrolic protons and thus has a "3-" charge once deprotonated (Figure 10). This, combined with their smaller cavity sizes make corroles well suited to stabilising metals of higher oxidation states[58] and thus suitable for activations of small molecules such as O_2[59] and H_2O.[60] As such, corrole-containing pacman molecules have been synthesised by Guilard and co-workers to create binuclear corrole or corrole/porphyrin compounds (Figure 10).[61, 62] It was found that binuclear cobalt- and heterobimetallic cobalt-containing porphyrin/corrole dyads were capable of catalysing the four-electron reduction of dioxygen to water.[63]

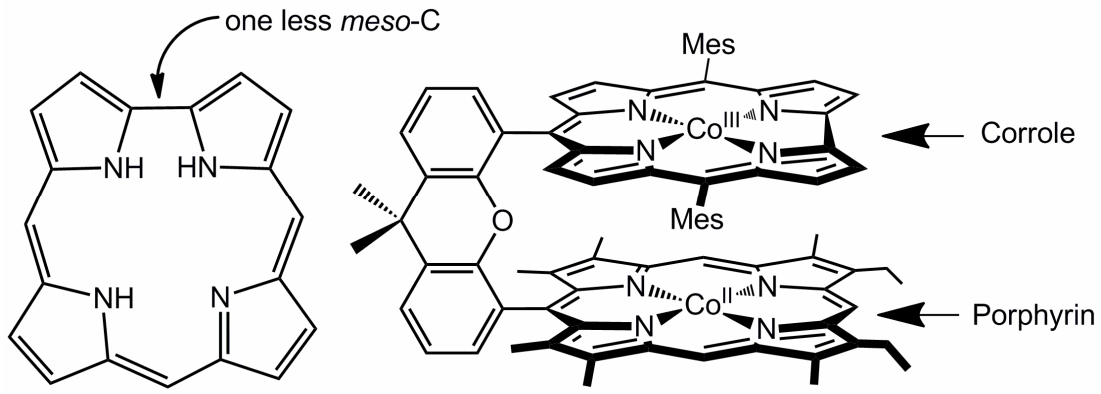

Figure 10: Corrole (left) and a porphyrin-corrole dyad by Guilard and co-workers[62] (right)

There are a number of further ligands based on porphyrins, including various types of expanded porpyrins,[64] in which macrocycles contain at least 17 atoms in cyclic conjugation with three or more pyrrole or other heterocyclic subunits.

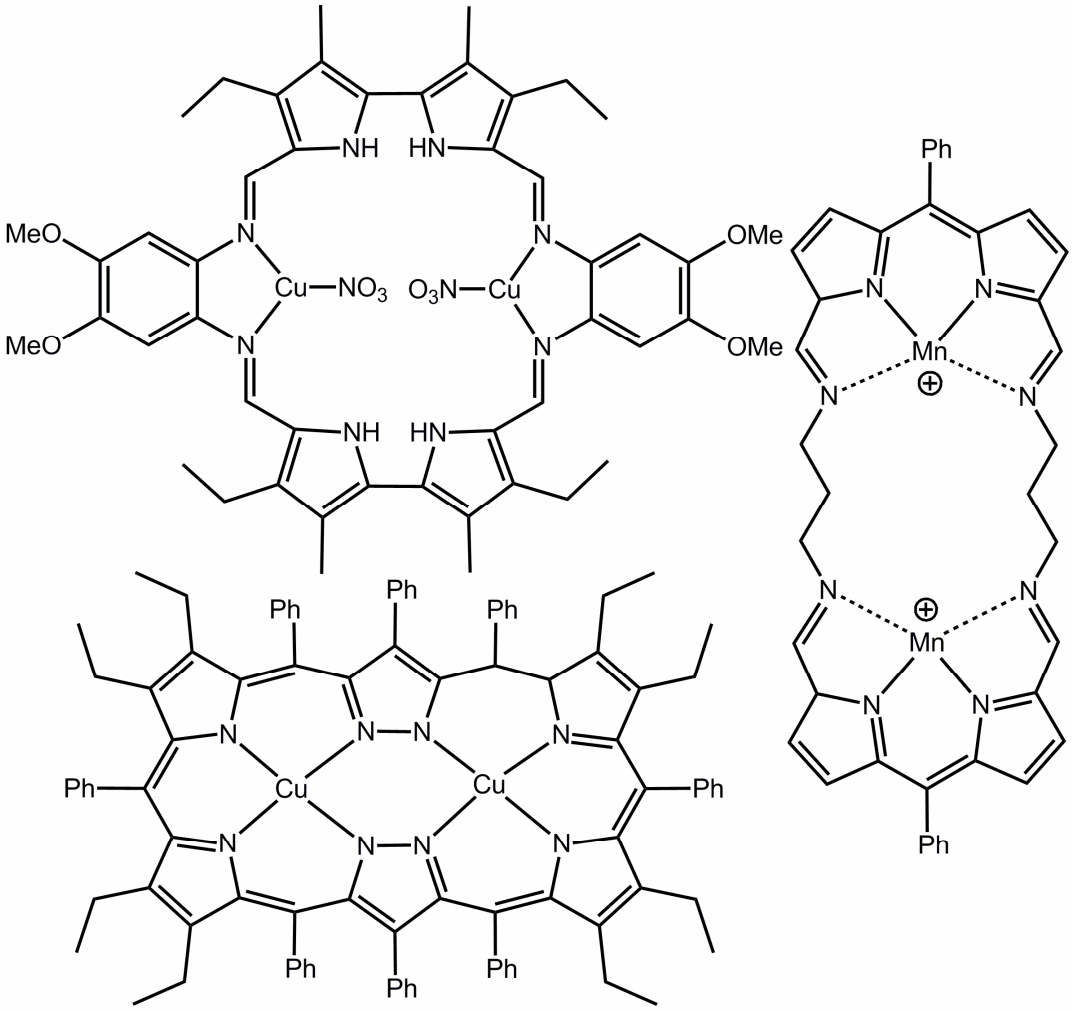

Figure 11: A Schiff-base macrocycle by the Sessler group[65] (top left), an accordion porphyrin[66] (right) and a Siamese twin porphyrin[67] (bottom left)

Meyer and co-workers recently published "Siamese twin porphyrins" (Figure 11),[67] containing a pyrazole-based macrocycle capable of binding two metal centres. Other porphyrin-based macrocycles include accordion porphyrins, where a flexible linker allows for large changes in metal-metal distances (Figure 11).[66] Furthermore, the Sessler group have also synthesised Schiff-base tetra-pyrrolic macrocycles capable of binding two metal centres (Figure 11).[65]

1.2.4 Schiff-base pacman-ligands and complexes

Despite the successes of pacman diporphyrins, especially as dioxygen reduction catalysts, their lengthy and challenging syntheses provide an obvious drawback. This is despite reductions in steps and increased yields over the course of their development. Thus ligands capable of mimicking the cofacial geometry and reactivity of pacman diporphyrins which are synthesised in a small number of high yielding steps from cheap starting materials are desirable. The Love[68] and Sessler[69] groups independently published a Schiff-base pyrrole macrocycle "H_4L", where the "H_4" denotes the four pyrrolic NHs (Scheme 5). Importantly, the synthesis is facile, in which the acid-templated condensation of 1,2-phenylenediamine, or related diamine, with a straightforwardly synthesised dipyrrole-dialdehyde was found to give solely the [2+2], symmetric macrocycle in good yield (greater than 60% over three steps, Scheme 5).

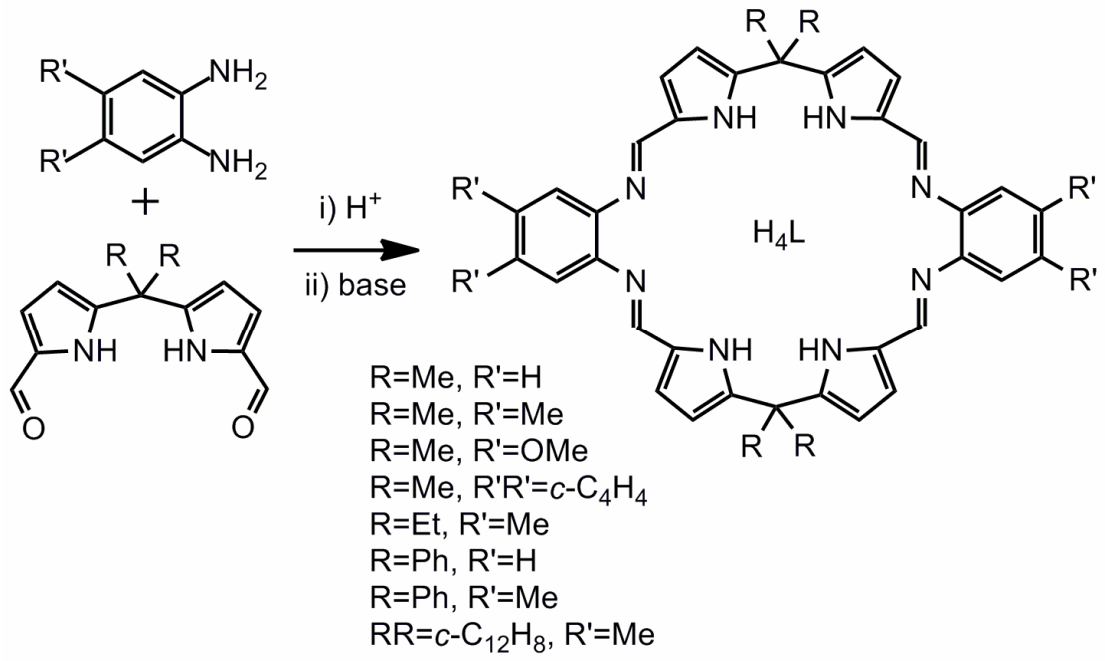

Scheme 5: General synthesis of Schiff-base pyrrole macrocycles. Many varieties have been synthesised[68, 70-73]

The macrocycle contains two N_4-donor pockets which, upon complexation of two metal centres, is capable of folding at the arene hinges into a wedge-shaped geometry that is reminiscent of pacman diporphyrins.[73] Under certain conditions, especially if the pyrrole nitrogens remain protonated, a bowl-shaped geometry is also obtained (Figure 12).[74]

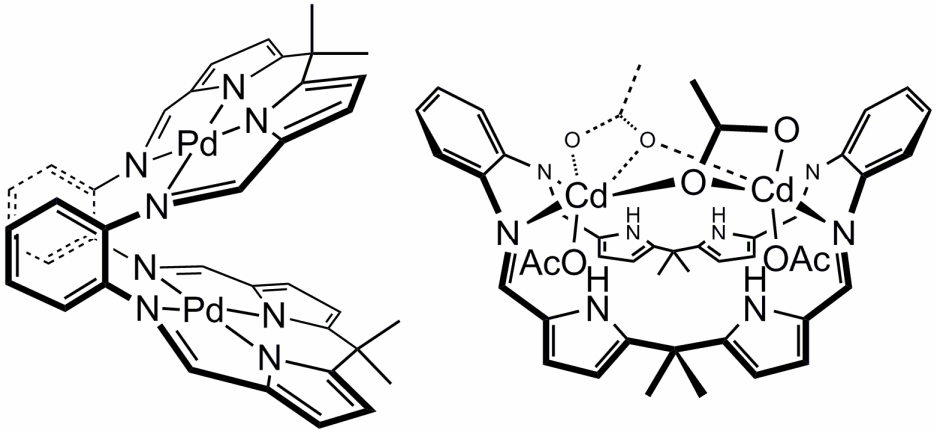

Figure 12: The Schiff-base pyrrole macrocycle is capable of forming a wedge-shaped pacman complex[68] (left) or a bowl-shaped complex[74] (right)

The ligand synthesis is open to modification at either the arene backbone or *meso*-position to fine tune its properties. A variety of Schiff-base pacman ligands have been synthesised and fully characterised, all of which are capable of adopting pacman geometry upon metal binding (Scheme 5). In contrast to diporphyrins, the *meso*-sp^3-carbon prevents full conjugation and the N_4-pockets are not cofacial, with the "bite" angle, defined as the angle between the metals and the midpoint centroid of the arene backbones, of about 60 °. The arene backbones are also found to twist, often forming π-π stacking interactions, though sometimes the two arene backbone units splay out at different angles forming a significant angle between them, the dihedral angle α. All three angles that define the structures are represented in Figure 13.

Various pacman-shaped homo-bimetallic complexes of these ligands have been reported, including complexes of Pd, Mn, Ni, Fe, Cu, Ti, V and Co with M···M separation ranging from 3.145 to 4.120 Å, twist angles ranging from 0.3 to 32.2 °, and bite angles from 52.1 to 64.8 ° depending on the ligand, metals and if any bridging atom(s) are found in the cleft.[68, 70, 73] Interestingly, the binuclear cobalt pacman complexes were shown to catalyse the four electron reduction of dioxygen to water akin to pacman porphyrins. Certain intermediates, including single crystal X-ray structures of dioxygen bound in the "mouth" of the pacman were also obtained.[70, 75] Unfortunately, poor turnover numbers were observed, and were thought to be due to formation of stable bridging oxo/hydroxo species as seen with pacman porphyrins.[71, 75, 76]

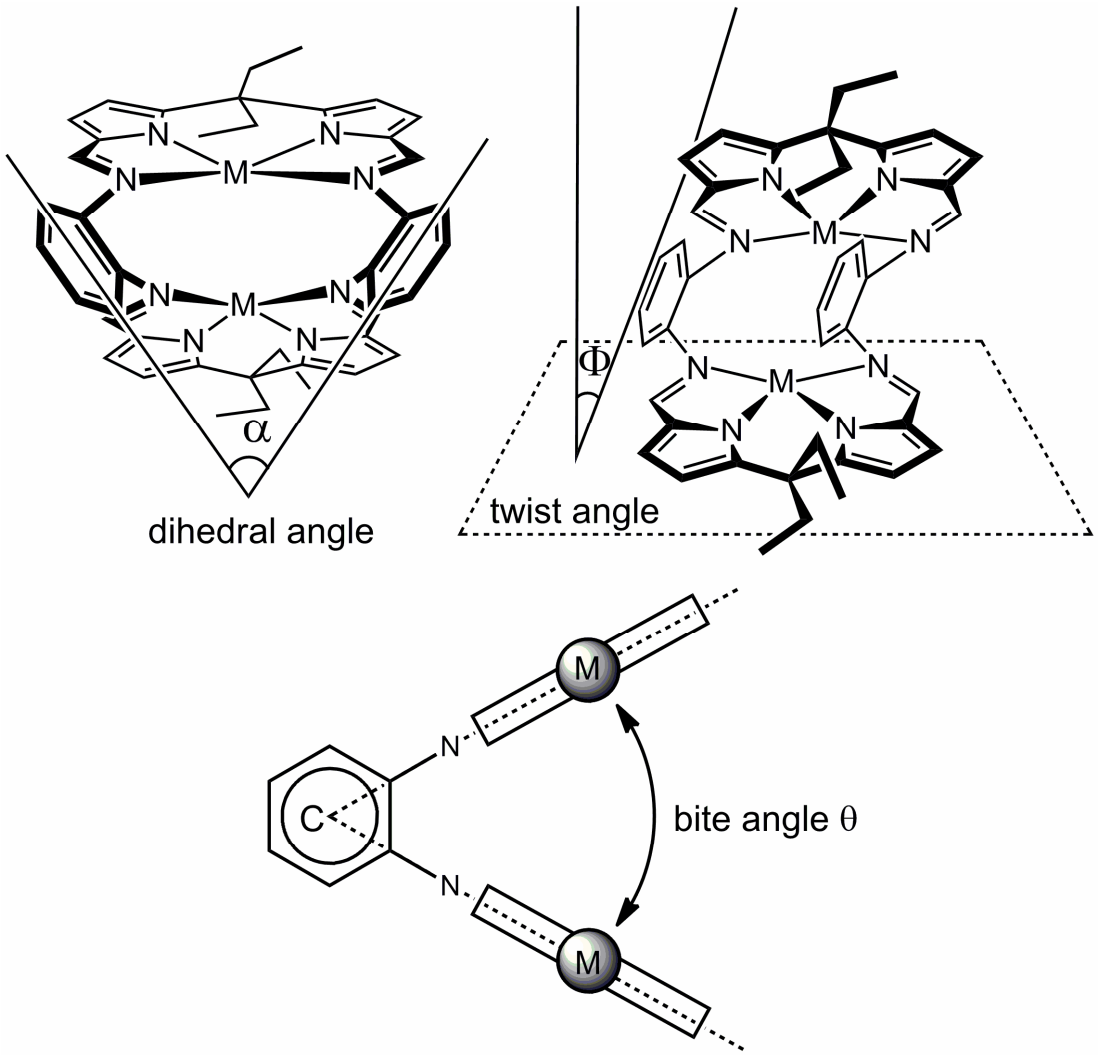

Figure 13: Diagrams defining the dihedral angle (α = angle between two aryl C_6 planes) twist angle Φ (angle between the normal to the MN_4 plane and aryl C_6 plane) and bite angle θ (C = bisector of the vector between the aryl ring centroids)

In an attempt to prevent single-atom bridging species being formed, a ligand with large bulky fluorenyl substituents in the *meso*-positions, and a ligand which employed a larger anthracene-hinge were synthesised (Figure 14).

It was hoped that a steric clash between the fluorenyl substituents would increase the metal-metal separation and disfavour μ-O formation; however, a μ-hydroxo species was identified by single crystal X-ray diffraction.[76] Investigations into binuclear-cobalt complexes of the anthracene-backboned ligand are currently awaiting publication but results show that these are also capable of catalysing the reduction of dioxygen to water. Furthermore, binuclear zinc complexes of this ligand have shown to form interesting zincate structures.[77]

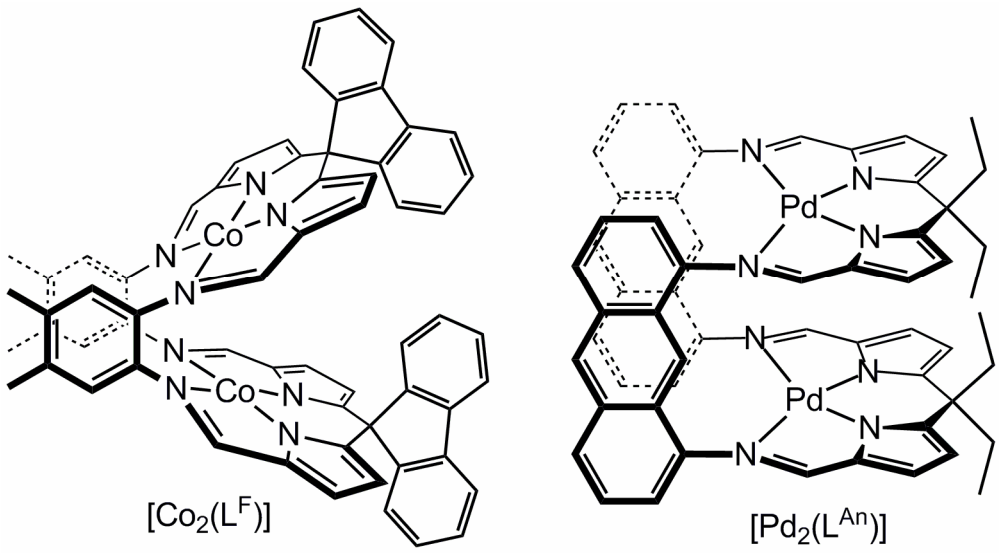

Figure 14: Pacman complexes of bulky fluorenyl ligand L^{F} [71] and anthracene backbone macrocycle L^{An} [77] designed to prevent single-atom bridged complexes

Disappointingly, reactions between the macrocycle and one equivalent of a transition-metal substrate, such as palladium acetate, yielded a mixture of mono-metallated complexes, doubly-metallated complexes and free ligand, H_4L. However, reaction with one equivalent of $[UO_2(THF)_2(N\{SiMe_3\}_2)_2]$ produced the mono-metallic complex $[(UO_2)(THF)(H_2L)]$ cleanly. It is thought the steric bulk of the linear UO_2^{2+} group disfavours coordination of a second UO_2^{2+}, leaving the second binding pocket free for further chemistry (Scheme 6).[78] By utilising this free pocket, it was possible to manipulate the now desymmetrised UO_2^{2+}, promoting reductive lithiation or silylation of the usually unreactive O=U=O group.[79, 80]

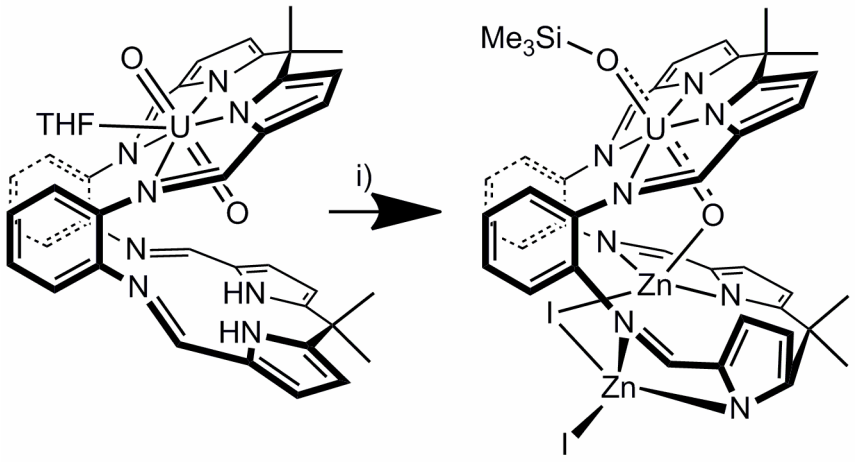

Scheme 6: Use of the free pocket allows for the reductive silylation of the uranyl unit[80]
i) $KN(SiMe_2)_2$, ZnI_2, THF -80 °C

1.3 Role of secondary coordination sphere control

Over 100 years ago it was suggested that the environment surrounding transition metal complexes affected their structure and reactivity.[81] Despite this, the vast majority of studies involving the synthesis and study of transition metal complexes have concentrated on the primary coordination sphere only. Although the primary coordination sphere does determine many properties of a given compound, the secondary coordination sphere also plays a vital role in influencing these properties. Management of both of these environments is thus vital to achieving many of the goals of synthetic inorganic chemistry. Despite this, studies into the effects of secondary coordination environments in both biological and synthetic metal-containing systems are a relatively recent endeavour.

1.3.1 Secondary coordination sphere control in nature.

The environment surrounding the active site of metalloproteins is not only important for proton and electron delivery, as discussed in Section 1.1.1, but also for the properties of the metal centre, any bound species, and the stability of any intermediates in chemical reactions.

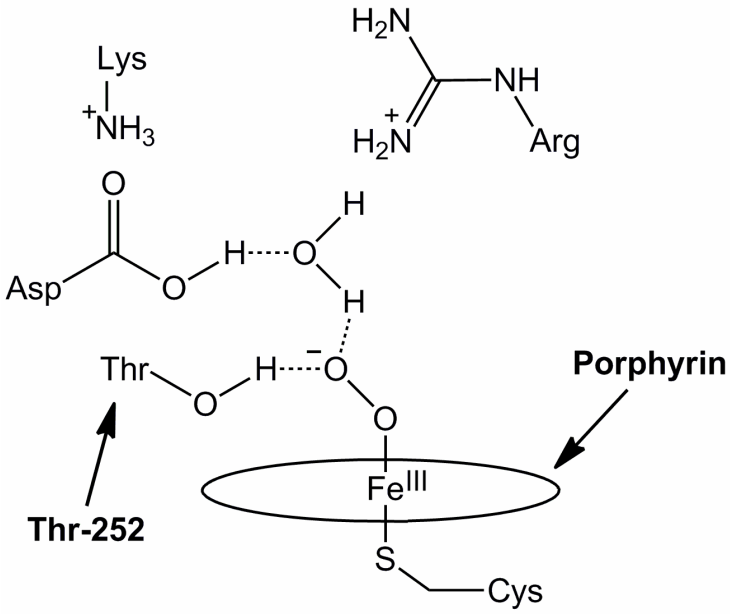

Figure 15: Active site of cytochrome P450, showing hydrogen-bonded intermediate

Cytochrome P450 catalyses the oxidation of organic substrates to alcohols and the mechanism has been heavily investigated.[82-85] Hydrogen bonding is required to initiate the cycle as well as to achieve selective reduction, with a proximal threonine

(Thr-252) vital for protein activity.[84] The hydroxyl group of Thr-252 stabilises the initial Fe-O_2 system formed and is also vital for the dioxygen to peroxide reduction step (Figure 15).[83, 85] Again hydrogen bonding is utilised to stabilise the iron-oxo system formed.[85, 86]

Ligands capable of hydrogen bonding to metal centres and bound species have been found in various proteins and aid in protein structure and function.[87] Furthermore, it has been found that certain blue-copper proteins with similar primary coordination environments display vastly different redox properties.[88] Reduction potentials range from 184 mV for stellacyanin[89] to 680 mV for rusticyanin,[90] a result thought to be due to the differences in secondary coordination environments.

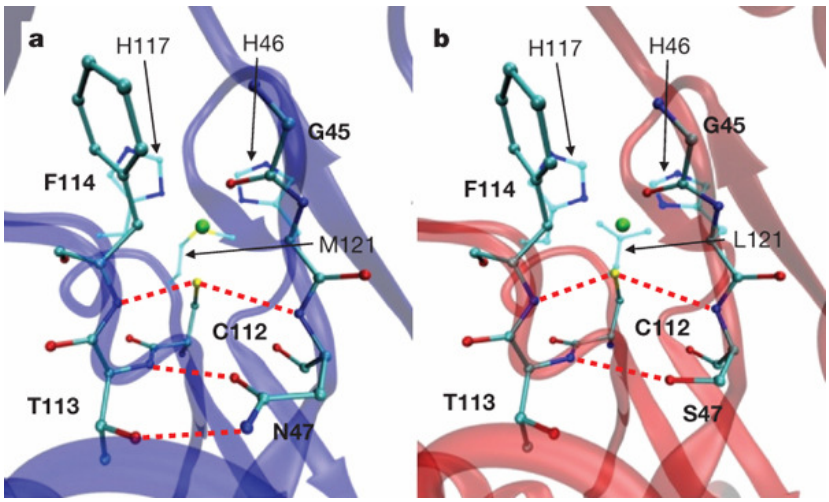

Figure 16: X-ray structures of two azurins, natural azurin (a) and a modified azurin (b) used by the Lu group. Dashed red lines show hydrogen bonding in the active site[91]

Lu and co-workers have studied cupredoxin azurin, a copper-based protein involved with various electron transfer reactions including photosynthesis, respiration and cell signalling.[92] They found that alteration of hydrogen bonding and hydrophobic groups in the outer-sphere environment (Figure 16) resulted in the ability to tune the redox properties of the protein over a 700 mV range, allowing access to reduction potentials not reached in naturally occurring proteins.[91] Mutants created by the Berry group introduced phenylaniline residues into the secondary coordination environment of azurin proteins, again resulting in alteration of redox properties.[93]

1.3.2 Secondary coordination control in synthetic complexes

The Borovik group are major contributors to research into synthetic complexes that incorporate secondary interactions.[86, 94-97] A series of tripodal cobalt complexes

were synthesised with three, two, one and no hydrogen-bonding urea groups and the effects of these alterations to the secondary coordination sphere on the properties of the complexes were investigated (Figure 17).[95]

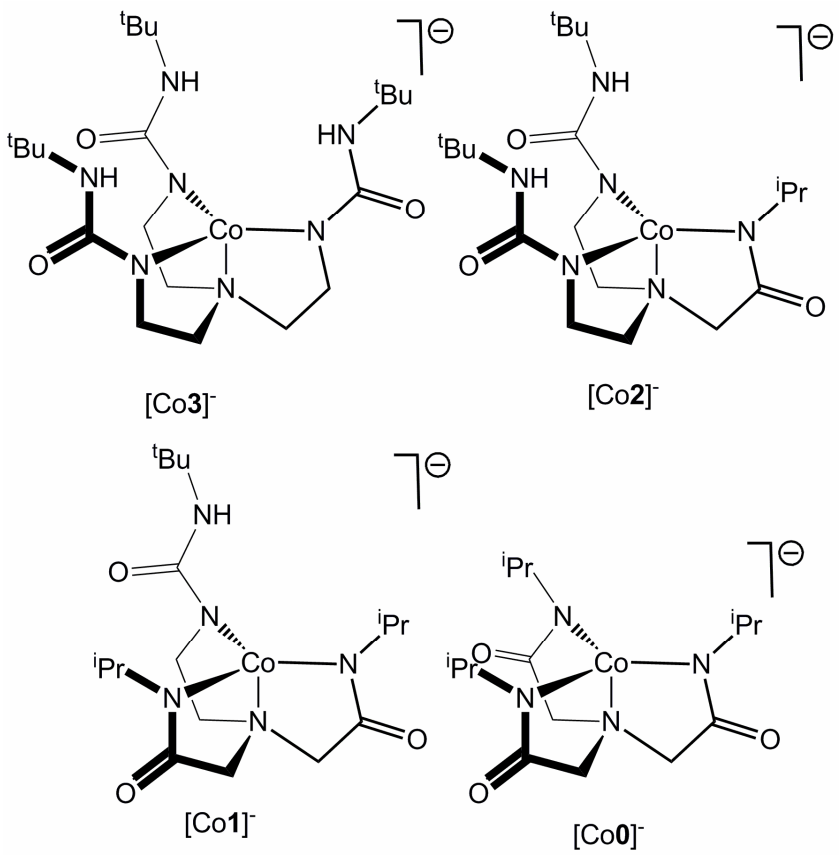

Figure 17: A series of complexes by the Borovik group altering the secondary coordination environment through use of urea groups[95]

Although there were difficulties in preparing bulk [Co**3**]$^-$ cleanly due to solubility problems, the bis, mono and zero urea-appended complexes ([Co**2**]$^-$, [Co**1**]$^-$ and [Co**0**]$^-$ respectively) were thoroughly investigated. It was found by single crystal X-ray diffraction and EPR spectroscopy that the primary coordination environments of these complexes were nearly-identical. Despite this, electrochemical investigations revealed differences in the Co(II)/Co(III) redox couple, with [Co**0**]$^-$ displaying a quasi-reversible feature whilst [Co**2**]$^-$ and [Co**1**]$^-$ only displayed an irreversible feature, with the anodic potential of these features scaling linearly with the number of H-bonds present (at -155, -240 and -385 mV respectively). It was found that [Co**2**]$^-$ reacted spontaneously with dioxygen, resulting in the formation of a Co^{III}-OH complex (Figure 18) whereas [Co**1**]$^-$ reacted only in the presence of excess oxygen. [Co**1**]$^-$ displayed a degree of reversibility by EPR and absorbance spectroscopy, whilst [Co**0**]$^-$ showed no

reactivity towards dioxygen at all. It was also shown that the lack of reactivity of [Co**0**]$^-$ was not due to steric effects as cyanide was found to bind to this complex. Overall, this work clearly demonstrates the importance of the secondary coordination sphere upon reactivity.[95]

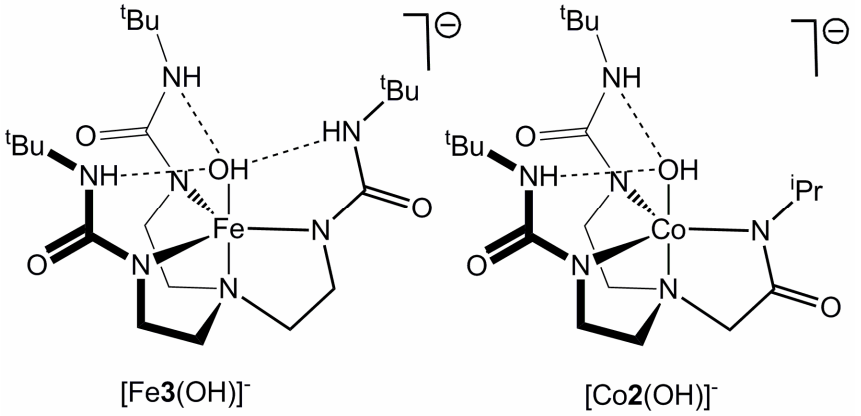

Figure 18: Iron[96] and cobalt[97]-hydroxo complexes studies by Borovik and co-workers

The same ligand set was also used to investigate the reactivity of iron complexes towards dioxygen to form Fe^{III}-OH complexes (Figure 18), employing single crystal X-ray diffraction, electrochemistry, EPR, IR and UV absorption spectroscopy. Despite almost identical primary coordination environments, the properties of these complexes were again found to change dramatically with alterations of the secondary coordination sphere. For example, the O-H stretching frequency decreased with an increasing number of H-bond donors.[96] Further to this, the Borovik group have synthesised related dinucleating ligands (Figure 19), the binuclear cobalt complexes of which were shown to bind anions as well as form a μ_2-OH complex which reacts with nitriles to form amides.[97]

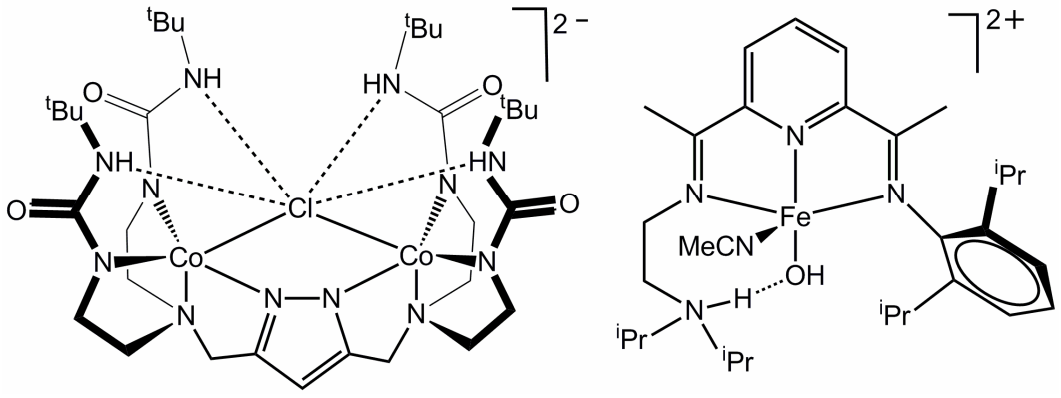

Figure 19: Dinucleating ligand complexes for secondary coordination sphere control by the Borovik group[97] (left) and a complex utilising H-bonds by Gilbertson and co-workers[98]

Terminal hydroxo ligands are thought to be active intermediates in many metalloenzymes, and are stabilised by amino acid residues in the secondary coordination sphere. The Gilbertson group used a pyridine-diimine ligand capable of intramolecular H-bonding to stabilise an Fe^{II}-OH group to investigate this type of intermediate (Figure 11).[98] Further examples of ligands containing groups capable of H-bond coordination include work by Kitajima and co-workers in which a stable manganese-peroxo complex was formed,[99] and zinc complexes of sulphur and pyridine donor tripodal ligands by the Berreau group (Figure 20).[100, 101] Mareque-Rivas and co-workers have synthesised zinc and copper-tripodal tetradentate ligand complexes and studied the binding of substrates in the cleft.[102, 103] Analogous to the work by Borovik, a series of zinc-chloride complexes of ligands with one, two and three amine arms were synthesised (Figure 20) and it was found that despite almost identical primary coordination environments, alteration of the secondary coordination environment caused large differences in the Zn-Cl bond lengths.[103]

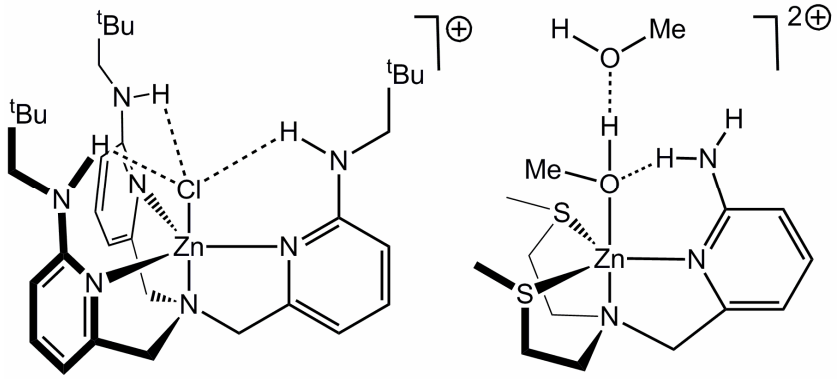

Figure 20: Amine tripod studied by the Mareque-Rivas group[103] (left) and sulphur-based tripod by Berreau and co-workers[100]

1.3.3 Picket-fence, Hanging-group, and Hangman porphyrins

There are many models of heme-proteins,[104] and one such example is picket-fence porphyrins (Figure 21). These systems, pioneered by Collman in 1975,[105] were synthesised to mimic the active site of oxygen-binding hemeproteins.[106] These complexes contain a pocket capable of binding dioxygen, whilst also shielding the pocket from coordination of a second metal.

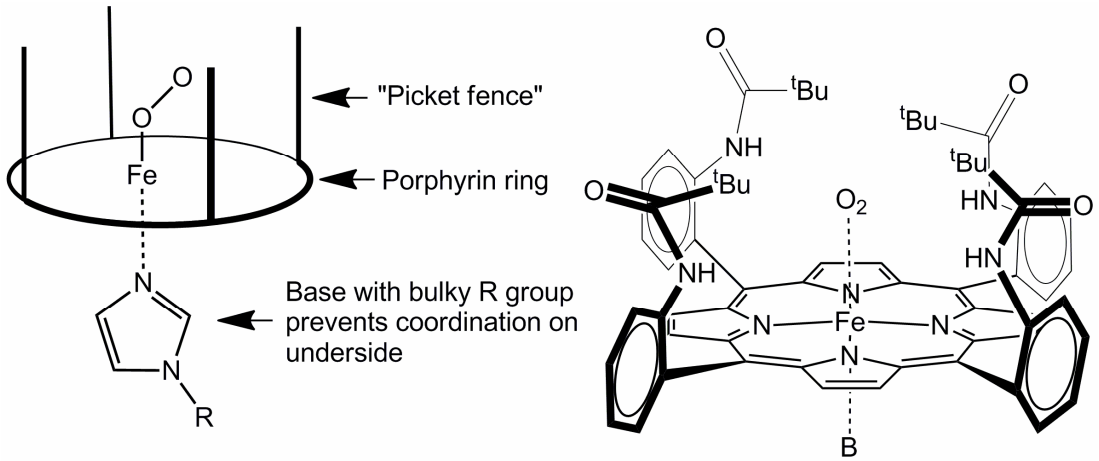

Figure 21: Picket fence porphyrin concept (left) and initial picket fence porphyrin synthesised by the Collman group[105] (right) B = methylimidazole

Positioning hydrogen-bonding groups on the *meso*-carbon caused them to be too far from the metal centre to be involved in H-bonding interactions. Despite this however, a weak dipole interaction was thought to stabilise the dioxygen complex.[107] Collman and co-workers have also used picket-fence porphyrins to synthesise functional heterobimetallic cytochrome c oxidase models, (Figure 22 and Chapter 3, Section 3.1).[108, 109] To overcome the problem of the pendant groups being too distant from any bound species, porphyrins with rigid groups which "hang" over the metal centre within H-bonding distances were synthesised. Reed and co-workers investigated a large series of such compounds in which one *meso*-amide group was changed for a variety of different groups such as amine, acetyl, benzofuran, urea, indole and phenol groups (Figure 22). It was found that introduction of one phenylurea group caused a nine-fold increase in dioxygen affinity relative to the tetra-amide picket fence porphyrin seen above.[110] The Chang group used Kemp's triacid as a hanging group and found that in this case dramatically higher dioxygen binding affinities with increases in temperature from -42 to 0 °C were observed (Figure 22).[111]

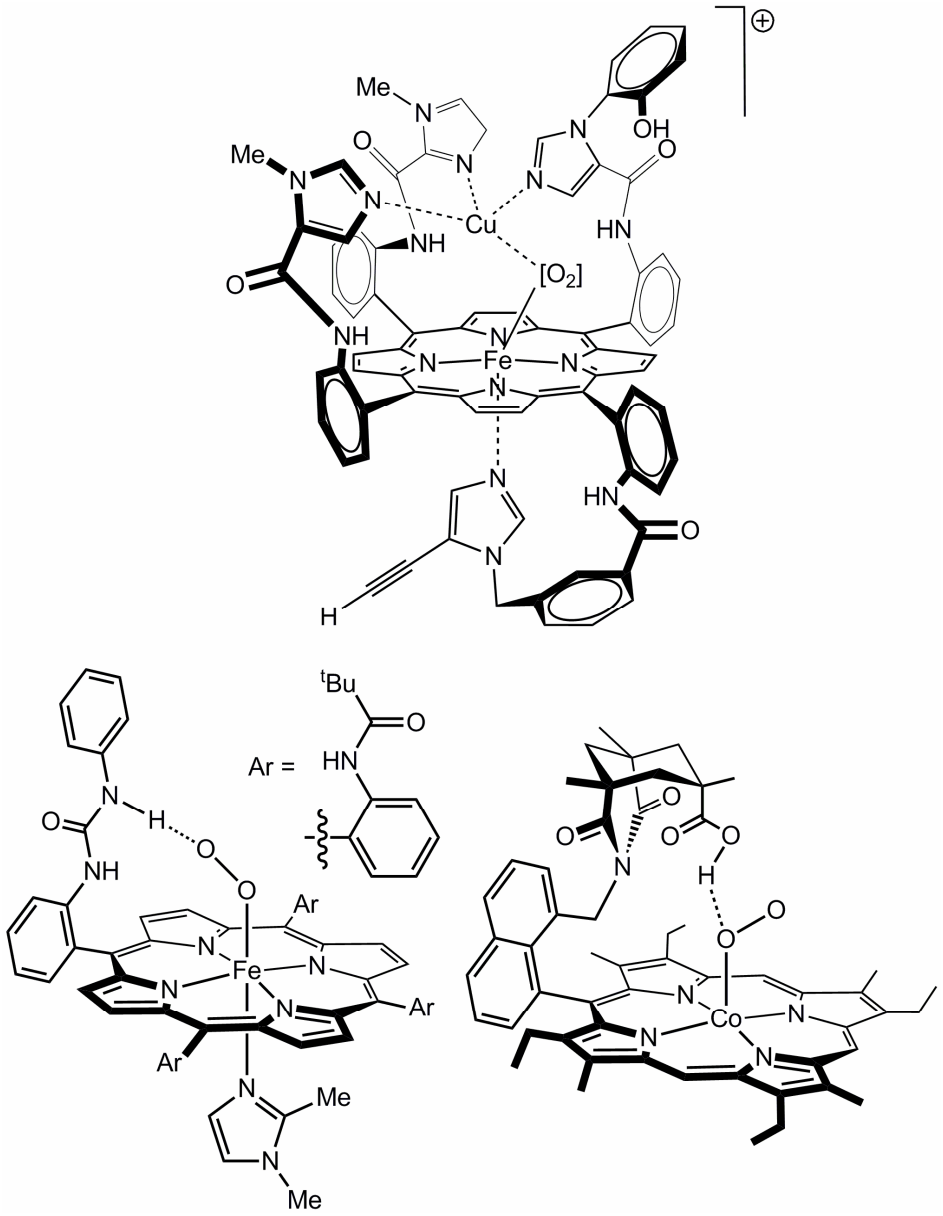

Figure 22: Cytochrome c oxidase model by the Collman group[108] (top). "Hanging group" porphyrins capable of binding dioxygen by the Reed group[110] (bottom left) and Chang and co-workers[111] (bottom right)

A merger of the concepts in hanging-group porphyrins together with single-pillared pacman diporphyrins by the Nocera group led to the development of "hangman" porphyrins in which a rigid xanthene or dibenzofuran backbone positions a "hanging" group above the metal centre.[112, 113] A solid-state structure of an Fe-OH hangman complex included a water molecule in the cleft H-bonded to both the Fe-OH and the hanging group leading to comparisons to the heme water channel. It was envisaged that the hanging group could be used to stabilise intermediates *via* H-bonding and to facilitate proton delivery to bound substrates, an effective coupling of proton and

electron delivery.[3] It was later found that iron (III) hangman complexes were capable of catalysing the disproportionation of hydrogen peroxide to oxygen and water (Scheme 7).[113, 114]

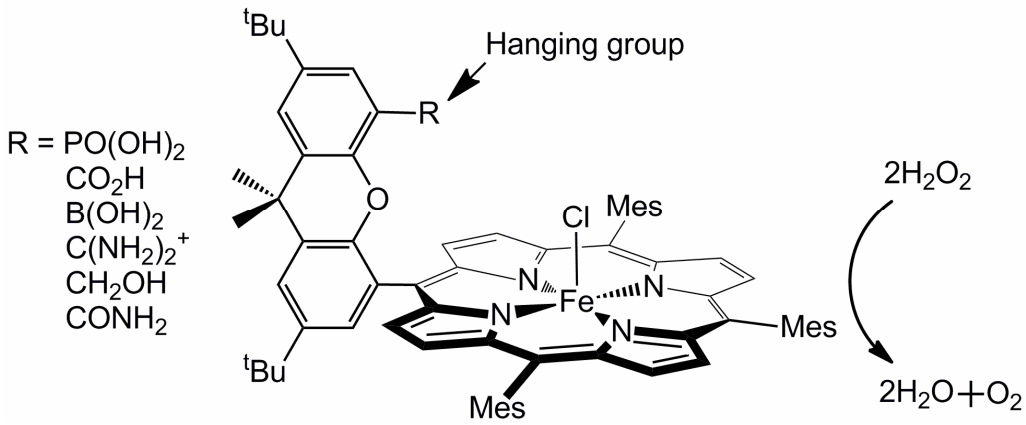

Scheme 7: General structure of a hangman porphyrin[114]

In one study, the hanging group was systematically changed and the activity of the resulting complexes investigated. Initial rates of reaction increased with decreasing pKa values, although employing a carboxylic acid hanging group resulted in turnover numbers five times higher than the next highest (when R = $PO(OH)_2$).[114] Dioxygen reduction by hangman complexes under electrocatalytic conditions was investigated and the full four electron reduction to water was observed, despite the absence of a second metal centre (Scheme 8).[3]

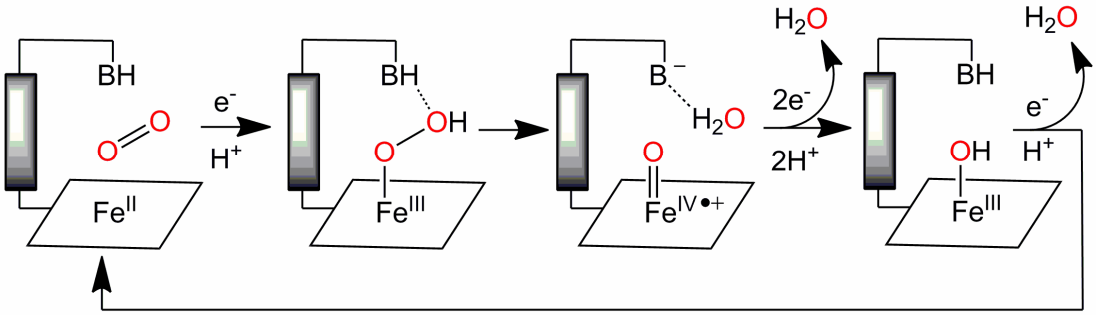

Scheme 8: Suggested mechanism for the four electron reduction of dioxygen catalysed by an iron hangman complex under electrocatalytic conditions. B = acid/base hanging group[3]

It was later found that a cobalt hangman complex could also catalyse the full four electron reduction of dioxygen to water under ambient conditions when an electron deficient porphyrin was used in conjunction with a carboxylic acid hanging group (see Chapter 3, Section 3.1).[115] Porphyrin platforms bearing two rigid hangman-groups have also been synthesised although their catalytic activity has not been investigated.[116]

Additionally hangman-appended, salen-based manganese complexes have been synthesised by the Nocera group and found to catalyse the epoxidation of 1,2-dihydronapthalene and the disproportionation of hydrogen peroxide (Figure 23).[117, 118] The modular synthesis of these complexes is thought to allow for fine tuning of their properties through alteration of both primary and secondary coordination spheres.[119] Furthermore, corrole-based, cobalt-hangman complexes have recently been synthesised and were shown to reduce dioxygen to water; iron complexes were also found capable of catalysing the disproportionation of H_2O_2 (Figure 23).[120, 121]

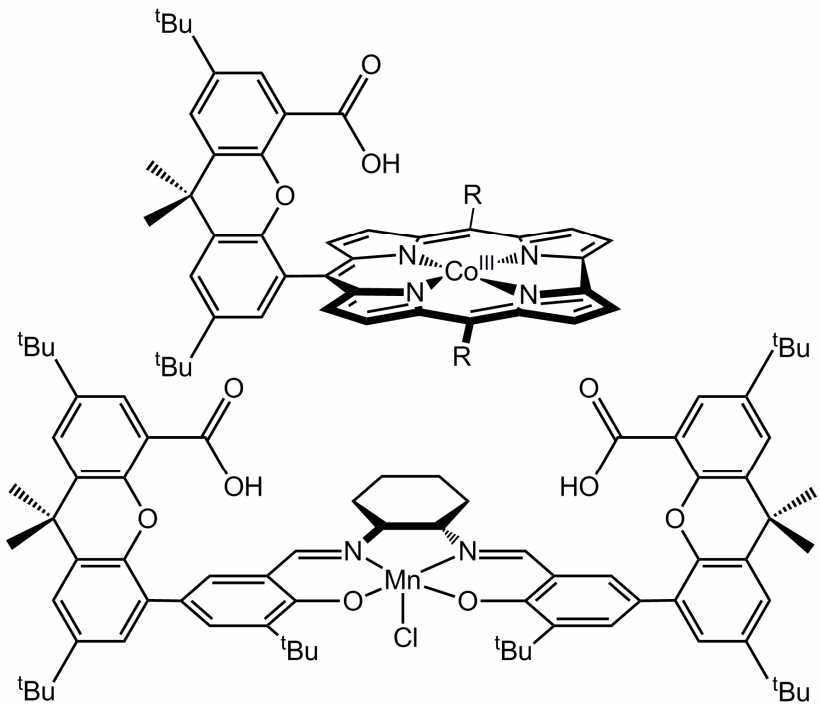

Figure 23: Corrole-hangman[120] R = C_6F_5 (top) and Salen-hangman complex[117] (bottom) by the Nocera group

1.4 Outlook

In conclusion, the function of metalloenzymes can be understood in terms of both their primary and secondary coordination spheres. It has also been shown that synthetic systems should also consider the secondary, as well as primary coordination spheres in their designs should the ultimate application of catalytic transformations be achieved. Cofacial diporphyrins have been shown to be effective catalysts for the PCET reduction of dioxygen to water, an important reaction to the further development of a hydrogen fuel cell economy. Certain complexes of Schiff-base pyrrole macrocycles are structurally similar to pacman porphyrins and although less catalytically active, are more

straightforwardly synthesised. Hangman porphyrins have shown secondary coordination control *via* hanging acid/base groups that can also promote catalytic reduction of dioxygen to water.

As such, this thesis describes the synthesis and characterisation of a range of macrocycles that are designed to be not only capable of adopting a pacman conformation designed but also integrate secondary sphere control. The ultimate aim of synthesising these compounds is to assess their catalytic application towards small molecule transformations, such as in the reduction of dioxygen to water.

1.5 References

[1] *U.S. Department of Energy: International Energy Outlook 2010, Energy Information Association: http://www.eia.doe.gov/oiaf/ieo/world.html*, **2010**.

[2] N. S. Lewis, D. G. Nocera, *Proc. Natl. Acad. Sci.* **2006**, *103*, 15729.

[3] J. L. Dempsey, A. J. Esswein, D. R. Manke, J. Rosenthal, J. D. Soper, D. G. Nocera, *Inorg. Chem.* **2005**, *44*, 6879.

[4] T. R. Cook, D. K. Dogutan, S. Y. Reece, Y. Surendranath, T. S. Teets, D. G. Nocera, *Chem. Rev.* **2011**, *110*, 6474.

[5] T. Tsukihara, H. Aoyama, E. Yamashita, T. Tomizaki, H. Yamaguchi, K. Shinzawa-Itoh, R. Nakashima, R. Yaono, S. Yoshikawa, *Science* **1995**, *269*, 1069; T. Tsukihara, H. Aoyama, E. Yamashita, T. Tomizaki, H. Yamaguchi, K. Shinzawa-Itoh, R. Nakashima, R. Yaono, S. Yoshikawa, *Science* **1996**, *272*, 1136.

[6] G. T. Babcock, M. Wikstrom, *Nature* **1992**, *356*, 301; K. Muramoto, K. Ohta, K. Shinzawa-Itoh, K. Kanda, M. Taniguchi, H. Nabekura, E. Yamashita, T. Tsukihara, S. Yoshikawa, *Proc. Natl. Acad. Sci.* **2010**, *107*, 7740.

[7] B. G. Malmstroem, *Chem. Rev.* **1990**, *90*, 1247.

[8] S. I. Chan, *Proc. Natl. Acad. Sci.* **2010**, *107*, 8505; P. Brzezinski, G. Larsson, *Biochim. Biophys. Acta-Bioenerg* **2003**, *1605*, 1; P. Brzezinski, A.-L. Johansson, *Biochim. Biophys. Acta-Bioenerg* **2010**, *1797*, 710.

[9] K. Faxen, G. Gilderson, P. Adelroth, P. Brzezinski, *Nature* **2005**, *437*, 286.

[10] C. W. Hoganson, M. A. Pressler, D. A. Proshlyakov, G. T. Babcock, *Biochim. Biophys. Acta-Bioenerg* **1998**, *1365*, 170.

[11] K. N. Ferreira, T. M. Iverson, K. Maghlaoui, J. Barber, S. Iwata, *Science* **2004**, *303*, 1831.

[12] J. S. Vrettos, J. Limburg, G. W. Brudvig, *Biochim. Biophys. Acta-Bioenerg* **2001**, *1503*, 229; V. L. Pecoraro, M. J. Baldwin, M. T. Caudle, W. Y. Hsieh, N. A. Law, *Pure Appl. Chem.* **1998**, *70*, 925.

[13] C. Tommos, G. T. Babcock, *Acc. Chem. Res.* **1998**, *31*, 18.

[14] F. Liu, J. J. Concepcion, J. W. Jurss, T. Cardolaccia, J. L. Templeton, T. J. Meyer, *Inorg. Chem.* **2008**, *47*, 1727.

[15] S. W. Gersten, G. J. Samuels, T. J. Meyer, *J. Am. Chem. Soc.* **1982**, *104*, 4029.

[16] J. A. Gilbert, D. S. Eggleston, W. R. Murphy, D. A. Geselowitz, S. W. Gersten, D. J. Hodgson, T. J. Meyer, *J. Am. Chem. Soc.* **1985**, *107*, 3855.

[17] X. Yang, M.-H. Baik, *J. Am. Chem. Soc.* **2006**, *128*, 7476.

[18] K. Kinoshita, M. Yagi, M. Kaneko, *J. Mol. Catal. A* **1999**, *142*, 1.

[19] K. Nagoshi, M. Yagi, M. Kaneko, *Bull. Chem. Soc. Jpn.* **2000**, *73*, 2193.

[20] M. Yagi, T. Yamaguchi, M. Kaneko, *J. Mol. Catal. A* **1999**, *149*, 289; M. Yagi, E. Takano, M. Kaneko, *Electrochim. Acta* **1999**, *44*, 2493.
[21] M. Yagi, K. Kinoshita, M. Kaneko, *J. Phys. Chem.* **1996**, *100*, 11098.
[22] H. H. Petach, C. M. Elliott, *J. Electrochem. Soc.* **1992**, *139*, 2217; T. Wada, K. Tsuge, K. Tanaka, *Angew. Chem., Int. Ed. Engl.* **2000**, *39*, 1479.
[23] J. J. Concepcion, J. W. Jurss, J. L. Templeton, T. J. Meyer, *J. Am. Chem. Soc.* **2008**, *130*, 16462.
[24] J. J. Concepcion, J. W. Jurss, M. R. Norris, Z. Chen, J. L. Templeton, T. J. Meyer, *Inorg. Chem.* **2010**, *49*, 1277.
[25] J. Mola, E. Mas-Marza, X. Sala, I. Romero, M. Rodríguez, C. Viñas, T. Parella, A. Llobet, *Angew. Chem., Int. Ed. Engl.* **2008**, *47*, 5830; C. Sens, I. Romero, M. RodrÃguez, A. Llobet, T. Parella, J. Benet-Buchholz, *J. Am. Chem. Soc.* **2004**, *126*, 7798.
[26] H. Chen, R. Tagore, S. Das, C. Incarvito, J. W. Faller, R. H. Crabtree, G. W. Brudvig, *Inorg. Chem.* **2005**, *44*, 7661; J. Limburg, J. S. Vrettos, L. M. Liable-Sands, A. L. Rheingold, R. H. Crabtree, G. W. Brudvig, *Science* **1999**, *283*, 1524.
[27] A. Dimitrakopoulou, V. Psycharis, C. P. Raptopoulou, A. Terzis, V. Tangoulis, D. P. Kessissoglou, *Inorg. Chem.* **2008**, *47*, 7608; C. M. Zaleski, T.-C. Weng, C. Dendrinou-Samara, M. Alexiou, P. Kanakaraki, W.-Y. Hsieh, J. Kampf, J. E. Penner-Hahn, V. L. Pecoraro, D. P. Kessissoglou, *Inorg. Chem.* **2008**, *47*, 6127.
[28] Y. Gorlin, T. F. Jaramillo, *J. Am. Chem. Soc.* **2011**, *132*, 13612.
[29] M. W. Kanan, D. G. Nocera, *Science* **2008**, *321*, 1072.
[30] J. G. McAlpin, Y. Surendranath, M. DincaÌŒ, T. A. Stich, S. A. Stoian, W. H. Casey, D. G. Nocera, R. D. Britt, *J. Am. Chem. Soc.* **2010**, *132*, 6882; Y. Surendranath, M. W. Kanan, D. G. Nocera, *J. Am. Chem. Soc.* **2010**, *132*, 16501.
[31] D. A. Lutterman, Y. Surendranath, D. G. Nocera, *J. Am. Chem. Soc.* **2009**, *131*, 3838.
[32] M. W. Kanan, J. Yano, Y. Surendranath, M. DincaÌ†, V. K. Yachandra, D. G. Nocera, *J. Am. Chem. Soc.* **2010**, *132*, 13692.
[33] M. Dinca, Y. Surendranath, D. G. Nocera, *Proc. Natl. Acad. Sci.* **2010**, *107*, 10337.
[34] *J. Porph. Phthal*; K. M. Kadish, K. M. Smith, R. Guilard, *The Porphyrin Handbook*, Academic Press: New York, **2000**.
[35] C. Shi, B. Steiger, M. Yuasa, F. C. Anson, *Inorg. Chem.* **1997**, *36*, 4294; B. Steiger, C. Shi, F. C. Anson, *Inorg. Chem.* **1993**, *32*, 2107.
[36] F. C. Anson, C. Shi, B. Steiger, *Acc. Chem. Res.* **1997**, *30*, 437; C. Shi, F. C. Anson, *Inorg. Chem.* **1996**, *35*, 7928.
[37] P. A. Forshey, T. Kuwana, *Inorg. Chem.* **1983**, *22*, 699; P. A. Forshey, T. Kuwana, *Inorg. Chem.* **1981**, *20*, 693.
[38] J. P. Collman, K. Kim, *J. Am. Chem. Soc.* **1986**, *108*, 7847.
[39] J. P. Collman, C. M. Elliott, T. R. Halbert, B. S. Tovrog, *Proc. Natl. Acad. Sci. U. S. A.* **1977**, *74*, 18; B. C. Bookser, T. C. Bruice, *J. Am. Chem. Soc.* **1991**, *113*, 4208.
[40] J. P. Collman, P. Denisevich, Y. Konai, M. Marrocco, C. Koval, F. C. Anson, *J. Am. Chem. Soc.* **1980**, *102*, 6027.
[41] C. K. Chang, I. Abdalmuhdi, *J. Org. Chem.* **1983**, *48*, 5388; C. K. Chang, I. Abdalmuhdi, *Angew. Chem., Int. Ed. Engl.* **1984**, *23*, 164.
[42] C. J. Chang, Y. Deng, A. F. Heyduk, C. K. Chang, D. G. Nocera, *Inorg. Chem.* **2000**, *39*, 959.
[43] J. P. Collman, P. S. Wagenknecht, J. E. Hutchison, *Angew. Chem., Int. Ed. Engl.* **1994**, *33*, 1537.
[44] C. K. Chang, H. Y. Liu, I. Abdalmuhdi, *J. Am. Chem. Soc.* **1984**, *106*, 2725; R. R. Durand, C. S. Bencosme, J. P. Collman, F. C. Anson, *J. Am. Chem. Soc.* **1983**, *105*, 2710.

[45] Y. Le Mest, C. Inisan, A. Laouenan, M. L'Her, J. Talarmin, M. El Khalifa, J.-Y. Saillard, *J. Am. Chem. Soc.* **1997**, *119*, 6095.
[46] J. Rosenthal, D. G. Nocera, *Acc. Chem. Res.* **2007**, *40*, 543.
[47] C. L. Ni, I. Abdalmuhdi, C. K. Chang, F. C. Anson, *J. Phys. Chem.* **1987**, *91*, 1158.
[48] R. Guilard, S. Brandes, C. Tardieux, A. Tabard, M. L'Her, C. Miry, P. Gouerec, Y. Knop, J. P. Collman, *J. Am. Chem. Soc.* **1995**, *117*, 11721.
[49] C. J. Chang, Y. Deng, C. Shi, C. K. Chang, F. C. Anson, D. G. Nocera, *Chem. Commun.* **2000**, 1355.
[50] B. J. Pistorio, C. J. Chang, D. G. Nocera, *J. Am. Chem. Soc.* **2002**, *124*, 7884.
[51] Y. Deng, C. J. Chang, D. G. Nocera, *J. Am. Chem. Soc.* **1999**, *122*, 410.
[52] C. J. Chang, E. A. Baker, B. J. Pistorio, Y. Deng, Z.-H. Loh, S. E. Miller, S. D. Carpenter, D. G. Nocera, *Inorg. Chem.* **2002**, *41*, 3102.
[53] C. J. Chang, Z.-H. Loh, C. Shi, F. C. Anson, D. G. Nocera, *J. Am. Chem. Soc.* **2004**, *126*, 10013.
[54] H. Y. Liu, I. Abdalmuhdi, C. K. Chang, F. C. Anson, *J. Phys. Chem.* **1985**, *89*, 665.
[55] J. M. Hodgkiss, C. J. Chang, B. J. Pistorio, D. G. Nocera, *Inorg. Chem.* **2003**, *42*, 8270.
[56] J. Rosenthal, B. J. Pistorio, L. L. Chng, D. G. Nocera, *J. Org. Chem.* **2005**, *70*, 1885.
[57] J. Rosenthal, T. D. Luckett, J. M. Hodgkiss, D. G. Nocera, *J. Am. Chem. Soc.* **2006**, *128*, 6546.
[58] I. Wasbotten, A. Ghosh, *Inorg. Chem.* **2006**, *45*, 4910; I. Aviv-Harel, Z. Gross, *Chem. Eur. J.* **2009**, *15*, 8382.
[59] K. M. Kadish, J. Shen, L. Fremond, P. Chen, M. E. Ojaimi, M. Chkounda, C. P. Gros, J.-M. Barbe, K. Ohkubo, S. Fukuzumi, R. Guilard, *Inorg. Chem.* **2008**, *47*, 6726.
[60] Y. Gao, T. Akermark, J. Liu, L. Sun, B. Akermark, *J. Am. Chem. Soc.* **2009**, *131*, 8726.
[61] R. Guilard, F. Jérôme, C. P. Gros, J.-M. Barbe, Z. Ou, J. Shao, K. M. Kadish, *C. R. l'Academie. Sci., Ser. IIC-Chem.* **2001**, *4*, 245; F. Jerome, C. P. Gros, C. Tardieux, J.-M. Barbe, R. Guilard, *Chem. Commun.* **1998**, 2007; K. M. Kadish, Z. Ou, J. Shao, C. P. Gros, J.-M. Barbe, F. Jerome, F. Bolze, F. Burdet, R. Guilard, *Inorg. Chem.* **2002**, *41*, 3990.
[62] F. Jerome, C. P. Gros, C. Tardieux, J.-M. Barbe, R. Guilard, *New J. Chem.* **1998**, *22*, 1327.
[63] R. Guilard, F. Burdet, J.-M. Barbe, C. P. Gros, E. Espinosa, J. Shao, Z. Ou, R. Zhan, K. M. Kadish, *Inorg. Chem.* **2005**, *44*, 3972; K. M. Kadish, L. Fremond, J. Shen, P. Chen, K. Ohkubo, S. Fukuzumi, M. El Ojaimi, C. P. Gros, J.-M. Barbe, R. Guilard, *Inorg. Chem.* **2009**, *48*, 2571.
[64] R. Misra, T. K. Chandrashekar, *Acc. Chem. Res.* **2008**, *41*, 265.
[65] J. L. Sessler, E. Tomat, T. D. Mody, V. M. Lynch, J. M. Veauthier, U. Mirsaidov, J. T. Markert, *Inorg. Chem.* **2005**, *44*, 2125.
[66] W. A. Reiter, A. Gerges, S. Lee, T. Deffo, T. Clifford, A. Danby, K. Bowman-James, *Coord. Chem. Rev.* **1998**, *174*, 343.
[67] L. K. Frensch, K. Pröpper, M. John, S. Demeshko, C. Brückner, F. Meyer, *Angew. Chem., Int. Ed. Engl.* **2011**, *50*, 1420.
[68] G. Givaja, A. J. Blake, C. Wilson, M. Schroder, J. B. Love, *Chem. Commun.* **2003**, 2508.
[69] J. L. Sessler, W.-S. Cho, S. P. Dudek, L. Hicks, V. M. Lynch, M. T. Huggins, *J. Porph. Phthal.* **2003**, *7*, 97.
[70] G. Givaja, M. Volpe, M. A. Edwards, A. J. Blake, C. Wilson, M. Schröder, J. B. Love, *Angew. Chem., Int. Ed. Engl.* **2007**, *46*, 584.

[71] E. Askarizadeh, A. M. J. Devoille, D. M. Boghaei, A. M. Z. Slawin, J. B. Love, *Inorg. Chem.* **2009**, *48*, 7491.
[72] M. Volpe, S. D. Reid, A. J. Blake, C. Wilson, J. B. Love, *Inorg. Chim. Acta* **2007**, *360*, 273.
[73] G. Givaja, M. Volpe, J. W. Leeland, M. A. Edwards, T. K. Young, S. B. Darby, S. D. Reid, A. J. Blake, C. Wilson, J. Wolowska, E. J. L. McInnes, M. Schröder, J. B. Love, *Chem. Eur. J.* **2007**, *13*, 3707.
[74] G. Givaja, A. J. Blake, C. Wilson, M. Schroder, J. B. Love, *Chem. Commun.* **2005**, 4423.
[75] M. Volpe, H. Hartnett, J. W. Leeland, K. Wills, M. Ogunshun, B. J. Duncombe, C. Wilson, A. J. Blake, J. McMaster, J. B. Love, *Inorg. Chem.* **2009**, *48*, 5195.
[76] E. Askarizadeh, S. B. Yaghoob, D. M. Boghaei, A. M. Z. Slawin, J. B. Love, *Chem. Commun.* **2010**, *46*, 710.
[77] A. M. J. Devoille, P. Richardson, N. L. Bill, J. L. Sessler, J. B. Love, *Inorg. Chem.* **2011**, *50*, 3116.
[78] P. L. Arnold, A. J. Blake, C. Wilson, J. B. Love, *Inorg. Chem.* **2004**, *43*, 8206.
[79] P. L. Arnold, A.-F. Pecharman, E. Hollis, A. Yahia, L. Maron, S. Parsons, J. B. Love, *Nat. Chem* **2010**, *2*, 1056.
[80] P. L. Arnold, D. Patel, C. Wilson, J. B. Love, *Nature* **2008**, *451*, 315.
[81] A. Werner, *Ber. Deutsch. Chem. Ges.* **1912**, *45*, 121; A. Werner, *J. Liebigs An. Chem.* **1912**, *386*, 1.
[82] M. Sono, M. P. Roach, E. D. Coulter, J. H. Dawson, *Chem. Rev.* **1996**, *96*, 2841.
[83] N. C. Gerber, S. G. Sligar, *J. Am. Chem. Soc.* **1992**, *114*, 8742.
[84] S. A. Martinis, W. M. Atkins, P. S. Stayton, S. G. Sligar, *J. Am. Chem. Soc.* **1989**, *111*, 9252.
[85] I. Schlichting, J. Berendzen, K. Chu, A. M. Stock, S. A. Maves, D. E. Benson, R. M. Sweet, D. Ringe, G. A. Petsko, S. G. Sligar, *Science* **2000**, *287*, 1615.
[86] R. L. Shook, A. S. Borovik, *Inorg. Chem.* **2010**, *49*, 3646.
[87] Y. Lu, J. S. Valentine, *Curr. Opin. Struct. Biol.* **1997**, *7*, 495; L. Regan, *Trends Biochem. Sci.* **1995**, *20*, 280.
[88] E. I. Solomon, *Inorg. Chem.* **2006**, *45*, 8012.
[89] N. Sailasuta, F. C. Anson, H. B. Gray, *J. Am. Chem. Soc.* **1979**, *101*, 455.
[90] A. G. Sykes, A. G. Sykes, in *Advances in Inorganic Chemistry, Vol. Volume 36*, Academic Press, **1991**, pp. 377.
[91] N. M. Marshall, D. K. Garner, T. D. Wilson, Y.-G. Gao, H. Robinson, M. J. Nilges, Y. Lu, *Nature* **2009**, *462*, 113.
[92] C. Dennison, *Coord. Chem. Rev.* **2005**, *249*, 3025.
[93] S. M. Berry, M. H. Baker, N. J. Reardon, *J. Inorg. Biochem.* **2010**, *104*, 1071.
[94] C. E. MacBeth, R. Gupta, K. R. Mitchell-Koch, V. G. Young, G. H. Lushington, W. H. Thompson, M. P. Hendrich, A. S. Borovik, *J. Am. Chem. Soc.* **2004**, *126*, 2556.
[95] R. L. Lucas, M. K. Zart, J. Murkerjee, T. N. Sorrell, D. R. Powell, A. S. Borovik, *J. Am. Chem. Soc.* **2006**, *128*, 15476.
[96] J. Mukherjee, R. L. Lucas, M. K. Zart, D. R. Powell, V. W. Day, A. S. Borovik, *Inorg. Chem.* **2008**, *47*, 5780.
[97] R. L. Shook, A. S. Borovik, *Chem. Commun.* **2008**, 6095.
[98] A. J. Kendall, L. N. Zakharov, J. D. Gilbertson, *Inorg. Chem.* **2010**, *49*, 8656.
[99] N. Kitajima, H. Komatsuzaki, S. Hikichi, M. Osawa, Y. Moro-oka, *J. Am. Chem. Soc.* **1994**, *116*, 11596.
[100] L. M. Berreau, R. A. Allred, M. M. Makowska-Grzyska, A. M. Arif, *Chem. Commun.* **2000**, 1423.
[101] L. M. Berreau, M. M. Makowska-Grzyska, A. M. Arif, *Inorg. Chem.* **2001**, *40*, 2212.

[102] J. C. Mareque Rivas, R. Torres Martin de Rosales, S. Parsons, *Dalton Trans.* **2003**, 2156; J. C. M. Rivas, S. L. Hinchley, L. Metteau, S. Parsons, *Dalton Trans.* **2006**, 2316; J. C. M. Rivas, E. Salvagni, S. Parsons, *Dalton Trans.* **2004**, 4185; J. C. M. Rivas, E. Salvagni, R. Prabaharan, R. T. M. de Rosales, S. Parsons, *Dalton Trans.* **2004**, 172; G. Feng, J. C. Mareque-Rivas, R. Torres Martin de Rosales, N. H. Williams, *J. Am. Chem. Soc.* **2005**, *127*, 13470.

[103] J. C. M. Rivas, R. Prabaharan, R. T. M. de Rosales, L. Metteau, S. Parsons, *Dalton Trans.* **2004**, 2800.

[104] M. Momenteau, C. A. Reed, *Chem. Rev.* **1994**, *94*, 659.

[105] J. P. Collman, R. R. Gagne, C. Reed, T. R. Halbert, G. Lang, W. T. Robinson, *J. Am. Chem. Soc.* **1975**, *97*, 1427.

[106] J. P. Collman, *Acc. Chem. Res.* **1977**, *10*, 265.

[107] G. B. Jameson, R. S. Drago, *J. Am. Chem. Soc.* **1985**, *107*, 3017.

[108] J. P. Collman, N. K. Devaraj, R. A. Decreau, Y. Yang, Y.-L. Yan, W. Ebina, T. A. Eberspacher, C. E. D. Chidsey, *Science* **2007**, *315*, 1565.

[109] J. P. Collman, L. Fu, P. C. Herrmann, X. Zhang, *Science* **1997**, *275*, 949.

[110] G. E. Wuenschell, C. Tetreau, D. Lavalette, C. A. Reed, *J. Am. Chem. Soc.* **1992**, *114*, 3346.

[111] C. K. Chang, Y. Liang, G. Aviles, S.-M. Peng, *J. Am. Chem. Soc.* **1995**, *117*, 4191.

[112] C.-Y. Yeh, C. J. Chang, D. G. Nocera, *J. Am. Chem. Soc.* **2001**, *123*, 1513.

[113] C. J. Chang, L. L. Chng, D. G. Nocera, *J. Am. Chem. Soc.* **2003**, *125*, 1866.

[114] L. L. Chng, C. J. Chang, D. G. Nocera, *Org. Lett.* **2003**, *5*, 2421.

[115] R. McGuire Jr, D. K. Dogutan, T. S. Teets, J. Suntivich, Y. Shao-Horn, D. G. Nocera, *Chem. Sci.* **2010**, *1*, 411.

[116] C. J. Chang, C.-Y. Yeh, D. G. Nocera, *J. Org. Chem.* **2002**, *67*, 1403.

[117] J. Y. Yang, S.-Y. Liu, I. V. Korendovych, E. V. Rybak-Akimova, D. G. Nocera, *ChemSusChem* **2008**, *1*, 941.

[118] J. Y. Yang, D. G. Nocera, *J. Am. Chem. Soc.* **2007**, *129*, 8192.

[119] J. Y. Yang, D. G. Nocera, *Tetrahedron Lett.* **2008**, *49*, 4796.

[120] D. K. Dogutan, S. A. Stoian, R. McGuire, M. Schwalbe, T. S. Teets, D. G. Nocera, *J. Am. Chem. Soc.* **2011**, *133*, 131.

[121] M. Schwalbe, D. K. Dogutan, S. A. Stoian, T. S. Teets, D. G. Nocera, *Inorg. Chem.* **2011**, *50*, 1368.

Chapter 2: Synthesis and metallation reactions of H_2L^P and H_2L^{NMe}

2.1 Introduction

In Chapter 1, the importance of both secondary coordination sphere control and stabilisation of metal centres for small molecule activation was discussed. Furthermore, taking inspiration from nature, the ability to control the flow of both protons and electrons for proton-coupled electron transfer reactions, such as the interconversion of water and dioxygen, is also of paramount importance to the successful synthesis of any laboratory-based catalysis.

Though capable of acting as catalysts such as in the four-electron reduction of dioxygen to water, bimetallic complexes of single-pillared pacman diporphyrins[1, 2] and related Schiff-base pyrrole macrocycles by the Love[3-6] and Sessler groups[7] are not without their problems. For example, the formation of highly stable μ-oxo or μ-hydroxy species can result in the removal of the catalytically-active species from any catalytic cycle.[1, 4, 6] To overcome this issue with the pacman diporphyrins, Nocera and co-workers replaced one of the porphyrins with simple "hanging" groups, such as carboxylic acids. Though these new ligands now only complex one metal centre, there was a gain in secondary coordination sphere control through this hanging group. With carboxylic acid hanging groups, protons can be delivered to species bound within the ligand-cleft.[2, 8] Indeed, cobalt complexes of hangman porphyrins have even been shown, under certain conditions, to induce the full four-electron reduction of dioxygen to water, despite the presence of only one metal centre.[2, 8]

2.2 Ligand design and synthesis, H_2L^P and H_2L^{NMe}

2.2.1 Ligand design: H_2L^P and H_2L^{NMe}

With the successes of recently developed hangman porphyrins[2, 8, 9] it was decided to re-design the H_4L ligand and make an asymmetric version, with two distinctly different binding pockets (Scheme 1).

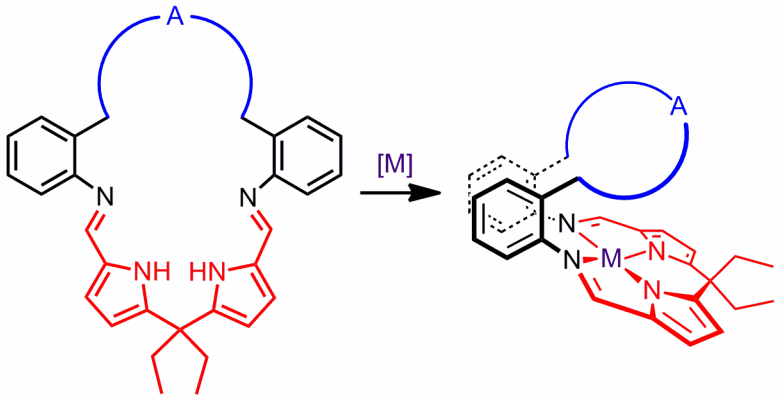

Scheme 1: Initial concept – Asymmetric macrocycle based on H_4L. A = binding pocket, M = metal

A folded-pacman geometry upon binding of a metal is expected and is crucial in order to place the free binding pocket (Scheme 1, blue) within close contact of the bound pocket (Scheme 1, red). A general synthesis of the type below was envisaged (Scheme 2). Such a synthesis would, if successful, be potentially very flexible with regards to the dichloride used, with many possible candidates such as polyglycols, thioethers, amines and amides (Scheme 2).

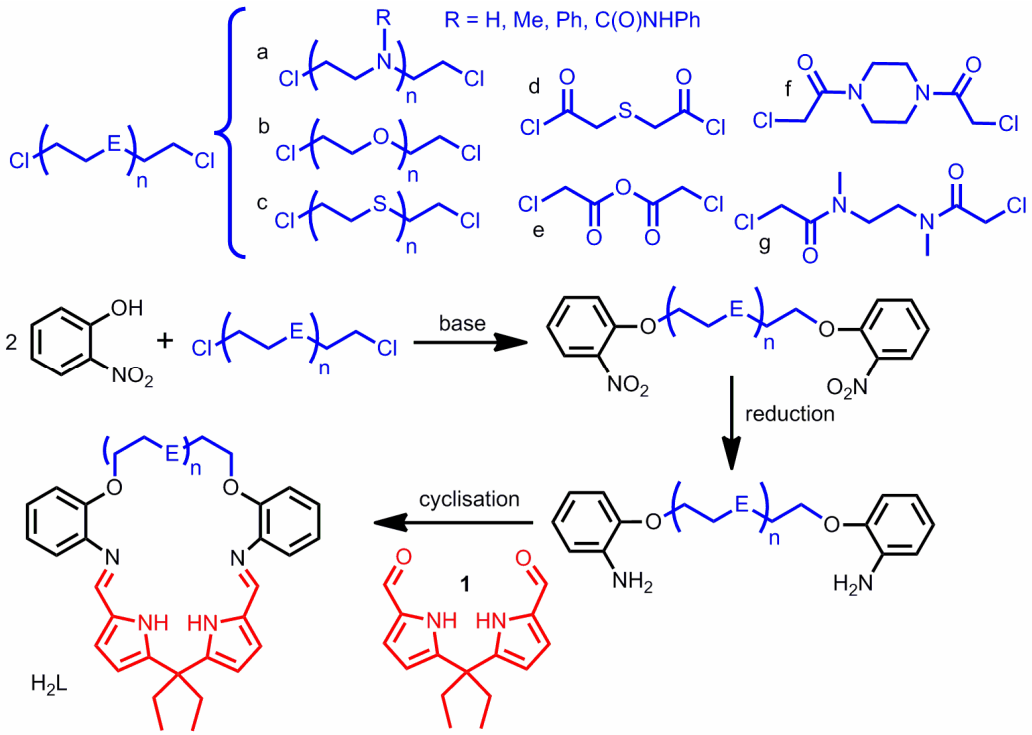

Scheme 2: Targeted synthesis towards asymmetric pacman macrocycles. a (R = H, n = 1, 2, HCl salt), b (n = 1, 2, 3) and e available from Sigma Aldrich. a (n = 1, R = Me,[10] Ph,[11] C(O)NHPh[12]), c (n = 2,[13] 3[14]), d,[15] f[16] and g[17] can be prepared from literature procedures

However, thioethers (c, Scheme 2) are mustard agents and so would require very careful handling. It was also feared that the carbonyls of compounds (Scheme 2, d-g) could cause further side reactions upon cyclisation. Side reactions could also be an issue with the use of a secondary amine (a, R = H),[18] and thus two initial targets were chosen (Scheme 3 and Scheme 4).

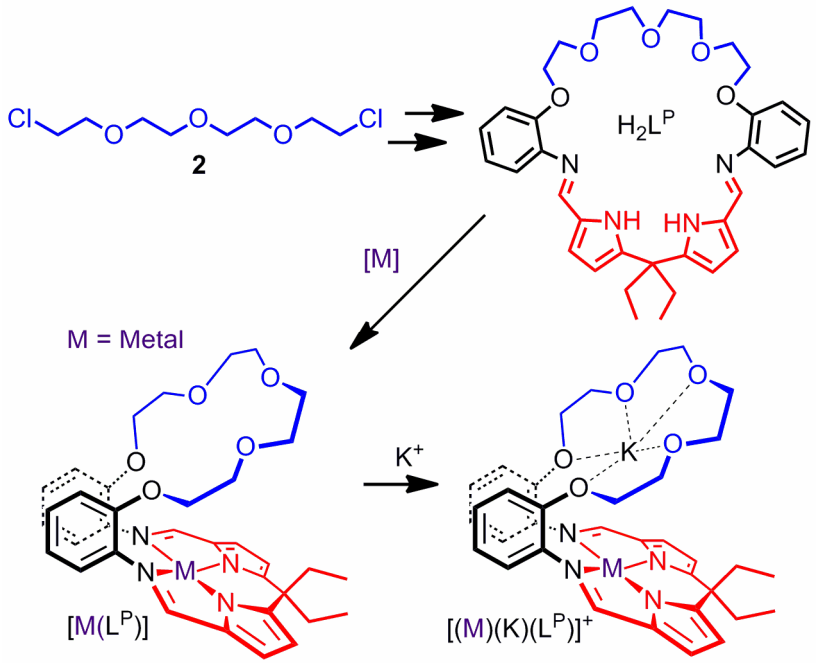

Scheme 3: Target 1 – H_2L^P synthesised from a poly-ether dichloride possesses the potential for cation binding

The polyglycol dichloride **2** is readily available from Sigma-Aldich. It was envisaged that upon folding, the poly-ether half of L^P macrocycle would be pre-organised for the binding of Group 1 metals akin to the crown-porphyrins (Scheme 3).[19] The investigations of Jux, Ivanovic-Burmazovic and co-workers involving superoxide binding to crown porphyrins showed that the addition of a Group 1 metal bound by the crown-ether drastically increased superoxide stability to the point that the complex was air stable (Figure 1).[20] Furthermore, crown ether ligands have been shown to bind protonated amines[21] as well as possessing a significant propensity for hydrogen bond acceptance by binding water (Figure 1).[19, 22, 23] Banfi and co-workers also found that the presence of an appended crown-ether on a porphyrin increased catalytic activity towards 1-dodecene epoxidation due to the crown-ether's ability for general acid/base stabilisation.[24]

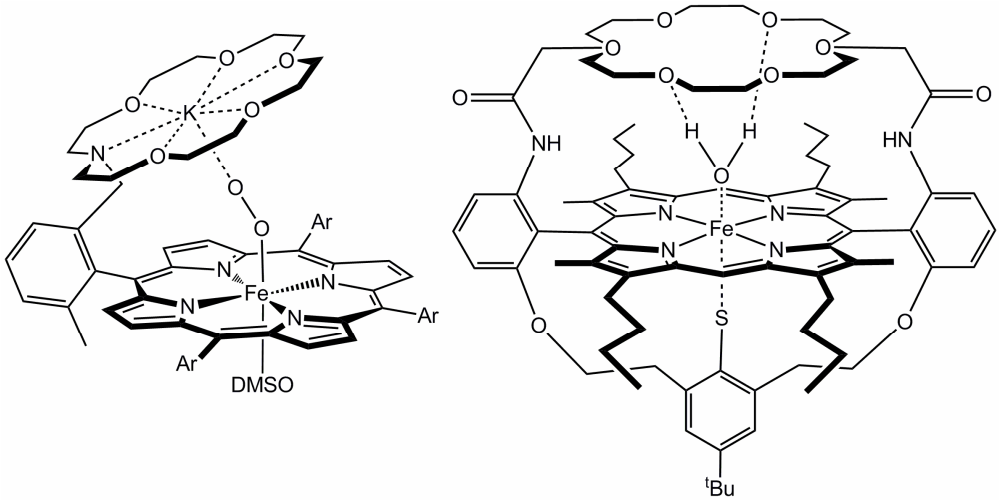

Figure 1: Potassium bound in the crown-ether of a crown porphyrin stabilises a bound superoxo in work by Jux and co-workers (Ar = *p*-^{t}Bu phenyl)[20] (left). Crown ethers can also be used to stabilise bound water, as shown by the Woggon group[22] (right)

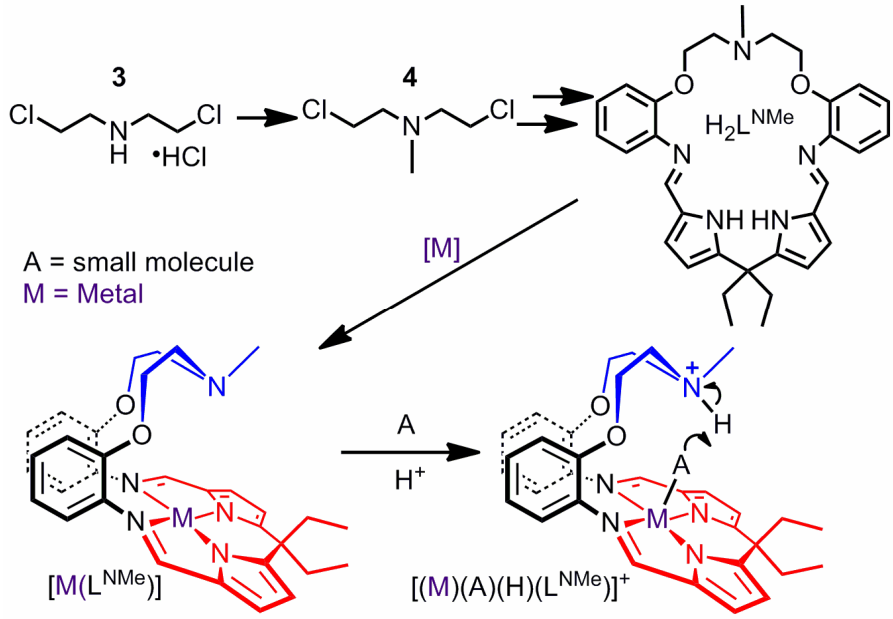

Scheme 4: Target 2 – H_2L^{NMe} synthesised from an amine dichloride. Possesses potential for proton delivery

The dichloride precursor of the second target ligand, H_2L^{NMe}, (Scheme 4) is known as the HCl salt of the secondary amine-dichloride **3**,[10] available cheaply from Sigma-Aldrich. The amine group of H_2L^{NMe} would be potentially protonatable, possibly leading to a proton channel, an important feature seen in biological systems such as in cytochrome P450,[25] a monooxygenase which reduces dioxygen to an alcohol and a

water molecule or in cytochrome c oxidase,[26] which catalyses the four electron reduction of dioxygen to water.

Furthermore, the apical amine gives the possibility of a charged second pocket as well as flexibility with regards to the introduction of an R-substituent of different functionalities. Once the proof of concept is obtained with R = Me, a variety of R groups capable of secondary coordination sphere control such as urea groups, secondary amines, or large blocking groups such as a 2,4,6-trimethylphenyl (mesityl) group could be employed. Different R-substituents could potentially be introduced either at the dichloride or dinitro stage or, should an R = H macrocycle be successfully synthesised, be incorporated at a later stage.

2.2.2 Ligand synthesis: H_2L^P and H_2L^{NMe}

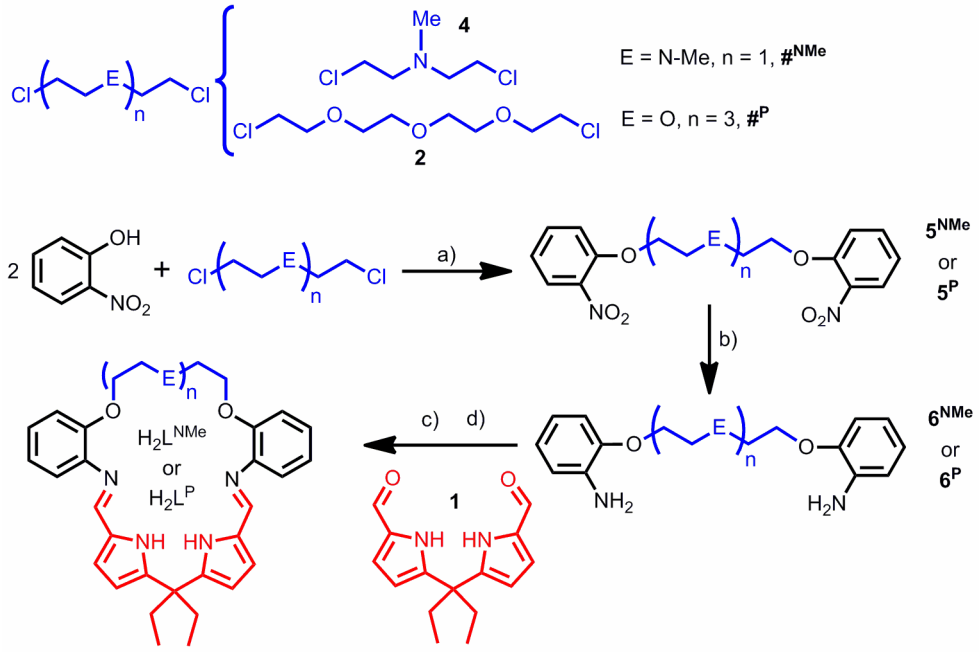

Scheme 5: Synthesis of H_2L^P and H_2L^{NMe}. a) K_2CO_3, DMF, 120 °C b) H_2, 10% Pd/C cat c) EtOH, 2.1 $BF_3{\cdot}OEt_2$ d) CH_2Cl_2, 7 M NH_3 (MeOH)

Reaction of 2-nitrophenol with either dichloride **2** or **4** in the presence of excess potassium carbonate in DMF at 120 °C gives the dinitro compounds $\mathbf{5^P}$ or $\mathbf{5^{NMe}}$ respectively. The reduction of these compounds, using a catalytic amount of 10 % Pd/C under an atmosphere of H_2, resulted in the formation of the corresponding amines $\mathbf{6^P}$ and $\mathbf{6^{NMe}}$ in moderate overall yield after workup (*ca.* 45 %, Scheme 5). The ^{1}H NMR spectra of the diamines shows the appearance of a resonance corresponding to NH_2 group at *ca.*

3.9 ppm, with the IR spectra showing the disappearance of the NO_2 absorbance at around 1610 and 1340 cm^{-1} and the appearance of the NH_2 stretch at approximately 3400 cm^{-1}. The [1+1] Schiff-base condensation reaction between the diamine and the straightforwardly-synthesised dialdehyde **1**[5] was achieved efficiently in the presence of $BF_3{\cdot}OEt_2$, giving the macrocycles H_2L^P and H_2L^{NMe} after neutralisation of the acid salt with a solution of NH_3 in MeOH. In contrast to the previously synthesised symmetrical ligands H_4L,[3, 27, 28] cyclisation reactions attempted using Brønsted acid catalysts such as CF_3COOH or *p*-$HOSO_2C_6H_4Me$ resulted in unidentifiable mixtures by ^1H NMR spectroscopy.

The formation of the macrocycle is supported by ^1H NMR spectroscopy (Figure 2) with a resonance at 8.03 (H_2L^{NMe}) or 8.29 ppm (H_2L^P) attributed to the imine N=C(H) proton. A further resonance at 8.69 (H_2L^{NMe}) and 9.13 ppm (H_2L^P) corresponds to the pyrrolic NH with aromatic C-H resonances at 7.00, 6.88, 6.67 and 6.82 ppm (H_2L^{NMe}) and 7.11, 7.50, 6.97 and 6.91 ppm (H_2L^P) and doublets at 6.51 and 6.19 ppm (H_2L^{NMe}) and 6.64 and 6.23 ppm (H_2L^P) indicative of the pyrrolic C-H; these assignments were supported by 2D NMR spectroscopy. A single quartet and triplet seen at 1.99 and 0.69 ppm (H_2L^{NMe}) and 2.12 and 0.80 ppm (H_2L^P) for the *meso*-ethyl groups infer flexibility in solution, which is corroborated by the ether/amine backbones protons, 4.00 and 2.86 ppm (H_2L^{NMe}) and 4.14, 3.83, 3.66 and 3.48 ppm (H_2L^P). A singlet resonance at 2.37 ppm is attributed to the N-CH_3 protons of the H_2L^{NMe} macrocycle.

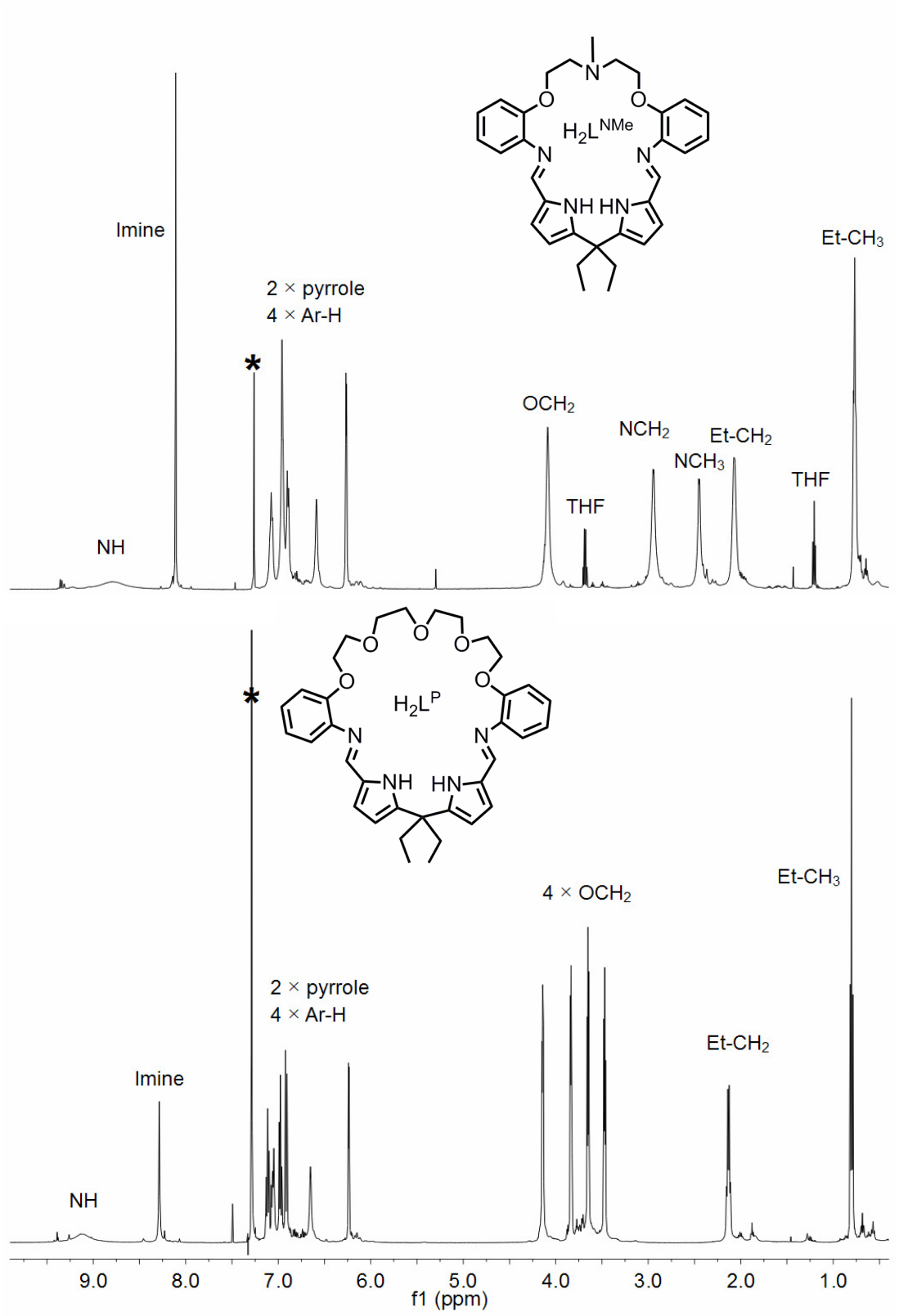

Figure 2: ^{1}H NMR spectra ($CDCl_3$) of H_2L^P (bottom) and H_2L^{NMe} (top). '*' denotes residual protio solvent

Unfortunately, efforts to further purify both macrocycles proved unsuccessful and the ^{1}H NMR spectra of both showed small broad resonances that appear closely related to the major product. Attempts at purification by column chromatography (silica or alumina) resulted in decomposition of the macrocycle. The successful syntheses of H_2L^{NMe} and H_2L^{P} were also confirmed by microanalysis and by IR spectroscopy, with absorptions at *ca.* 3200 (NH) and 1620 cm^{-1} (imine C=N). EI mass spectrometry also supports a [1+1] product, showing the molecular ion at 523 (H_2L^{NMe}) and 598 amu (H_2L^{P}). However, low intensity, high-mass peaks at 1046 and 1019 (H_2L^{NMe}) and 1198 and 1169 (H_2L^{P}) amu indicate the presence of a small amount of [2+2] product which accounts for the small, broad resonances in the ^{1}H NMR spectra. Further evidence for this [2+2] product will be discussed in Section 2.3.6. Unlike the symmetrical macrocycles H_4L, H_2L^{P} and H_2L^{NMe} are mildly water sensitive with ^{1}H NMR spectra showing the appearance of an aldehyde resonance at *ca.* 9.2 ppm when a sample was left exposed to air.

2.3 Complexes of (L^{P}) and (L^{NMe})

2.3.1 Synthesis of [Pd(L^{P})] and [Pd(L^{NMe})]

Palladium(II), with its d^8 electronic configuration prefers a diamagnetic square planar geometry, making it an ideal candidate to probe whether the new asymmetric ligands adopt a pacman geometry upon metal binding.

$$H_2L^{P/NMe} + Pd(OAc)_2 \xrightarrow[Toluene]{2\ NEt_3} [Pd(L^{P/NMe})]$$

Equation 1

A mixture of either ligand, H_2L^{NMe} or H_2L^{P}, with palladium acetate in toluene in the presence of NEt_3 leads to the isolation of the corresponding palladium complex as a yellow solid after workup in good yield (Equation 1).

The ^{1}H NMR spectra of [Pd(L^{NMe})] (Figure 3) shows the disappearance of the NH resonance at 8.69 ppm as well as the shifting of the imine resonance from 8.03 to 7.52 ppm, a characteristic also seen in the bimetallic complexes [Pd_2(L)].[3, 5, 28]

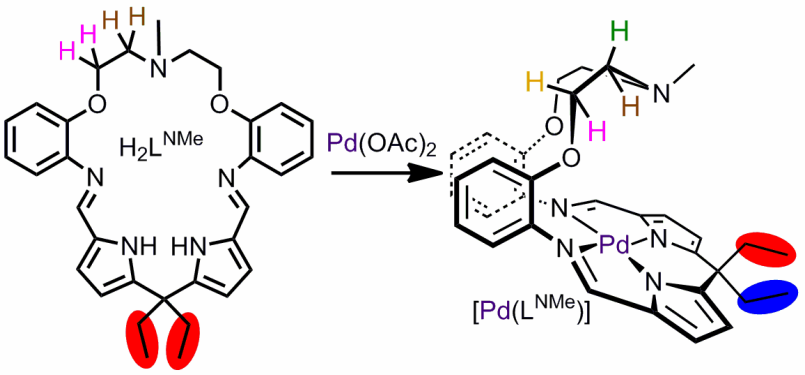

Scheme 6: Desymmetrication of the meso-ethyl groups and ether/amine protons of L^{NMe} upon folding to a rigid pacman geometry

As mentioned previously, a folded-pacman geometry of any complex formed is crucial for potential catalytic activity. A rigid pacman geometry in solution can be inferred from ^{1}H and $^{13}C\{^{1}H\}$ spectroscopy. The flexibility of the macrocycle H_2L^{NMe} causes resonances for the *meso*-ethyl groups (Scheme 6, left, red) to be equivalent, with the protons of the ether/amine CH_2 groups (Scheme 6, left, pink/brown) also equivalent. In a rigid pacman conformation, desymmetrisation of both the *meso*-ethyl groups and the protons of the ether/amine CH_2 backbone would be observed (Scheme 6, right). Thus analysis of the low frequency region of the ^{1}H NMR spectrum allows the solution-state structure to be determined (Figure 4). Two quartets at 2.16 and 2.07 ppm and two triplets at 0.56 and 0.53 ppm correspond to two *meso*-ethyl groups in different environments. The amine/ether backbone displays four separate resonances at 4.06, 3.60, 3.02 and 2.85 ppm, each integrated to two protons. Furthermore, the $^{13}C\{^{1}H\}$ NMR spectrum also displays resonances for two distinctive ethyl groups (CH_3 at 10.0 and 9.7 ppm, CH_2 at 46.5 and 37.0 ppm) with only two resonances corresponding to the amine/ether backbone carbons at 68.0 and 55.2 ppm observed. Therefore, a desymmetrisation of both the ethyl groups and the amine/ether protons supports a pacman conformation in solution for $[Pd(L^{NMe})]$.

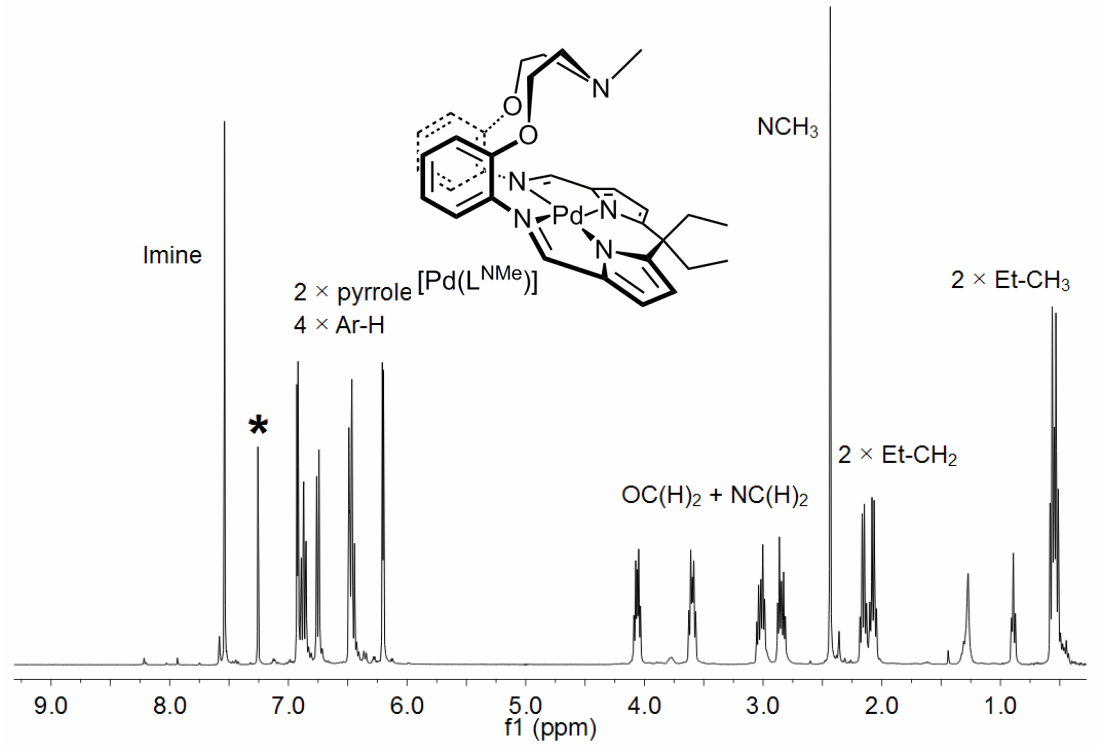

Figure 3: ^{1}H NMR spectra ($CDCl_3$) of [Pd(L^{NMe})]. '*' denotes residual protio solvent

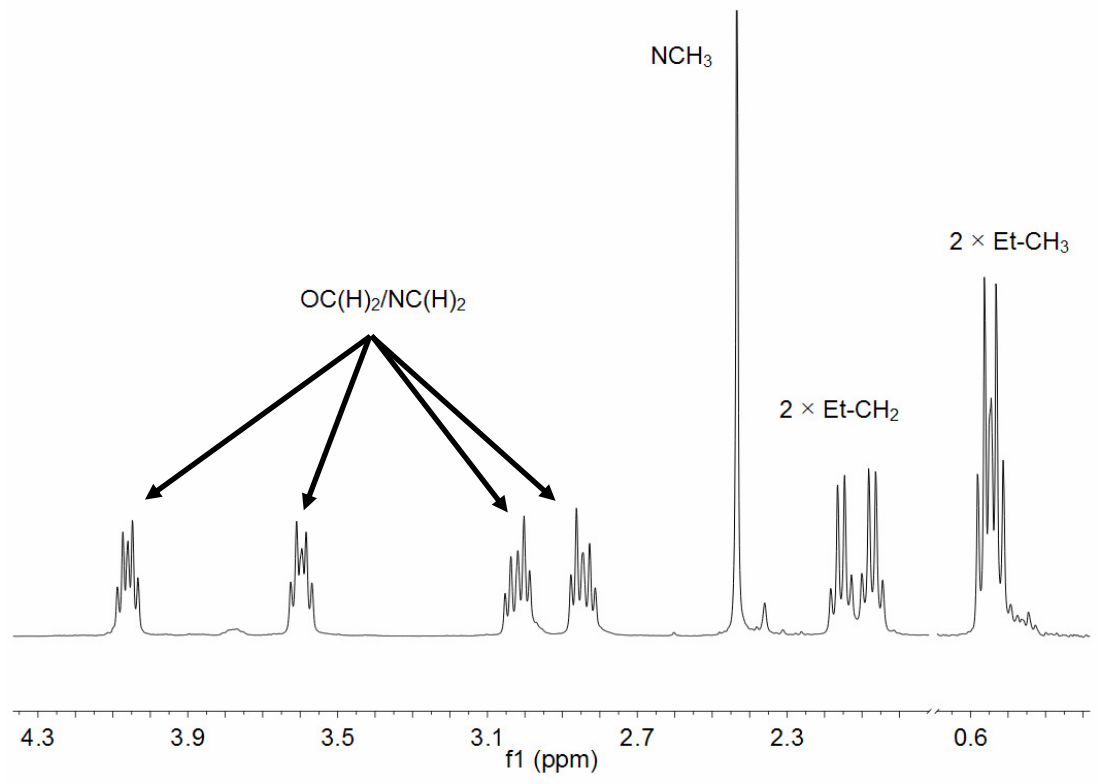

Figure 4: ^{1}H NMR spectra ($CDCl_3$) of [Pd(L^{NMe})] showing selected low-frequency regions to show the desymmetrisation of the meso-ethyl and ether/amine CH_2 protons

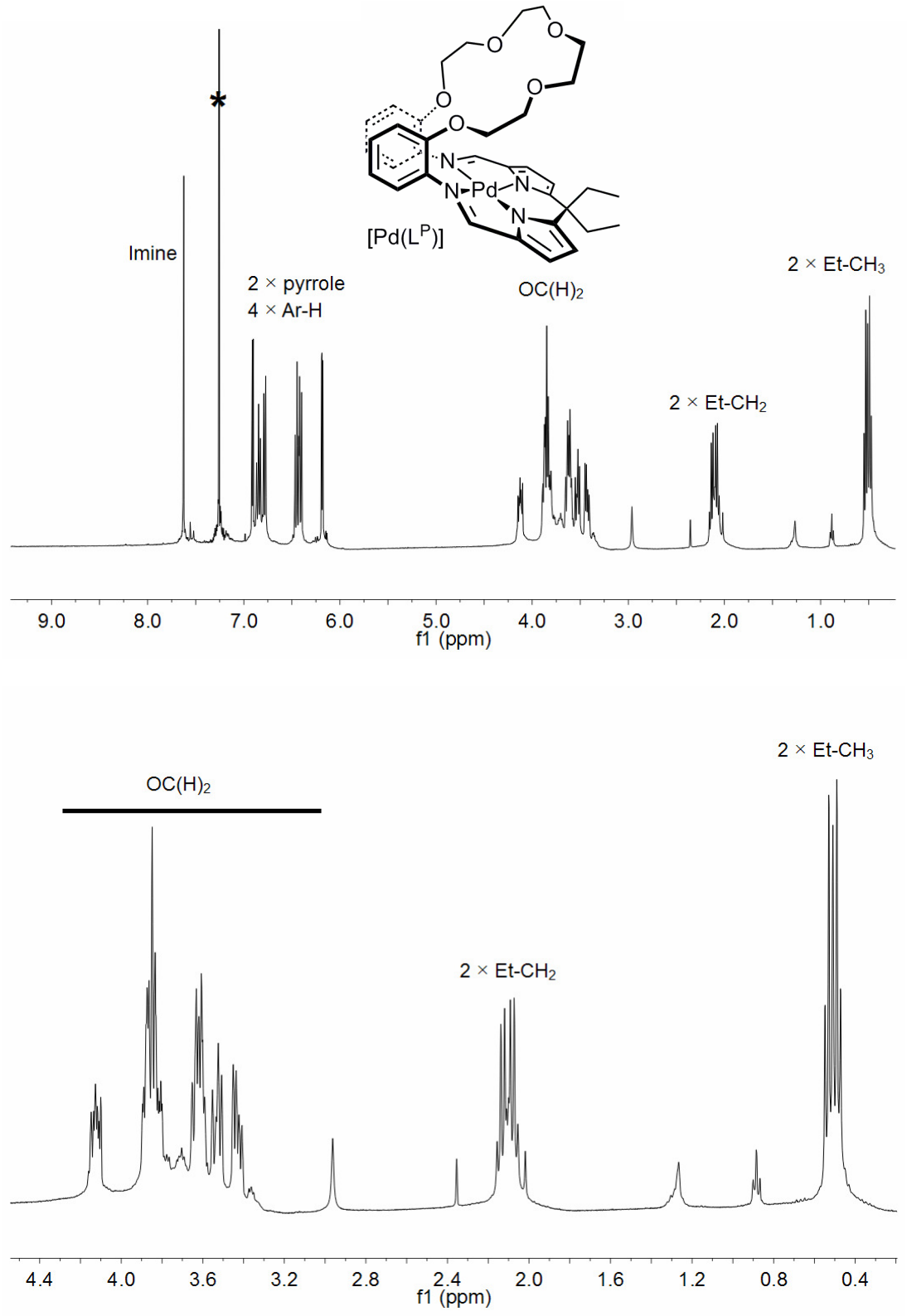

Figure 5: ^{1}H NMR spectra ($CDCl_3$) of [Pd(L^P)] (top) and [Pd(L^P)] showing selected low-frequency regions to show the desymmetrisation of the meso-ethyl and ether/amine CH_2 protons (bottom). '*' denotes residual protio solvent

The ^{1}H NMR spectrum of [Pd(L^{P})] (Figure 5) displays similar properties; a disappearance of the NH resonance at 9.13 ppm and a shifting of the imine resonance from 8.29 to 7.55 ppm. Two ethyl environments are observed (CH_2 at 2.05 and 2.01 ppm, CH_3 at 0.45 and 0.42 ppm) as well as desymmetrisation of the ether backbone protons (multiplet at 4.15 and overlapping multiplet resonances 3.9 – 3.3 ppm). Again analysis of the ^{13}C{^{1}H} NMR spectrum shows two ethyl environments (CH_2: 38.3 and 37.6 ppm, CH_3: 9.9 ppm – only one resonance was observed, but overlap was confirmed by analysis of the ^{1}H-^{13}C HSQC spectrum) but only four ether backbone carbons at 71.0, 70.5, 69.6 and 68.2 ppm. Thus metallation of both ligands with palladium result in pacman conformations in solution, with L^{NMe} forming an O-N-O binding pocket and L^{P} a pseudo 15-crown-5 pocket (Figure 6).

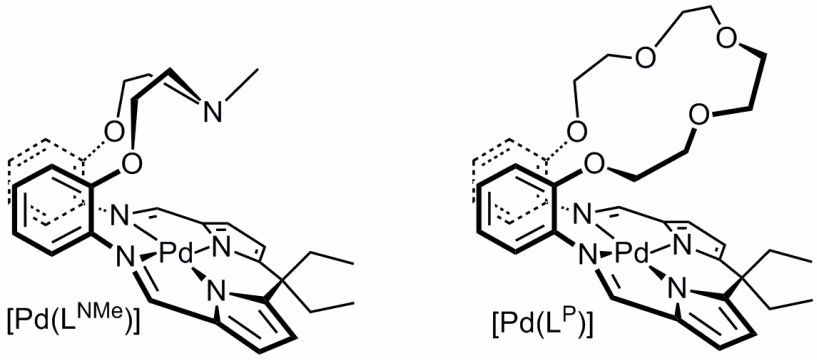

Figure 6: Pacman-shaped complexes [Pd(L^{NMe})] (left) and [Pd(L^{P})] (right)

The IR spectra of both complexes also show the loss of an NH stretch at *ca.* 3200 cm^{-1} and a shift in the imine absorption from 1620 to 1560 cm^{-1}, again as observed for the H_4L set of ligands upon metallation.[3, 5, 28] The EI mass spectra also show the molecular ions at 627 and 702 amu for [Pd(L^{NMe})] and [Pd(L^{P})] respectively, and microanalysis also supports the expected formulations. Once synthesised, unlike the free macrocycles, the palladium complex of either ligand is stable to both water and air, with the ^{1}H NMR spectra unchanged after weeks exposed to air.

Crystals of [Pd(L^{NMe})] suitable for X-ray diffraction analysis were grown from hexane solution whilst in Japan† (Figure 7, Table 1). The asymmetric unit contains two [Pd(L^{NMe})] molecules in slightly different conformations. Due to the similarity of the environment around the palladium, only one of the structures will be discussed.

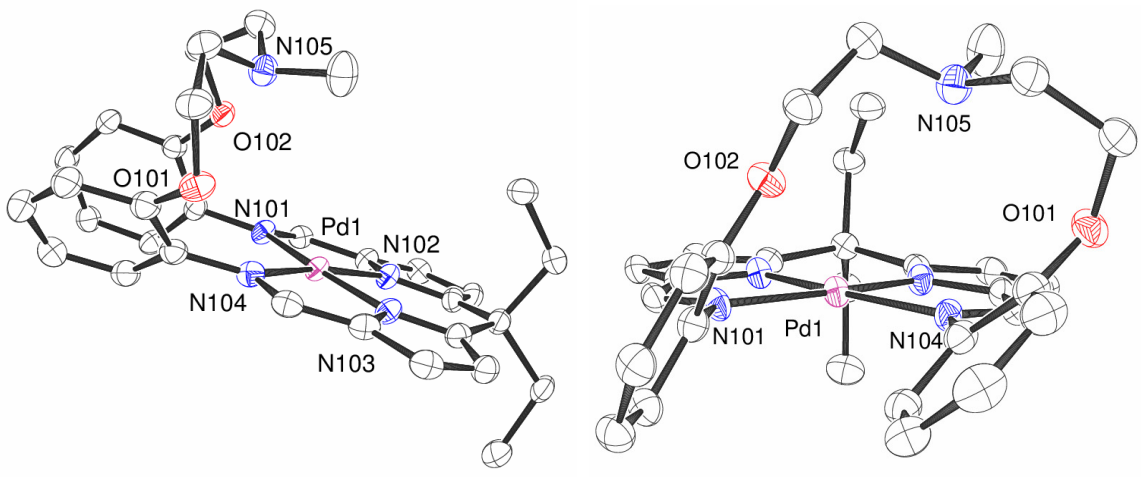

Figure 7: X-ray crystal structure of [Pd(L^{NMe})]. For clarity, all hydrogen atoms are omitted and displacement ellipsoids are drawn at 50% probability

Table 1: Selected bond lengths (Å) and angles (°) of [Pd(L^{NMe})]

Pd1-N101	2.096(2)	N101-Pd1-N102	79.96(9)
Pd1-N102	1.945(2)	N102-Pd1-N103	86.98(9)
Pd1-N103	1.943(2)	N103-Pd1-N104	80.07(9)
Pd1-N104	2.093(2)	Σ ∠ Pd1	359.92
Pd1···N_4	0.037	Twist Φ	23.41/45.40
N101-Pd1-N104	112.91(9)	Dihedral α	23.23

The complex is unambiguously a folded-pacman conformation in the solid state, and correlates well to the solution structure. The geometry at the palladium is very similar to that seen in the symmetric ligand palladium complexes [Pd_2(L)]. Palladium-imine (2.093(2)–2.096(2) Å) and palladium-pyrrole bond lengths (1.945(2)–1.943(2) Å) are comparable to [Pd_2(L)] complexes (Pd-N_{im} 2.043(7)–2.096(2) Å, Pd-N_{py} 1.928(4)–1.947(4) Å).[3, 5, 28] Bond angles are also comparable with N_{im}-Pd-N_{im} (112.91(9) °) and N_{im}-Pd-N_{py} (79.96(9)–80.07(9) °) similar to those of [Pd_2(L)] N_{im}-Pd-N_{im} (109.9(4)–119.7(5) °), N_{im}-Pd-N_{py} (79.7(3)–81.4(4) °)[3, 5, 28]. The N_{py}-Pd-N_{py} angle of (86.98(9) °) is marginally more acute than in the [Pd_2L] complexes N_{py}-Pd-N_{py} (88.01(17)–88.8(3) °), though similar that of other bimetallic complexes of L (N_{py}-M-N_{py} (84.80(13)–88.8(3) °).[28]

The conformation of the two [Pd(L^{NMe})] molecules in the asymmetric unit differ due to the orientation of the N-Me group, with one orientated towards, and the other away from, the palladium centre (Figure 8, Table 2).

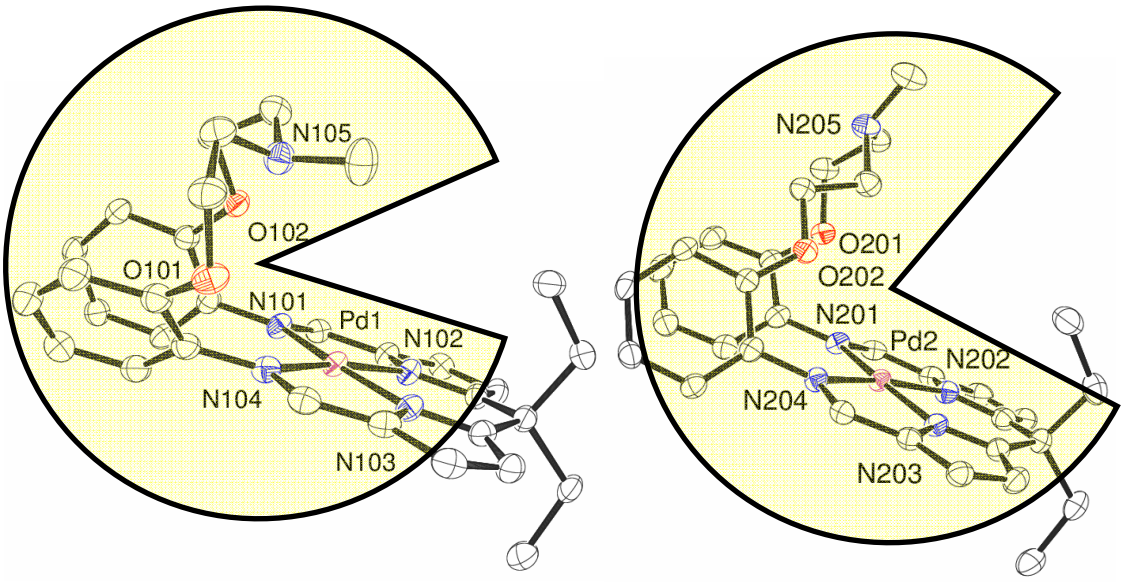

Figure 8: X-ray crystal structure of [Pd(L^{NMe})] showing the two crystallographically independent [Pd(L^{NMe})] complexes in the asymmetric unit. Complexes considered as "open-mouth" and a "closed mouth" pacman. For clarity, all hydrogen atoms are omitted and displacement ellipsoids are drawn at 50% probability

Table 2: Selected bond lengths (Å) and angles (°) of [Pd(L^{NMe})] showing difference between the two [Pd(L^{NMe})] complexes in the asymmetric unit

	Pd1	Pd2
Pd···N105/205	4.356	5.449
O101/201···Pd	4.660	3.245
O102/202···Pd	3.456	4.577
Twist Φ	23.41/45.40	28.97/46.75
Dihedral α	23.23	18.25

The flipping and twisting of the ether/amine backbone causes the nitrogen of this backbone to move by almost 1.1 Å, a feature which could be important should groups other than a methyl be employed for proton delivery. These two structures could be considered as an "open mouth" and a "closed mouth" pacman (Figure 8). Furthermore, the increased flexibility of the ether/amine backbone compared to the more rigid

symmetric version allows the aryl hinges to twist to a much greater angle (23.41–46.75 °) compared to reported structures of the type $[M_2(L)]$ (0.3–32.2 °)[7, 28]

2.3.2 Synthesis of $[K_2(L^P)]$ and $[K_2(L^{NMe})]$

Although the syntheses of $[Pd(L^P)]$ and $[Pd(L^{NMe})]$ from $Pd(OAc)_2$ were successful, an alternative route that would favour the formation of a greater variety of metal complexes of L^P and L^{NMe} was sought. Previously, the *in-situ* formation of $[K_4(L)]$ has facilitated the synthesis of $[Co_2(L)]$, $[Pd_2(L)]$,[5] $[Ni_2(L)]$,[28] $[(VCl)_2(L)]$ and $[(TiCl)_2(L)]$ through salt elimination methods.[29] Thus it was envisaged a similar route could be used with (L^P) and (L^{NMe}).

$$H_2L^{P/NMe} + 3\,KH \xrightarrow[THF]{} [K_2(L^{P/NMe})] + H_2$$

Equation 2

Addition of dry THF to a mixture of $H_2L^{P/NMe}$ and excess potassium hydride resulted in immediate effervescence of hydrogen. After stirring for four hours a colour change from yellow to red was observed and effervescence had ceased, giving $[K_2(L^{P/NMe})]$ in quantitative yield (Equation 2). The ^1H NMR spectra (double solvent suppression H_8-THF/C_6D_6 capillary) of both complexes showed the disappearance of the NH resonance at around 9.5 ppm and a single imine resonance at *ca.* 8.3 ppm. The low frequency region of the spectra shows only one *meso*-ethyl environment (Et-CH_3, 1.06 (L^P), 1.10 ppm (L^{NMe})) with resonances for the *meso*-ethyl-CH_2 and ether/amine backbone lost beneath the suppressed THF resonances. The $^{13}C\{^1H\}$ NMR spectra also indicate one ethyl environment with Et-CH_2 and Et-CH_3 resonances at 30.98 and 9.65 ppm (L^{NMe}) and 29.05 and 9.14 ppm (L^P) indicating that the geometries of $[K_2(L^{NMe})]$ and $[K_2(L^P)]$ are fluxional in solution. This contrasts to the potassium salt of a symmetric version of the ligand in which two environments for *endo*- and *exo-meso* substituents were observed.[29] The successful syntheses of $[K_2(L^{P/NMe})]$ is also confirmed by microanalytical data and by EI mass spectroscopy, the latter showing parent peaks at 599 ($[K_2(L^{NMe})]$) and 674 amu ($[K_2(L^P)]$). Furthermore, the IR spectra show the disappearance of the NH stretch at *ca.* 3200 cm^{-1} and a shift in the imine absorbance from *ca.* 1620 to 1560 cm^{-1}. Crystals of $[K_2(L^P)]$ suitable for single crystal X-ray diffraction were grown by slow diffusion of hexane into a H_8-THF/C_6D_6 solution of $[K_2(L^P)]$ (Table 3, Figure 9).

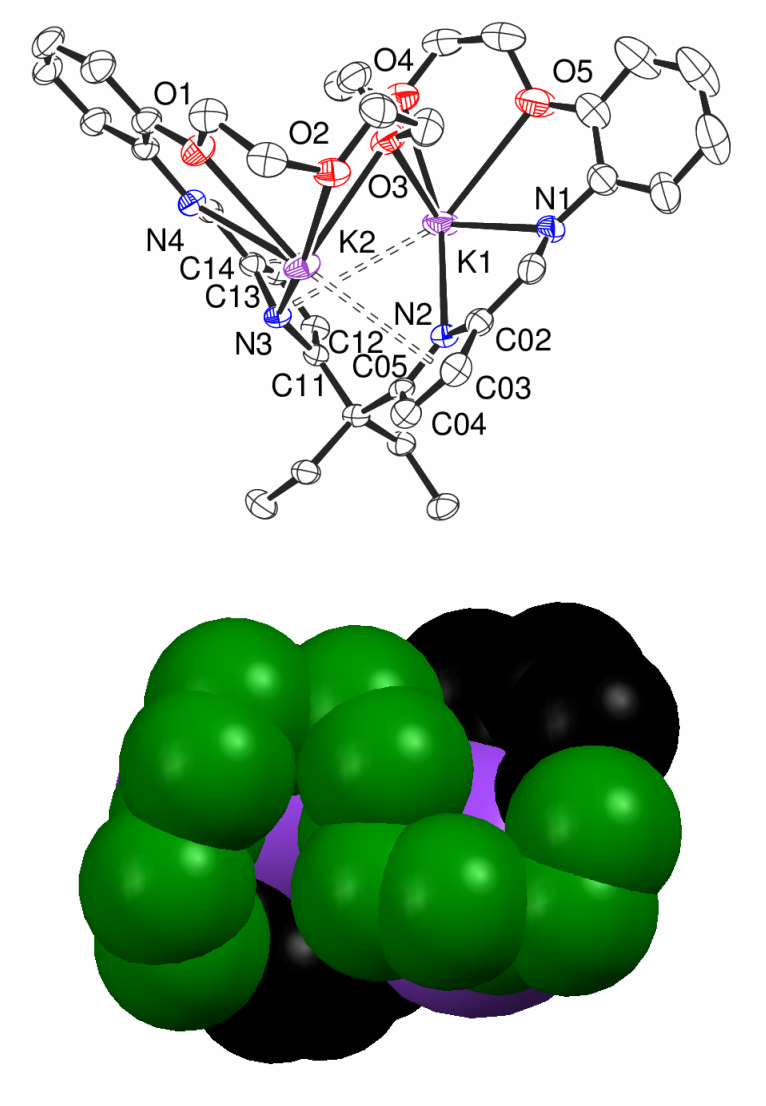

Figure 9: X-ray crystal structure of $[K_2(L^P)]$ (top), for clarity, all hydrogen atoms are omitted and displacement ellipsoids are drawn at 50% probability. Space-filling model of $[K_2(L^P)]$ showing only the macrocyclic backbone illustrating helicate-type structure (bottom).

Table 3: Selected bond lengths (Å) and angles (°) of [$K_2(L^P)$]

K1-N1	2.830(3)	K1-O5	3.134(3)
K1-N2	2.683(2)	K1···K2	4.434
K2-N3	2.715(2)	N3-K2-N4	62.20(7)
K2-N4	2.871(2)	N4-K2-O1	53.45(6)
K2-O1	3.017(2)	O1-K2-O2	56.86(6)
K2-O2	2.750(2)	O2-K2-O3	59.76(7)
K2-O3	2.908(2)	O3-K1-O4	52.56
K1-O3	3.540	O4-K1-O5	55.60(7)
K1-O4	2.625(2)	O5-K1-N1	52.82(7)
η^5 K2···C02-C05/N2 centroid	3.276	N1-K1-N2	63.48(7)
η^5 K1···C11-C14/N3 centroid	3.460	O1-K2-(C02-C05/N2 centroid)	167.75
η^6 K1···(C16'-C21'centroid)	3.386	O5-K1-(C11-C14/N3 centroid)	152.75
η^6 K2··· (C16'-C21'centroid)	3.590		

The solid state structure was found to be a twisted helicate-type structure with two benzene solvent molecules of crystallisation. Helicate structures will also be discussed in Section 2.3.6. Further inspection of the structure reveals interactions between each potassium and the π-system of the arene-backbone units of adjacent molecules (C16–C21), so adopting an inter-molecular η^6-bonding mode (Figure 10).

Each potassium atom is seven-coordinate, each bound in a κ^1 binding mode to one pyrrolic and one imine nitrogen, three ether oxygens (one bridging between two potassium atoms), in a η^5-fashion to a pyrrolic π-system and in a η^6-mode to the arene-backbone π-system; however, some of these interactions are very weak.

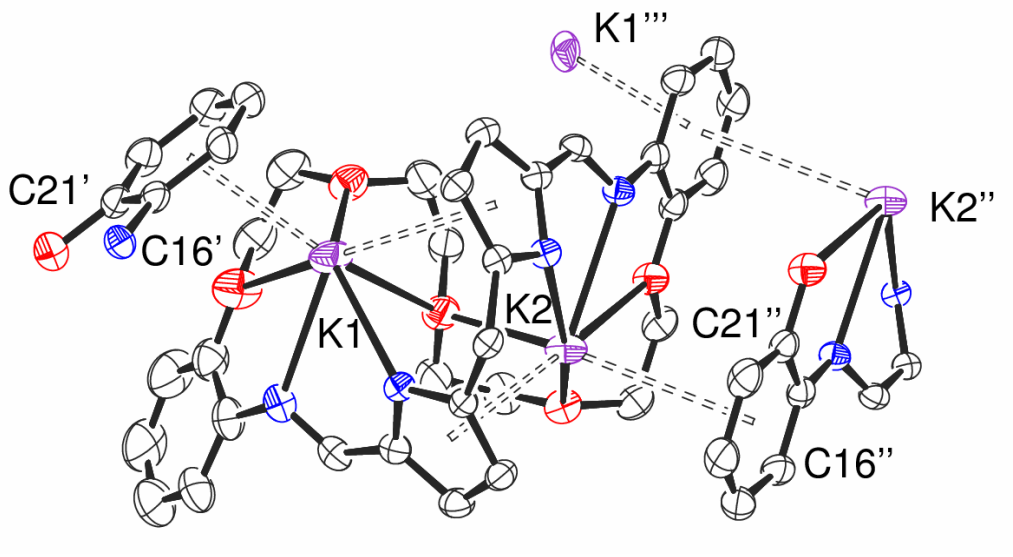

Figure 10: X-ray crystal structure of [$K_2(L^P)$] showing intermolecular interactions with the π-system of adjacent macrocycles. For clarity, all hydrogen atoms and *meso*-ethyl groups are omitted and displacement ellipsoids are drawn at 50% probability

The K-N_{py} distances of 2.683(2)–2.715(2) Å are shorter than those of the symmetric ligand K_4L (2.811(2)–2.915(3) Å)[29] and the one reported porphyrin structure (2.740(7)–2.794(6) Å).[30] These distances are more comparable to those seen in imine-pyrrole chelates (Figure 11, left) previously reported by the Love group (2.676(3)–2.976(3) Å),[31] and can be attributed to the increased flexibility of the (L^P) ligand compared to the pacman macrocycles L. The K-η^5 centroid distances of 3.276 (K2) and 3.460 (K1) Å are, however, very long. In both [K_4(L)] and in the imine-pyrrole chelate **7** (Figure 11, left and bottom right), the K-η^5-centroid distances of 2.962 and 2.903 Å, respectively, are appreciably shorter. The longest reported K-η^5-pyrrole distance is 3.309 Å for a niobium complex of a tripodal ligand, reported by the Gambarotta group, (Figure 11, top right)[32] is also shorter than in [$K_2(L^P)$], though a space-filling model of [$K_2(L^P)$] does imply a weak interaction between the pyrrole and K1.

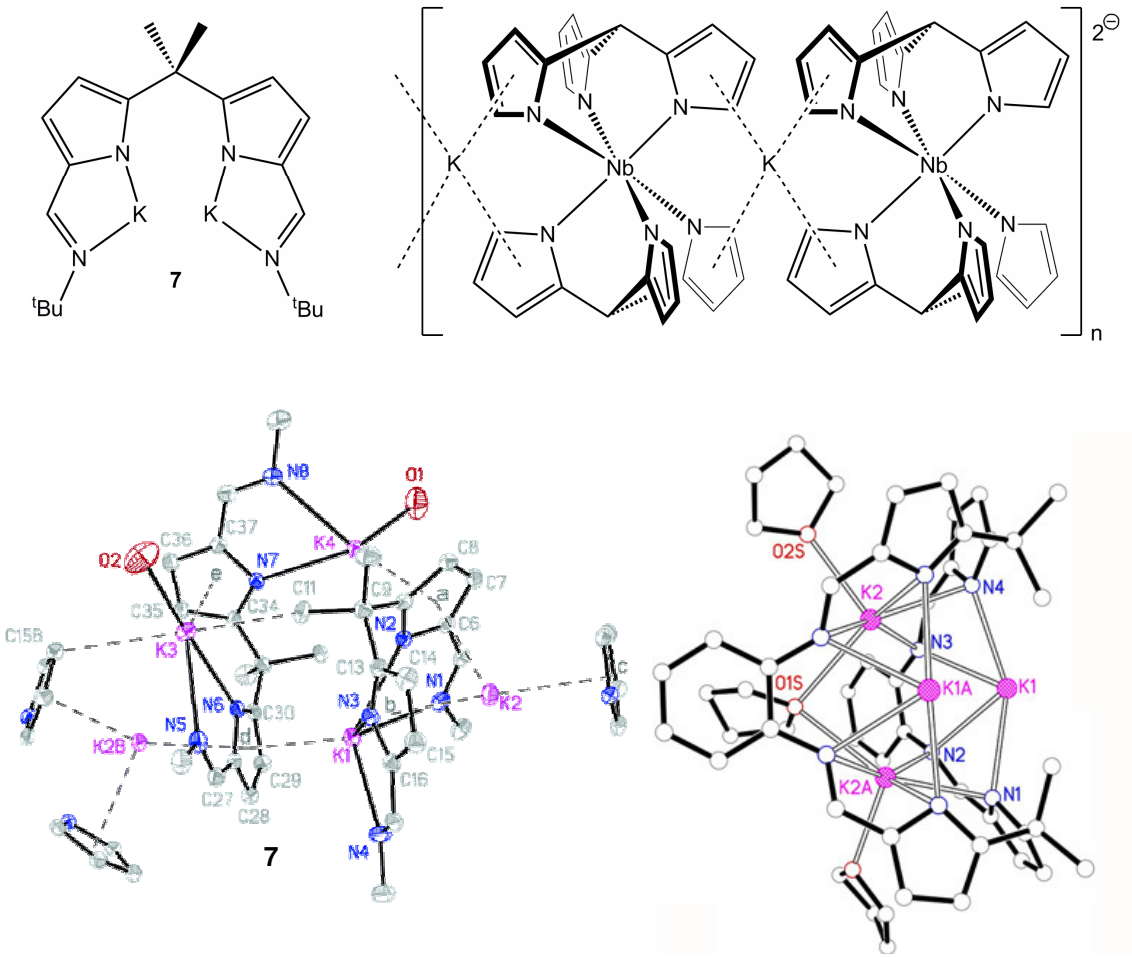

Figure 11: The Imine-pyrrole chelate potassium complex synthesised by the Love group **7** (top left) and X-ray crystal structure of this[31] (bottom left). A niobium complex of a pyrrolic tripodal ligand synthesised by Gambarotta and co-workers[32] (top right), X-ray crystal structure of symmetric ligand [K_4L] reported by the Love group[29] (bottom right)

K-N_{im} bond lengths of 2.820(3) and 2.871(2) Å are comparable to the imine-pyrrole chelate **7** and [K_4(L)] at 2.787(3)–2.966(3) Å[31] and 2.834(2)–2.840(3) Å,[29] respectively. The majority of K-O distances (2.750(2)–3.134(3) Å) are of a standard length though μ_2-O3 is only weakly bonding to K1 (3.540 Å) compared to K2 (2.908(2) Å), which is compensated by the relatively short K1-O4 distance of 2.625(2) Å.[33] Intermolecular interactions between potassium and the arene-backbones (K-centroid-C16'-C21', 3.386 and 3.590 Å) are also weak, with reported K-η^6-arene-centroid distance ranging from around 2.752 to 3.406 Å;[34] again, a space-filling model of [$K_2(L^P)$] does infer only a weak interaction.

Attempted bulk isolation of the potassium salts [$K_2(L^P)$] and [$K_2(L^{NMe})$] by either precipitation with hexane or by removal of the THF solvent under vacuum proved

problematic, with some decomposition to the free ligand $H_2(L^{P/NMe})$ observed in the ^1H NMR spectrum, as seen with $[K_4(L)]$. Therefore, $[K_2(L^{P/NMe})]$ was synthesised *in-situ* in any attempted metallations involving the potassium salt.

With the potassium salts $[K_2(L^{P})]$ and $[K_2(L^{NMe})]$ successfully synthesised, routes into new complexes of $(L^{P/NMe})$ were available.

2.3.3 Cobalt complexes of (L^{P}) and (L^{NMe})

As discussed in Chapter 1, various cobalt complexes have been shown to be active in oxygen reduction chemistry, notwithstanding hangman porphyrins and the symmetric ligand system $[Co_2(L)]$. Though capable of the four electron reduction of dioxygen to water, the formation of a stable μ-oxo/hydroxo species removes the complex from the catalytic cycle, causing a poor turnover number, especially the case with $[Co_2(L)]$.[6, 35] As mentioned in the introduction to this chapter, the ligands (L^{P}) and (L^{NMe}) have been designed with the view of preventing formation of this μ-O group.

$$H_2L^{P/NMe} + 3\ KH \xrightarrow[THF]{} [K_2(L^{P/NMe})] \xrightarrow[THF]{CoCl_2} [Co(L^{P/NMe})] + 2\ KCl$$

Equation 3

Reaction of $CoCl_2$ with *in-situ* generated $[K_2(L^{P/NMe})]$ leads to the formation of the cobalt complexes $[Co(L^{P})]$ and $[Co(L^{NMe})]$ in good yield (*ca.* 65 %, Equation 3) after workup as red solids. The ^1H NMR spectra of these complexes are paramagnetically shifted and broadened: $[Co(L^{P})]$ displays 19 resonances ranging from 69 to -40 ppm (Figure 13, top) and $[Co(L^{NMe})]$ 13 resonances between 72 and -43 ppm. The number and integral values of these resonances, allowing for overlap of resonances, are consistent with a solution-state pacman conformation of both complexes Furthermore, the IR spectra show the disappearance of the NH stretch at *ca.* 3200 cm^{-1} and the shifting of the imine absorbance from *ca.* 1620 to 1560 cm^{-1} and are indicative of metal binding. The EI mass spectra display parent ions at 580 ($[Co(L^{NMe})]$) and 655 amu ($[Co(L^{P})]$) and elemental analysis supports the formulation. Crystals of $[Co(L^{P})]$ and $[Co(pyr)(L^{P})]$ suitable for single crystal X-ray diffraction were grown by hexane diffusion into a THF solution and a THF/pyridine solution of $[Co(L^{P})]$ respectively (Figure 12, Table 4). The asymmetric unit cell of $[Co(L^{P})]$ contains two crystallographically-independent $[Co(L^{P})]$ complexes, and, due to their similarity, only one is discussed.

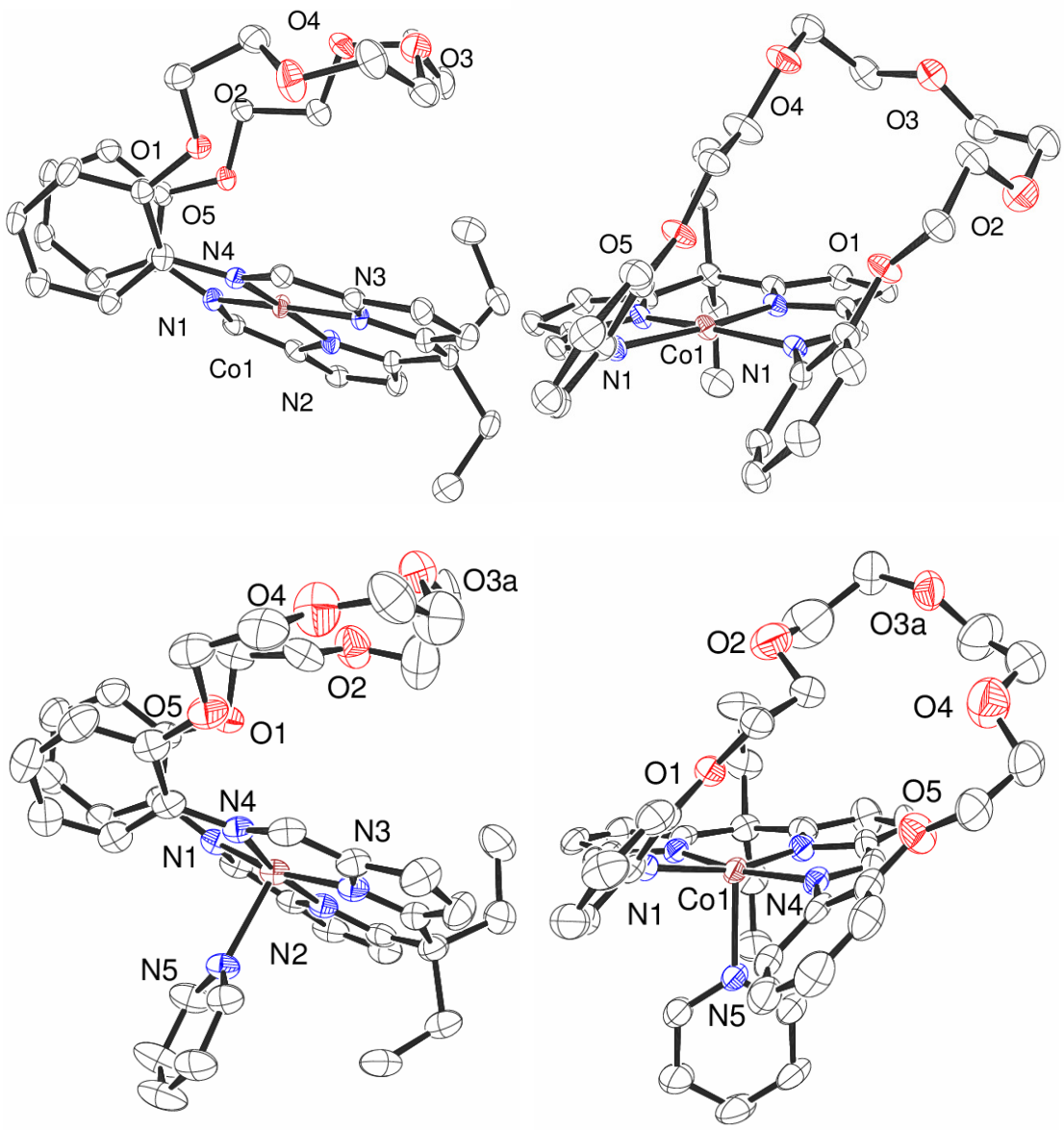

Figure 12: X-ray crystal structure of [Co(L^P)] (top) and [Co(pyr)(L^P)] (bottom). For clarity, all hydrogen atoms are omitted and displacement ellipsoids are drawn at 50% probability. Disorder in polyether backbone of [Co(pyr)(L^P)] resulted in the parting of atoms between O2 and O4, for clarity, only one conformation is shown

Both molecules clearly demonstrate wedge-shaped pacman conformations with the cobalt of [Co(L^P)] sitting in the centre of a square planer environment (Σ angles at Co 360.12 °) bound by two imine and two pyrrolic nitrogens. The addition of pyridine results in a distorted square-based pyramidal binding mode at Co with the pyridine as the axial ligand. The presence of pyridine causes the position of Co1 to shift by *ca.* 0.2 Å, from 0.042 Å below the imine-pyrrole N_4 plane (i.e. *endo*-to the cleft) to 0.169 Å *exo* to

the cleft. This is accompanied by a slight increase in the mean cobalt-imine (1.981 to 2.026 Å) and cobalt-pyrrole bond lengths (1.855 to 1.872 Å). Despite this, the Co(II)-N_{im} bond lengths of both complexes (1.981(4)–2.0335(18) Å) are similar to those of dicobalt complexes of the symmetric ligands (1.856(7)–1.984(4) Å)[4, 5, 35] though longer than Co(II)-salen complexes (1.838(3)–1.888(7)).[36]

Table 4: Selected bond lengths (Å) and angles (°) of [Co(L^P)] and [Co(pyr)(L^P)]

	[Co(L^P)]	[Co(pyr)(L^P)]
Co1-N101	1.981(4)	2.0335(18)
Co1-N102	1.852(3)	1.8818(18)
Co1-N103	1.858(3)	1.8624(19)
Co1-N401	1.981(4)	2.0187(17)
Co1-N5	-	2.1514(17)
N_4···Co1···N5	-	87.95
Co1···N_4	0.042	0.169
N1-Co1-N4	107.68(15)	107.92(8)
N1-Co1-N2	82.29(16)	81.62(8)
N2-Co1-N3	87.62(16)	86.61(8)
N3-Co1-N4	82.53(16)	82.43(8)
Σ ∠ Co1	360.12	358.58
Co1···O01	4.443	4.737
Co1···O05	2.823	3.250
Twist Φ	55.25/50.55	54.08/43.18
Dihedral α	13.92	21.50

Likewise, the Co(II)-N_{py} bond lengths (1.852(3)–1.8818(18) Å) are also comparable to the symmetric analogues (1.847–1.970(8) Å)[4, 5, 35] and analogous porphyrin complexes (1.923(2)–2.071(2) Å).[37] The cobalt-N_{pyr} distance of 2.1514(17) Å is also standard compared to salen complexes (2.135(7)–2.262(12) Å).[38] The

conformations of the ether backbone are very different between the two structures and reflect the large degree of flexibility in this section of the macrocycle.

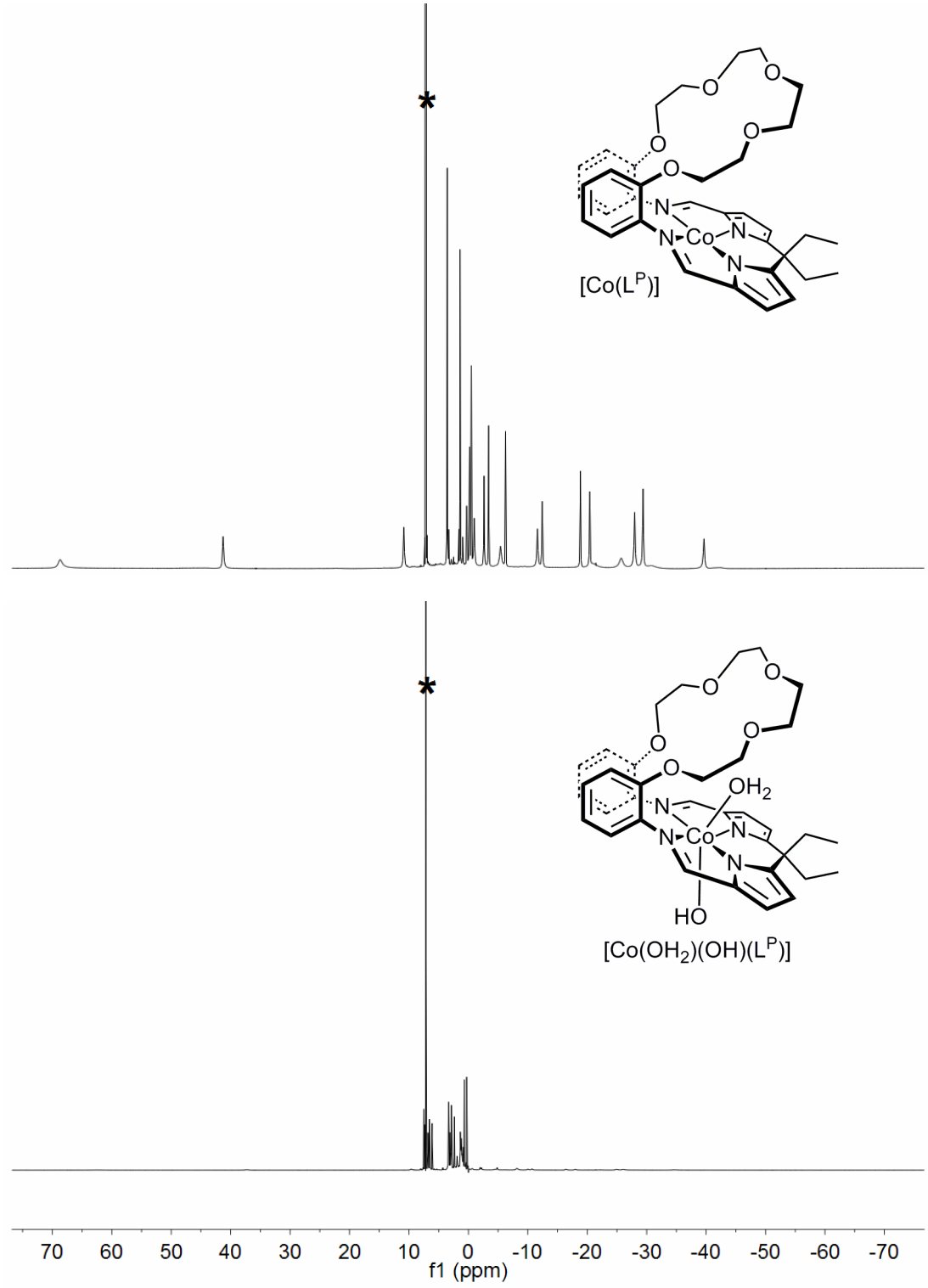

Figure 13: ^{1}H NMR spectra (C_6D_6) of [Co(L^P)] (top), [Co(L^P)] exposed to air to give [Co(OH_2)(OH)(L^P)], wide sweep width (bottom) '*' denotes residual protio solvent

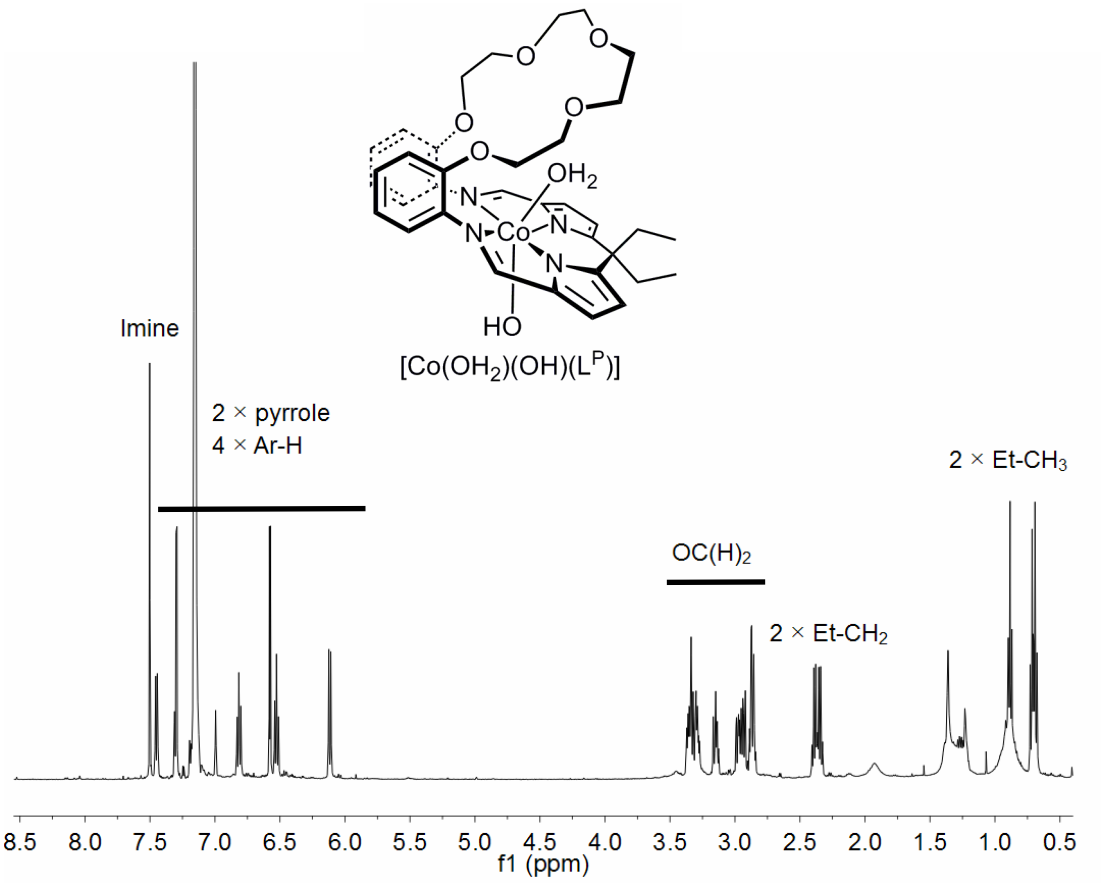

Figure 14: ^{1}H NMR spectra (C_6D_6) of [Co(OH_2)(OH)(L^P)] '*' denotes residual protio solvent

Exposure of [Co(L^P)] or [Co(L^{NMe})] to air results in spontaneous aerobic oxidation to Co(III) complexes. The ^{1}H NMR spectra of these cobalt complexes display resonances in the diamagnetic region only (Figure 13, bottom), and are consistent with the presence of low-spin octahedral Co(III) d^6. The ^{1}H NMR spectrum of [Co(OH_2)(OH)(L^P)] displays resonances indicative of a wedge-shaped conformation in solution (Figure 14). As such, desymmetrised ethyl resonances are observed at 0.71 and 0.68 ppm (CH_3) and 2.38 and 2.35 ppm (CH_2) as well as dissimilar ether-proton environments as broad multiplet resonances at 3.38–3.26 (6H), 3.17–3.11 (2H), 3.01–2.91 (4H), and 2.89–2.83 ppm (4H). The two ethyl environments are reflected in the ^{13}C{^{1}H} NMR spectrum at 10.30 and 9.98 ppm (CH_3) and 38.79 and 38.35 (CH_2) with four ether-CH_2 resonances at 70.06, 70.04, 68.66 and 67.95 ppm showing that only the ether-backbone protons are desymmetrised, as seen with the pacman complex [Pd(L^P)]. Slow diffusion of hexane into an air-saturated benzene solution of [Co(OH_2)(OH)(L^P)] gave a large amount of red-brown crystals suitable for single crystal X-ray diffraction (Figure 15, Table 5).

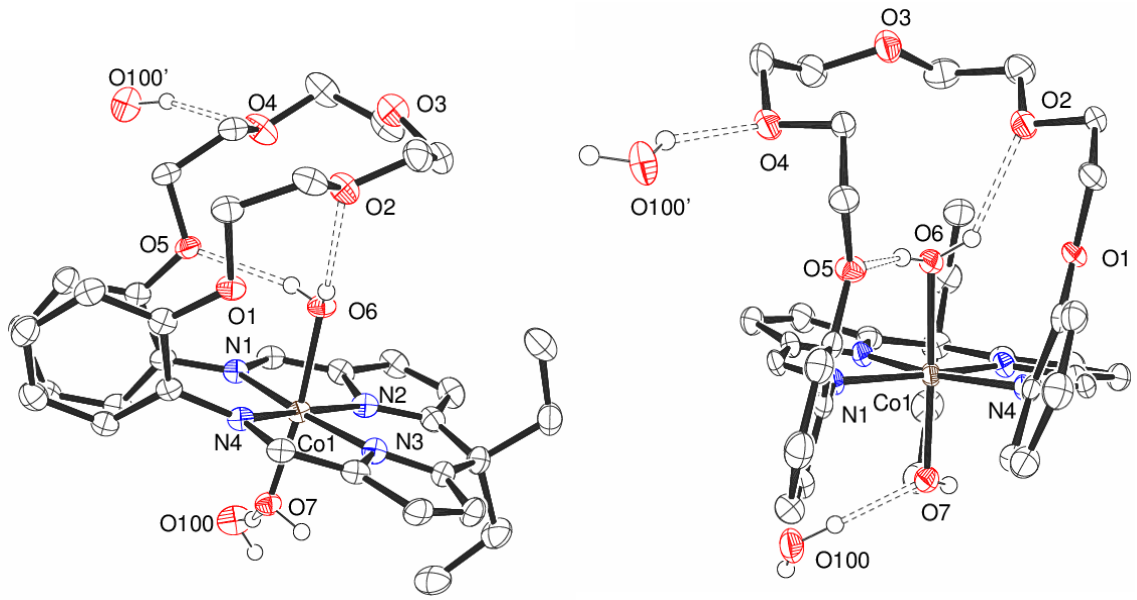

Figure 15: X-ray crystal structure of $[Co(OH_2)(OH)(L^P)]\cdot H_2O$. For clarity, all hydrogen atoms, except for those on O6, O7 and O100 (which were found from the difference map and refined with restraints) and partially occupied waters of crystallisation are omitted and displacement ellipsoids are drawn at 50% probability

Table 5: Selected bond lengths (Å) and angles (°) of $[Co(OH_2)(OH)(L^P)]\cdot H_2O$

Co1-N1	1.996(3)	O6-Co1-O7	173.67(10)
Co1-N2	1.883(3)	Co1···N_4	0.040
Co1-N3	1.872(3)	N1-Co1-N4	107.59(11)
Co1-N4	2.009(3)	N1-Co1-N2	82.62(12)
Co1-O6	2.033(2)	N2-Co1-N3	87.05(12)
Co1-O7	1.880(2)	N3-Co1-N4	82.71(11)
O7···O100	2.668	Σ ∠ Co1	359.97
O100···O4'	3.119	Twist Φ	17.35/10.03
O2···O6	2.940	Dihedral α	10.11
O5···O6	2.873	O1/5···Co1	3.723/4.004

The asymmetric unit of $[Co(OH_2)(OH)(L^P)]$ shows that the Co(III) cation is pseudo-octahedral and bound equatorially by four macrocyclic nitrogens, with an axial water molecule *endo* to the cleft and hydroxide *exo* to the cleft (O6-Co1-O7 173.67(10) °). The Co-N distances (1.996(3)–2.009(3) Å (imine) and 1.872(3)–1.883(3)

Å (pyrrole)) are similar to that of [Co(L^P)] and [Co(pyr)(L^P)] (1.981(1)–2.0335(18) Å (imine) and 1.852(3)–1.8818(18) Å (pyrrole)). The water bound within the macrocyclic cleft (Co-O6 2.033(2) Å) is further stabilised by hydrogen bonding to the poly-ether backbone (O2···O6 2.940, O5···O6 2.873 Å) resulting in a substantial decrease twist in the arene backbone and polyether unit compared to [Co(L^P)] (from *ca.* 50 to 15 °). The hydroxide is bound at a distance of 1.880(2) Å from the cobalt with the assignment of a hydroxide confirmed by analysis of this bond length. The Co1-O7 distance is shorter than the Co-O bond distances in salen-based and porphyrin Co-OH_2 complexes (1.964(7)–2.354(14) Å[39] and 1.9298(6)–2.114(8) Å[40] respectively) and is consistent with reported Co(III)-OH bond distances (1.882(5)–1.883(6) Å).[41]

Further inspection of the structure of [Co(OH_2)(OH)(L^P)] shows that a water molecule forms an intermolecular hydrogen bond to the *exogenous* hydroxide (O7···O100 2.668 Å) which, in turn, hydrogen bonds to the oxygen (O4') of the poly-ether backbone of an adjacent macrocycle (O100···O4' 3.119 Å). These interactions result in the formation of a supramolecular hydrogen bonded, crenellated cyclic hexamer (Figure 16).[42]

Adjacent pacman complexes are found alternating above and below the median plane. Expanding the solid state structure further reveals that the crenellated hexamer structure interlocks to form columnar motifs. These columns form a channel of approximately 7.6 Å in diameter which is occupied by approximately four waters of crystallisation per hexamer (Figure 17). However, the electron density in the channel could not be satisfactorily modelled, so it is likely to be a one dimensional chain of water molecules.

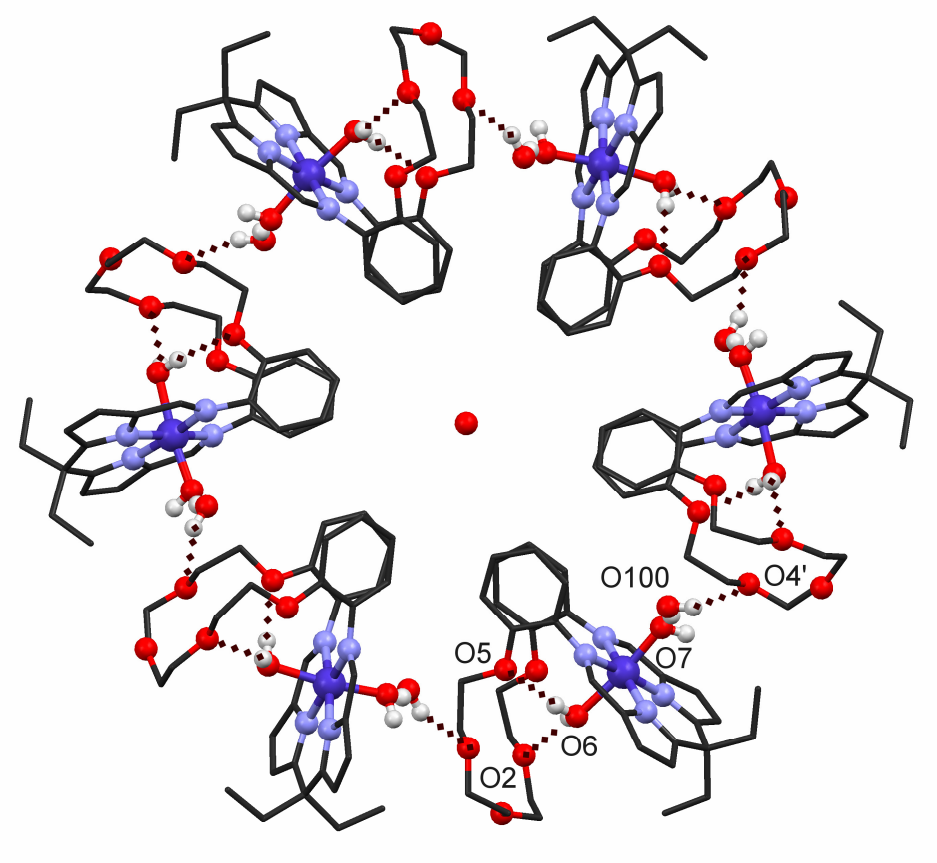

Figure 16: X-ray crystal structure of the extended structure of $[Co(OH_2)(OH)(L^P)]$. For clarity, all hydrogen atoms except those located on O6, O7, and O100, are omitted[42]

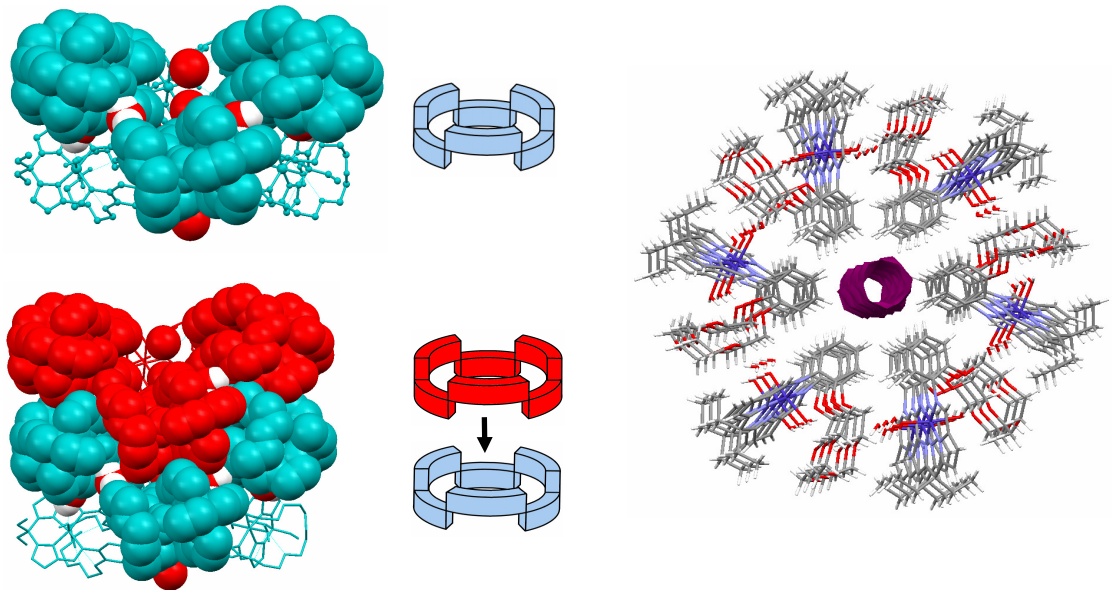

Figure 17: X-ray crystal structure of $[Co(OH_2)(OH)(L^P)]$ extended structure showing crenellated structure, with hexamer cartoon (top left) and interlocking of crenellated hexamers to form columns, with cartoons (bottom left). Void analysis in Mercury of the solid state structure of $[Co(OH_2)(OH)(L^P)]\cdot H_2O$ (spherical probe radius of 1.15 Å) (right)

Each column is further arranged in a hexagonal fashion creating a honey-comb structure (Figure 18).

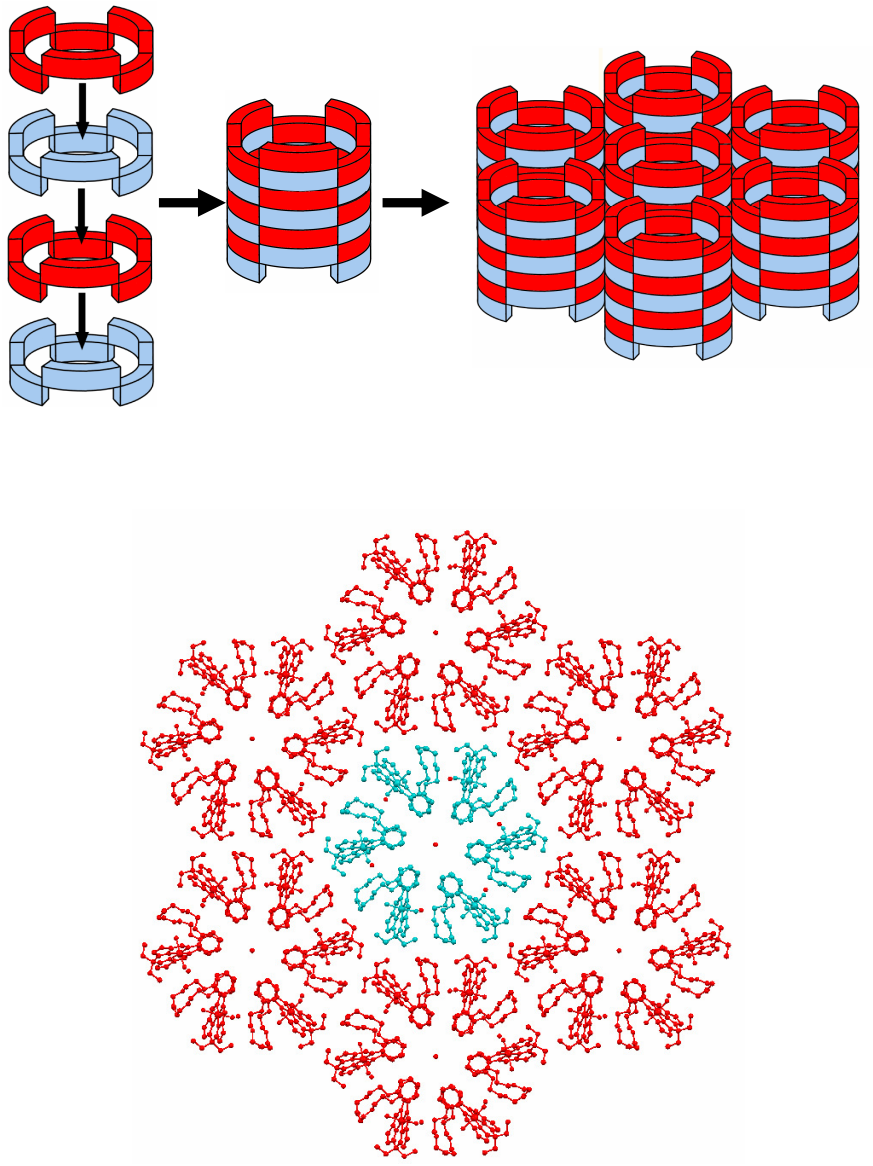

Figure 18: Cartoon showing the stacking of $[Co(OH_2)(OH)(L^P)]$ hexamers (top) and X-ray crystal structure of $[Co(OH_2)(OH)(L^P)]$ extended structure showing honey-comb structure of stacked hexamers (bottom)

There are many examples of cyclic assemblies of metal complexes through hydrogen bonding[43] and one such is the supramolecular ring formed by the assembly of $[Fe_2(\eta^5\text{-}C_5H_4CH_2CH_2OH)_2(CO)_2(\mu\text{-}CO)_2]$ units published by Braga and co-workers (Figure 19);[44] H-bonding of the terminal hydroxides forms a $(OH)_6$-ring in a manner similar to solid state structures of certain alcohols.

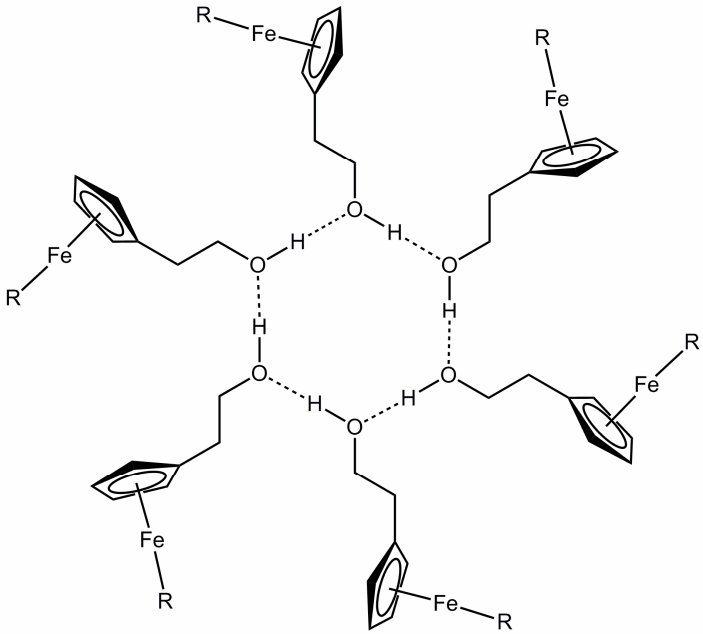

Figure 19: H-bonded wheel by the Braga group. R = $(CO)_2(\mu\text{-}CO)_2Fe(\eta^5\text{-}C_5H_4CH_2CH_2OH)$[44]

Metal oxide or oxometallate wheels and giant "nano-rings" have also been synthesised through bridging covalent interactions and are being studied for their application towards single molecular magnets.[45-47] For example, the Cronin group have studied the formation of giant Mo_{160} rings, held *via* oxo bridges[47] whereas Winpenny and co-workers have published work investigating the properties of transition metal wheels. Here, introducing one or more different transition metals into the ring, as well as altering ring size, shape and bridging group, drastically altered their magnetic properties (Figure 20).[45]

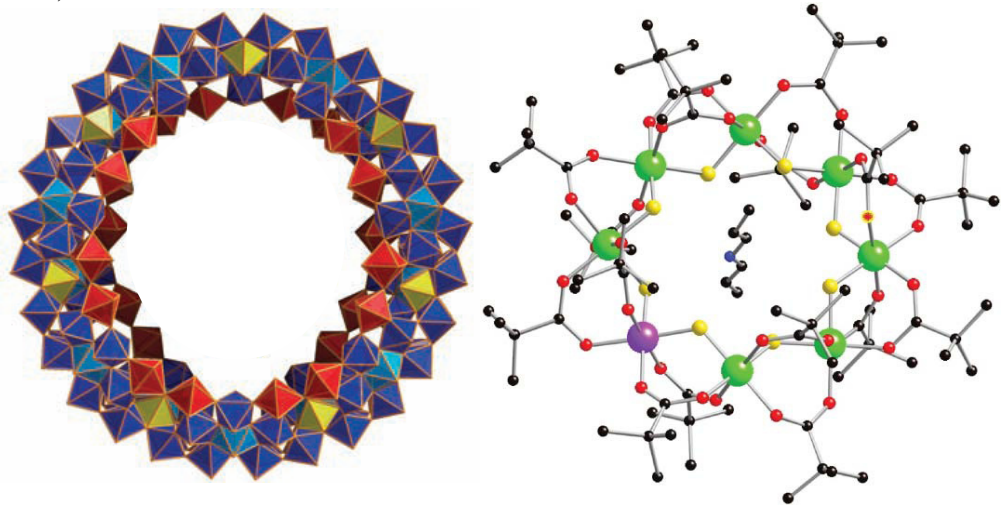

Figure 20: Giant Mo_{160} ring studied by the Cronin group[47] (left, colours indicate different Mo-containing polyhedra) and heteronuclear wheel developed by Winpenny and co-workers (right, green = chromium purple = nickel).[45]

The Hannon group have shown that π-stacking interactions between trinuclear helixcate complexes results in crystallisation in a hexagonal fashion with nano-scale channels (Figure 21).[48]

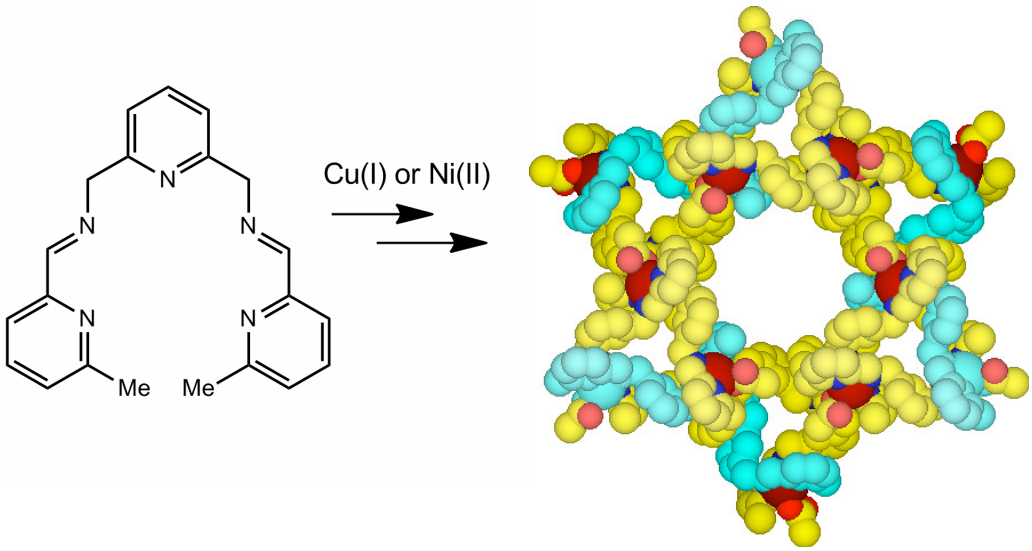

Figure 21: Hannon and co-workers crystallised a series of hexagonal complexes with nano-scale channels[48]

However, large cyclic structures in which discrete metal complexes retain potential catalytic function are rare, investigations into the catalytic chemistry and post-synthetic modifications of metal-organic frameworks have only been published relatively recently.[49]

Tsuchida and co-workers have reported the synthesis of a salen-based oxo-vanadium ring from equimolar mixtures of [VO(salen)] and [{O=V(salen)}$_2$(μ-F)][BF_4]. Weak intermolecular interactions between the vanadyl units of [VO(salen)] complexes result in a hexagonal cell creating a nano-scale channel decorated further by [{O=V(salen)}$_2$(μ-F)][BF_4] complexes on the outside (Figure 22, left). A view of the core of the wheel from the side (Figure 22, right) shows a crenellated ordering of the [VO(salen)] units in a manner similar to that seen in the [Co(L^P)]-based wheel, though analysis of distances between complexes in the vanadyl complex indicates a much weaker intermolecular interaction compared to that seen for [Co(L^P)].

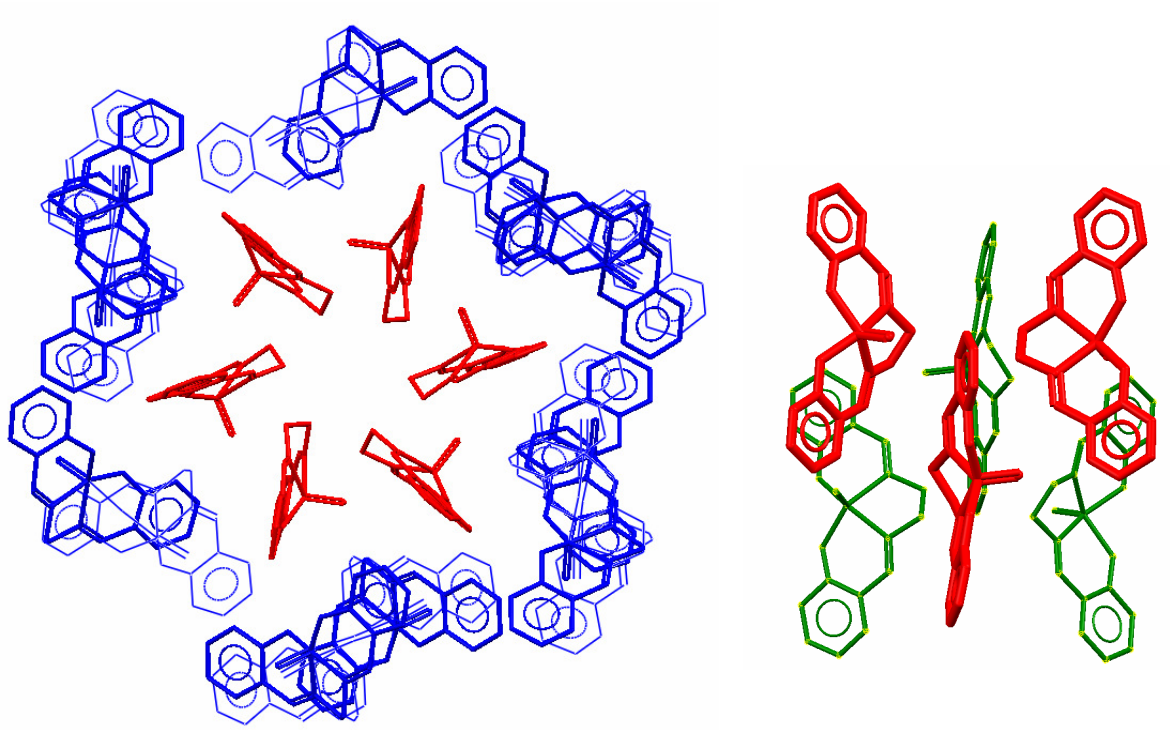

Figure 22: X-ray crystal structure of (left) [VO(salen)] (red) /[{O=V(salen)}$_2$(μ-F)][BF_4] wheel (blue) view from the top and (right) [VO(salen)] core as view from the side (red = near from point of view, green = further away) from the Tsuchida group[50]

There are also examples of porphyrin-based wheel complexes, though these have been generated by covalent interactions. These have been synthesised for various applications such as for their light-harvesting properties,[51] formation of 3D networks[51] and towards strained molecular wires[52] (Figure 23).

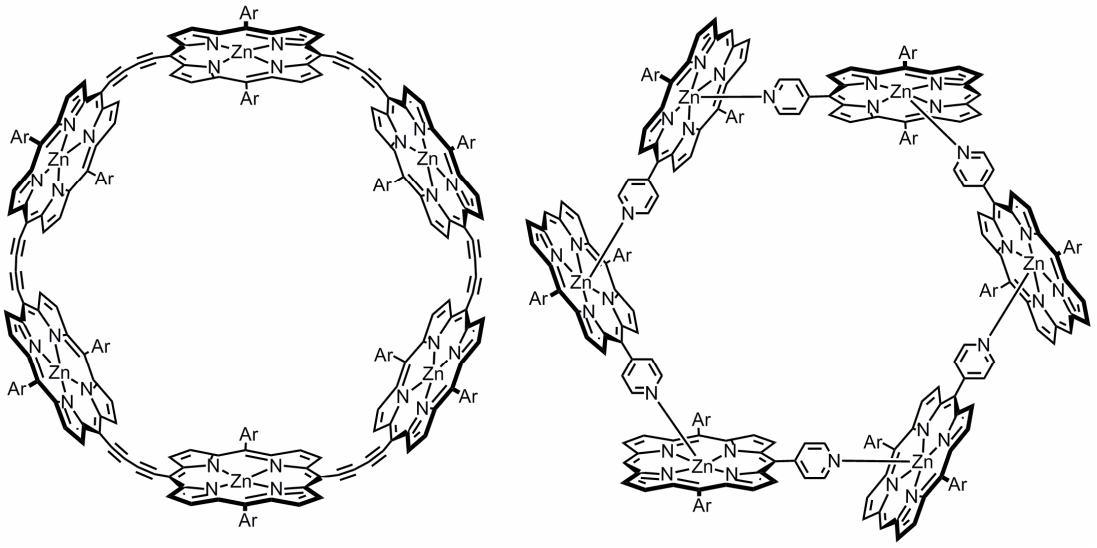

Figure 23: Porphyrin wheels synthesised by Anderson and co-workers to create strained molecular wires (left)[52] the Hosseini and Bulach group to synthesise 3D networks (right)[51]

Microanalysis of $[Co(OH_2)(OH)(L^P)]\cdot H_2O$ also supports formulation with the IR spectrum displaying broad absorbances at 3468 and 3413 cm^{-1} corresponding to O-H stretches. Crystallisation of this cobalt wheel from benzene is repeatable.

The stability of the $[Co(OH_2)(OH)(L^P)]\cdot H_2O$ wheel in solution was probed. When dissolved in a 50:50 toluene : methanol solution, the ESI mass spectrum showed no peaks corresponding to a cyclic structure in solution with peaks at *m/z* = 655 and 625 corresponding to $[Co(L^P)]$ and $[Co(L^P)]$-2Me respectively. Further peaks were observed corresponding to adducts of $[Co(L^P)]$ such as a MeO-adduct at 687 amu, with Na and K adducts at 679 and 695 amu respectively. However, in the absence of protic solvent and using mixtures of toluene and acetonitrile, aggregates were observed in solution, with a trimer $[[Co(L^P)]_3(OH_2)(OH)_2]^+$ peak at 2019 amu in the cryospray mass spectrum. Peaks corresponding to the monomer and dimer were also present but no heavier ions were observed.

Addition of MeOD to a C_6D_6 solution of the $[Co(OH_2)(OH)(L^P)]\cdot H_2O$ hexamer caused shifts its ^1H NMR spectrum such as the O-CH_2 and the *meso*-ethyl group resonances become less complex; this suggests that a potentially monomeric, less rigid complex has formed (Figure 24).

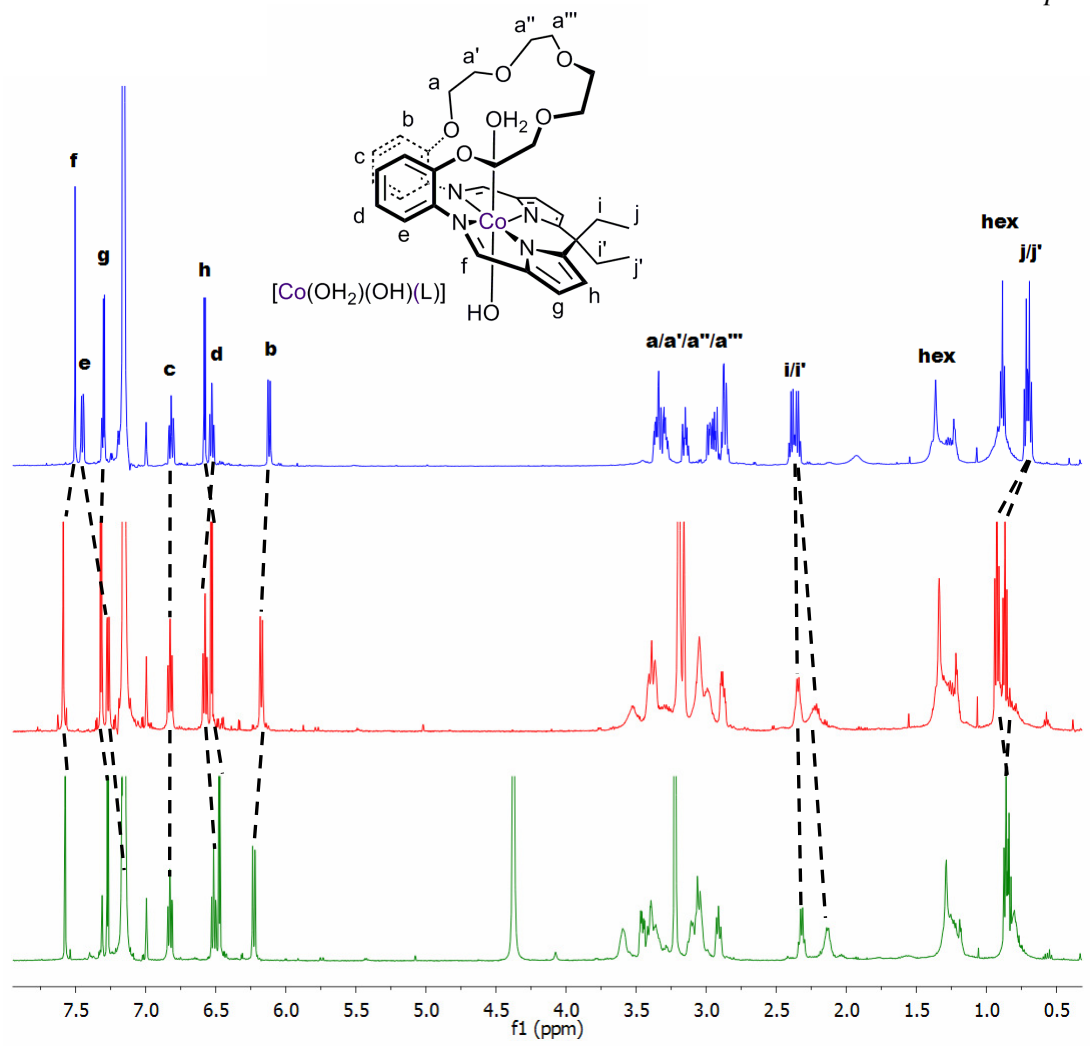

Figure 24: ^{1}H NMR spectrum of [Co(OH$_2$)(OH)(L^P)] in C_6D_6 (top, blue), C_6D_6 with one drop of MeOD (middle, red), C_6D_6 and excess MeOD (bottom, green)

The ^{1}H NMR nOe spectrum of the hexamer in C_6D_6 shows intramolecular nOe interactions as well as potential, though weak, intermolecular nOe between OCH_2 and arene/imine protons (Figure 25).

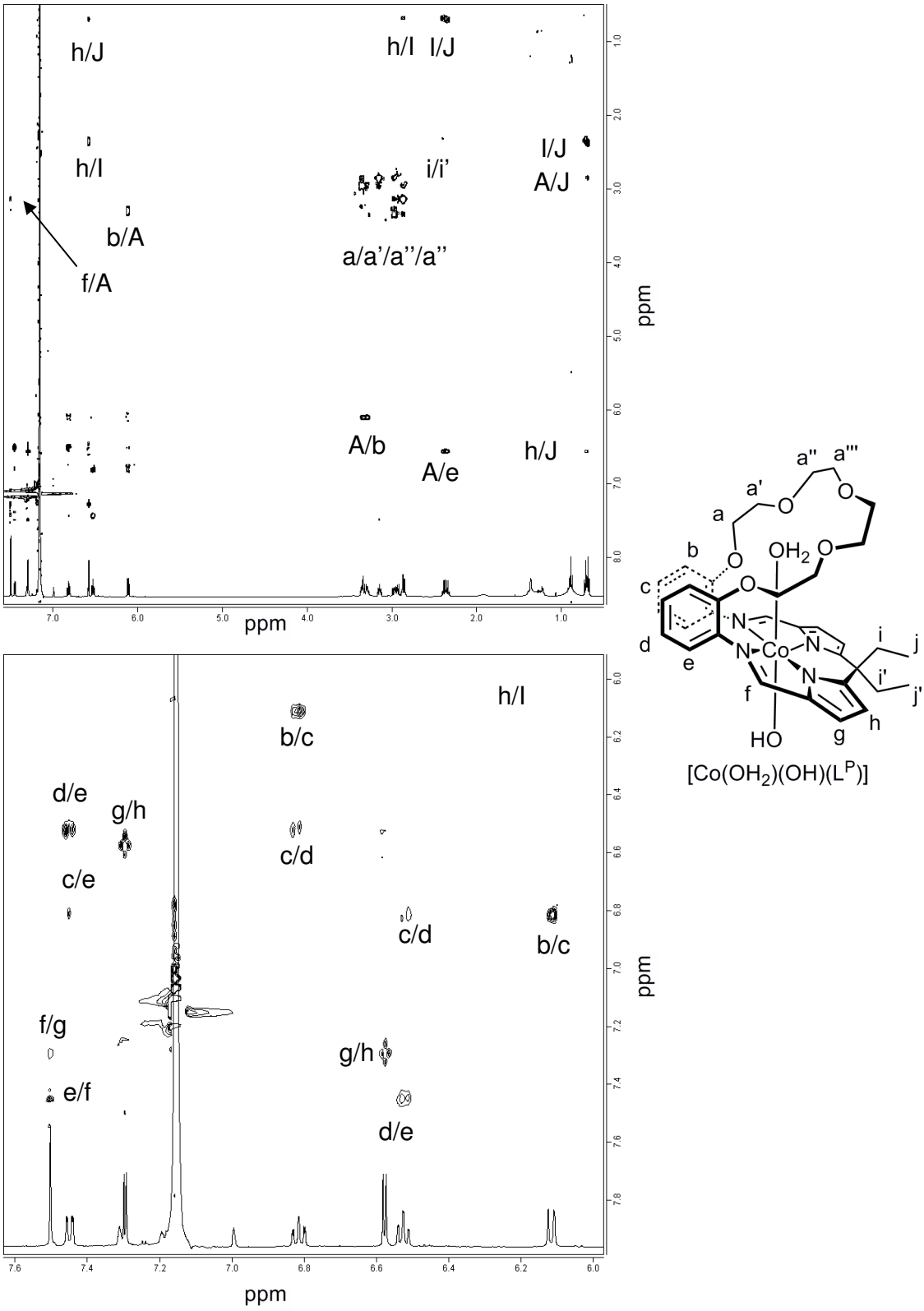

^{1}H-^{1}H-nOe NMR (C_6D_6) of [Co(OH_2)(OH)(L)] (top) and showing arene region only (bottom). Letters correspond to assignments in figure (right) with A = a, a', a'' and/or a''', I = i and/or i' with J = j and/or j'

However, some of the interactions between the ethereal and arene/imine protons persist upon addition of MeOD and thus their identity is unclear. Therefore, it can be assumed that the cyclic hexamer shows only limited stability in protic solvents although a degree of aggregation does occur in the absence of such solvents.

Air-oxidation of [Co(L^P)] in THF in the presence of LiI leads to the isolation of [Co(OH_2)(I)(L^P)]. Again resonances in the ^{1}H NMR spectrum, recorded in H_8-THF/C_6D_6, are in the diamagnetic region only from 8.04 to 1.05 ppm and indicate a pacman structure in solution. Two ethyl environments at 1.15 and 1.05 ppm (Et-CH_3) and 2.55 and 2.65 ppm (Et-CH_2) are observed though desymmetrisation of the ether-backbone protons cannot be seen due to the suppression of the H_8-THF resonances. Microanalysis and EI mass spectrometry support the formulation, with a parent ion peak in the mass spectrum seen at 781 amu for the M^+–H_2O. Broad absorptions at 3424 and 3242 cm^{-1} in the IR spectrum are also indicative of the bound water. A crystal suitable for single crystal X-ray diffraction was grown by hexane diffusion into a THF solution (Figure 25, Table 6).

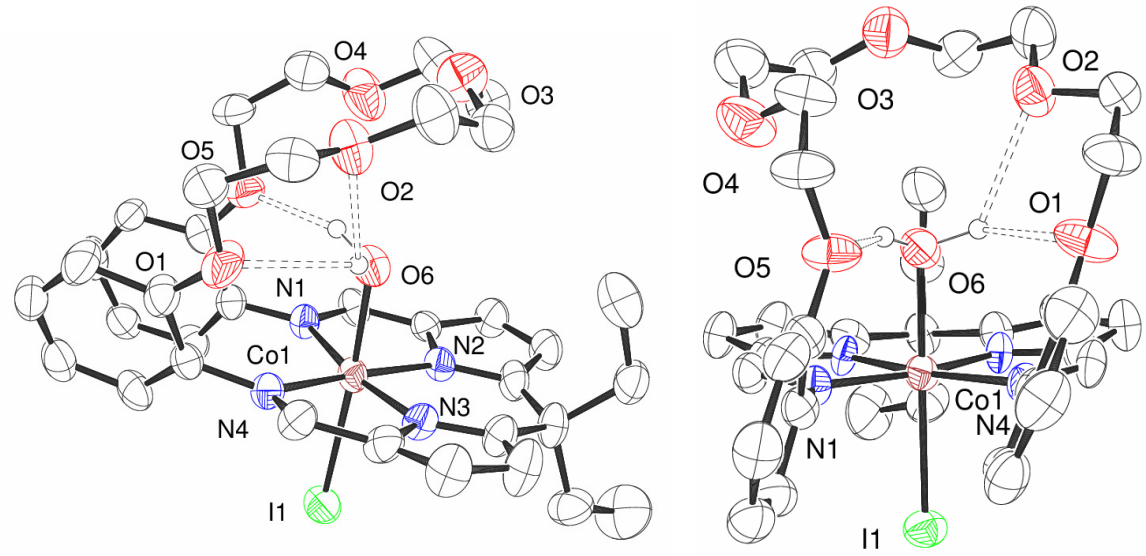

Figure 25: X-ray crystal structure of [Co(OH_2)(I)(L^P)]. For clarity, all hydrogen atoms except those on O6 are omitted and displacement ellipsoids are drawn at 50% probability

Table 6: Selected bond lengths (Å) and angles (°) of $[Co(OH_2)(I)(L^P)]$

Co1-N1	2.024(7)	Co1···N_4	0.052
Co1-N2	1.882(6)	N1-Co1-N4	107.3(3)
Co1-N3	1.868(7)	N1-Co1-N2	82.3(3)
Co1-N4	1.984(6)	N2-Co1-N3	87.0(3)
Co1-O6	2.019(6)	N3-Co1-N4	83.1(3)
Co1-I1	2.5569(13)	Σ ∠ Co	359.70
O1···O6	3.237	Twist Φ	76.80/67.86
O2···O6	3.112	Dihedral α	10.23
O5···O6	2.843	O1/5···Co1	3.715/4.054
O6-Co1-I1	176.58(17)		

The asymmetric unit of $[Co(OH_2)(I)(L^P)]$ is comparable to that of $[Co(OH_2)(OH)(L^P)]$. However, the lack of a hydrogen-bond donor in the exogenous-axial position prevents the formation of any supramolecular architecture as seen in the hydroxide complex. In $[Co(OH_2)(I)(L^P)]$, the cobalt adopts a distorted octahedral geometry with the iodide *exo* to the cleft and the water molecule within the cleft, so forming the axial ligands. No counterions were found in the structure thereby supporting the Co(III) oxidation state. The water is bound at a Co-O distance of 2.019(6) Å, similar to that of the *exo*-OH structure at 2.033(2) Å. The water is further stabilised by hydrogen bonding to the ethereal oxygens O1, O2 and O5 of the polyether at 3.237, 3.112 and 2.843 Å respectively. The cobalt sits in the N_4-plane (Co···N_4 0.052 Å) with Co-N_{im} (1.984(6) and 2.024(7) Å) and Co-N_{py} distances (1.868(7) and 1.882(6) Å) comparable to those of $[Co(OH_2)(OH)(L^P)]$ (Co-N_{im} 1.996(3) and 2.009(3) Å, Co-N_{py} 1.883(3) and 1.872(3) Å) and $[Co(L^P)]$ (Co-N_{im} 1.981(4) Å, Co-N_{py} 1.852(3) and 1.858(3) Å) and are thus of a standard length. The Co-I distance of 2.5569(13) Å is shorter than that reported for a similar salen Co-I complex (2.714(1) Å)[53] but is within the range of other reported Co(III)-I bond distances (2.510(5)–2.7178(11) Å)[54]

Although a clean product could not be isolated when exposing [Co(L^{NMe})] to air, a crystal suitable for X-ray diffraction was isolated from a mixture of [Co(L^{NMe})] and KCl in benzene in the presence of air (Figure 26, Table 7).

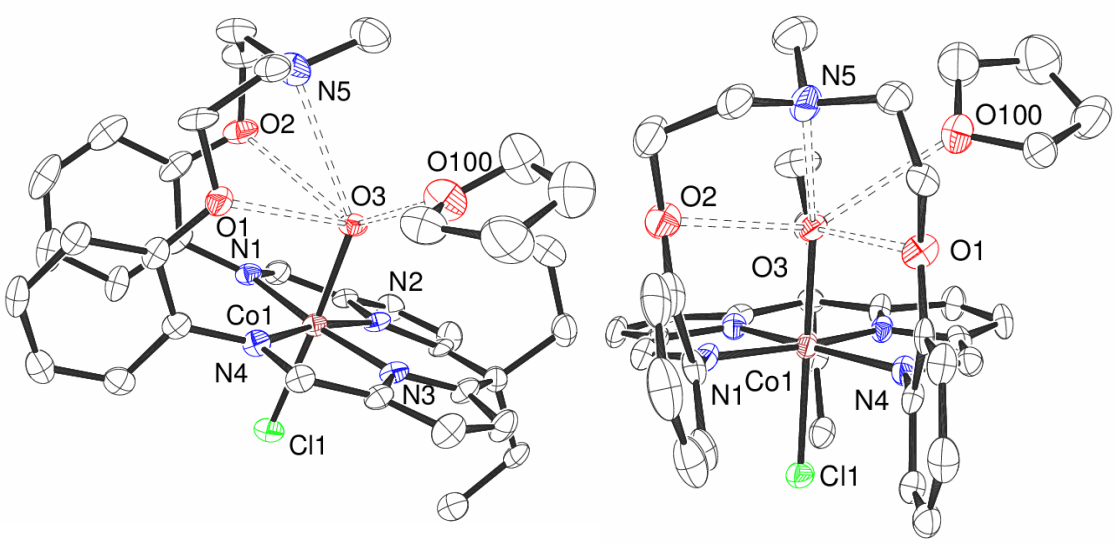

Figure 26: X-ray crystal structure of [Co(OH_2)(Cl)(L^{NMe})]. For clarity, all hydrogen atoms are omitted and displacement ellipsoids are drawn at 50% probability

Table 7: Selected bond lengths (Å) and angles (°) of [Co(OH_2)(Cl)(L^{NMe})]

Co1-N1	1.993(6)	N1-Co1-N2	82.9(3)
Co1-N2	1.880(6)	N2-Co1-N3	86.8(3)
Co1-N3	1.866(6)	N3-Co1-N4	83.0(3)
Co1-N4	1.999(6)	Σ ∠ Co1	360.00
Co1-O3	2.010(5)	Twist Φ	74.92/88.82
Co1-Cl	2.220(2)	Dihedral α	19.20
Co1···N5	4.714	O1/2···Co1	3.832/3.940
O3-Co1-Cl	177.08(17)	O1/2···O3	3.126/3.160
Co1···N_4	0.013	O100···O3	2.934
N1-Co1-N4	107.3(3)	O3···N5	2.991

Again, a pacman motif is maintained with the cobalt centre in a distorted octahedral environment with axial chloride and a molecule of water bound exogenous and endogenous to the cleft, respectively. No counterion was found and thus a cobalt(III)

oxidation state is assigned. The Co1-O3 (water) bond length (2.010(5)Å) is similar to those in the [Co(OH_2)(L^P)] complexes (2.019(6)-2.033(2) Å) and is stabilised by hydrogen bonding to the ether (O3···O1/O2 3.126/3.160 Å) and amine (O3···N5 2.991 Å) substituents from the upper half of the ligand. Furthermore, a THF molecule is bound within hydrogen-bonding distance to the water in the cleft at a distance of O3···O100 2.934 Å, comparable to that of literature values (2.518–3.510 Å).[55] The cobalt sits in the N_4 plane (Co···N_4 0.013 Å), with Co-N_{im} (1.993(6)/1.999(6) Å) and Co-N_{py} (1.866(6)/1.880(6) Å) bond distances comparable to the cobalt-(L^P) complexes reported here. The Co1-Cl bond length of 2.220(2) Å is slightly shorter than that of salen (2.2382(6)–2.5513(17) Å)[40, 56] and porphyrin complexes (2.243(2)–2.271(2) Å).[57]

The electrochemistry of [Co(L^P)] and [Co(L^{NMe})] under nitrogen was studied by cyclic voltammetry, both complexes displayed a Co(II)/Co(III) and a Co(I)/Co(II) wave at -0.18 and -2.27 V ([Co(L^{NMe})]) and -0.12 and -2.29 V ([Co(L^P)]) respectively (vs Fc^+/Fc). The electrochemistry of both complexes is discussed in Chapter 3 Section 3.4.

2.3.4 Titanium and Vanadium complexes of (L^P) and (L^{NMe})

Complexes of group 4 and 5 metals have been shown to form highly reactive N_2-bridged compounds upon reduction (Figure 27).[58]

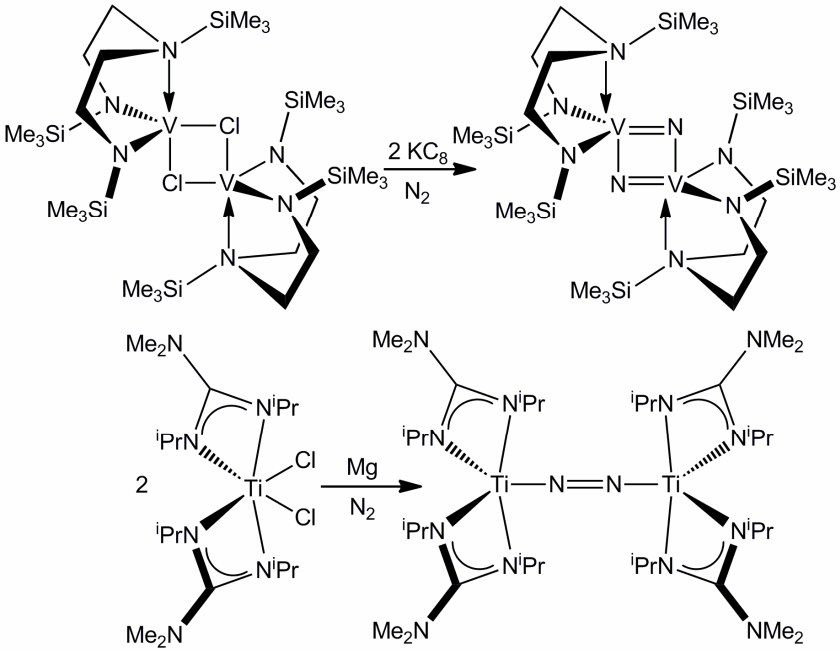

Figure 27: Examples of N_2 activation by V[59] and Ti[60] complexes upon reduction

The Bergman and Arnold groups showed that the reduction of a titanium dichloride complex of guanidinate ligands forms a dinitrogen complex which undergoes hetero-atom abstraction upon exposure to substrates containing nitrogen, oxygen or sulfur to yield imido, or bridging dioxo or sulfido complexes.[60] Cloke and co-workers have also shown that the reduction under nitrogen of a binuclear vanadium complex of bulky silylamino(disilylamido) ligands results in N_2 cleavage and the formation of bridged-nitrido complexes (Figure 27).[61]

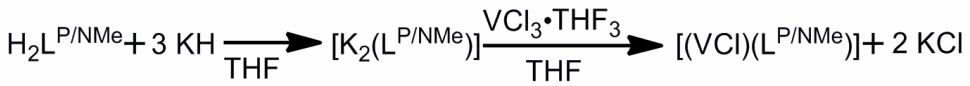

Equation 4

Addition of *in-situ* prepared $[K_2(L^{P/NMe})]$ to a stirring suspension of $VCl_3{\cdot}(THF)_3$ caused an immediate change in colour from pink to deep red, so resulting in the formation of the complexes $[(VCl)(L^{P})]$ and $[(VCl)(L^{NMe})]$ in moderate yield (*ca.* 60 %) as red solids after workup (Equation 4). The products are highly paramagnetic and are silent in their ^1H NMR spectra. The EI mass spectra display low intensity parent peaks at 683 ($[(VCl)(L^{P})]$) and 607 amu ($[(VCl)(L^{NMe})]$), with higher intensity peaks showing the loss of the chloride ligand. Elemental analysis for both complexes supports their formulation. The IR spectra show the disappearance of the NH stretch at *ca.* 3200 cm^{-1} as well as the expected shifting of the imine absorbance from *ca.* 1620 to 1560 cm^{-1}. The V-Cl stretches should occur in the far-IR region (*ca.* 300-400 cm^{-1})[62] and so could not be determined. Crystals of $[(VCl)(L^{P})]$ suitable for X-ray crystallography were grown by slow diffusion of hexanes into a THF solution (Table 8, Figure 28). It is clear from the structure that the sample has become contaminated by some water impurity present in the glove-box atmosphere. The pacman-shaped complex contains a vanadium atom in the 3+ oxidation state, bound in a distorted octahedral environment with a hydrogen-bonded water molecule found within the cleft.

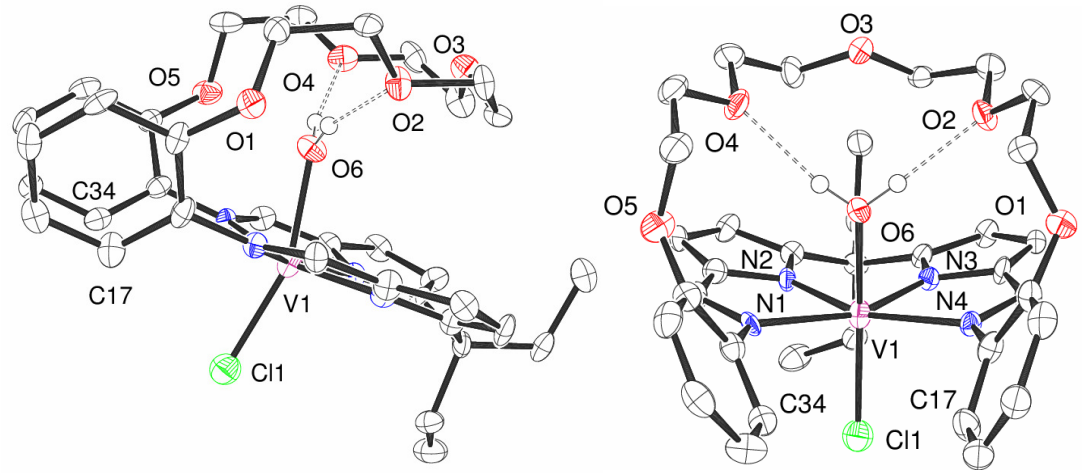

Figure 28: X-ray crystal structure [(VCl)(OH_2)(L^P)]. For clarity, all hydrogen atoms except those of O6 are omitted and displacement ellipsoids are drawn at 50% probability

Table 8: Selected bond lengths (Å) and angles (°) of [(VCl)(OH_2)(L^P)]

V1-N1	2.195(3)	O2···O6	2.753
V1-N2	2.023(3)	O4···O6	2.804
V1-N3	1.998(3)	O2···O6···O4	102.01
V1-N4	2.198(3)	O6-V1-Cl	158.58(8)
V1-Cl	2.2390(12)	C17···Cl	3.694
V1···N_4	0.186	C34···Cl	3.742
N1-V1-N4	121.00(10)	O1···V1	4.635
N1-V1-N2	77.47(11)	O5···V1	4.604
N2-V1-N3	82.19(11)	Σ ∠ V1	358.11
N3-V1-N4	77.45(11)	Twist Φ	33.88/24.45
V1-O6	2.111(3)	Dihedral α	55.91

The vanadium atom sits slightly outside of the cleft, 0.186 Å from the N_4-plane, bound by two imine and two pyrrolic nitrogens. The vanadium-N_{im} distances of 2.195(3) and 2.198(3) Å are slightly longer than for a similar complex of the symmetric ligand (*ca.* 2.14 Å)[29] and are fairly long compared to V(III)-salen complexes (2.042(3)–2.166(3) Å)[63] though are within values of other V(III)-N_{im} complexes (2.003(8)–2.242(3) Å).[64] There are a few examples of structurally-characterised vanadium(III) complexes, with

V-N_{py} distances of ranging from 1.952(3) to 2.119(6) Å[65] similar to those reported here (1.998(3)–2.023(3) Å). The axially-bound chloride resides *exo* to the cleft, with a bond distance of 2.2390(12) Å, shorter than that in the binuclear analogue (*ca.* 2.32 Å) as well as being short compared to V(III)-salen complexes (2.286(4)–2.352(2) Å).[66] The arene backbone units have splayed open, so forming an angle of 55.91°, that is similar to that seen in binuclear vanadium,[29] uranyl[67] and alkyl-tin[27] complexes of the symmetric ligand L. The chloride is slightly bent towards the arene with a O6-V1-Cl1 angle of 158.58(8)° leading to a weak interaction between the chloride and arene groups (Cl-C_{arene} *ca.* 3.7 Å). An axially-bound water molecule resides within the cleft. The V1-O6 bond distance of 2.111(3) Å is characteristic of a V(III)-OH_2 bond and not an oxidized V(IV)=O bond. Examples of V(III)-water interactions are relatively rare, with the V1-O6 bond distance being only slightly longer than reported V(III)-OH_2 distances (1.970(3)–2.108(2) Å).[68] Bond lengths of octahedral V(IV)=O are considerably shorter and are in the region of 1.578(2)–1.631(3) Å.[69] The water molecule is further stabilised by hydrogen bonding to the polyether oxygens O2 and O4 distances of 2.753 and 2.804 Å from O6. Thus the contamination of [(VCl)(L^P)] with water has again demonstrated the ability of the free binding pocket to stabilise incoming small molecules through a combination of metal-ligand and hydrogen-bonding interactions.

Crystals of [(VCl)(L^{NMe})] suitable for single crystal X-ray diffraction were grown from hexane diffusion into a THF solution (Figure 29), although the poor quality of the data is reflected with an R-factor of over 10 % (10.23 %); as such, while the connectivity can be elucidated the geometric data will not be discussed.

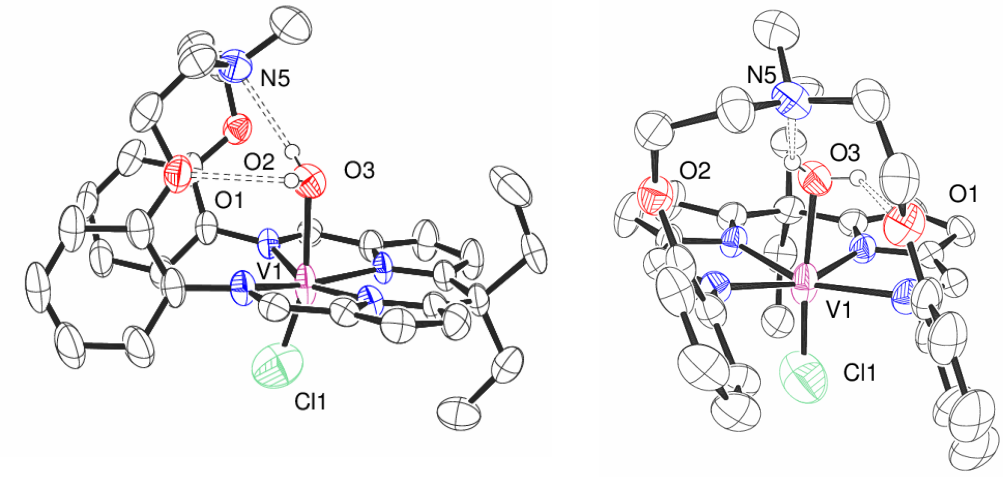

Figure 29: X-ray crystal structure [(VCl)(OH_2)(L^{NMe})]. For clarity, all hydrogen atoms, except those of O3 are omitted and displacement ellipsoids are drawn at 50% probability

Again, some water impurity present in the glovebox atmosphere has resulted in the binding of water inside the cleft of the pacman-shaped structure. Some interaction between the amine N5, the ethereal oxygens, and the water molecule is suggested by their proximity.

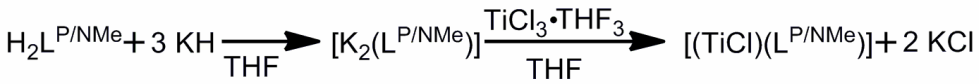

Equation 5

The salt elimination reaction using $TiCl_3{\cdot}(THF)_3$ instead of $VCl_3{\cdot}(THF)_3$ results in the formation of $[(TiCl)(L^P)]$ and $[(TiCl)(L^{NMe})]$ in moderate yields (*ca.* 50 %, Equation 5). Again, the complexes are highly paramagnetic and silent in their ^1H NMR spectra, though their formulations are supported by elemental analysis. Parent ion peaks were seen in the EI mass spectra at 604 (L^{NMe}) and 679 amu (L^P). Once again, the IR spectra show the disappearance of the NH stretch at *ca.* 3200 cm^{-1} and the shifting of the imine absorbance from 1620 to 1580 cm^{-1}.

Crystals of $[(TiCl)(L^P)]$ suitable for X-ray diffraction studies were grown by the slow diffusion of hexanes into a THF solution (Figure 30, Table 9).

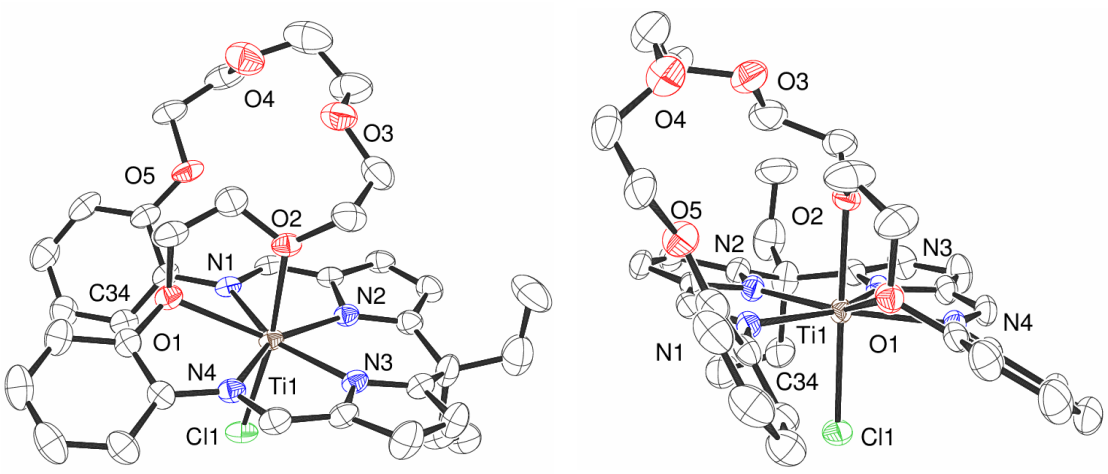

Figure 30: X-ray crystal structure $[(TiCl)(L^P)]$. For clarity, all hydrogen atoms are omitted and displacement ellipsoids are drawn at 30% probability

Table 9: Selected bond lengths (Å) and angles (°) of [(TiCl)(L^P)]

Ti1-N1	2.285(2)	C17···Cl	4.430
Ti1-N2	2.117(3)	C34···Cl	3.616
Ti1-N3	2.150(3)	O1···Ti1	2.382(2)
Ti1-N4	2.195(2)	O2-Ti1	2.219(2)
Ti1-Cl	2.3843(11)	O5···Ti1	4.656
Ti1···N_4	0.015	O1-Ti-Cl1	102.41(6)
N1-Ti1-N4	134.41(10)	O2-Ti-Cl1	172.30(7)
N1-Ti1-N2	75.01(9)	Σ ∠ Ti1	359.99
N2-Ti1-N3	77.16(9)	Twist Φ	55.03/26.58
N3-Ti1-N4	73.41(10)	Dihedral α	29.81

Unusually, the titanium adopts a distorted 7-coordinate pentagonal bipyramidal environment with four nitrogen donors (two pyrrolic, two imino) and one ethereal oxygen in the equatorial plane and a chloride and ethereal oxygen occupying the axial sites. This structure is the only one of all the pacman-H_2L-based complexes which are either seven-coordinate or in which the free binding pocket directly binds to the metal centre bound in the N_4 plane. The highly oxophilic nature of titanium has resulted in a large distortion of the ligand, causing one of the arene backbone units to twist heavily to accommodate the binding of two ethereal oxygens to the titanium; however, the overall pacman geometry is maintained. The two Ti-N_{im} bond lengths (Ti1-N4 2.195(2) and Ti1-N1 2.285(2) Å) differ from each other by 0.09 Å which is likely the result of steric interactions. Similar to [(VCl)(L^P)], the Ti-N_{im} bond lengths (2.195(2) and 2.285(2) Å) are longer than those of Ti(III)-salen complexes (2.106(4)–2.139(9))[70] though the bond N4-Ti1, at 2.285(2) Å is the longest Ti-N_{im} bond known (a search of titanium(III)-N_{im} complexes gives the longest Ti-N bond length as 2.268(3) Å).[71] This is accompanied by a very obtuse N_{im}-Ti-N_{im} bond angle of 134.41(10) ° that is attributed to the heavily-twisted arene backbone. The Ti-N_{py} distances (2.117(3)/2.150(3) Å) are comparable to the few known structures of Ti(III)-pyrrole complexes (2.096(4)–2.136(2)

Å).[72] The ether backbone forms an equatorial interaction with the titanium, with a Ti1-O1 distance of 2.382(2) Å, and a stronger axial bond with a Ti1-O2 bond length of 2.219(2) Å. These bond lengths are comparable to previously reported Ti(III)-ether bonds (2.109(4)–2.232(2) Å).[73] The chloride is bound *exo* to the cleft at a Ti1-Cl1 distance of 2.3843(11) Å, which is of a standard nitrogen/oxygen-bound-Ti(III)-Cl distance (2.324(2)–2.415(2) Å).[74] As seen with the structure of $[(VCl)(OH_2)(L^P)]$, there is also a weak interaction between the chloride and one of the arene backbones, with a C34···Cl1 distance of 3.616 Å.

As mentioned previously, reduction of vanadium and titanium complexes can lead to dinitrogen activation. It was envisaged that reduction of $[(VCl)(L^{P/NMe})]$ or $[(TiCl)(L^{NMe})]$ could lead to a similar end.

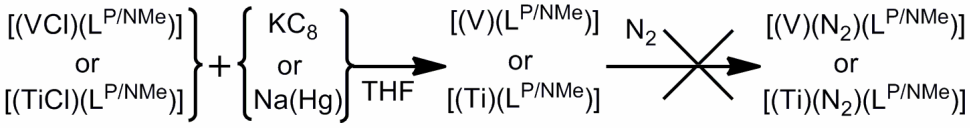

Equation 6

Reaction of the VCl complexes of either ligand with either KC_8 or Na(Hg) in THF led to a dramatic colour change from red to deep green (Equation 6). The product was very air sensitive, decomposing to a red/brown instantly upon exposure to air. Likewise, reductions of the TiCl complexes caused a colour change from red to a deeper red. The ^1H NMR spectra were again silent and a study of the IR spectra showed no absorbance corresponding to bound N_2, expected at around 1706-2100 cm^{-1};[75] Raman spectroscopic measurements were not undertaken. Furthermore, a repeat of the reduction of vanadium compounds under argon seemingly yielded the same deep green compound. Attempts to crystallise these complexes have thus far been unsuccessful and therefore more investigation is needed to characterise these complexes. However, a red crystal of a decomposition product of the reduced form of $[(VCl)(L^P)]$, $[V(O)(L^P)]$, presumably due to reaction with some dioxygen impurity in the glove box, was grown from hexane diffusion into a THF solution and its X-ray structure determined (Figure 31, Table 10).

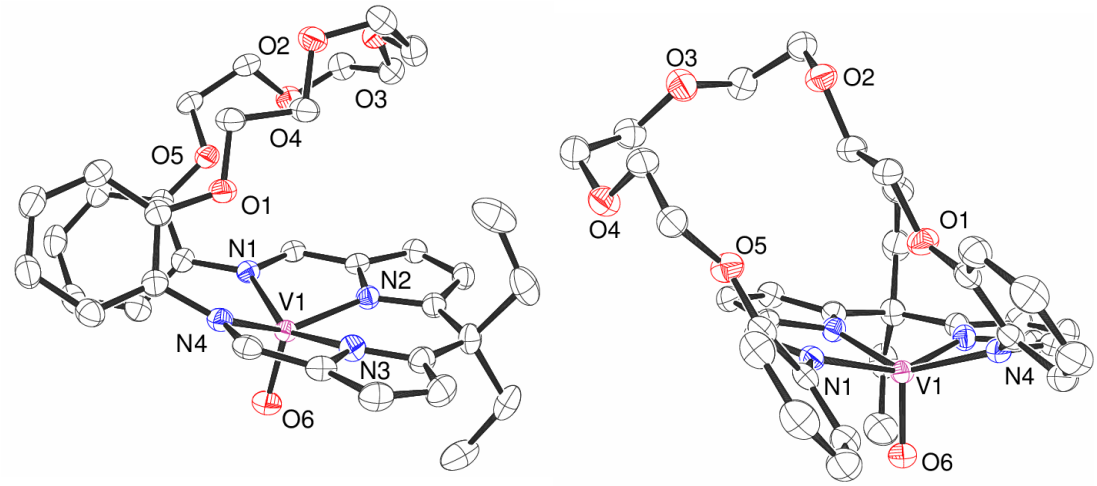

Figure 31: X-ray crystal structure [V(O)(L^P)]. For clarity, all hydrogen atoms are omitted and displacement ellipsoids are drawn at 50% probability

Table 10: Selected bond lengths (Å) and angles (°) of [(VO)(L^P)]

V1-N1	2.1347(17)	N1-V1-N4	108.22(7)
V1-N2	1.9954(17)	N1-V1-N2	78.54(7)
V1-N3	2.0048(17)	N2-V1-N3	80.88(7)
V1-N4	2.1125(17)	N3-V1-N4	77.57(7)
V1-O6	1.5936(15)	Σ ∠ V1	345.21
V1···O1	3.143	Twist Φ	53.78/52.51
V1···N_4	0.523	Dihedral α	19.16

The vanadium atom adopts a distorted square-based pyramidal geometry and is positioned 0.523 Å out of the N_4-plane *exo* to the cleft. An oxo group is bound *exo* to the cleft, which contrasts to the structures of binuclear complexes of the symmetrical ligand L in which the V(IV)=O oxo is found within the cleft and bridging to remaining V(III) present in the other binding pocket. The V-O6 distance of 1.5936(15) Å is similar to V(IV)=O bonds seen in porphyrin (1.584(4)–1.620(2) Å)[76, 77] and salen (1.588(3)–1.614(4) Å).[78]

The V-N_{py} distances (1.9954(17)–2.0048(17) Å) are similar to those found in porphyrin V(IV)=O complexes (2.011(9)–2.117(3) Å)[77, 79] with the V-N_{im} bond lengths 2.1125(17) and 2.1347(17) also similar to salen V(IV)=O complexes (2.002(3)–2.127(3)

Å).[80] There is possibly a weak interaction between the vanadium V1 and O1 of the polyether backbone, similar to that seen for [(TiCl)(L^P)] but at an elongated distance of 3.143 Å.

2.3.5 Synthesis of [Mg($L^{P/NMe}$)]

$$H_2L^{P/NMe} + Mg(^nBu)_2 \xrightarrow[THF]{} [Mg(L^{P/NMe})] + 2\ ^nBuH$$

Equation 7

The successful route into novel metal complexes of (L^P) and (L^{NMe}) by salt elimination reactions of the potassium salts [$K_2(L^P)$] and [$K_2(L^{NMe})$] with metal chlorides suggested that routes using Group 2 metal complexes could be possible. As such, it was found that the reaction of a heptane solution of dibutyl-magnesium with either macrocycle leads to a change from a yellow/orange to a bright yellow dichroic solution yielding the magnesium complexes [Mg(L^P)] or [Mg(L^{NMe})] in greater than 93 % yield (Equation 7).

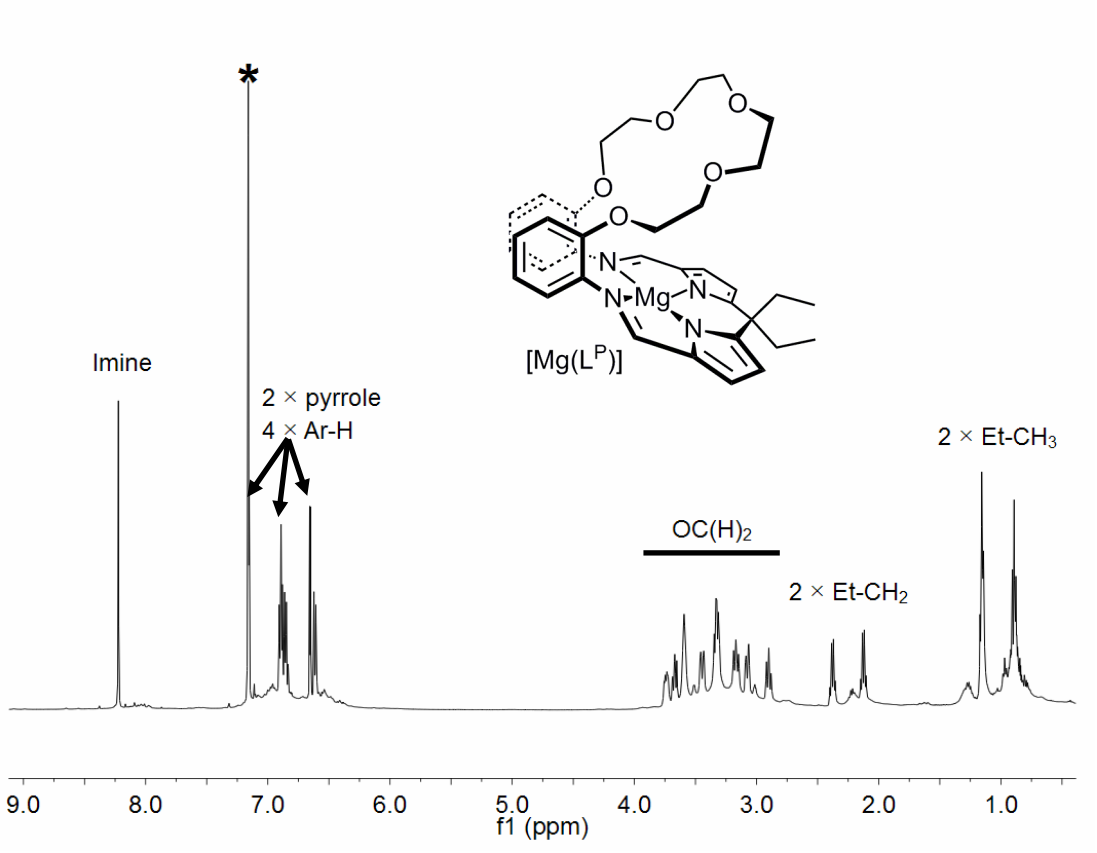

Figure 32: ^{1}H NMR spectrum (C_6D_6) of [Mg(L^P)]. '*' denotes residual protio solvent

The ^{1}H NMR spectra of these complexes supports pacman geometries in solution with two *meso*-ethyl resonances and the desymmetrisation of the ether/amine backbone (Figure 32). The ^{1}H NMR spectrum of [Mg(L^{P})] displays two triplets at 1.16 and 0.89 ppm and two quartets at 2.38 and 2.12 ppm, corresponding to two ethyl environments, and seven separate multiplet resonances between 3.75 and 2.90 ppm, six integrating to two protons and one to four protons, assigned to the desymmetrised ether backbone. The two *meso*-ethyl environments are also observed in the ^{13}C{^{1}H} NMR spectrum at 11.48 and 10.52 ppm (CH_3) and 41.47 and 34.33 ppm (CH_2) with only four ether-CH_2 resonances at 71.04, 70.72, 70.63 and 70.24 ppm indicating only the protons of the ether backbone are desymmetrised.

Similarly, the ^{1}H NMR spectrum of [Mg(L^{NMe})] displays two ethyl environments at 0.95 and 0.85 ppm (CH_3) and two overlapping resonances between 2.31–2.21 ppm (CH_2); these data are reflected in the ^{13}C{^{1}H} NMR spectrum at 10.48 and 10.19 ppm (CH_3) and 38.67 and 38.03 ppm (CH_2). Again, resolution of the amine/ether CH_2 protons is observed (four multiplets at *ca.* 3.58, 3.03, 2.42 and 2.05 ppm) with only two corresponding ^{13}C{^{1}H} NMR resonances (55.48 and 48.83 ppm). All of these assignments were confirmed by COSY and ^{1}H-^{13}C HSQC NMR analysis.

Furthermore, the ^{1}H NMR spectra of both complexes show the disappearance of the NH resonance at *ca.* 9.2 ppm, the loss of which is also seen in the IR spectra along with a shifting of the imine absorbance from *ca.* 1620 to 1565 cm^{-1}. The EI mass spectrum shows a molecular ion peak for [Mg(L^{P})] at 621 amu with a peak at 503 amu corresponding to fragmented [Mg(L^{NMe})]–Et–Me. Both complexes were characterised by elemental analysis.

Unfortunately, attempts at synthesising complexes *via* salt-elimination reactions of [Mg($L^{P/NMe}$)] resulted in a mixture of products by ^{1}H NMR spectroscopy. With successful synthesis already demonstrated *via* [K_2($L^{P/NMe}$)], it was decided to concentrate on using the potassium salt route in any reactions with metal halides.

2.3.6 Synthesis of [Fe($L^{P/NMe}$)], [Mn($L^{P/NMe}$)] and [2+2]-ligand complexes

Enzymes containing iron or manganese are capable of carrying out transformations of small molecules that are challenging to replicate in a laboratory environment. For example, Photosystem II catalyses water oxidation in plants and

contains a multi-nuclear manganese-calcium cubane at its active site. Furthermore, iron containing proteins such as cytochrome c oxidase,[81] which reduces dioxygen to water, nickel-iron hydrogenase,[82] which oxidises H_2, and iron-molybdenum nitrogenase[83] which fixes nitrogen to ammonia, are ubiquitous in nature. Furthermore, iron and manganese complexes of cofacial diporphyrins[2, 84] and iron complexes of hangman porphyrins have been shown to carry out oxygen redox chemistry.[2, 85] As mentioned in Chapter 1, monomeric Fe-OH (Fe^{II} or Fe^{III}) complexes are rare due to the propensity to form bridged oxo/hydroxo system, as seen with pacman porphyrins and the symmetric Schiff-base pyrrole macrocycle.[7, 86] As such, attempts were made to synthesise Fe and Mn complexes of L^P and L^{NMe}.

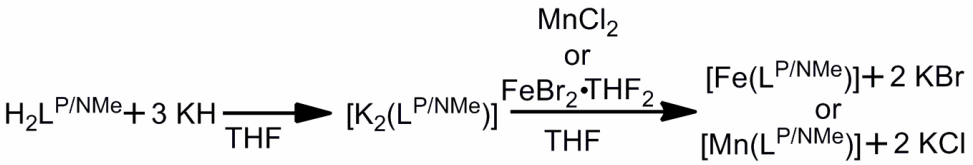

Equation 8

The filtration of *in-situ* generated $[K_2(L^P)]$ or $[K_2(L^{NMe})]$ onto a stirring suspension of $FeBr_2{\cdot}THF_2$ in THF resulted in a colour change from orange to deep red and the isolation of the iron complexes $[Fe(L^P)]$ or $[Fe(L^{NMe})]$ after work up (yield *ca.* 60 %, Equation 8). The ^1H NMR spectra of these complexes are paramagnetically shifted and broadened, though the number of resonances and their integrals are consistent with pacman geometries. Parent ion peaks are seen in the EI mass spectra at 577 ($[Fe(L^{NMe})]$) and 652 amu ($[Fe(L^P)]$), and though the isotope pattern is consistent with formation of $[Fe(L^{P/NMe})]$, low intensity, high mass peaks are also seen in the mass spectrum of $[Fe(L^P)]$ at 1304 and 1277 and indicate the presence of a small amount of a higher cyclisation product. The IR spectra show the disappearance of the NH stretch at *ca.* 3200 cm^{-1} and the imine absorbance shifting to *ca.* 1560 cm^{-1}, from 1620 cm^{-1}. The elemental analysis of $[Fe(L^{NMe})]$ supports its formulation.

In a similar manner, the salt-elimination reaction of $[K_2(L^{P/NMe})]$ with $MnCl_2$ resulted in a colour change from red to deep red and the formation of $[Mn(L^P)]$ or $[Mn(L^{NMe})]$. The ^1H NMR spectra are silent, and with all crystallisation attempts unsuccessful, the structures of these complexes cannot be deduced. However, elemental analysis support their formulations, and the mass spectra exhibit molecular ions at

*m/*z = 577 [Mn(L^{NMe})] and 651 [Mn(L^{P})]. Furthermore, the standard loss of NH stretch and shift in the imine absorbance to *ca.* 1560 cm^{-1} were again observed.

Attempts to grow crystals of [Fe($L^{P/NMe}$)] and [Mn($L^{P/NMe}$)] were unsuccessful. However, a small amount of crystalline material corresponding to [2+2] ligand by-products were isolated from THF solutions of [Fe(L^{P})] and [Mn(LP)] (Scheme 7, Figure 33, Table 11).

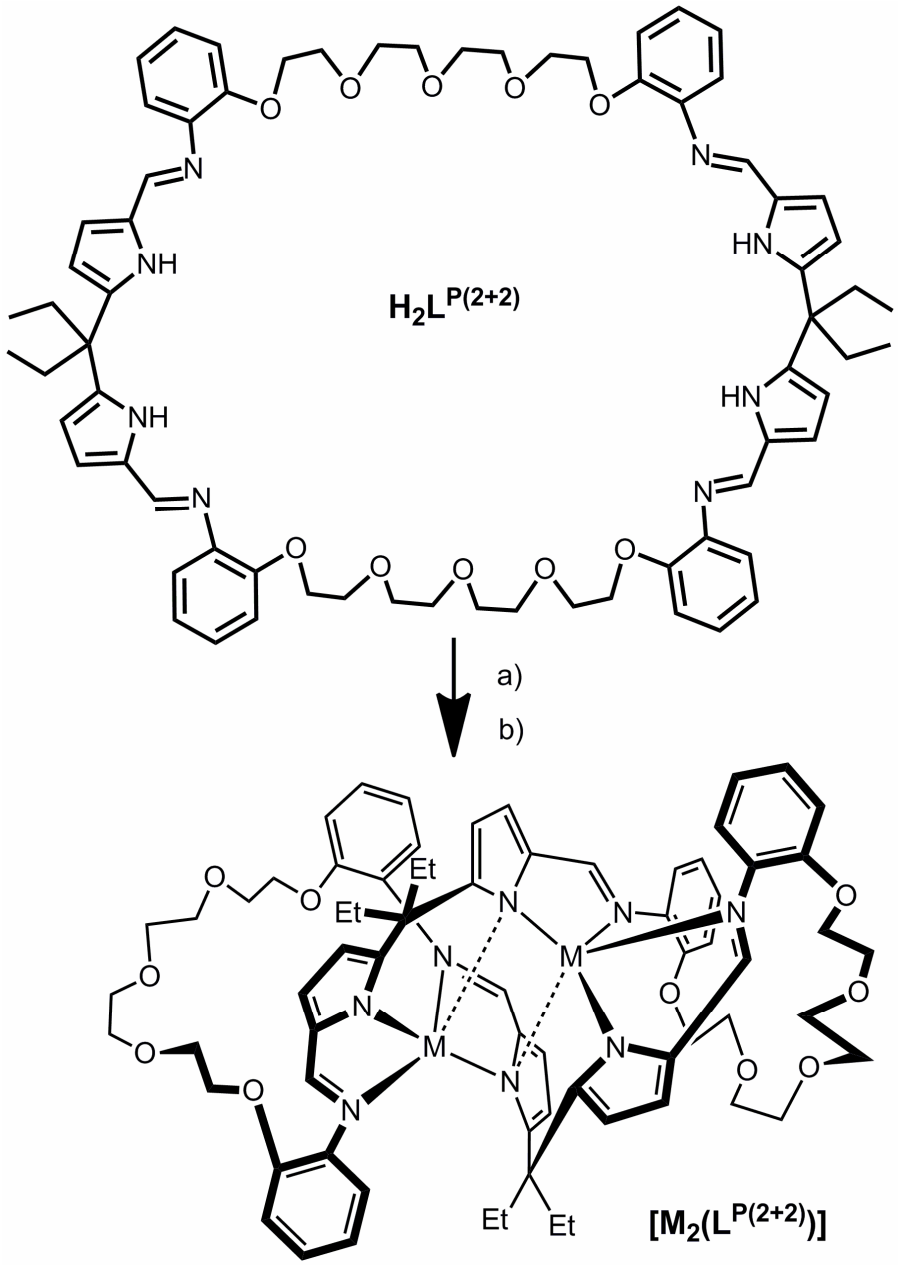

Scheme 7: [2+2] ligand $H_2L^{P(2+2)}$ (top) helicate [$M_2(L^{P(2+2)})$] (M = Mn or Fe) (bottom). a) 3 KH, THF b) 2 $FeBr_2$·THF_2 or 2 $MnCl_2$, THF

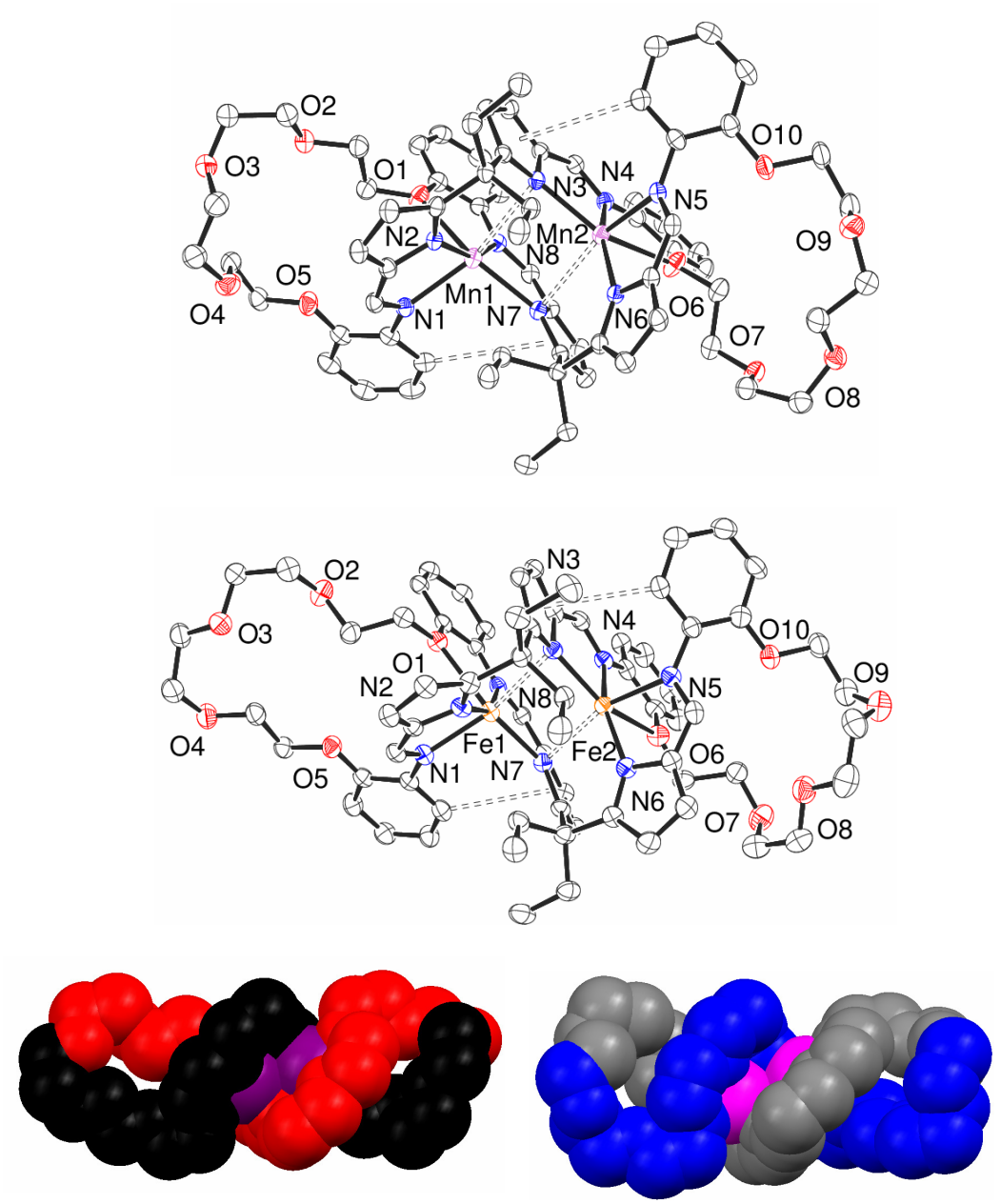

Figure 33: X-ray crystal structure of [2+2] ligand complexes [$Mn_2(L^{P(2+2)})$] (top) and [$Fe_2(L^{P(2+2)})$] (middle). For clarity, all hydrogen atoms are omitted and displacement ellipsoids are drawn at 50% probability. Space filling model shows helical structure of [$Fe_2(L^{P(2+2)})$] (bottom left) and [$Mn_2(L^{P(2+2)})$] (bottom right), for clarity only the macrocyclic backbone is shown

As stated earlier, the ^{1}H NMR spectra of $H_2L^{P/NMe}$ showed the presence of small, broad resonances similar to the major resonances, and the mass spectrum indicated the possible formation of small amounts of a [2+2] cyclisation product. The crystals grown from solutions of [$Fe(L^P)$] and [$Mn(L^P)$] support this observation.

Table 11: Selected bond lengths (Å) and angles (°) of [[$Fe_2(L^{P(2+2)})$] and [$Mn_2(L^{P(2+2)})$]

	[$Fe_2(L^{P(2+2)})$]	[$Mn_2(L^{P(2+2)})$]
M-N_{im}	2.118(4)/2.130(4)	2.1536(15)/2.1622(15)
M-N_{im} (axial)	2.192(4)/2.216(4)	2.2293(15)/2.2505(15)
M-N_{py}	2.049(4)–2.178(4)	2.0943(15)–2.2205(15)
M1···M2	3.151	3.521
O···M	2.508/2.474	2.4658(13)/2.5145(15)
N_{im}-M-N_{im}	99.84(14)/99.14(14)	107.84(6)/109.84(5)
N_{im}-M-N_{py}	79.48(14)–79.92(14)	78.22(6)–79.27(6)
N_{py}-M-N_{py}	127.44(14)/126.83(15)	124.69(6)/124.52(5)
N_{im}-M-O	68.79/68.46	66.72(5)/67.53(5)
N_{py}-M-O	84.20/84.80	89.87(5)/88.94(5)
N_3O···M	0.023/0.002	0.101/0.096

The complexes of a [2+2] L^P-ligand ($L^{P(2+2)}$) adopt a twisted, helicate structure. The imine-pyrrole core of these Fe and Mn complexes are similar in structure. The metals reside in a distorted octahedral environment, slightly out of an N_3O plane (N_3O···Fe 0.002 and 0.023 Å, N_3O···Mn 0.101 and 0.096 Å) made from two pyrrolic and one imine-nitrogen and an ethereal oxygen. A further imino-nitrogen occupies one axial position with the other a weak interaction between the metal and the nitrogen of another pyrrole (M···N distance of 2.530 and 2.565 Å (Fe) and 2.770 and 2.795 (Mn) Å). The Fe-N_{py} distances (2.049(4)–2.178(4) Å) and Fe-N_{im} distances (2.118(4)–2.130(4) Å) are longer than that of imine-pyrrole chelates (Scheme 9, **8**) (Fe-N_{py} 2.016(2) and 2.021(2) Å, Fe-N_{im} 2.104(2) and 2.107(2) Å) and symmetric ligand iron-complexes (Fe-N_{py} 2.009(7)–2.025(6), Fe-N_{im} 2.096(6)–2.176(4) Å).[7] These distances are however within the ranges of iron-porphyrin (Fe-N_{py} 1.972(4)–2.261(5))[87] and iron-imine complexes (1.984(2)–2.241(5)).[88] Mn-N distances (Mn-N_{py} 2.0943(15)–2.2205(15) Å, Mn-N_{im} 2.1536(15)/2.1622(15) Å) are similar to that of Mn complexes of imine-pyrrole chelates (Scheme 9, **8**) (Mn-N_{py} 2.086(2) Å, Mn-N_{im} 2.162(2) and 2.169 Å).[89]. An intramolecular face-to-edge π-stacking interaction between and arene hinge and a

pyrrole unit is also observed for these two complexes (C_{arene}-centroid$_{py}$ 3.361 and 3.336 Å (Fe), 3.632 and 3.969 Å (Mn)). Intermolecular π-stacking is present in [$Mn_2(L^{P(2+2)})$] between two arene units (centroid$_{arene}$-centroid$_{arene}$ 3.579 Å) as well as weak face-to-edge π-stacking interactions C_{arene}-centroid$_{py}$ 3.955 Å).

Further to these $L^{P(2+2)}$ complexes, a crystal suitable for single crystal X-ray diffraction studies was grown by hexane diffusion into a THF solution of [$Co(L^{NMe})$] yielding a [2+2] L^{NMe}-ligand complex of cobalt [$Co_2(L^{NMe(2+2)})$] (Scheme 8, Figure 34, Table 12).

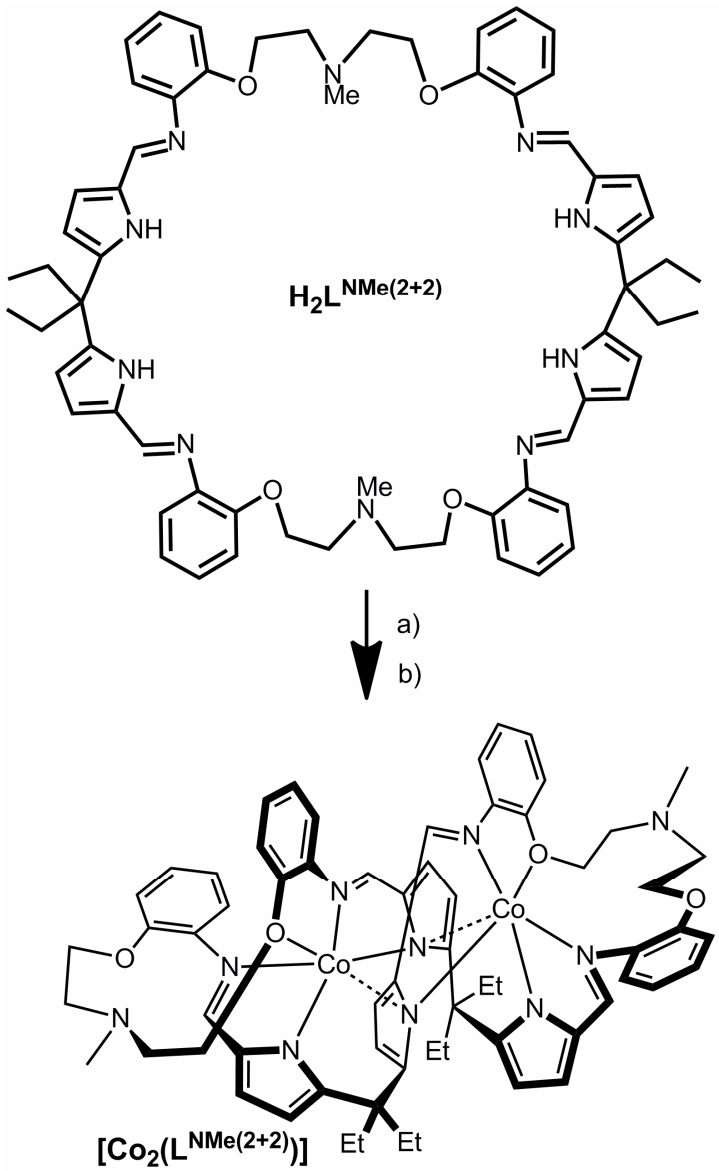

Scheme 8: [2+2] ligand $H_2L^{NMe(2+2)}$ (top) helicate [$Co_2(L^{NMe(2+2)})$] (bottom). a) 3 KH, THF b) 2 $CoCl_2$, THF

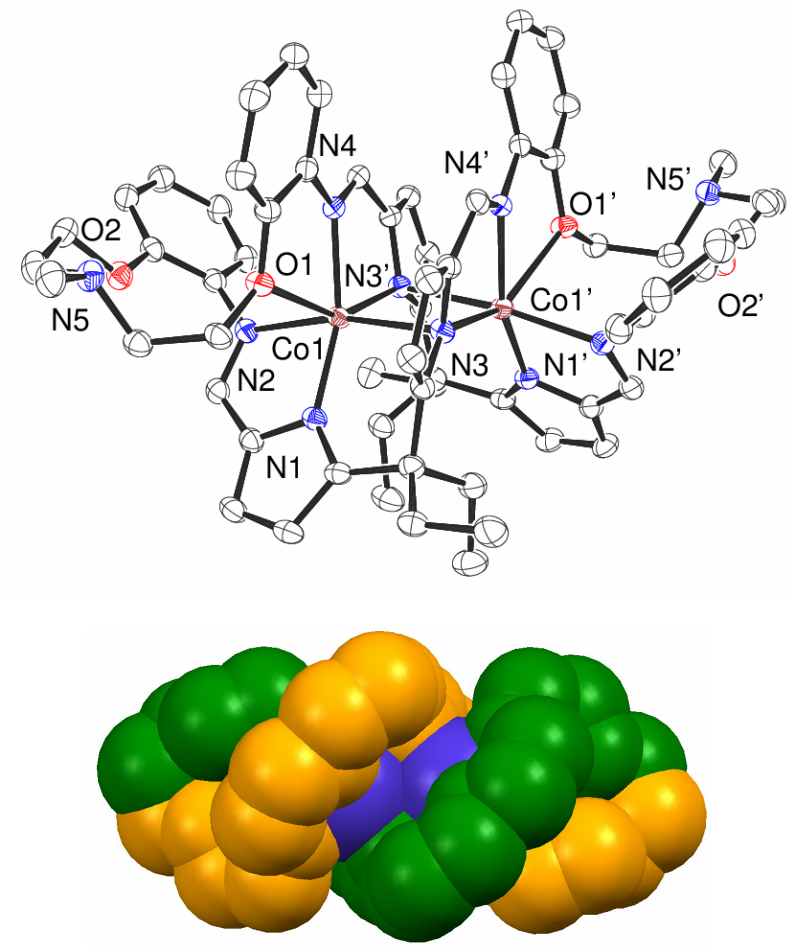

Figure 34: X-ray crystal structure of [2+2] ligand complexes [$Co_2(L^{NMe(2+2)})$] (top). For clarity, all hydrogen atoms are omitted and displacement ellipsoids are drawn at 50% probability. Space filling model shows helical structure of [$Co_2(L^{NMe(2+2)})$] (bottom). For clarity, only the macrocyclic backbone is shown

Table 12: Selected bond lengths (Å) and angles (°) of [$Co_2(L^{NMe(2+2)})$]

Co1-N1	2.125(2)	N4-Co1-N3	81.05(7)
Co1-N2	1.997(2)	N2-Co1-N3	125.04(7)
Co1-N3	2.1642(19)	N2-Co1-N1	98.74(8)
Co1-N4	2.072(2)	N4-Co1-O1	68.68
Co1···O1	2.488	N2-Co1-O1	85.21
Co1···Co1'	3.104	N_3O···Co1	0.024
N1-Co1-N4	98.74(8)		

Again, a twisted helicate structure is observed. The cobalt sits in a distorted octahedral environment, residing 0.024 Å out of an N_3O-equatorial plane. The axial ligands comprise of an imine nitrogen as well as a weak pyrrole-N interaction (Co···N_{py} 2.481 Å) akin to the above $L^{P(2+2)}$ complexes. Co-N bond distances (Co-N_{py} 1.997(2) and 2.1642(19) Å and Co-N_{im} 2.072(2) and 2.125(2) Å) are slightly longer than corresponding imine-pyrrole chelate (Scheme 9) (Co-N_{py} 1.980(3) and 1.989(3) Å and Co-N_{im} 2.047(3) and 2.055(3) Å) as well as marginally longer than symmetric ligand cobalt complexes (Co-N_{py} 1.847–1.970(8) Å, N_{im} 1.856(7)–1.984(4) Å)[5, 35] and [Co(L^P)] complexes (Co-N_{py} 1.852(3)–1.8818(18) Å, Co-N_{im} 1.981(1)–2.0335(18) Å). Intermolecular face-to-edge π-stacking interactions between two arene units ($centoid_{arene}$- $centoid_{arene}$ 3.438 Å) are also observed.

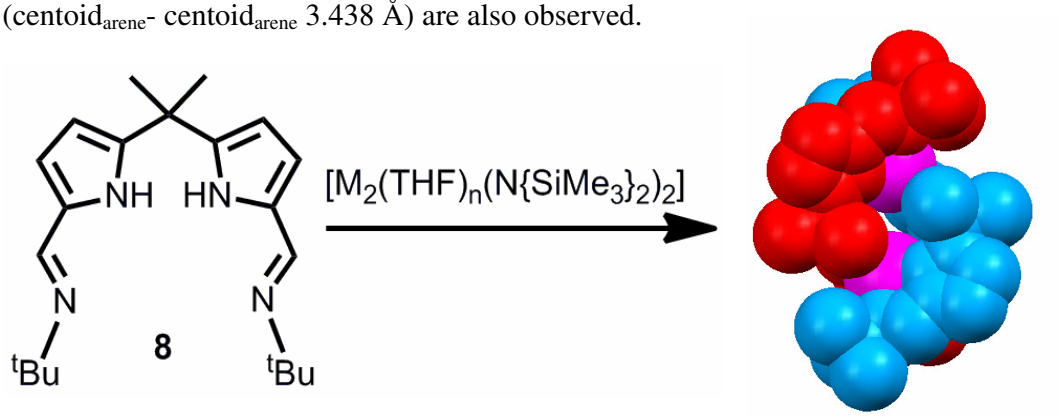

Scheme 9: Synthesis of a bis-metallated helicate from an imine-pyrrole chelate. Space-filling crystal structure shows the two ligands (red and blue) bound to two metal centres (pink). (M = Mn n = 2, Fe n = 1, Co n = 2)[89]

The imine-pyrrole core of all three [2+2]-ligand helicate complexes closely resemble that of helicates of imine-pyrorle chelates synthesised by the Love group (Scheme 9). In all cases, twisting around the *meso*-carbon allows adjacent pyrrole units to complex two metal centres with spontaneous formation of helicate structures. The presence of ether/amine groups in the [2+2]-ligands enable a distorted octahedral, rather than distorted tetrahedral, coordination as seen with complexes of **8**. This results in much shorter M···M distances compared to the imine-pyrrole chelates ([2+2] M···M distances 3.151 (Fe), 3.521 (Mn) and 3.104 Å (Co) compared to 4.689, 4.751 and 4.914 Å respectively). The M···M separations do indicate some metal-metal interactions, albeit weak ones. A similarity between the two systems however is the presence of a major and minor groove motif, thought to be due to a degree of π-π-stacking between imine/pyrrole

and arene groups (Figure 35), further inspection of the structure revealed a racemic mixture of helicates are present in the unit cell.

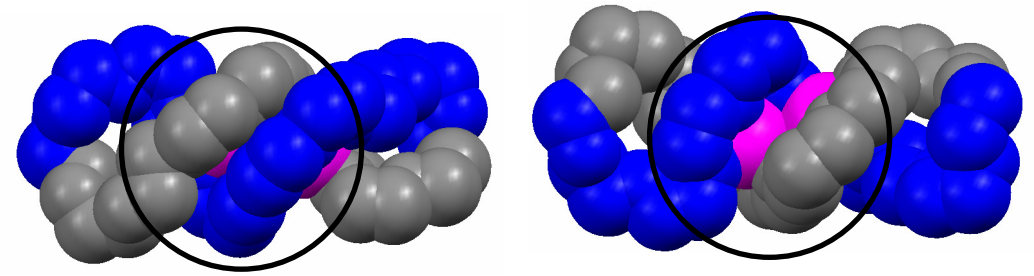

Figure 35: Space-filling models of [$Mn_2(L^{P(2+2)})$] showing the minor (left) and major groove (right). For clarity, only the macrocyclic backbone is shown

Thus, the flexibility of the ether/amine linkers does not hinder the formation of helical structures as seen with the discreet imine-pyrrole chelates **8**. It is thought that the [2+2] ligand complexes crystallised preferentially and only represent a small fraction of the bulk. The molecular ion peaks in the mass spectra of bulk [$Fe(L^P)$], [$Mn(L^P)$] and [$Co(L^{NMe})$] show an isotope pattern consistent with a [1+1] ligand complex with high-mass peaks of a very low intensity. Work on synthesising [2+2] ligands in preference to [1+1] or the linking of imine/pyrrole chelates with other flexible linkers is yet to be investigated.

2.3.7 Group 1 metal binding by complexes of L^P

It was envisaged that the poly-ether backbone of L^P would be able to bind alkali-metal cations due to its close resemblance to 15-crown-5 (Figure 36).

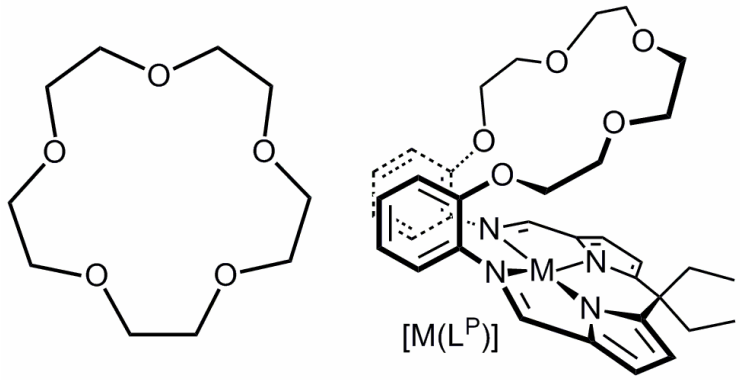

Figure 36: 15-crown-5 (left) is comparable to the polyether binding pocket of [$M(L^P)$] (right). M = metal

Though not a true crown-ether, there are many examples of quasi-crown ethers binding Group one cations, for example in the binding of potassium by calixarene-based

polyethers by the Kim group,[90] sodium by Lai and co-workers[91] or lithium by the Merz and Lex groups (Figure 37).[92]

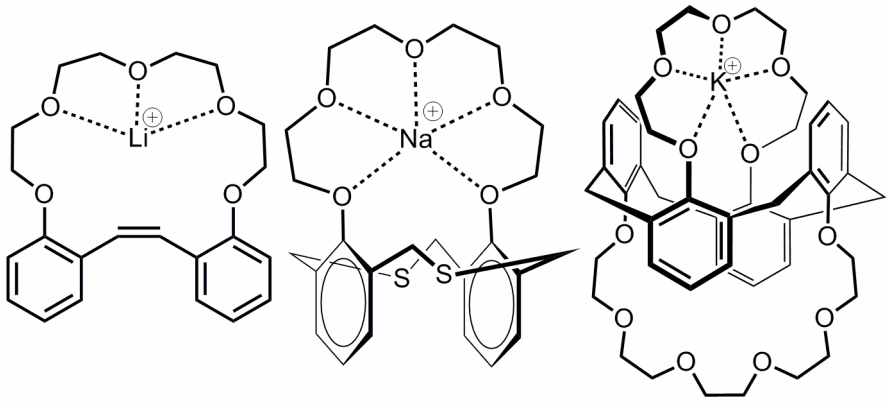

Figure 37: Examples of quasi-crown ethers binding group 1 metals by the Merz and Lex group[92] (left), the Lai group[91] (middle) and Kim and co-workers[90] (right)

Unfortunately, all efforts to use complexes of L^P to bind Group 1 metals were unsuccessful. It was envisaged that reaction with a potassium salt such as KCl would result in K^+ binding due the potential to form a bridged structure. The addition of salts such as LiCl, LiBr, LiI, NaCl, NaBr, $NaBF_4$, KCl, KBr, KI and KPF_6 to metal complexes of L^P (Scheme 10) resulted in either isolation of starting materials or, in the case of the cobalt complexes, the binding of a halide to the oxidised metal centre, combined presumably with the formation of KOH.

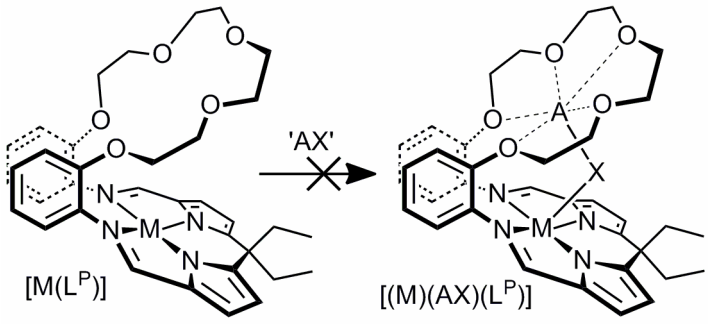

Scheme 10: Attempts at Group 1 incorporation have so far been unsuccessful

The addition of Group 1 metal salts such as KI or LiI to $[M(L^P)]$ complexes in THF showed no chemical shift changes in the ^1H NMR spectrum which implies that binding does not occur.

2.4 Conclusion

Two new [1+1] macrocycles, L^P and L^{NMe}, have been synthesised selectively and in high yield by a straightforward, three or four step route. The macrocycles contain two distinct binding pockets: an N_4 pocket, consisting of two imine and two pyrrole nitrogen donors as well as a neutral poly-ether (L^P) or ether/amine (L^{NMe}) binding pocket. These macrocycles have been shown to fold into a wedge-shaped pacman geometry in both the solid and solution state upon metallation. The successful syntheses of the complexes $[Pd(L^P)]$, $[Pd(L^{NMe})]$, $[K_2(L^P)]$, $[K_2(L^{NMe})]$, $[Co(L^P)]$, $[Co(L^{NMe})]$, $[(VCl)(L^P)]$, $[(VCl)(L^{NMe})]$, $[(TiCl)(L^P)]$, $[(TiCl)(L^{NMe})]$, $[Mg(L^P)]$, $[Mg(L^{NMe})]$, $[Fe(L^P)]$, $[Fe(L^{NMe})]$, $[Mn(L^P)]$ and $[Mn(L^{NMe})]$ have been described and characterised. Most complexes have been shown to adopt a pacman conformation in the solid and solution state, except for the potassium salt complexes $[K_2(L^{P/NMe})]$; further investigation is needed to determine the structures of $[Fe(L^{P/NMe})]$ and $[Mn(L^{P/NMe})]$. Exposure of $[Co(L^P)]$ or $[Co(L^{NMe})]$ to air results in oxidation to Co(III) complexes concurrent with the coordination of a molecule of water within the cleft. This feature underlines the ability of these macrocycle to engage in secondary sphere hydrogen-bonding interactions. Furthermore, a potential new area of supramolecular chemistry research has been uncovered. The air oxidation of $[Co(L^P)]$ and subsequent crystallisation from a benzene solution results in the formation of a six-membered pacman crenellated wheel structure which stack in the solid state to form large columns that are formed around a water channel. Attempts to activate dinitrogen through the reduction of vanadium and titanium complexes of L^P and L^{NMe} requires further study, as does the study of the reactivity of all of these complexes towards small molecules such as CO, CO_2 or H_2. Further to this, evidence for the formation of [2+2]-ligand products was uncovered with the crystallisation of $[Fe_2(L^{P(2+2)})]$, $[Mn_2(L^{P(2+2)})]$ and $[Co_2(L^{NMe(2+2)})]$ with all three complexes adopting helicate-type structure in the solid state. With the successful synthesis and characterisation of L^P and L^{NMe} complexes, studies into ligand modification will be discussed in the next chapter.

2.5 References

† Funded by the Japanese Society for the Promotion of Science (JSPS) summer program, two months were spent at the Tokyo Institute of Technology under the supervision of Prof. Hiroyuki Kawaguchi during summer 2009. Though the main focus of the research carried out in Japan was on niobium chemistry (see Chapter 4), the solid-state structure of [Pd(L^{NMe})] was gained whist in Japan. Data were collected with the help of Dr. Yutaka Ishida.

[1] C. J. Chang, Z.-H. Loh, C. Shi, F. C. Anson, D. G. Nocera, *J. Am. Chem. Soc.* **2004**, *126*, 10013; R. Guilard, F. Jérôme, C. P. Gros, J.-M. Barbe, Z. Ou, J. Shao, K. M. Kadish, *C. R. l'Academie. Sci., Ser. IIC Chem.* **2001**, *4*, 245.

[2] J. Rosenthal, D. G. Nocera, *Acc. Chem. Res.* **2007**, *40*, 543.

[3] G. Givaja, A. J. Blake, C. Wilson, M. Schroder, J. B. Love, *Chem. Commun.* **2003**, 2508.

[4] G. Givaja, M. Volpe, M. A. Edwards, A. J. Blake, C. Wilson, M. Schröder, J. B. Love, *Angew. Chem., Int. Ed. Engl.* **2007**, *46*, 584.

[5] E. Askarizadeh, A. M. J. Devoille, D. M. Boghaei, A. M. Z. Slawin, J. B. Love, *Inorg. Chem.* **2009**, *48*, 7491.

[6] E. Askarizadeh, S. B. Yaghoob, D. M. Boghaei, A. M. Z. Slawin, J. B. Love, *Chem. Commun.* **2010**, *46*, 710.

[7] J. M. Veauthier, W.-S. Cho, V. M. Lynch, J. L. Sessler, *Inorg. Chem.* **2004**, *43*, 1220.

[8] R. McGuire Jr, D. K. Dogutan, T. S. Teets, J. Suntivich, Y. Shao-Horn, D. G. Nocera, *Chem. Sci.* **2010**, *1*, 411.

[9] C.-Y. Yeh, C. J. Chang, D. G. Nocera, *J. Am. Chem. Soc.* **2001**, *123*, 1513.

[10] C.-S. Chang, Y.-T. Lin, S.-R. Shih, C.-C. Lee, Y.-C. Lee, C.-L. Tai, S.-N. Tseng, J.-H. Chern, *J. Med. Chem.* **2005**, *48*, 3522.

[11] X. Shen, H. Liu, Y. Li, S. Liu, *Macromolecules* **2008**, *41*, 2421.

[12] G. R. Pettit, D. S. Blonda, R. A. Upham, *Can. J. Chem.* **1965**, *43*, 1798

[13] J. M. Desper, D. R. Powell, S. H. Gellman, *J. Am. Chem. Soc.* **1990**, *112*, 4321.

[14] I. Vujasinovic, J. Veljkovic, K. Mlinaric-Majerski, *J. Org. Chem.* **2004**, *69*, 8550.

[15] V. B. Gawandi, H. Mohan, J. P. Mittal, *J. Chem. Soc., Perkin Trans. 2* **1999**, 1425.

[16] J. Wang, T. Zeng, M.-L. Li, E.-H. Duan, J.-S. Li, *Acta Crystallogr., Sect. E.* **2006**, *62*, 2912.

[17] M. J. Belousoff, M. B. Duriska, B. Graham, S. R. Batten, B. Moubaraki, K. S. Murray, L. Spiccia, *Inorg. Chem.* **2006**, *45*, 3746.

[18] H. Adams, R. Bastida, D. E. Fenton, B. E. Mann, L. Valencia, *Eur. J. Org. Chem.* **1999**, *1999*, 1843.

[19] P. Even, B. Boitrel, *Coord. Chem. Rev.* **2006**, *250*, 519.

[20] K. Durr, B. P. Macpherson, R. Warratz, F. Hampel, F. Tuczek, M. Helmreich, N. Jux, I. Ivanovic-Burmazovic, *J. Am. Chem. Soc.* **2007**, *129*, 4217.

[21] F. D'Souza, R. Chitta, S. Gadde, M. E. Zandler, A. S. D. Sandanayaka, Y. Araki, O. Ito, *Chem. Commun.* **2005**, 1279.

[22] M. Lochner, M. Meuwly, W.-D. Woggon, *Chem. Commun.* **2003**, 1330.

[23] L. Michaudet, P. Richard, B. Boitrel, *Tetrahedron Lett.* **2000**, *41*, 8289.

[24] S. Banfi, A. Manfredi, F. Montanari, G. Pozzi, S. Quici, F. Ursino, *J. Mol. Catal. A* **1996**, *113*, 369.

[25] T. I. Oprea, G. Hummer, A. E. Garcia, *Proc. Natl. Acad. Sci. U. S. A.* **1997**, *94*, 2133.

[26] R. M. Henry, C.-H. Yu, T. Rodinger, R. Pomès, *J. Mol. Biol.* **2009**, *387*, 1165.

[27] J. W. Leeland, A. M. Z. Slawin, J. B. Love, *Organometallics* **2010**, *29*, 714.

[28] G. Givaja, M. Volpe, J. W. Leeland, M. A. Edwards, T. K. Young, S. B. Darby, S. D. Reid, A. J. Blake, C. Wilson, J. Wolowska, E. J. L. McInnes, M. Schröder, J. B. Love, *Chem. Eur. J.* **2007**, *13*, 3707.
[29] M. Volpe, S. D. Reid, A. J. Blake, C. Wilson, J. B. Love, *Inorg. Chim. Acta* **2007**, *360*, 273.
[30] J. Arnold, D. Y. Dawson, C. G. Hoffman, *J. Am. Chem. Soc.* **1993**, *115*, 2707.
[31] S. D. Reid, A. J. Blake, C. Wilson, J. B. Love, *Inorg. Chem.* **2005**, *45*, 636.
[32] M. Tayebani, S. Conoci, K. Feghali, S. Gambarotta, G. P. A. Yap, *Organometallics* **2000**, *19*, 4568.
[33] S.-Z. Fu, D.-Q. Wang, J.-M. Dou, *Acta Crystallogr., Sect. E.* **2007**, *63*, m1522; M. J. Zaworotko, C. R. Kerr, J. L. Atwood, *Organometallics* **1985**, *4*, 238; J.-M. Lu, S. V. Rosokha, S. V. Lindeman, I. S. Neretin, J. K. Kochi, *J. Am. Chem. Soc.* **2005**, *127*, 1797.
[34] A. F. Richards, M. Brynda, P. P. Power, *J. Am. Chem. Soc.* **2004**, *126*, 10530; P. B. Hitchcock, M. F. Lappert, G. A. Lawless, B. Royo, *J. Chem. Soc., Chem. Commun.* **1993**, 554.
[35] M. Volpe, H. Hartnett, J. W. Leeland, K. Wills, M. Ogunshun, B. J. Duncombe, C. Wilson, A. J. Blake, J. McMaster, J. B. Love, *Inorg. Chem.* **2009**, *48*, 5195.
[36] W.-B. Yuan, H.-Y. Wang, J.-F. Du, S.-W. Chen, Q. Zhang, *Acta Crystallogr., Sect. E.* **2006**, *62*, m3504; G. Fachinetti, C. Floriani, P. F. Zanazzi, A. R. Zanzari, *Inorg. Chem.* **1978**, *17*, 3002.
[37] D. V. Konarev, S. S. Khasanov, G. Saito, R. N. Lyubovskaya, Y. Yoshida, A. Otsuka, *Chem. Eur. J.* **2003**, *9*, 3837; V. V. Smirnov, E. K. Woller, S. G. DiMagno, *Inorg. Chem.* **1998**, *37*, 4971.
[38] P. Charpin, M. Nierlich, D. Vigner, M. Lance, P. Thuery, J. Zarembowitch, F. D'Yvoire, *J. Chem. Crystall.* **1988**, *18*, 429; N. Bresciani, M. Calligaris, G. Nardin, L. Randaccio, *J. Chem. Soc., Dalton Trans.* **1974**, 498.
[39] M. J. Rodríguez, M. I. Fernández, A. M. González-Noya, M. Maneiro, R. Pedrido, M. Vázquez, B. Donnadieu, M. R. Bermejo, *Z. Anorg. Allg. Chem.* **2005**, *631*, 2161.
[40] J. Xing, *Acta Crystallogr., Sect. E.* **2009**, *65*, m468.
[41] P. V. Bernhardt, E. J. Hayes, *Inorg. Chem.* **2002**, *41*, 2892; M. Ghiladi, J. T. Gomez, A. Hazell, P. Kofod, J. Lumtscher, C. J. McKenzie, *Dalton Trans.* **2003**, 1320.
[42] J. W. Leeland, F. J. White, J. B. Love, *Chem. Commun.* **2011**, *47*, 4132.
[43] L. Brammer, in *Crystal Design: Structure and Function, Vol. 7* (Ed.: G. R. Desiraju), John Wiley & Sons, Ltd, **2003**; D. Braga, F. Grepioni, G. R. Desiraju, *Chem. Rev.* **1998**, *98*, 1375.
[44] D. Braga, F. Grepioni, P. Sabatino, G. R. Desiraju, *Organometallics* **1994**, *13*, 3532.
[45] M. Affronte, S. Carretta, G. A. Timco, R. E. P. Winpenny, *Chem. Commun.* **2007**, 1789.
[46] N. Hoshino, A. M. Ako, A. K. Powell, H. Oshio, *Inorg. Chem.* **2009**, *48*, 3396; H. Imai, T. Akutagawa, F. Kudo, M. Ito, K. Toyoda, S.-i. Noro, L. Cronin, T. Nakamura, *J. Am. Chem. Soc.* **2009**, *131*, 13578; D.-L. Long, R. Tsunashima, L. Cronin, *Angew. Chem., Int. Ed. Engl.* **2010**, *49*, 1736; T. C. Stamatatos, S. Mukherjee, K. A. Abboud, G. Christou, *Chem. Commun.* **2009**, 62.
[47] H. N. Miras, G. J. T. Cooper, D.-L. Long, H. Bogge, A. Muller, C. Streb, L. Cronin, *Science* **2010**, *327*, 72.
[48] J. Hamblin, F. Tuna, S. Bunce, L. J. Childs, A. Jackson, W. Errington, N. W. Alcock, H. Nierengarten, A. Van Dorsselaer, E. Leize-Wagner, M. J. Hannon, *Chem. Eur. J.* **2007**, *13*, 9286.
[49] Z. Wang, S. M. Cohen, *Chem. Soc. Rev.* **2009**, *38*, 1315; J. Lee, O. K. Farha, J. Roberts, K. A. Scheidt, S. T. Nguyen, J. T. Hupp, *Chem. Soc. Rev.* **2009**, *38*, 1450.

[50] K. Oyaizu, E. Tsuchida, *J. Am. Chem. Soc.* **2003**, *125*, 5630.
[51] E. Kuhn, V. Bulach, M. W. Hosseini, *Chem. Commun.* **2008**, 5104.
[52] M. Hoffmann, J. Kärnbratt, M.-H. Chang, L. M. Herz, B. Albinsson, H. L. Anderson, *Angew. Chem., Int. Ed. Engl.* **2008**, *47*, 4993.
[53] C. T. Cohen, C. M. Thomas, K. L. Peretti, E. B. Lobkovsky, G. W. Coates, *Dalton Trans.* **2006**, 237.
[54] N. Bricklebank, S. M. Godfrey, C. A. McAuliffe, R. G. Pritchard, *J. Chem. Soc., Dalton Trans.* **1996**, 157; R. Beck, H.-F. Klein, *Z. Anorg. Allg. Chem.* **2008**, *634*, 1971.
[55] A. Voituriez, A. B. Charette, *Adv. Syn. Catal.* **2006**, *348*, 2363; J. L. Sessler, D. Seidel, C. Bucher, V. Lynch, *Chem. Commun.* **2000**, 1473; D.-H. Won, D.-W. Yoon, S.-J. Hong, K. S. Ha, J. L. Sessler, C.-H. Lee, *Bull. Korean Chem. Soc.* **2006**, *27*, 925.
[56] J. Welby, L. N. Rusere, J. M. Tanski, L. A. Tyler, *Inorg. Chim. Acta* **2009**, *362*, 1405.
[57] J.-i. Setsune, H. Takeda, S. Ito, Y. Saito, Y. Ishimaru, K. Fukuhara, Y. Saito, T. Kitao, T. Adachi, *Inorg. Chem.* **1998**, *37*, 2235; O. P. Anderson, D. K. Lavallee, *J. Am. Chem. Soc.* **1977**, *99*, 1404.
[58] J. A. Pool, E. Lobkovsky, P. J. Chirik, *Nature* **2004**, *427*, 527; M. P. Shaver, M. D. Fryzuk, *Adv. Syn. Catal.* **2003**, *345*, 1061; M. D. Fryzuk, J. B. Love, S. J. Rettig, V. G. Young, *Science* **1997**, *275*, 1445; M. D. Fryzuk, S. A. Johnson, *Coord. Chem. Rev.* **2000**, *200-202*, 379; N. Kuganathan, J. C. Green, H.-J. Himmel, *New J. Chem.* **2006**, *30*, 1253.
[59] R. Ferguson, E. Solari, C. Floriani, D. Osella, M. Ravera, N. Re, A. Chiesi-Villa, C. Rizzoli, *J. Am. Chem. Soc.* **1997**, *119*, 10104.
[60] S. M. Mullins, A. P. Duncan, R. G. Bergman, J. Arnold, *Inorg. Chem.* **2001**, *40*, 6952.
[61] G. K. B. Clentsmith, V. M. E. Bates, P. B. Hitchcock, F. G. N. Cloke, *J. Am. Chem. Soc.* **1999**, *121*, 10444.
[62] E. F. King, M. L. Good, *Spectrochim. Acta, Part A* **1973**, *29*, 707; A. Arquero, P. Souza, J. A. García-Vázquez, J. R. Masaguer, *Trans. Met. Chem.* **1985**, *10*, 424.
[63] K. Yamamoto, K. Oyaizu, E. Tsuchida, *J. Am. Chem. Soc.* **1996**, *118*, 12665; J.-Q. Wu, L. Pan, N.-H. Hu, Y.-S. Li, *Organometallics* **2008**, *27*, 3840.
[64] D. Reardon, F. o. Conan, S. Gambarotta, G. Yap, Q. Wang, *J. Am. Chem. Soc.* **1999**, *121*, 9318; S. Ciurli, C. Floriani, A. Chiesi-Villa, C. Guastini, *J. Chem. Soc., Chem. Commun.* **1986**, 1401.
[65] K. Ejsmont, R. Kubiak, *Acta Crystallogr., Sect. C.* **1998**, *54*, 1844; D. Reardon, J. Guan, S. Gambarotta, G. P. A. Yap, D. R. Wilson, *Organometallics* **2002**, *21*, 4390.
[66] M. Mazzanti, C. Floriani, A. Chiesi-Villa, C. Guastini, *Inorg. Chem.* **1986**, *25*, 4158; D. G. McCollum, G. P. A. Yap, L. Liable-Sands, A. L. Rheingold, B. Bosnich, *Inorg. Chem.* **1997**, *36*, 2230.
[67] P. L. Arnold, A. J. Blake, C. Wilson, J. B. Love, *Inorg. Chem.* **2004**, *43*, 8206.
[68] N. S. Dean, L. M. Mokry, M. R. Bond, C. J. O'Connor, C. J. Carrano, *Inorg. Chem.* **1996**, *35*, 2818; M. Kosugi, S. Hikichi, M. Akita, Y. Moro-oka, *Inorg. Chem.* **1999**, *38*, 2567; J. C. Dutton, G. D. Fallon, K. S. Murray, *J. Chem. Soc., Chem. Commun.* **1990**, 64; K. Kanamori, T. Okayasu, K. Okamoto, *Chem. Lett.* **1995**, *24*, 105; K. Kanamori, K. Yamamoto, O. Takako, N. Matsui, K. Okamoto, W. Mori, *Bull. Chem. Soc. Jpn.* **1997**, *70*, 3031.
[69] C. D. Beard, R. J. Barrie, J. Evans, W. Levason, G. Reid, M. D. Spicer, *Eur. J. Inorg. Chem.* **2006**, *2006*, 4391; C. J. Carrano, M. Mohan, S. M. Holmes, R. de la Rosa, A. Butler, J. M. Charnock, C. D. Garner, *Inorg. Chem.* **1994**, *33*, 646.

[70] S. J. Coles, M. B. Hursthouse, D. G. Kelly, A. J. Toner, N. M. Walker, *J. Organomet. Chem.* **1999**, *580*, 304; M. Pasquali, F. Marchetti, A. Landi, C. Floriani, *J. Chem. Soc., Dalton Trans.* **1978**, 545.
[71] F. Calderazzo, U. Englert, G. Pampaloni, R. Santi, A. Sommazzi, M. Zinna, *Dalton Trans.* **2005**, 914.
[72] R. Crescenzi, E. Solari, C. Floriani, A. Chiesi-Villa, C. Rizzoli, *Organometallics* **1996**, *15*, 5456; A. Spannenberg, V. V. Burlakov, P. Arndt, M. Klahn, U. Rosenthal, *Z. Kristallogr.-New Cryst. Struct* **2007**, *222*, 192.
[73] D. G. Sekutowski, G. D. Stucky, *Inorg. Chem.* **1975**, *14*, 2192; T. Matsuo, H. Kawaguchi, M. Sakai, *J. Chem. Soc., Dalton Trans.* **2002**, 2536.
[74] M. Talja, M. Klinga, M. Polamo, E. Aitola, M. Leskelä, *Inorg. Chim. Acta* **2005**, *358*, 1061; M. Mazzanti, J.-M. Rosset, C. Floriani, A. Chiesi-Villa, C. Guastini, *J. Chem. Soc., Dalton Trans.* **1989**, 953.
[75] N. C. Smythe, R. R. Schrock, P. Muller, W. W. Weare, *Inorg. Chem.* **2006**, *45*, 9197; H. Gailus, G. Woitha, D. Rehder, *J. Chem. Soc., Dalton Trans.* **1994**, 3471; T. E. Hanna, E. Lobkovsky, P. J. Chirik, *J. Am. Chem. Soc.* **2004**, *126*, 14688.
[76] F. S. Molinaro, J. A. Ibers, *Inorg. Chem.* **1976**, *15*, 2278.
[77] Y. Kashiyama, M. Shiro, R. Tada, Ookouchi, *Chem. Lett.* **2007**, *36*, 706.
[78] Y. Abe, K. Nakabayashi, N. Matsukawa, H. Takashima, M. Iida, T. Tanase, M. Sugibayashi, H. Mukai, K. Ohta, *Inorg. Chim. Acta* **2006**, *359*, 3934; G. Hoshina, S. Ohba, M. Tsuchimoto, *Acta Crystallogr., Sect. C.* **1999**, *55*, 1451.
[79] R. Harada, H. Okawa, T. Kojima, *Inorg. Chim. Acta* **2005**, *358*, 489.
[80] J.-P. Costes, S. Shova, J. M. C. Juan, N. Suet, *Dalton Trans.* **2005**, 2830; K. I. Smith, L. L. Borer, M. M. Olmstead, *Inorg. Chem.* **2003**, *42*, 7410.
[81] T. Tsukihara, H. Aoyama, E. Yamashita, T. Tomizaki, H. Yamaguchi, K. Shinzawa-Itoh, R. Nakashima, R. Yaono, S. Yoshikawa, *Science* **1995**, *269*, 1069.
[82] A. Volbeda, Y. Montet, X. Vernède, E. C. Hatchikian, J. C. Fontecilla-Camps, *Int. J. Hydrogen Energy* **2002**, *27*, 1449; A. Volbeda, M.-H. Charon, C. Piras, E. C. Hatchikian, M. Frey, J. C. Fontecilla-Camps, *Nature* **1995**, *373*, 580.
[83] B. K. Burgess, D. J. Lowe, *Chem. Rev.* **1996**, *96*, 2983.
[84] R. Guilard, S. Brandes, A. Tabard, N. Bouhmaida, C. Lecomte, P. Richard, J.-M. Latour, *J. Am. Chem. Soc.* **1994**, *116*, 10202.
[85] L. L. Chng, C. J. Chang, D. G. Nocera, *Org. Lett.* **2003**, *5*, 2421.
[86] A. J. Kendall, L. N. Zakharov, J. D. Gilbertson, *Inorg. Chem.* **2010**, *49*, 8656; J. M. Hodgkiss, C. J. Chang, B. J. Pistorio, D. G. Nocera, *Inorg. Chem.* **2003**, *42*, 8270.
[87] J. P. Collman, J. L. Hoard, N. Kim, G. Lang, C. A. Reed, *J. Am. Chem. Soc.* **1975**, *97*, 2676; J. P. Battioni, I. Artaud, D. Dupre, P. Leduc, I. Akhrem, D. Mansuy, J. Fischer, R. Weiss, I. Morgenstern-Badarau, *J. Am. Chem. Soc.* **1986**, *108*, 5598.
[88] S. Ross, T. Weyhermuller, E. Bill, K. Wieghardt, P. Chaudhuri, *Inorg. Chem.* **2001**, *40*, 6656; G. J. P. Britovsek, J. England, S. K. Spitzmesser, A. J. P. White, D. J. Williams, *Dalton Trans.* **2005**, 945.
[89] S. D. Reid, A. J. Blake, W. Kockenberger, C. Wilson, J. B. Love, *Dalton Trans.* **2003**, 4387.
[90] J. S. Kim, W. K. Lee, I.-H. Suh, J.-G. Kim, J. Yoon, J. H. Lee, *J. Org. Chem.* **2000**, *65*, 7215.
[91] J. Xu, Y.-H. Lai, *Org. Lett.* **2002**, *4*, 3211.
[92] A. Merz, T. Futterer, J. Lex, H. Inerowicz, *Angew. Chem., Int. Ed. Engl.* **1997**, *36*, 278.

Chapter 3: Modifications to asymmetric macrocycles and their complexes

3.1 Introduction

Once proof of principal has been established for a given ligand set, tailoring of reactivity through ligand modification is the next important step. The evolution of pacman porphyrins, as discussed in chapter one, started with doubly-strapped cofacial diporphyrins,[1] through two generations of single-pillared diporphyrins[2] to end with hangman porphyrins.[3-5] At each step, alteration of the arene backbone, porphyrin substituents or, in the case of hangman porphyrins, the hanging group, has been found to alter reactivity. One such example is demonstrated with cobalt hangman porphyrins (Figure 1) which found using an electron deficient porphyrin platform, such as employing a pendant fluorenyl arene substituents, resulted in the full four electron reduction of dioxygen to water, rather than the expected two electron reduction.[4]

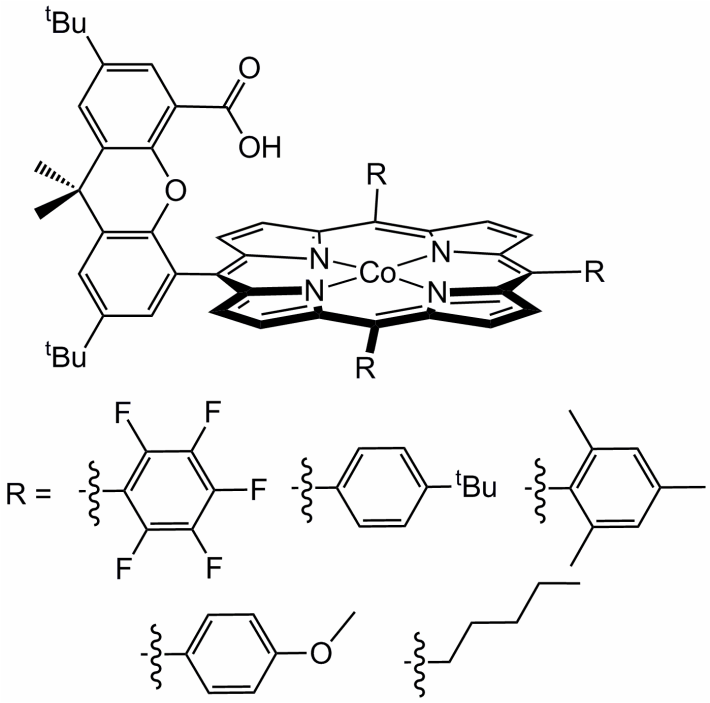

Figure 1: Hangman porphyrin with different possible porphyrin substituents. If R = fluoro-arene, the complex catalyses the full four electron reduction of dioxygen to water

Modifications of the Schiff-base pacman macrocycle synthesised by the Love and Sessler groups has also been achieved. As mentioned in Chapter 1, alteration of the

arene backbone to include methyl groups improved ligand and complex solubility[6, 7] whereas the use of an anthracene backbone drastically increased metal-metal separation.[8]

Use of differing *meso*-substituent also altered the core structure and reactivity of pacman complexes formed.[6, 7, 9] Using ethyl-groups again improved solubility whereas the introduction of bulky fluorenyl groups prevents solvent interactions in the cleft of the complex enabling new bridging superoxo and hydroxo cobalt complexes to be isolated.[10]

The synthesis of hetero-bimetallic complexes as well as the introduction of groups capable of secondary coordination sphere control is highly desirable. For example, Collman and co-workers have synthesised a functional model of cyctochrome-c-oxidase which binds both cobalt and copper cations at a porphyrin and an azamacrocycle, respectively (Figure 2).[11]

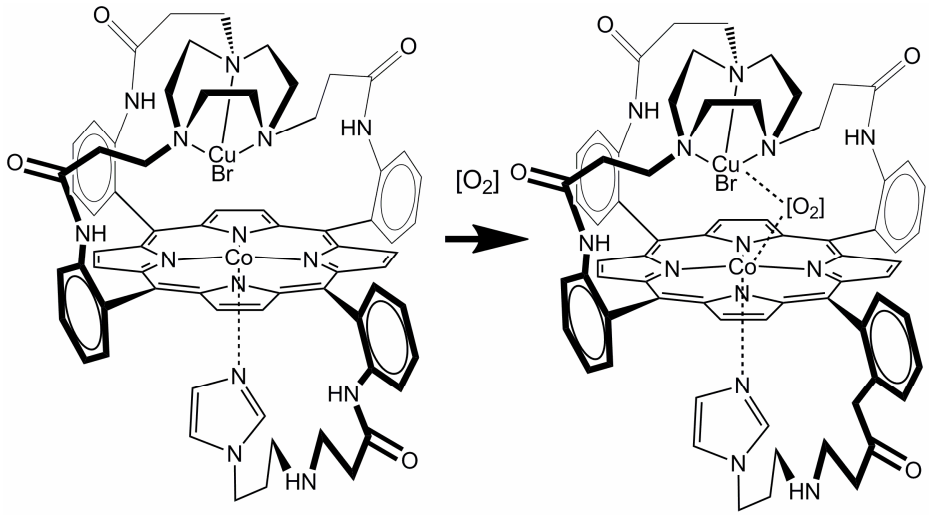

Figure 2: Hetero bimetallic cytochrome-c-oxidase model synthesised by the Collman group binds O_2.[11]

Furthermore, it is advantageous to have a potentially charged second binding pocket, rather than a neutral one, as seen with H_2L^P and H_2L^{NMe}. This would introduce more flexibility with regards to complexation of a second metal and potentially provide an increase in the stability of the binding of that metal centre.

3.2 Modification of the *meso*-group

3.2.1 *meso*-fluorenyl ligands H_2L^{FP} and H_2L^{FNMe}

As discussed in Chapter 1, it is possible to introduce a large, bulky fluorenyl substituent in the *meso*-position of the pyrrole-based dialdehyde in the formation of a [2+2] Schiff-base-symmetric macrocycle to form H_4L^F. Thus it was reasoned the same dialdehyde could be incorporated into ligands of the type H_2L^P and H_2L^{NMe} (Scheme 1). The fluorenyl dialdehyde **9** is straightforwardly synthesised in two steps from pyrrole and 9-fluorenone.[8]

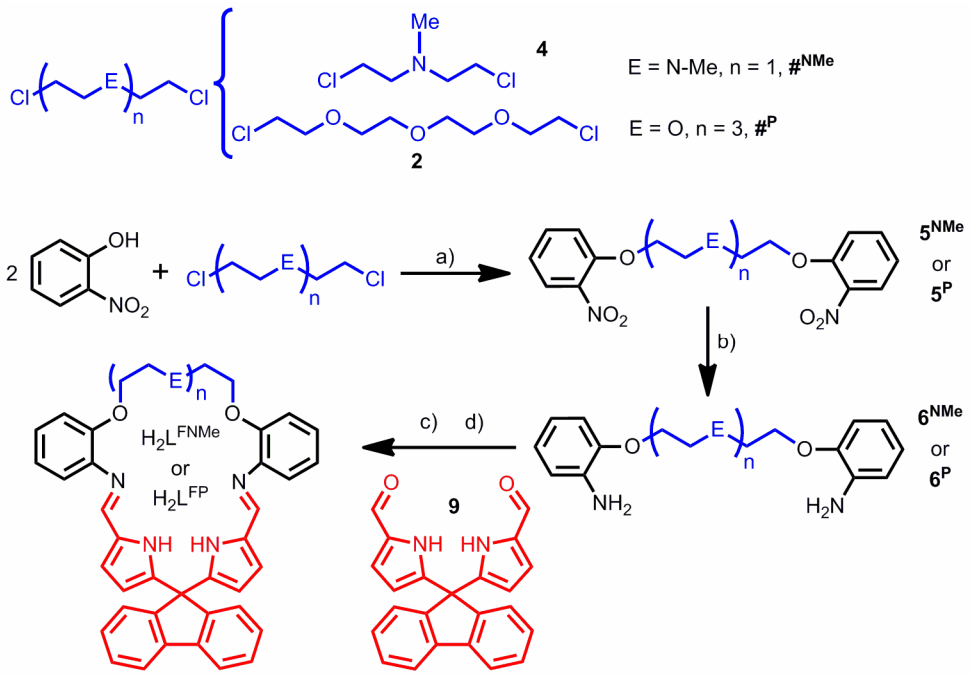

Scheme 1: Synthesis of H_2L^{FP} (E = O, n = 3) and H_2L^{FNMe} (E = NMe, n = 1). a) K_2CO_3, DMF, 120 °C b) H_2, 10% Pd/C cat c) EtOH, 2.1 $BF_3{\cdot}OEt_2$, overnight (L^{FNMe} = RT, L^{FP} = 40 °C) d) CH_2Cl_2, 7 M NH_3 (MeOH)

The straightforward syntheses of diamines $\mathbf{6^P}$ and $\mathbf{6^{NMe}}$ from 2-nitrophenol and dichlorides **2** and **4** was described in chapter two. In work carried out with Miss Berengere Escuyer†, the [1+1] Schiff-base cyclisation was achieved by the addition of $BF_3{\cdot}OEt_2$, followed by that of a NH_3 solution in MeOH, giving H_2L^{FP} and H_2L^{FNMe} in good yield (*ca.* 68 %) as yellow powders. These are much higher yields than the corresponding *meso*-ethyl macrocycles, H_2L^P and H_2L^{NMe} (40 and 57 % respectively), and furthermore, the crude material is much purer by ^{1}H NMR spectroscopy. However, due to the poor solubility of the fluorenyl-dialdehyde a longer reaction time of *ca.* 16 h was required. Formation of a cyclic product is corroborated by analysis of the ^{1}H NMR

spectrum (Figure 3, Figure 4), which displays an imine resonance at 8.17 (H_2L^{FP}) and 8.16 ppm (H_2L^{FNMe}) with a broad resonance at 9.52 (H_2L^{FP}) and 9.50 ppm (H_2L^{FNMe}) corresponding to the pyrrolic NH. Multiplet arene resonances for the arene backbone and *meso*-fluorenyl substituent, each of which integrated to two protons unless stated, are observed at 7.81, 7.75, 7.45, 7.38, 7.12, 6.98 (4H) and 6.89 ppm (H_2L^{FP}) and 7.93, 7.81, 7.44, 7.38, 7.34 and 7.01 (4H) ppm (H_2L^{FNMe}) with pyrrolic CH doublets seen at 6.57 and 6.08 ppm (H_2L^{FP}) and 6.51 and 5.83 ppm (H_2L^{FNMe}). Four resonances corresponding to the ethereal backbone of H_2L^{FP} are present at 4.16, 3.90, 3.78 and 3.62 ppm with the ether/amine backbone protons of H_2L^{FNMe} at 4.22 and 3.08 ppm with the NMe singlet at 2.64 ppm. As seen with the *meso*-ethyl precursors, H_2L^{FP} and H_2L^{FNMe} are mildly air and water sensitive, with the appearance of an aldehyde resonance in the ^{1}H NMR spectrum at around 8.9 ppm if left exposed to air. Though the synthesis of these macrocycles is cleaner than the corresponding ethyl-versions, especially in the L^{FP} case, a method of further purification could not be found.

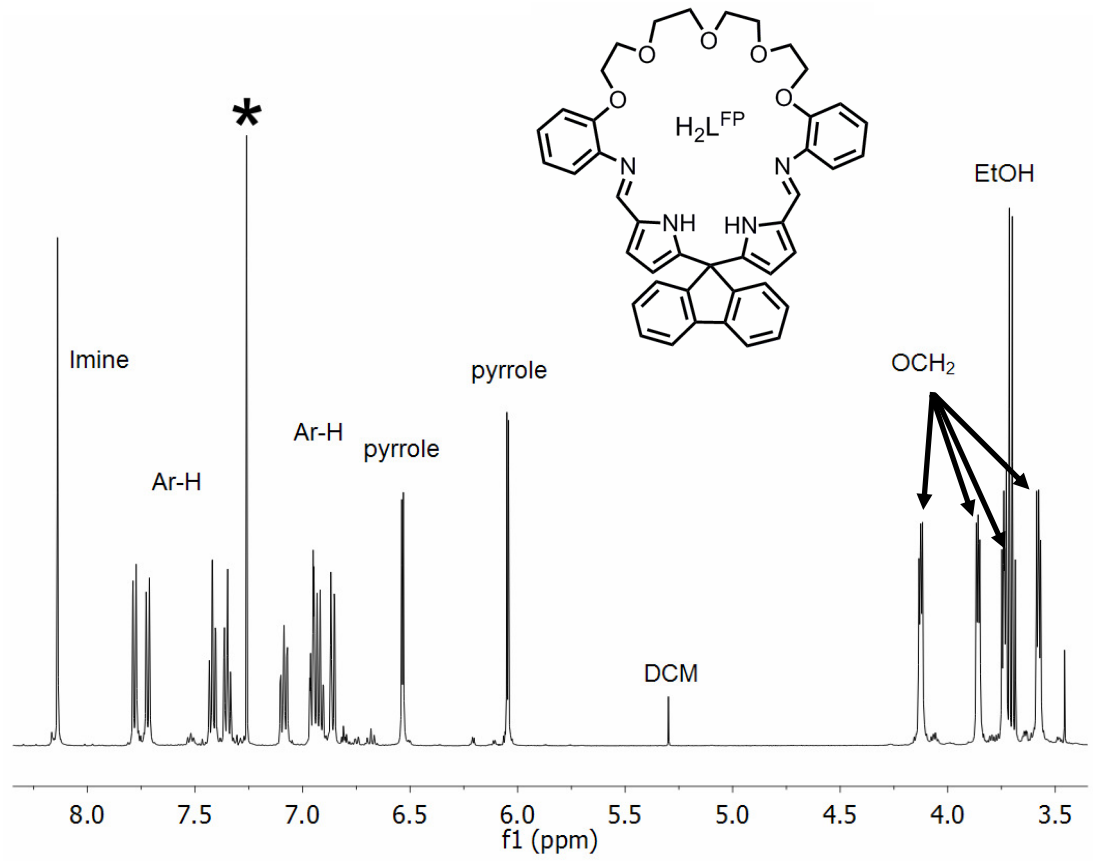

Figure 3: ^{1}H NMR spectra ($CDCl_3$) of H_2L^{FP}. '*' denotes residual protio solvent

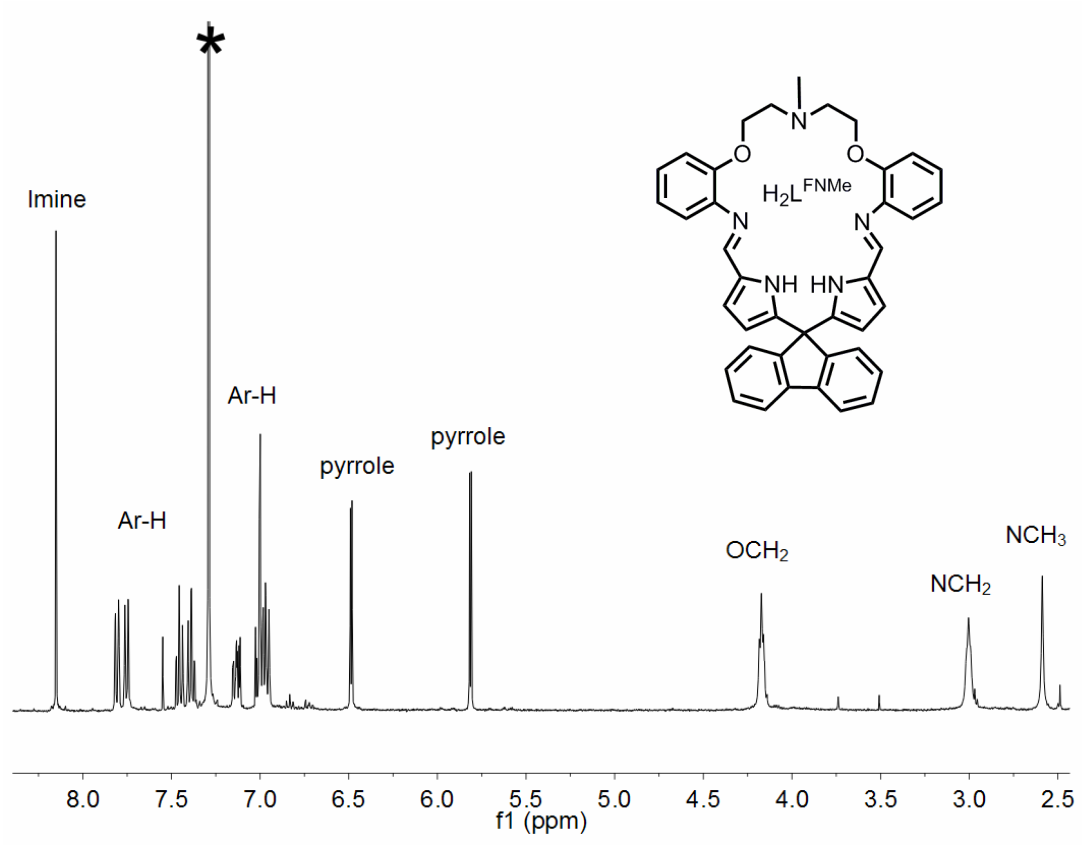

Figure 4: ^{1}H NMR spectra ($CDCl_3$) of H_2L^{FNMe}. '*' denotes residual protio solvent

Formation of a [1+1] cyclic product is also supported by the EI mass spectrum which displays a parent ion peak at 692 (H_2L^{FP}) and 617 amu (H_2L^{FNMe}), the isotope pattern of which is consistent with a [1+1] product; furthermore, no higher mass peaks corresponding to [2+2] impurities were seen, in contrast to H_2L^{P} and H_2L^{NMe}. Microanalysis also supports the formulations of both macrocycles and the IR spectra display a broad NH stretch at *ca.* 3200 cm^{-1} with the imine absorbance present at *ca.* 1620 cm^{-1}. A crystal of H_2L^{FNMe} suitable for single crystal X-ray diffraction was grown by hexane diffusion into a THF solution (Figure 5, Table 1). Two crystallographically-independent H_2L^{FNMe} molecules were found in the asymmetric unit cell, and, due to their similarity, only one will be discussed.

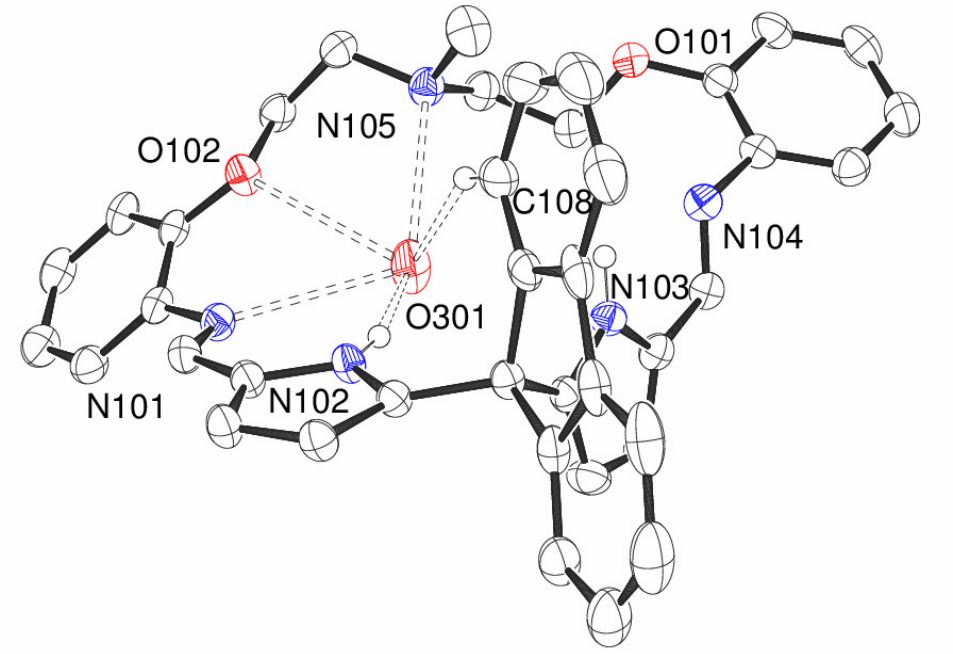

Figure 5: X-ray crystal structure of [H_2L^{FNMe}]. For clarity, all hydrogen atoms except those on N102, N103 and C108 are omitted and displacement ellipsoids are drawn at 50% probability

Table 1: Selected bond lengths (Å) and angles (°) of H_2L^{FNMe}

C101-N101	1.284(2)	N101···O301	2.914
N102-C102	1.376(2)	N102···O301	2.847
C102-C103	1.384(3)	N105···O301	2.863
C103-C104	1.411(3)	C108···O301	3.610
C104-C105	1.378(2)	C140-N101-C101	120.25(16)
C105-N102	1.364(2)	N101-C101-C102	121.73(17)
O102···O301	3.046		

In the solid state, the macrocycle adopts a shallow-bowl conformation with the *meso*-fluorenyl group twisted out of the macrocyclic plane (N_4-plane – fluorenyl angle 69.36 °). A water molecule is found hydrogen bonded to one half of the macrocycle, with the macrocycle displaying both hydrogen bond donor and acceptor properties *via* five different donor/acceptor groups present (O301-donor distances: -N101 2.914, -O102 3.046, -N105 2.863 Å, O301-acceptor distances: -N102 2.847 and -C108 3.610 Å). A similarly weak interaction between the fluorenyl (C108) and the bound water was seen in

a related binuclear cobalt complex of the symmetric, fluorenyl macrocycle ($C_{fluorenyl}$-O 3.386 Å) and could play a role in any future catalytic investigations. The second pyrrolic nitrogen (N103) is not involved in any further bonding. All the bond distances observed are similar to those of related symmetric macrocycles employing either the *meso*-fluorenyl or other *meso*-substituents, such as the imine (C101–N101 1.284(2) Å) compared to 1.280(8)–1.289(3) Å and C_{arene}-N101-C101 bond angle of 120.25(16) °, compared to 119.7(5)–121.0(3) ° for related symmetric macrocycles.[7, 8]

Thus two new ligands, H_2L^{FP} and H_2L^{FNMe} have been synthesised in a higher yielding, cleaner synthesis than the corresponding *meso*-ether macrocycles H_2L^{P} and H_2L^{NMe}.

3.3 Complexes of L^{FP} and L^{FNMe}

With the successful synthesis of H_2L^{FP} and H_2L^{FNMe}, metallation reactions analogous to H_2L^{P} and H_2L^{NMe} were attempted, also with the help of Miss Berengere Escuyer.

3.3.1 Synthesis of [Pd(L^{FP})] and [Pd(L^{FNMe})]

The palladium complexes of the fluorenyl ligands were targeted to see if a pacman conformation results from metallation in solution.

$$H_2L^{FP/FNMe} + Pd(OAc)_2 \xrightarrow[CH_2Cl_2]{2\ NEt_3} [Pd(L^{FP/FNMe})]$$

Equation 1

Reaction of either ligand with palladium acetate in CH_2Cl_2 in the presence of NEt_3 resulted in the formation of the palladium complexes [Pd(L^{FP})] or [Pd(L^{FNMe})] as yellow solids in moderate yields (*ca*. 38 %, Equation 1).

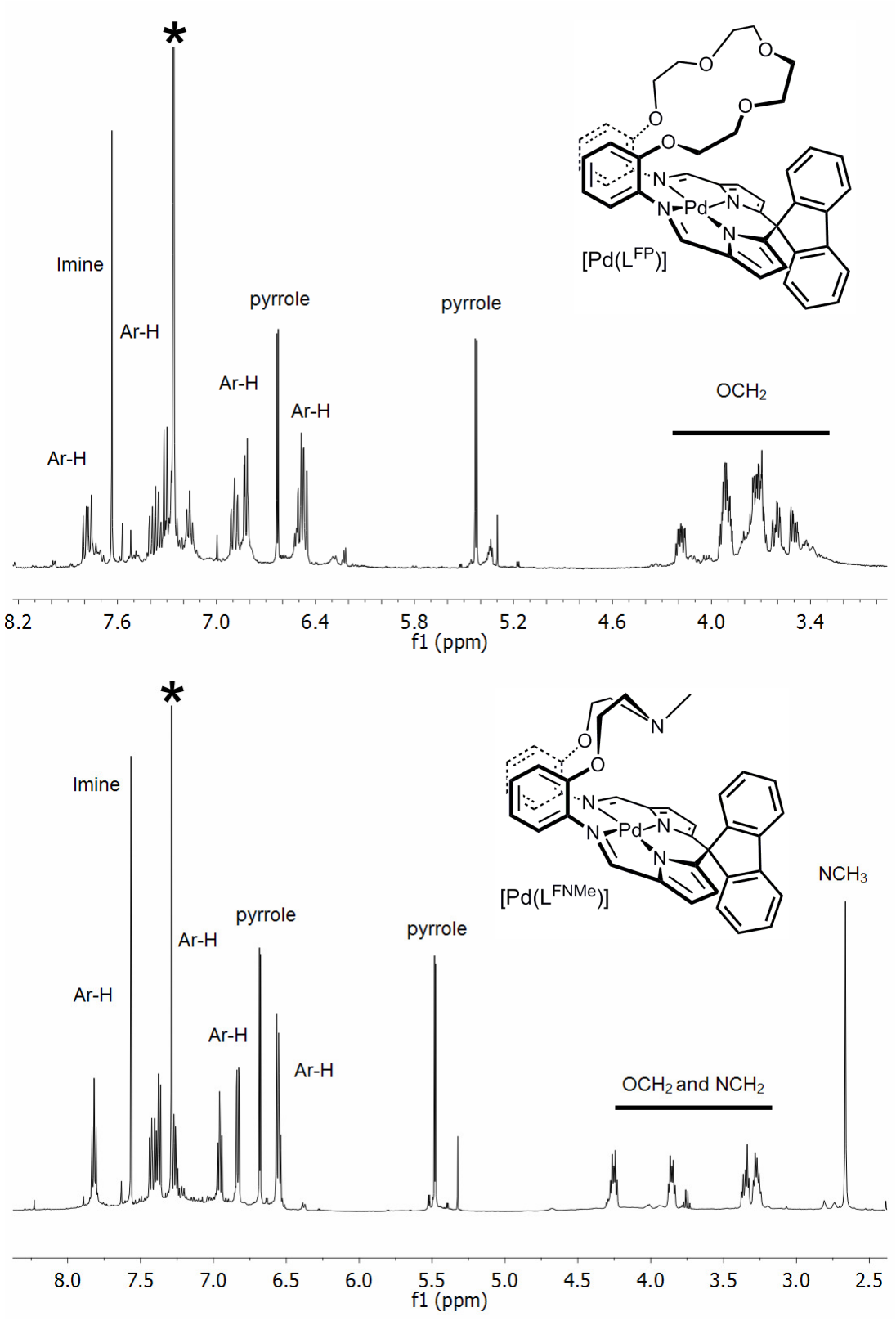

Figure 6: ^{1}H NMR spectra ($CDCl_3$) of [Pd(L^{FP})] (top) and [Pd(L^{FNMe})] (bottom). '*' denotes residual protio solvent

The ^{1}H NMR spectra of [Pd(L^{FP})] and [Pd(L^{FNMe})] (Figure 6, top and bottom respectively) show shifts in the imine resonances from 8.17 to 7.63 ppm (L^{FP}) and 8.16 to 7.57 ppm (L^{FNMe}). The splitting of the ethereal-backbone protons of [Pd(L^{FP})] are observed as a series of multiplets (integral values in brackets) at around 4.20 (2H), 3.91 (4H), 3.72 (6H), 3.61 (2H) and 3.50 ppm (2H), reflected also in the amine/ether protons of [Pd(L^{FNMe})], with four resonances, each integrating to two protons at around 4.26, 3.85, 3.35 and 3.28 ppm thus indicating a pacman geometry in solution. However, unlike the L^{P} and L^{NMe} analogues, splitting of the *meso*-substituents is not observed in the ^{1}H NMR spectra as expected, with only eight aromatic resonances seen (four arene backbone, four fluorenyl). The desymmetrisation of the fluorenyl group is however supported in the ^{13}C{^{1}H} NMR spectra, and by ^{1}H-^{13}C HSQC NMR spectroscopy. Both [Pd(L^{FP})] and [Pd(L^{FNMe})] display fifteen CH resonances in the aromatic region (four arene backbone, eight fluorenyl, two pyrrolic and one imine) and eight quaternary carbon resonances in the same region (two arene backbone, two pyrrolic, four fluorenyl) thus confirming a solution-state pacman geometry.

The EI mass spectra show parent ions at 721 amu for [Pd(L^{FNMe})] and 796 amu for [Pd(L^{FP})], with the isotope pattern consistent with [1+1] complexes only. Microanalytical data also support the formulations and the IR spectra show the loss of the NH stretch at around 3200 cm^{-1} and a shift in the imine absorbance from *ca*. 1620 to 1555 cm^{-1} which supports metallation. Crystals suitable for single crystal X-ray crystallography were grown from a saturated hexane solution of [Pd(L^{FNMe})] (Table 2, Figure 7).

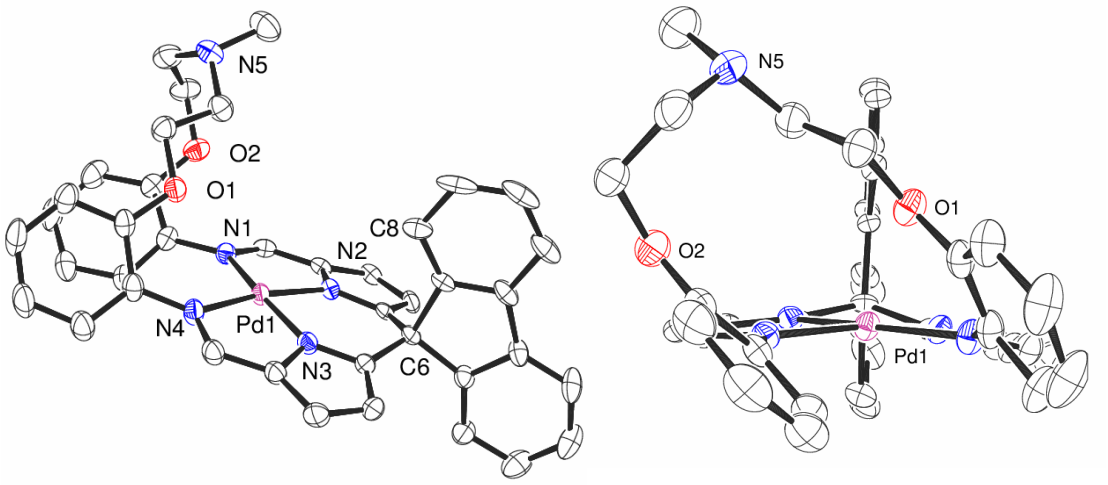

Figure 7: X-ray crystal structure of [Pd(L^{FNMe})]. For clarity, all hydrogen atoms are omitted and displacement ellipsoids are drawn at 50% probability

Table 2: Selected bond lengths (Å) and angles (°) of [Pd(L^{FNMe})]

Pd-N1	2.078(2)	*meso*C-plane ^ N_4 plane	23.50
Pd-N2	1.941(2)	fluorenyl-plane ^ N_4 plane	89.45
Pd-N3	1.934(2)	N1-Pd-N4	111.95(9)
Pd-N4	2.080(2)	N1-Pd-N2	79.99(9)
C8···Pd	4.013	N2-Pd-N3	87.87(9)
O1···Pd	3.232	N3-Pd-N4	80.01(9)
O2···Pd	4.620	Σ ∠ Pd	359.82
N5····Pd	5.610	Twist Φ	43.40/30.19
Pd···N_4	0.076	Dihedral α	26.82

The complex [Pd(L^{FNMe})] clearly adopts a wedge-shaped pacman geometry in the solid state. The palladium sits in the N_4-plane (Pd···N_4 0.076 Å) in a distorted square planar environment (Σ Pd angles = 359.82 °). The palladium-nitrogen bond distances (Pd-N_{im} 2.078(2)–2.080(2) Å, Pd-N_{py} 1.934(2)–1.941(2) Å) are marginally shorter than those of [Pd(L^{NMe})] (Pd-N_{im} 2.093(2)–2.096(2) Å, Pd-N_{py} 1.943(2)–1.945(2) Å, see Chapter 2) but are comparable to related symmetric macrocycle complexes (Pd-N_{im} 2.043(7)–2.096(2) Å, Pd-N_{py} 1.928(4)–1.947(4) Å).[7-9] The fluorenyl is bent at a slight angle around the *meso*-carbon (C6) towards the cleft at an angle of 23.50 ° relative to the N_4-plane, a feature also seen with the symmetric fluorenyl macrocycle [$Pd_2(L^F)$] (19.46 and 22.45 °).

Therefore the ligands H_2L^{FP} and H_2L^{FNMe}, upon complexation of a metal, are capable of folding into a rigid pacman-geometry in both the solution and solid state, as seen with H_2L^P and H_2L^{NMe}.

3.3.2 Synthesis of [$K_2(L^{FP})$], [$K_2(L^{FNMe})$], [$Mg(L^{FP})$] and [$Mg(L^{FNMe})$]

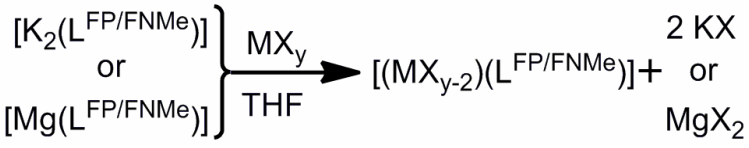

Equation 2

As with $L^{P/NMe}$, the syntheses of K and Mg complexes of L^{FP} and L^{FNMe} was attempted in order to facilitate salt elimination reactions with metal halides.

Equation 3

Deprotonation of either macrocycle with excess potassium hydride leads to immediate effervescence of gas and the formation of $[K_2(L^{FP})]$ or $[K_2(L^{FNMe})]$ (Equation 3). ^1H and $^{13}C\{^1H\}$ NMR (H_8-THF/C_6D_6) spectra of both potassium complexes indicate non-pacman conformations in solution with only eight aromatic CH resonances observed, with multiplets (integrating to 2H unless stated) present at 8.31, 8.00, 7.52 (6H), 7.45, 7.28 and 7.21 ppm for $[K_2(L^{FP})]$ and 7.71, 7.64, 7.15, 7.07, 6.96, 6.85 and 6.78 ppm (4H) for $[K_2(L^{FNMe})]$. Resonances corresponding to the ether/amine protons could not be seen due to suppressed H_8-THF, with singlet imine resonances at 8.42 ppm for $[K_2(L^{FP})]$ and 8.01 ppm for $[K_2(L^{NMe})]$. The EI mass spectra also show parent ion peaks at *m/z* = 768 $[K_2(L^{FP})]$ and 693 $[K_2(L^{FNMe})]$ with the composition of $[K_2(L^{FNMe})]$ also supported by microanalysis. A disappearance of the NH stretch in the IR spectra at *ca.* 3200 cm^{-1}, and a shifting of the imine absorbances from *ca.* 1620 to 1560 cm^{-1} were also observed. In a manner similar to $[K_2(L^{P})]$, $[K_2(L^{NMe})]$, and potassium salts of the symmetric macrocycle $[K_4(L)]$, isolation and storage of bulk material proved problematic and so reactions with metal halides involved the *in-situ* formation of $[K_2(L^{FP})]$ or $[K_2(L^{FNMe})]$.

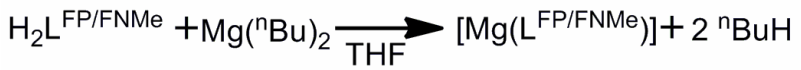

Equation 4

Reaction of either macrocycle with a heptane solution of dibutylmagnesium resulted in the formation of $[Mg(L^{FP})]$ and $[Mg(L^{FNMe})]$ in good yields (*ca.* 93 %$^+$) as yellow solids (Equation 4). The ^1H NMR spectrum of $[Mg(L^{FP})]$ (Figure 8, top) displays eight aromatic resonances, each integrating to 1H at 8.23, 7.80, 7.67, 7.58, 7.46 and two overlapping resonances at 7.41–7.33 ppm as well as corresponding CH resonances in the $^{13}C\{^1H\}$ spectrum (a total of 15 CH and 8 quaternary resonances in the high-frequency region). Furthermore, the ether OCH_2 protons were split into a series of overlapping multiplets from 3.44 to 2.77 ppm, consistent with a pacman-geometry in solution.

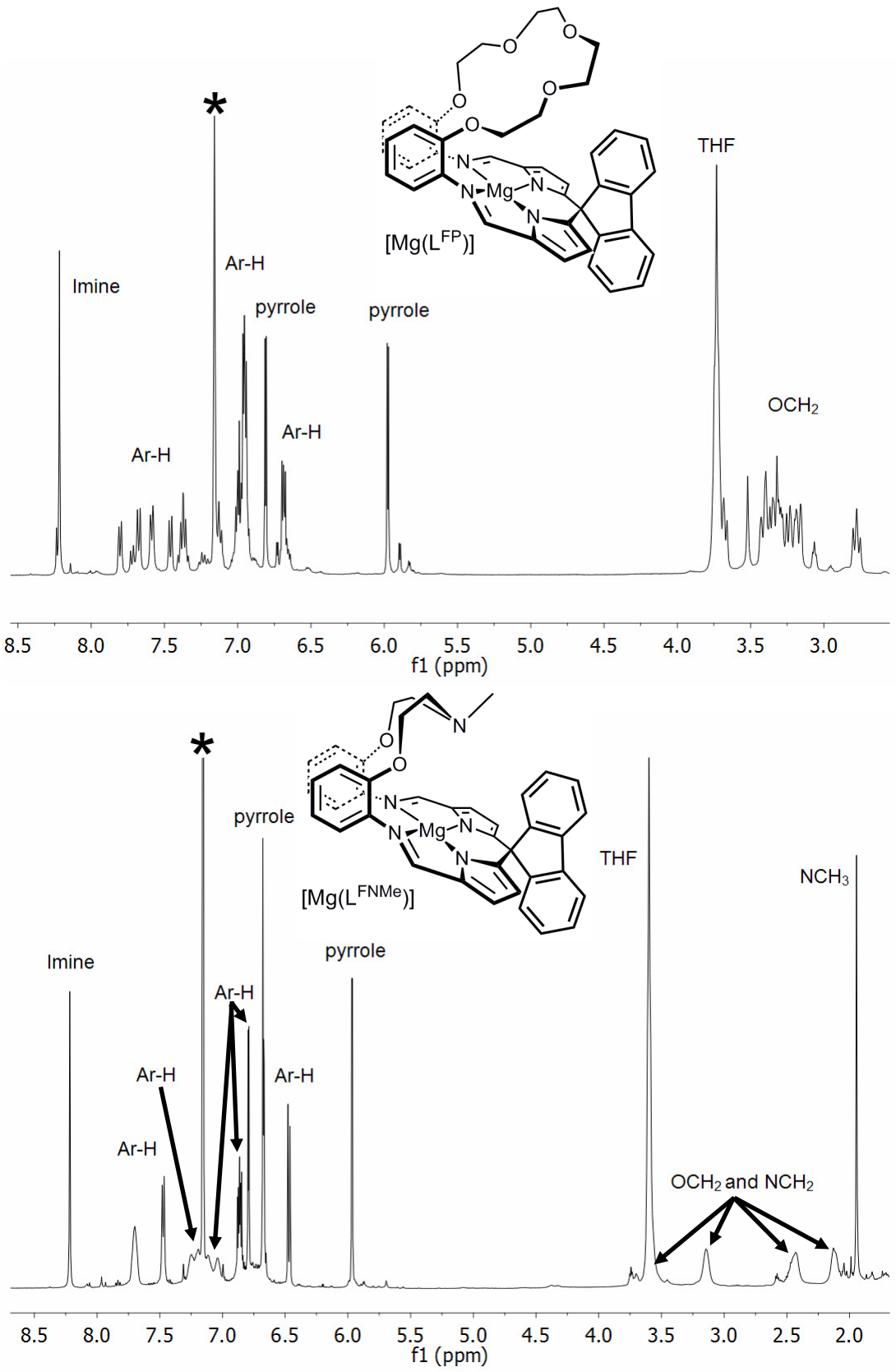

Figure 8: ^{1}H NMR spectra (C_6D_6) of [Mg(L^{FP})] (top) and [Mg(L^{FNMe})] (bottom). '*' denotes residual protio solvent

Similarly, the ^{1}H NMR spectrum of [Mg(L^{FNMe})] (Figure 8, bottom) also shows a series of overlapping multiplets at 7.70 (2H), 7.47 (2H), 7.32–6.99 (8H), 6.90–6.84 (6H), 6.69–6.65 (4H) and 6.47 (2H) indicating desymmetrisation of the fluorenyl group, which is also confirmed by the ^{13}C{^{1}H} NMR spectrum that shows 15 CH and 8 quaternary resonances between 160 and 112 ppm. Four separate resonances corresponding to the ether/amine protons at 3.56, 3.14, 2.45 and 2.13 ppm are also observed in the ^{1}H NMR spectrum confirming that [Mg(L^{FNMe})] is also in a pacman conformation in solution. Resonances corresponding to the ether/amine backbone and fluorenyl group of [Mg(L^{FNMe})] are broad and shallow indicating a degree of fluxionality in solution. Resonance assignments were confirmed by ^{1}H-^{13}C HSQC NMR spectroscopy. There is no sign of an NH stretch at 3200 cm^{-1} in the IR spectra, with the imine absorbance shifting from *ca*. 1620 to 1565 cm^{-1} and parent ion peaks are seen in the EI mass spectra at 714 [Mg(L^{FP})] and 639 amu [Mg(L^{FNMe})].

3.3.3 Synthesis of [Co(L^{FP})] and [Co(L^{FNMe})]

With the successful synthesis of [Co(L^{P})] and [Co(L^{NMe})], the syntheses of [Co(L^{FP})] and [Co(L^{FNMe})] *via* [K_2(L^{FP})] and [K_2(L^{FNMe})] were also attempted in the hope of studying what effect introduction of the fluorenyl group had on these complexes.

$$H_2L^{NMes} + 3\ KH \xrightarrow[THF]{} [K_2(L^{NMes})] \xrightarrow[THF]{CoCl_2} [Co(L^{NMes})] + 2\ KCl$$

Equation 5

Reaction of *in-situ* generated [K_2(L^{FP})] or [K_2(L^{FNMe})] with one equivalent of cobalt dichloride resulted in the formation of the cobalt complexes [Co(L^{FP})] or [Co(L^{FNMe})] in poor yield (*ca*. 20 %) as red solids (Equation 5). The ^{1}H NMR spectra are paramagnetically shifted and broadened, though the number of resonances and the values of their integrals are consistent with a pacman-shape in solution. Specifically, [Co(L^{FP})] displays 22 resonances between 60 and -37 ppm, including eight which integrate to 1H corresponding to a desymmetrised fluorenyl group, as well as seven resonances indicating dissimilar ethereal protons (one resonance integrating to 4H is assumed to be two overlapping 2H resonances). Similarly, the ^{1}H NMR spectrum of [Co(L^{FNMe})] displays 19 resonances from 45 to -18 ppm, with six resonances integrating to 1H, with two 1H resonances overlapping, eleven resonances integrated to 2H and one 3H resonance. Elemental analysis supports the formulation of [Co(L^{FNMe})] and the EI mass spectra show parent ion peaks at 674 for [Co(L^{FNMe})] and 749 amu for [Co(L^{FP})]. The IR

spectra also show the loss of the NH stretch at 3200 cm^{-1} and the standard shifting of the imine absorption from 1620 to 1560 cm^{-1}. Exposure of [Co(L^{FP})] and [Co(L^{FNMe})] to air results in ^{1}H NMR spectra in the diamagnetic region, indicative of Co(III) complexes similar to those seen for air-exposed [Co(L^{P})] and [Co(L^{NMe})] in Chapter 2. Although the isolation of the highly insoluble [Co(OH_2)(OH)(L^{FNMe})] was not successful, the isolation of [Co(OH_2)(OH)(L^{FP})] was possible. The ^{1}H NMR spectrum of [Co(OH_2)(OH)(L^{FP})] displays a series of multiplets, some of which overlap, in the arene region 7.78–6.18ppm, which indicates desymmetrisation of the fluorenyl group, with overlapping multiplets from 3.48–2.72 ppm indicative of dissimilar backbone ethereal protons. Ligand desymmetrisation is also mirrored in the $^{13}C\{^{1}H\}$ NMR spectrum with 15 CH and 8 quaternary carbon resonances between 163 and 106 ppm and is also indicative of a pacman geometry in solution. Microanalysis supports the formulation and the IR spectrum shows absorptions at 3409 and 3232 cm^{-1} that are assigned to OH stretches. Crystals of [Co(OH_2)(OH)(L^{FP})] suitable for X-ray diffraction were grown from an air-saturated toluene solution of [Co(L^{FP})] (Figure 9). Unfortunately, due to poor quality of the data leading to a high R factor of 12.9 %, an in-depth discussion of the structure is not possible.

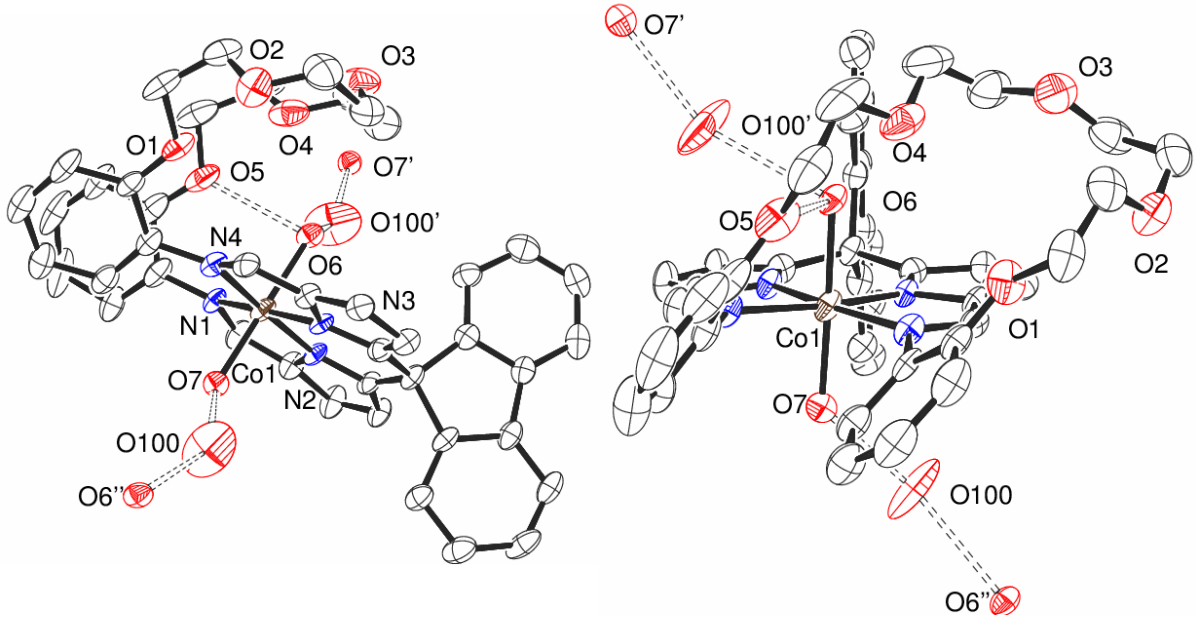

Figure 9: X-ray crystal structure of [Co(OH_2)(OH)(L^{FP})]. For clarity, all hydrogen atoms are omitted and displacement ellipsoids are drawn at 30% probability

The complex displays a pacman structure in which Co1 adopts a distorted octahedral geometry. Comparison to the asymmetric unit of $[Co(OH_2)(OH)(L^P)]$ suggests that the axial ligands are water and hydroxide, with the water O6 within the cleft and the hydroxide O7 outside the cleft . The arene hinges and polyether backbone are heavily twisted, with only O5 hydrogen bonded to the water within the cleft. Though this structure does not display the same supramolecular cylindrical structure as $[Co(OH_2)(OH)(L^P)]$, a hydrogen-bonded chain of pacman units is observed. The exogenous hydroxide is hydrogen bonded to a second water molecule (O7···O100 2.475 Å), which is in turn is hydrogen bonded to the endogenous water of an adjacent pacman complex (O100···O6' 2.677 Å), so creating a Co-pacman "water wire" (Figure 10).

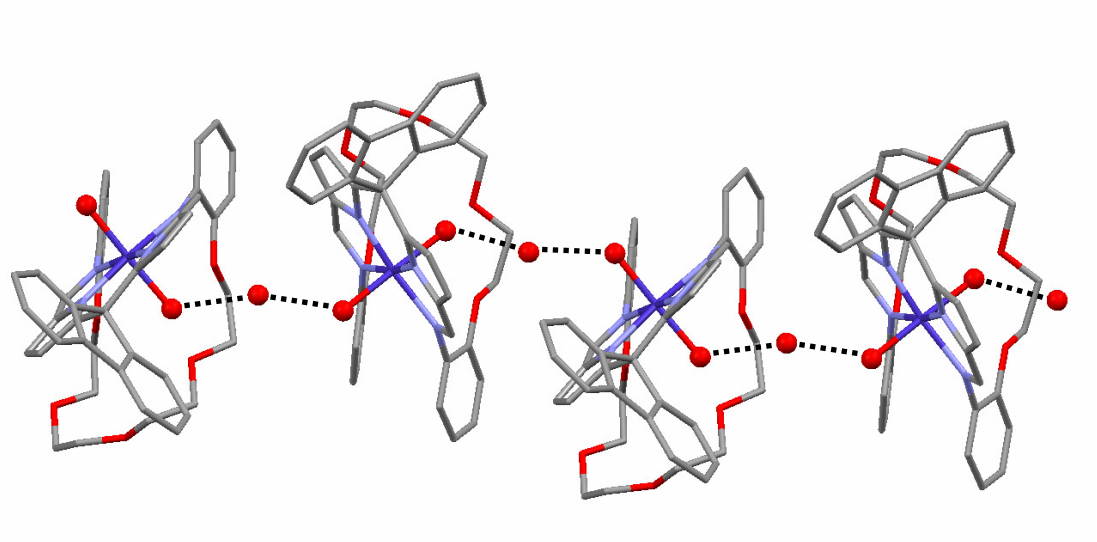

Figure 10: X-ray crystal structure of $[Co(OH_2)(OH)(L^{FP})]$ showing extended structure

3.4 Investigations into the redox chemistry of the cobalt and palladium complexes $[M(L^P)]$, $[M(L^{NMe})]$, $[M(L^{FP})]$ and $[M(L^{FNMe})]$ by cyclic voltammetry

Due to the observation that the cobalt complexes $[Co(L^P)]$, $[Co(L^{NMe})]$, $[Co(L^{FP})]$ and $[Co(L^{FNMe})]$ undergo oxidation from Co(II) to Co(III) upon exposure to air, the electrochemistry of these compounds were investigated by cyclic voltammetry. In an effort to gain insight into any ligand-based redox features, the cyclic voltammograms (CV) of $[Pd(L^P)]$, $[Pd(L^{NMe})]$, $[Pd(L^{FP})]$ and $[Pd(L^{FNMe})]$ were also recorded. All experiments were conducted in dry THF with Bu_4NBF_4 electrolyte (0.2 M) and complex (1.0 $mmoldm^{-3}$) under an atmosphere of N_2 and referenced to ferrocene (Fc/Fc^+ = 0 V). Scans were conducted at 400, 200, 100, 50 and 25 mVs^{-1} and all features scanned

starting from both the most positive and most negative vertex point. All cyclic voltammograms can be found in CD-Appendix 1.

The complexes [Pd(L^P)] and [Pd(L^{NMe})] showed no features within the THF window (*ca*. -3.0 to 1.0 V) (Figure 11). A broad feature present in the CV of [Pd(L^{NMe})] at 0.2 V when scanning at 200 mVs^{-1} was also present in the background and so was ignored.

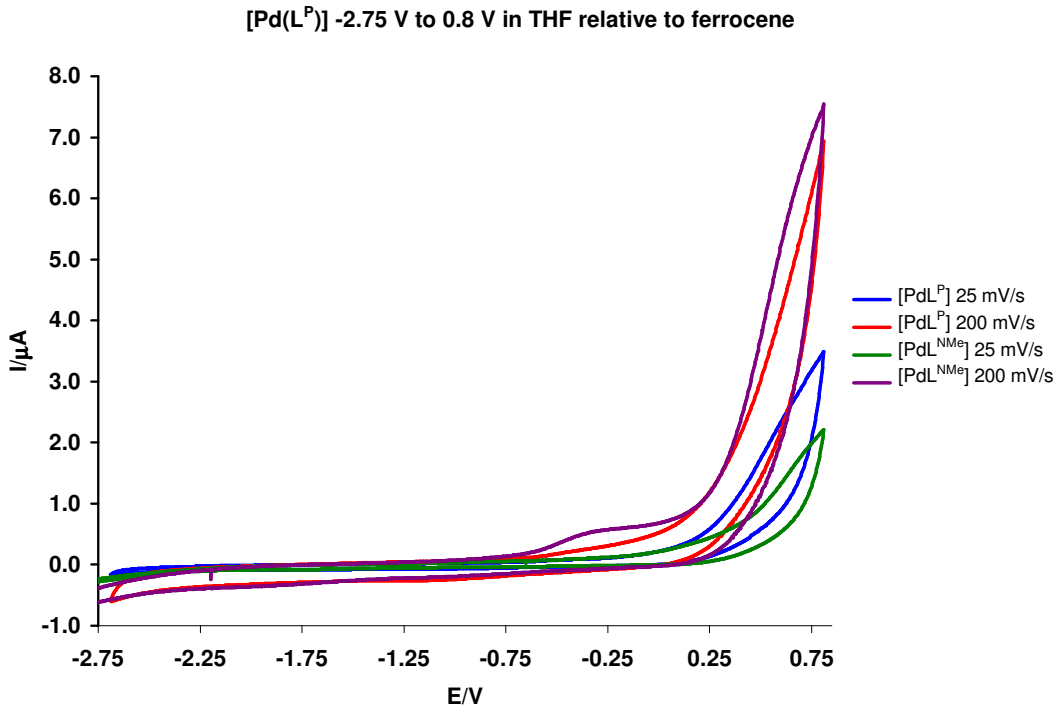

Figure 11: Cyclic voltammogram of [Pd(L^P)] and [Pd(L^{NMe})] in THF (Bu_4NBF_4, Fc/Fc^+)

In contrast, the CVs of [Co(L^P)] revealed a quasi-reversible Co(II)/(III) wave with half-wave potential ($E_{1/2}$) of -0.12 V and a reversible Co(I)/(II) wave at -2.29 V (Figure 12).

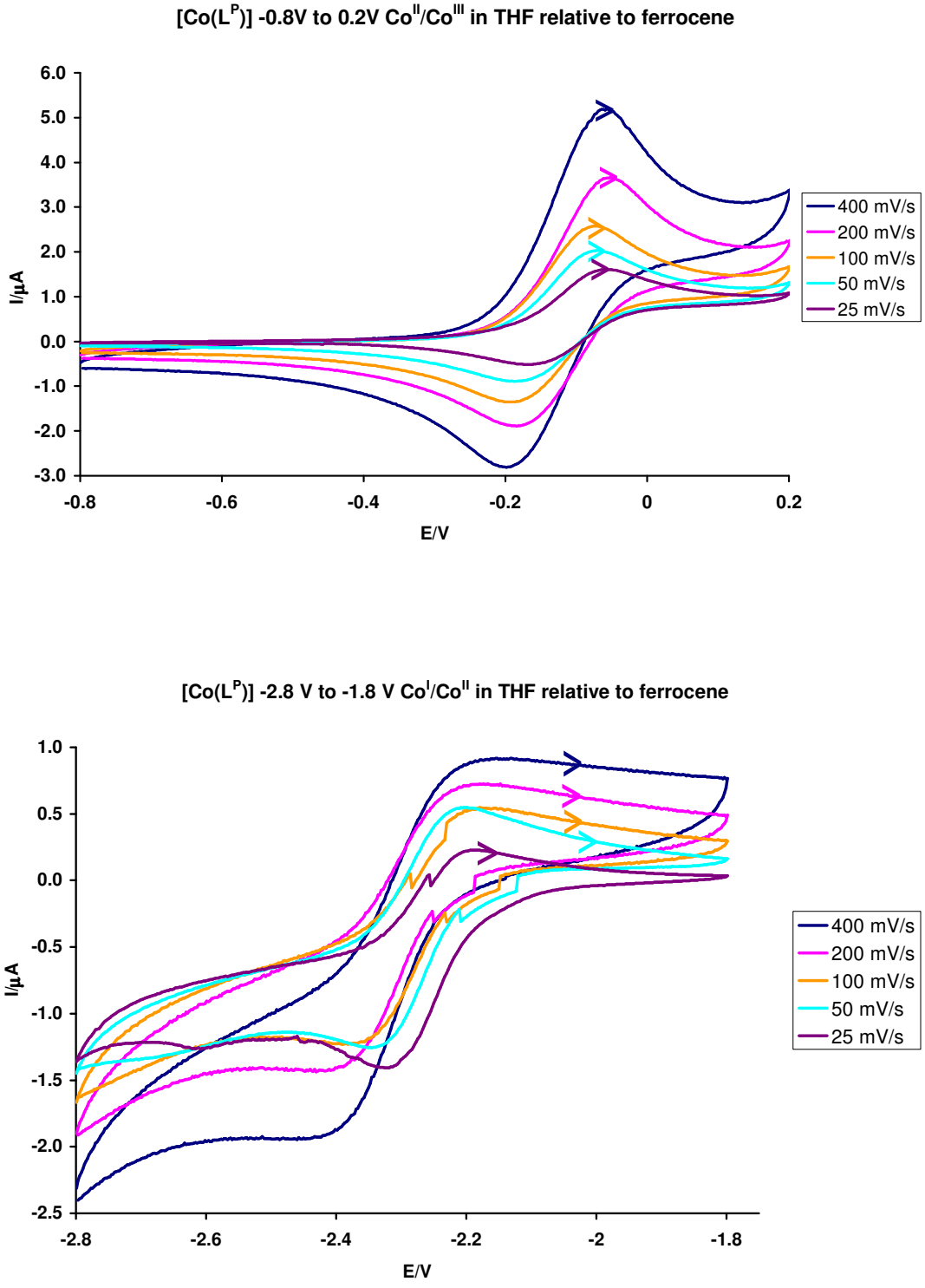

Figure 12: Cyclic voltammogram of [Co(L^P)] showing a quasi-reversible waves at $E_{1/2}$ = -0.12 V (top) and reversible wave at -2.29 V (bottom) in THF (Bu_4NBF_4, Fc/Fc^+)

Likewise, the CVs of [Co(L^{NMe})] displays similar quasi-reversible waves with a Co(II)/(Co(III) wave at $E_{1/2}$ = -0.18 V and a Co(I)/Co(II) wave at -2.27 V. Thus the

Co(II)/Co(III) couple occurs at a slightly more positive potential for [Co(L^{P})] than [Co(L^{NMe})] ($E_{1/2}$ = -0.12 and -0.18 V respectively) with almost identical Co(I)/Co(II) features at $E_{1/2}$ = -2.29 ([Co(L^{P})]) and -2.27 V ([Co(L^{NMe})]) (Figure 13).

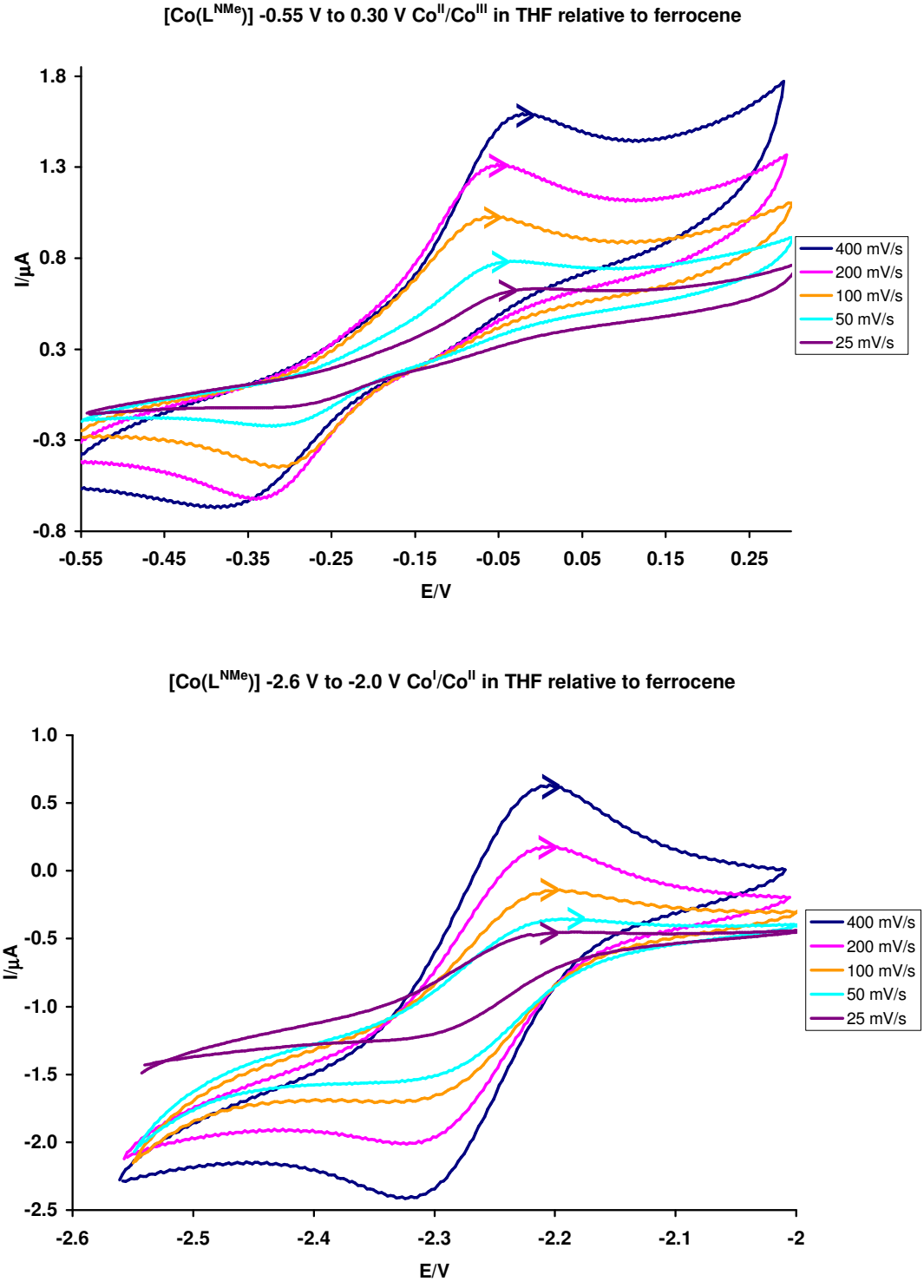

Figure 13: Cyclic voltammogram of [Co(L^{NMe})] showing quasi-reversible waves at $E_{1/2}$ = -0.18 V(top) and 2.27 V (bottom) in THF (Bu_4NBF_4, Fc/Fc^+)

Electrochemical properties under O_2, akin to those undertaken for cobalt complexes of symmetric ligands[12] and pacman-diporphyrin complexes,[3, 13] are yet to be investigated.

It was found that the introduction of the fluorenyl group to the macrocycle has a large effect on the electrochemistry of its complexes. While the palladium complex [Pd(L^P)], with *meso*-ethyl substituents, showed no redox chemistry, the *meso*-fluorenyl-substituted complex [Pd(L^{FP})] displayed three features, a reversible wave at $E_{1/2}$ = -2.44 V, a quasi-reversible wave at $E_{1/2}$ = 0.00 V and an irreversible feature at E_{pc} = 0.58 V. By comparison to the cobalt complex [Co(L^{FP})] (Figure 14) as well as with [Co(L^{FNMe})] and [Pd(L^{FNMe})], the waves centred at $E_{1/2}$ = -2.44 and 0.0 V are tentatively assigned to ligand-based redox reactions, i.e. [Pd(L^{FP})$^-$]/[Pd(L^{FP})] and [Pd(L^{FP})]/[Pd(L^{FP})$^+$] respectively. The irreversible feature at around E_{pc} = 0.58 V, which is a weak feature in which the signal diminishes upon repeated scans, is attributed to the palladium-centred Pd(II)/Pd(0) reduction.[14] Due to problems with the equipment when scanning from -3 to 1 V with the [Pd(L^{FP})], there were errors in the signal at sub -1.5 V potentials; however, scans from -2.9 to -1.9 V enable isolation of a feature in this region.

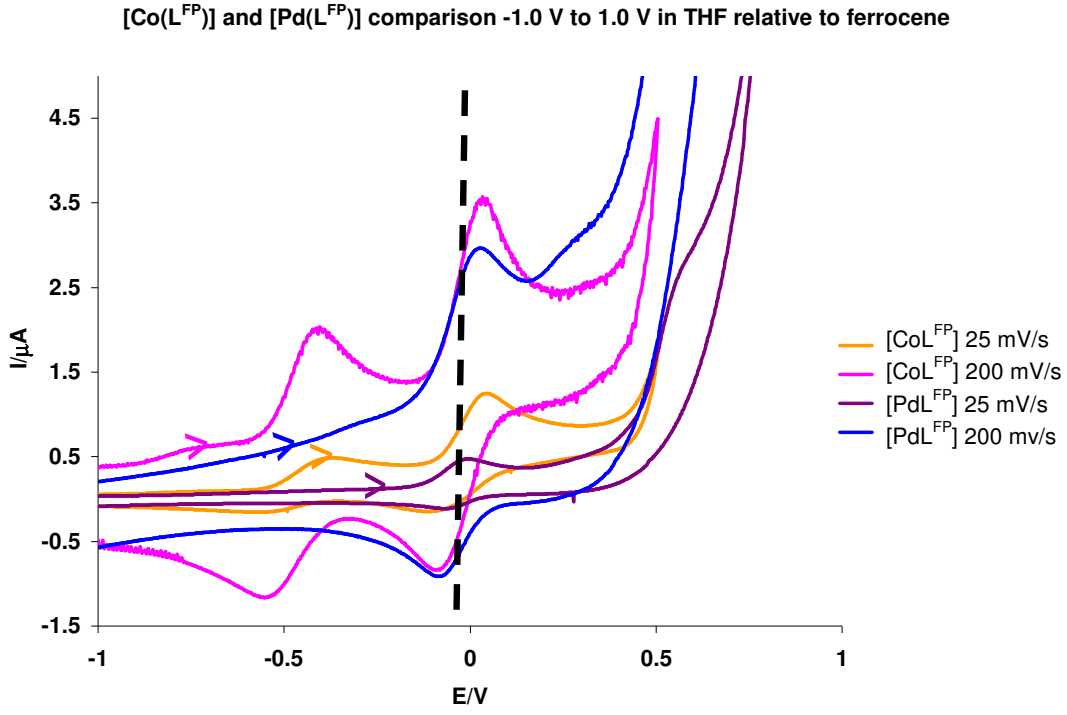

Figure 14: Cyclic voltammogram of [Co(L^{FP})] and [Pd(L^{FP})] for comparison in THF (Bu_4NBF_4, Fc/Fc^+). Dashed line showing feature at around -0.05 V is common to both complexes

The CVs of [Co(L^{FP})] also shows three features, and are assigned to a reversible ligand-based [Co(L^{FP})$^-$]/[Co(L^{FP})] redox couple at $E_{1/2}$ = -2.12 V, a quasi-reversible ligand-based [Co(L^{FP})]/[Co(L^{FP})$^+$] couple at $E_{1/2}$ = -0.01 V, and a quasi-reversible cobalt-based Co^{II}/Co^{III} wave at $E_{1/2}$ = -0.46 V. Thus, the introduction of the cobalt has little effect on the ligand-based [M(L^{FP})]/ [M(L^{FP})$^+$] feature compared to the palladium ($E_{1/2}$ = -0.01 V for [Co(L^{FP})], 0.00 V for [Pd(L^{FP})]) although there is a large 0.32 V shift in the [M(L^{FP})$^-$]/ [M(L^{FP})] wave from $E_{1/2}$ = -2.44 V for the palladium complex to -2.12 V for the cobalt. Unfortunately, a Co^I/Co^{II} couple could not be identified.

Data gained from the CVs of [Pd(L^{FNMe})] and [Co(L^{FNMe})] are less well defined. [Pd(L^{FNMe})] displays an irreversible wave at approximately E_{pc} = 0.2 V and a poorly defined wave at E_{pa} = -2.50 V attributed to ligand-based [Pd(L^{FNMe})]/[Pd(L^{FNMe})$^+$] and [Pd(L^{FNMe})$^-$]/[Pd(L^{FNMe})] couples, respectively, by comparison to [Pd(L^{FP})] (showing equivalent waves at $E_{1/2}$ = 0.00 V and -2.44 V). [Co(L^{FNMe})] showed three waves including a ligand-based quasi-reversible [Co(L^{FNMe})$^-$]/[Co(L^{FNMe})] wave at $E_{1/2}$ = -2.12 V and an irreversible wave at around E_{pc} = 0.05 V that is attributed to a ligand-based [Co(L^{FNMe})]/[Co(L^{FNMe})$^+$] couple. Unlike the L^{FP} complexes, the ligand-based [M(L^{FNMe})]/[M(L^{FNMe})$^+$] couple shows a large difference in potential between the palladium (E_{pc} = 0.2 V) and cobalt complex (E_{pc} = 0.05 V) as well as a shift in the ([M(L^{FNMe})$^-$]/[M(L^{FNMe})] ligand-based feature, with the cobalt complex wave ($E_{1/2}$ = -2.12 V) occurring at a more positive potential than the palladium complex (E_{pa} = -2.50 V). An ill-defined oxidation/reduction at around -0.6 V could be due to a Co(II)/Co(III) couple, by comparison to [Co(L^{FP})], which shows a Co(II)/Co(III) feature at $E_{1/2}$ = -0.46 V.

It is therefore clear that the large, aromatic fluorenyl group has a dramatic effect on the electrochemistry of these complexes. Not only are ligand oxidation and reductions possible, but the Co(II)/Co(III) oxidation/reduction has shifted by *ca*. –0.4 V relative to the complexes containing *meso*-ethyl substituents (Co(II)/Co(III) wave at $E_{1/2}$ = -0.12 V [Co(L^P)], -0.46 V [Co(L^{FP})], -0.18 V [Co(L^{NMe})] and *ca*. -0.6 V [Co(L^{FNMe})]). Unfortunately attempts at studying the redox chemistry of these complexes by rotating ring disk electrochemistry, as carried out by Nocera and co-workers on cofacial[3] and hangman[4] porphyrins, were unsuccessful with no repeatable signal observed for any cobalt complexes. Further work is required to confirm assignments of these oxidation/reductions by spectroelectrochemistry.

3.5 Modification of ligand *via* ligand precursors

The syntheses of various macrocycles were attempted by altering the ligand precursors, some with more success than others.

3.5.1 Attempted synthesis of H_4L^2, $H_2L^{amideNH/amideNMe}$ H_2L^{Urea} and H_2L^{NH}

With the successful synthesis of the macrocycles H_2L^P and H_2L^{NMe} from 2-nitrophenol, it was thought a "3-pocket" macrocycle could be synthesised from 2,6-dinitro-*p*-cresol using a similar method (Scheme 2).

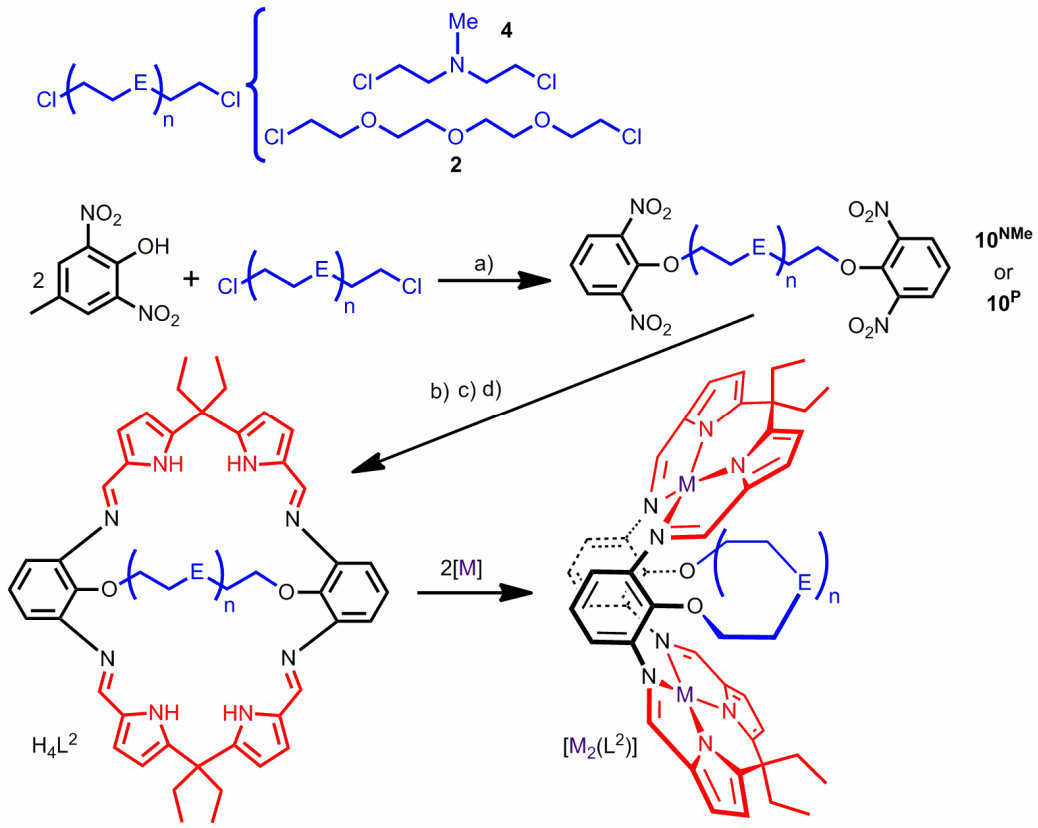

Scheme 2: Attempted synthesis of "3-pocket" macrocycle H_2L^2 from 2, 6-dinitro-p-cresol. E= NMe, n=1 or E=O, n=3. a) K_2CO_3, DMF, 120 °C. b) H_2, Pd/C c) dialdehyde, $BF_3{\cdot}OEt_2$ d) NH_3, MeOH

Unfortunately, all attempts at synthesising the tetra-nitro compound $\mathbf{10}^{P/NMe}$ were unsuccessful; no clean product was isolated by ^{1}H NMR spectroscopy, with the majority of the sample corresponding to unreacted starting materials.

It was also thought an amide-based macrocycle could help fine-tune reactivity as well as hold potential for interesting secondary coordination sphere control. The diamine $\mathbf{11}^{amideNH}$, published by the Nasman group, was chosen due to its one step, facile synthesis from cheap starting materials.[15] Unfortunately, despite varying solvents, acids

(Brønsted and Lewis acids), temperature, reaction time and also attempting template reactions, no macrocyclic product was isolated (Scheme 3). Furthermore, similar problems were encountered during cyclisation when using the tertiary amine **11**$^{\mathbf{amideNMe}}$.

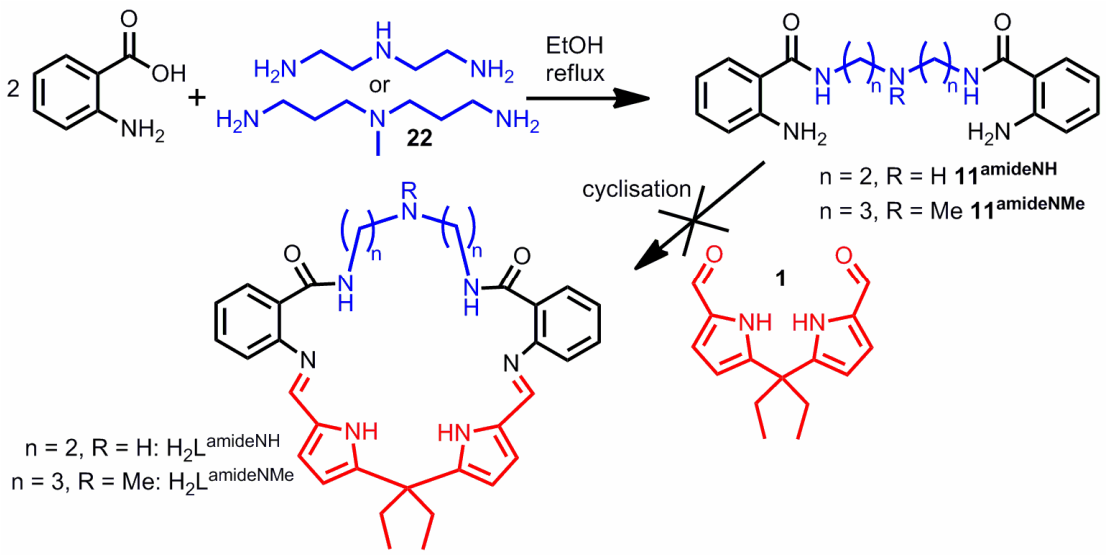

Scheme 3: Attempted synthesis of an asymmetric amide macrocycle

Introducing a urea group to the amine dichloride **3** is desirable due to its potential for secondary coordination sphere control. Using a method developed by Lijinsky and Taylor[16] it was thought the phenyl-urea-appended dichloride **12** was synthesised (Scheme 4). However, reaction of dichloride **3** with phenylisocyanate followed by that of 2-nitrophenol did not yield the desired product.

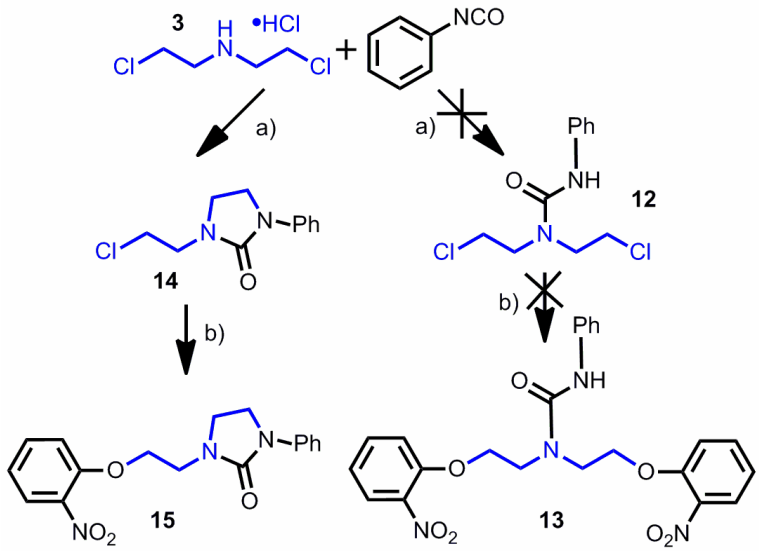

Scheme 4: Attempted initial reactions towards a urea-functionalised macrocycle a) KOH, H_2O, toluene, petroleum ether, phenylisocyanate, reflux b) 2-nitrophenol, K_2CO_3, DMF, 120 ℃

Though a clean, crystalline product was isolated in good yield, the ^{1}H NMR spectrum of the product revealed resonances corresponding to four alkyl CH_2 environments at 4.29 (2H), 3.85–3.78 (4H) and 3.77 ppm (2H) and not the expected two, indicating formation of imidazolidinone **15**; this assignment was also supported by the ESI mass spectrum which displayed a parent ion at 327 amu. Further investigation revealed the formation of an imidazolidinone actually occurs during workup of the initial dichloride step (step a-Scheme 4).[17]

However, since heating can cause this cyclisation reaction and the reaction with 2-nitrophenol was carried out at 120 °C, attempts at urea-based macrocycles were not investigated further. Despite this, a synthesis of a urea-based dinitro compound may be possible starting from other alkyl-[16, 18] and arene-[19] appended urea dichlorides although further work is required.

With attempts at forming an amine-based macrocycle with a urea appendage unsuccessful, synthesis of a macrocycle containing a secondary amine functionality was attempted. Should such a macrocycle be formed, it could open up a wealth of possibilities with regards to modification of the macrocycle *via* this secondary amine. Potential further modifications include ureas,[16], carbamates,[20] amides[21] or alkyl substituents.[22]

Unfortunately the reaction of the secondary amine hydrochloride with 2-nitrophenol led to an unidentified mixture of products by ^{1}H NMR spectroscopy (Scheme 5).

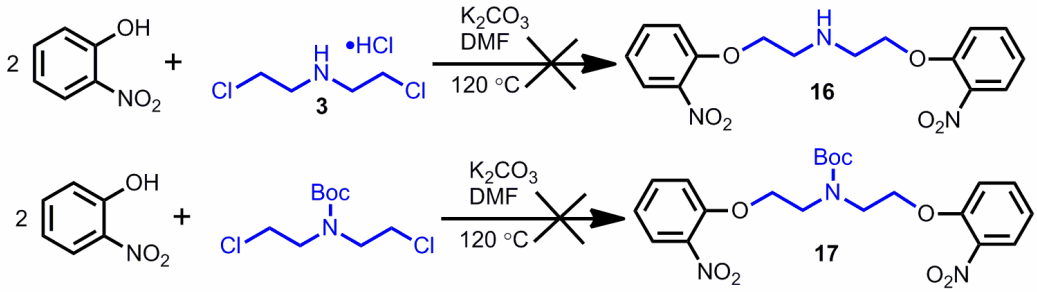

Scheme 5: Initial reactions towards a secondary amine macrocycle

Boc protection of the dichloride **3** is known,[23] however, the product was not found to be stable under the high temperatures used for the dinitro-compound formation (Scheme 5). The reaction was also attempted at the lower temperature of 80 °C with similar results. Despite this, there is scope for using alternative protecting groups in the

future, such as triphenylmethylamine or tosylamide, which may withstand the conditions used.

3.5.2 Synthesis of H_2L^{NMes}

Two macrocycles, H_2L^{NMe} and H_2L^{FNMe}, have been synthesised using a small methyl-appended amine. Due to the small methyl group, the metallated "MN_4" pocket of the macrocycle remains very exposed, and therefore a bulky N-substituent could help to block/protect this. Based on a related phenyl derivative by Lui and co-workers,[24] a 2,4,6-trimethylphenyl (Mes) substituted amine dichloride starting material was synthesised. All the following work on L^{NMes} ligands and complexes was carried out alongside Mr Colin Finn‡. A mixture of 2,4,6-trimethylaniline and 2-chloroethanol was heated in the presence of NaOH, this was followed by addition of $POCl_3$ and resulted in the desired dichloride product **19** (Scheme 6). The macrocycle H_2L^{NMes} was synthesised in a manner similar to H_2L^{NMe} (Scheme 7).

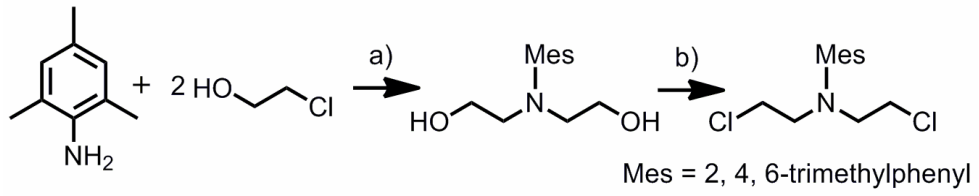

Scheme 6: Synthesis of 2,4,6-trimethylphenyl dichloride ligand precursor a) 20 % NaOH, 120 °C b) $POCl_3$, 110 °C

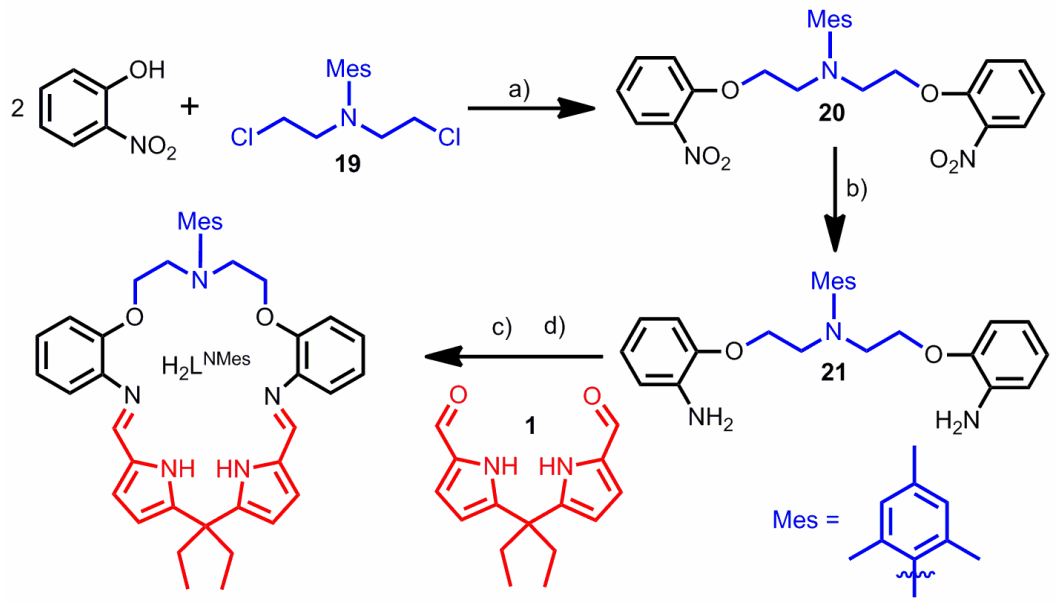

Scheme 7: Synthesis of H_2L^{NMes} a) K_2CO_3, DMF, 120 °C b) 10 % Pd/C cat. H_2 c) $BF_3{\cdot}OEt_2$, EtOH d) NH_3, MeOH, CH_2Cl_2

Reaction of the dichloride compound **19** with 2-nitrophenol followed by reduction using a Pd/C catalyst under an atmosphere of H_2 provided the diamine precursor **21**. Condensation of this diamine with the dialdehyde **1** in the presence of $BF_3{\cdot}OEt_2$ in EtOH, followed by workup in CH_2Cl_2 with an NH_3 solution in MeOH gave H_2L^{NMes} in a good yield (77 %) as a yellow solid.

Cyclisation is inferred in the ^1H NMR spectrum (Figure 15), which shows a singlet resonance at 8.12 ppm that is consistent with formation of an imine. The pyrrolic NH is seen as a broad resonance at 8.84 ppm with aromatic resonances between 7.03 and 6.75 ppm corresponding to the four arene-backbone (multiplets at 7.01 (2H), 6.93–6.90 (4H) and 6.75 (2H) ppm) and one mesityl CH resonance (6.80 ppm). Pyrrolic doublets are present at 6.75 and 6.61 ppm, with two resonances for the ether/amine backbone at 3.84 and 3.52 ppm. Singlets observed at 2.22 and 2.20 ppm correspond to the *para*- and *ortho*-mesityl-CH_3 groups respectively, one *meso*-ethyl environment is seen with resonances at 2.06 (CH_2) and 0.82 ppm (CH_3). Unfortunately, some small, broad resonances are again associated with each main resonance indicating a small amount of [2+2] macrocycle formation.

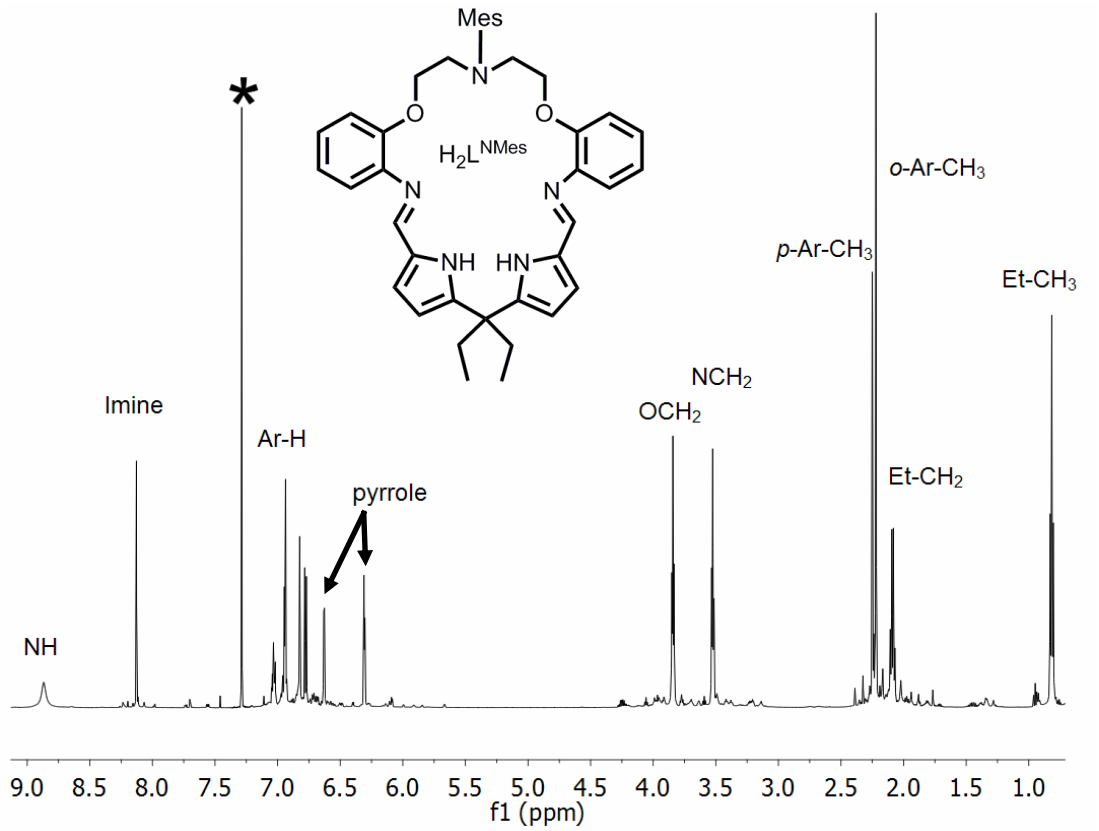

Figure 15: ^1H NMR spectra ($CDCl_3$) of $H_2L^{NMes.}$ '*' denotes residual protio solvent

The successful synthesis of H_2L^{Mes} is also supported by the IR spectrum which displays an NH stretch at 3437 cm^{-1} and an imine absorbance at 1624 cm^{-1}. Microanalysis supports its formulation and the EI mass spectrum shows a parent ion at 627 amu; however, some low intensity peaks at 1254 and 1228 amu indicate that a small amount of higher cyclised product is present.

3.5.3 Complexes of H_2L^{NMes}

Again, alongside Mr Colin Finn,‡ reaction of palladium acetate with the macrocycle H_2L^{NMes} in the presence of NEt_3 gave the complex $[Pd(L^{NMes})]$ as a yellow powder in good yield (68 %) (Equation 6).

$$H_2L^{NMes} + Pd(OAc)_2 \xrightarrow[\text{Toluene}]{2\ NEt_3} [Pd(L^{NMes})]$$

Equation 6

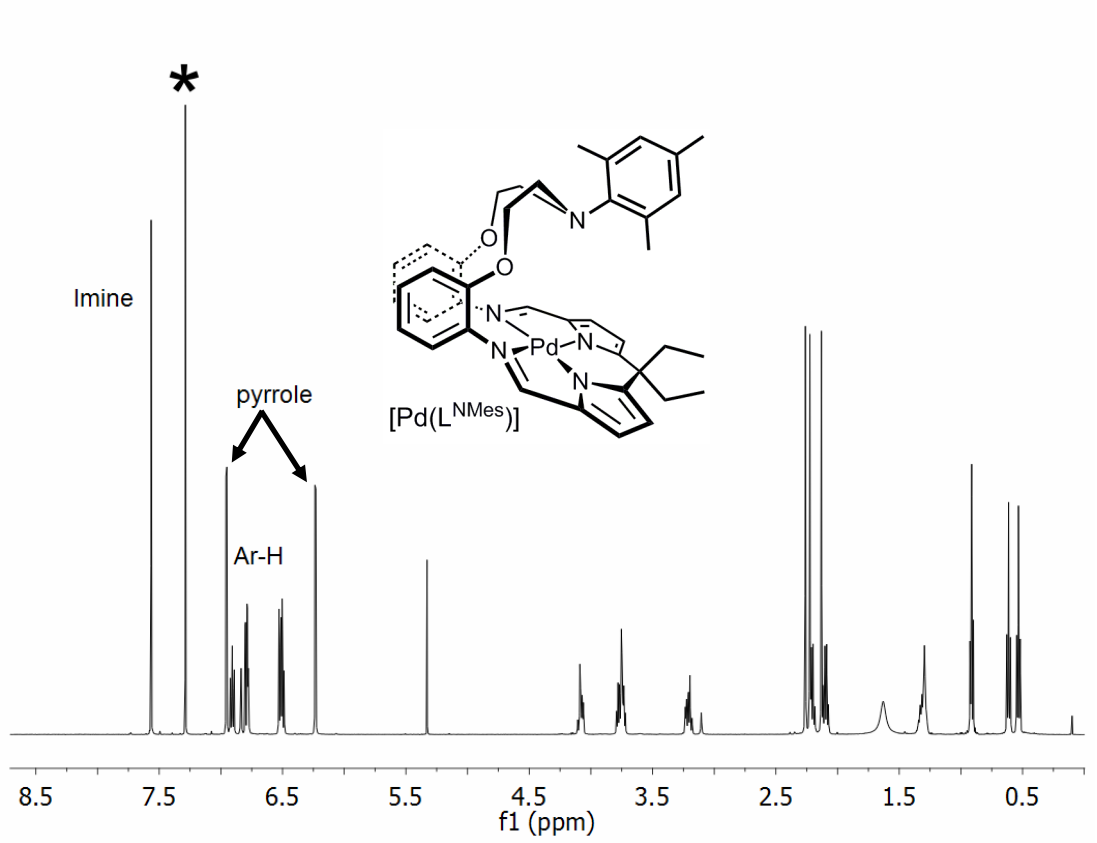

Figure 16: ^1H NMR spectra ($CDCl_3$) of $[Pd(L^{NMes})]$. '*' denotes residual protio solvent

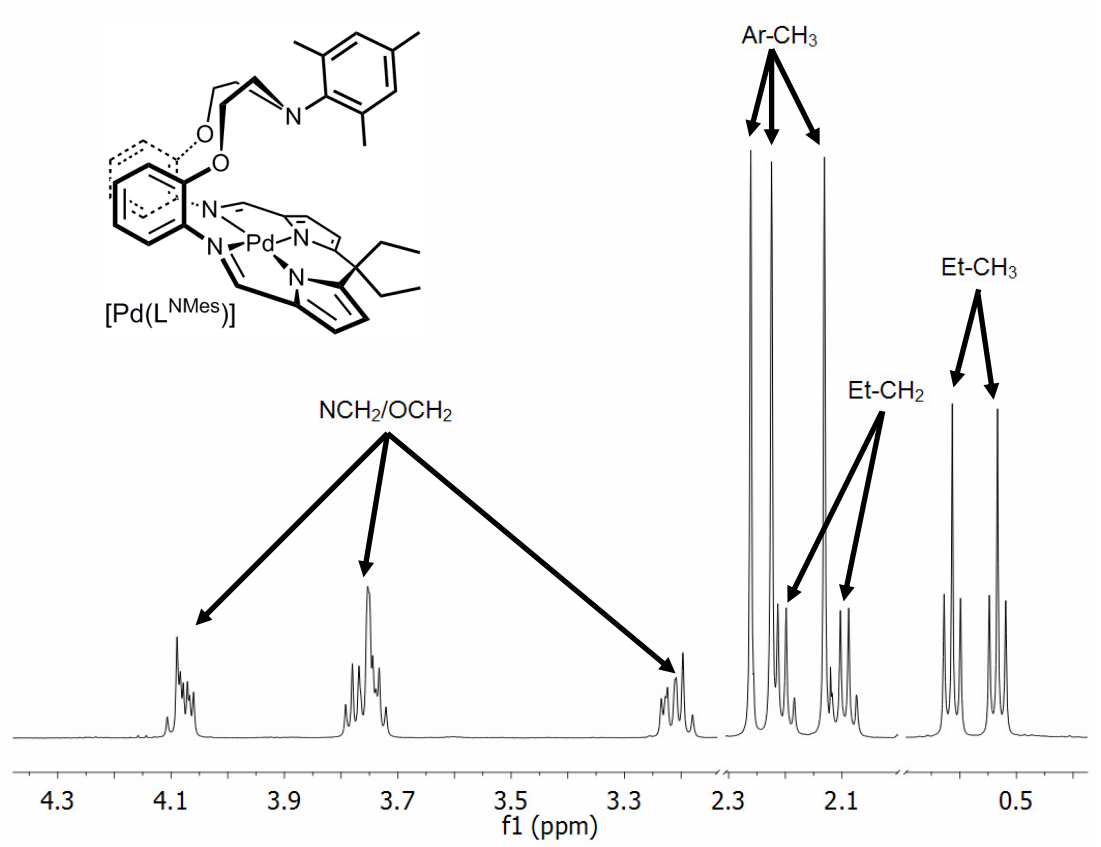

Figure 17: ^{1}H NMR spectra ($CDCl_3$) of [Pd(L^{NMes})] showing alkyl region only (bottom)

A pacman geometry in solution is confirmed by ^{1}H and $^{13}C\{^{1}H\}$ NMR spectroscopy which shows the desymmetrisation of *meso*-ethyl groups and ether/amine backbone protons (Figure 16, Figure 17). In particular, the ^{1}H NMR spectrum shows two sets of quartets at 2.17 and 2.07 ppm (Et-CH_2) and triplets at 0.58 and 0.51 ppm (Et-CH_3) which are mirrored in the $^{13}C\{^{1}H\}$ NMR spectrum with resonances at 9.9 and 9.4 ppm (Et-CH_3) 36.7 and 38.9 ppm (Et-CH_2). The ^{1}H NMR spectrum also shows ether/amine backbone protons as multiplets at 4.05, 3.77–3.69 (two overlapping multiplets) and 3.18 ppm. Further to this, the imine has shifted from 8.13 to 7.54 ppm upon metallation. Interestingly, the mesityl group is also desymmetrised with two resonances seen at 6.80 and 6.74 ppm for the aromatic protons and 2.23, 2.20 and 2.10 ppm for the three methyl groups; these features are also mirrored in the $^{13}C\{^{1}H\}$ NMR spectrum. This lack of symmetry suggests that free-rotation around the N-C(Mes) bond is restricted. In order to investigate this further, crystals of [Pd(L^{NMes})] suitable for single crystal X-ray diffraction were grown from a saturated hexane solution (Figure 18, Table 3).

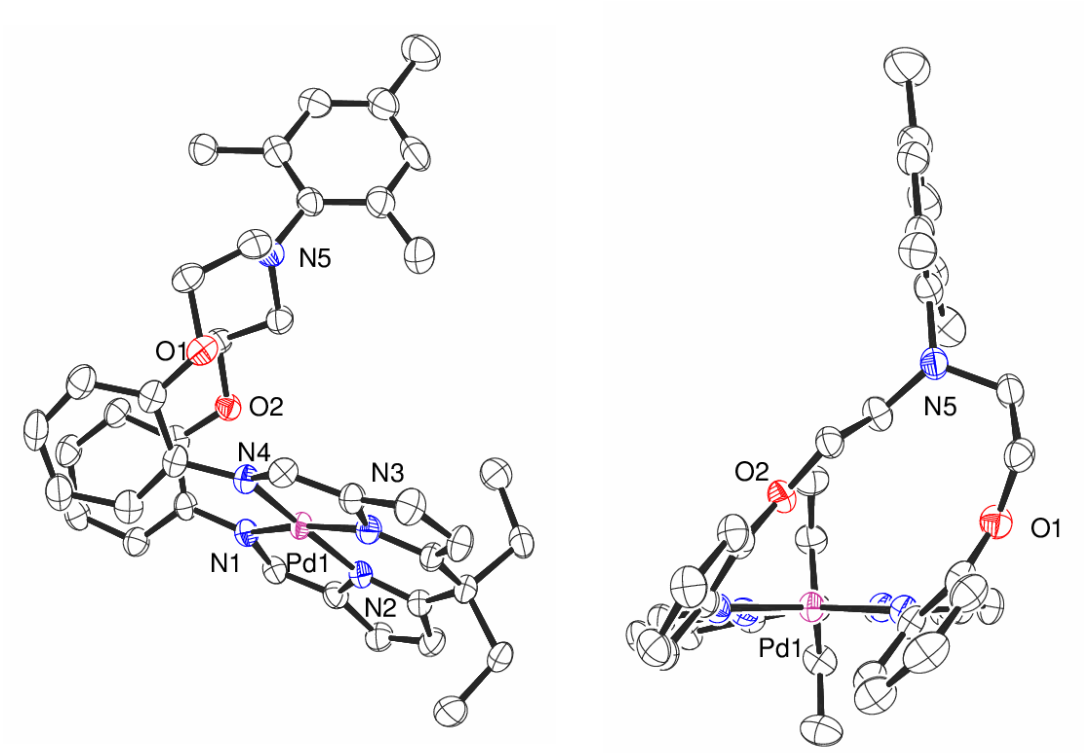

Figure 18: X-ray crystal structure of [Pd(L^{NMes})] For clarity, all hydrogen atoms are omitted and displacement ellipsoids are drawn at 50% probability

Table 3: Selected bond lengths (Å) and angles (°) of [Pd(L^{NMes})]

Pd-N1	2.082(3)	O2···Pd	3.156
Pd-N2	1.934(3)	N1-Pd-N4	111.88(12)
Pd-N3	1.940(3)	N1-Pd-N2	80.09(13)
Pd-N4	2.092(3)	N2-Pd-N3	87.79(14)
Pd···N5	5.543	N3-Pd-N4	80.20(13)
Pd···C32	5.946	Σ ∠ Pd	359.96
Pd ···N_4	0.044	Twist Φ	34.64/40.69
O1···Pd	4.605	Dihedral α	16.66

A clear pacman geometry is observed in the solid state, with the palladium sitting in the N_4-plane (Pd···N_4 0.044 Å) in a distorted square-planar environment. Due to the bulky mesityl group, the arene-hinges have a significant lateral-twist (34.64/40.69 °) compared to symmetric macrocycle complexes (0.3 to 32.2 °).[7-9, 25] These twist values

are however comparable to Pd complexes of other asymmetric macrocycles ([Pd(L^{NMe})] Φ = 23.41–46.75 °, [Pd(L^{FNMe})] Φ = 30.19/43.40 °, see Chapter 2).

The amine-palladium separation (N5···Pd 5.543 Å) is comparable to those in related complexes ([Pd(L^{NMe})] 4.356/5.440 Å, [Pd(L^{FNMe})] 5.610 Å). The palladium-N_{im} and N_{py} distances (Pd-N_{im} 2.082(3)/2.092(3) Å, Pd-N_{py} 1.934(3)/1.940(3) Å) are comparable to those of [Pd(L^{FNMe})] (Pd-N_{im} 2.078(2)–2.080(2) Å, Pd-N_{py} 1.934(2)–1.941(2) Å) and [Pd(L^{NMe})] (Pd-N_{im} 2.093(2)–2.096(2) Å, Pd-N_{py} 1.943(2)–1.945(2) Å). As expected from the solution NMR data, the bulky mesityl group is desymmetrised, with the mesityl-arene ring almost perpendicular to the N_4-plane at an angle of 84.23 °. There is possibly a weak π-π interaction between this mesityl group and the arene-hinge of an adjacent complex with the distance between ring-centroids being 4.512 Å. With regards to the solution-state structure, arene-amines are known to have restricted rotation due to electron donation of the nitrogen lone pair into the π system of the arene; however, this would cause the mesityl group to be roughly parallel with the N_4-plane. As such, it is likely that the restricted rotation is caused by a combination of the steric demand of the *o*-methyl substituents and the rigid pacman geometry. The chemical composition of [Pd(L^{NMes})] is also supported by microanalysis and the EI mass spectrum shows the parent ion at *m/z* = 731. The IR spectrum shows the disappearance of the NH stretch at 3437 cm^{-1} and a shifting in the imine absorbance from 1624 to 1560 cm^{-1}, as seen in the metallation of the other asymmetric macrocycles.

$$H_2L^{NMes} + 3\ KH \xrightarrow[THF]{} [K_2(L^{NMes})] \xrightarrow[THF]{CoCl_2} [Co(L^{NMes})] + 2\ KCl$$

Equation 7

Addition of *in-situ* generated [$K_2(L^{NMes})$] to a stirring suspension of $CoCl_2$ resulted in the formation of [Co(L^{NMes})] as a red solid (Equation 6). The ^1H NMR spectrum is paramagnetically shifted and broadened, displaying 20 resonances between 74 and -43 ppm which are consistent with a solution-state pacman geometry (Figure 19). The IR spectrum supports metallation with the absence of an NH stretch at 3437cm^{-1} and a shifting of the imine absorbance from 1624 to 1558 cm^{-1}. The formulation is confirmed by microanalysis and by EI mass spectrometry, showing a peak at 684 amu, consistent with [Co(L^{NMes})]. Crystals suitable for single crystal X-ray crystallography were grown from a hexane solution of [Co(L^{NMes})] (Figure 20, Table 4).

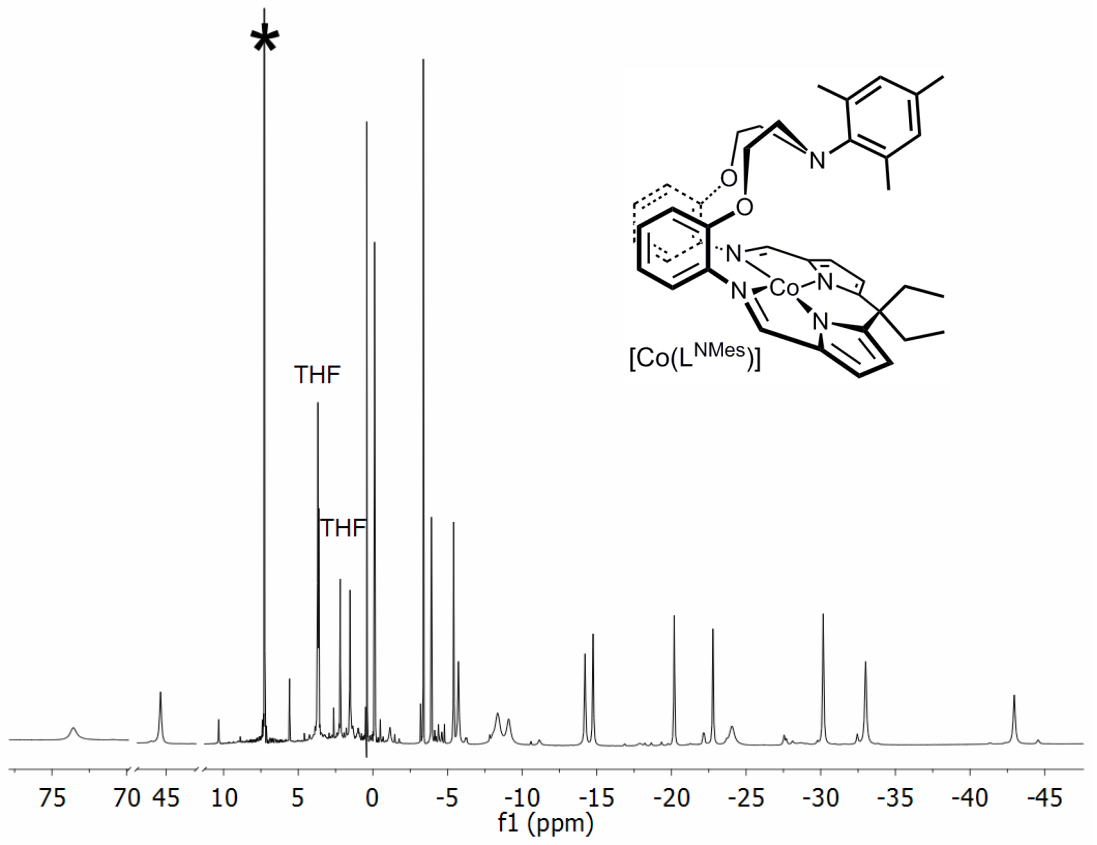

Figure 19: ^{1}H NMR spectra (C_6D_6) of [Co(L^{NMes})]. For clarity, only selected regions shown '*' denotes residual protio solvent

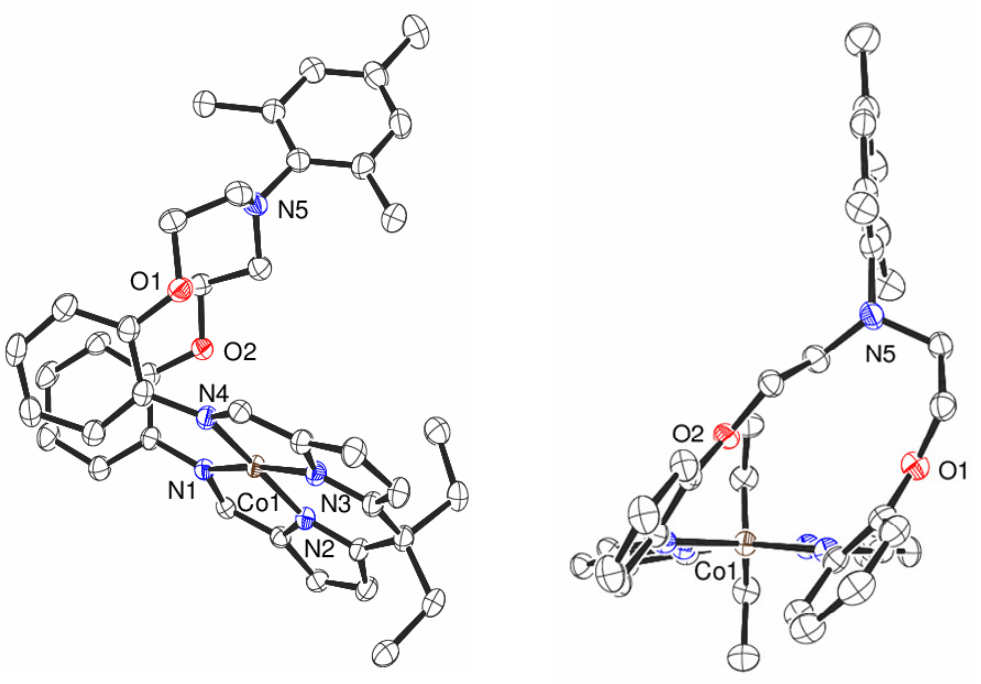

Figure 20: X-ray crystal structure of [Co(L^{NMes})]. For clarity, all hydrogen atoms are omitted and displacement ellipsoids are drawn at 50% probability

Table 4: Selected bond lengths (Å) and angles (°) of [Co(L^{NMes})]

Co1-N1	1.977(2)	O2···Co1	4.500
Co1-N2	1.862(2)	N1-Co1-N4	107.60(8)
Co1-N3	1.864(2)	N1-Co1-N2	82.38(9)
Co1-N4	1.999(2)	N2-Co1-N3	87.17(9)
Co1···N5	5.600	N3-Co1-N4	82.76(9)
Co1···C32	6.065	Σ ∠ Co1	359.91
Co1···N_4	0.056	Twist Φ	58.19/52.07
O1···Co1	3.143	Dihedral α	18.48

The overall structure is similar to that of [Pd(L^{NMes})] with a pacman conformation observed and the cobalt residing in a square-planar environment, 0.056 Å from the N_4-plane. Co-N distances (Co1-N_{im} 1.977(2)–1.999(2) Å, Co1-N_{py} 1.862(2)–1.864(2) Å) are consistent with those seen in other asymmetric ligand cobalt complexes (Co-N_{im} 1.981(1)–2.0335(18) Å, Co-N_{py} 1.852(3)–1.8818(18) Å). Further to this there is potentially a weak interaction between the cobalt and one of the ethereal linkers (Co1···O1 3.143 Å). As with [Pd(L^{NMes})], the bulky Mes group is orientated away from the metal centre resulting in a N5···Co1 distance of 5.600 Å and the arene backbones are heavily twisted (Φ = *ca.* 55°) but are comparable to other Co(II) complexes of asymmetric ligands (43.18–55.25 °). The Mes group is also found roughly perpendicular to the N_4-plane at an angle of 85.16 ° with the Mes group desymmetrised, agreeing with the ^{1}H NMR spectrum.

[Co(L^{NMes})] is yet to be investigated for reactivity towards any small molecules.

3.5.4 Synthesis and complexation of $H_2L^{(NH)NMe}$

In a modification to a tris-silylamine ligand set first reported by Cloke and co-workers (Figure 21, top left),[26] the Mountford group synthesised zirconium and scandium complexes of a three-carbon bridged silyl-amine ligand.[27, 28] The zirconium complex of this ligand was shown to be an efficient olefin polymerisation catalyst (Figure 21, top right).[27]

Recently, work on a related, two carbon-bridged system has also been shown to undergo nitrile, isonitrile, CO_2, isocyanate and alkyne insertion into Ti=N_α bonds in hydrazido complexes of this ligand (Figure 21, bottom).[29]

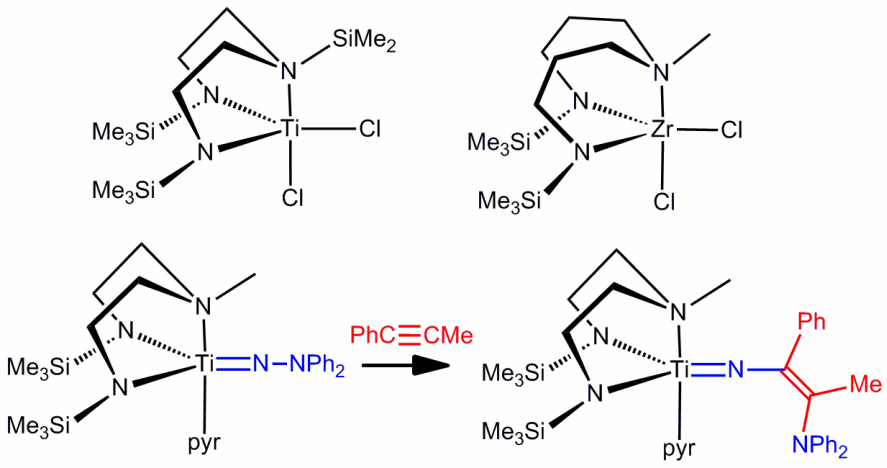

Figure 21: A tris-silylamine ligand complex by Cloke and co-workers (top left). A three-carbon bridged ligand-zirconium complex precursor to an olefin polymerisation catalyst (top right), titanium complexes of a two-carbon bridged ligand undergoes alkyne insertion into the N_α of a hydrazido bond (bottom)

Tin, bismuth, gallium, and aluminium complexes[30, 31] of this two carbon-bridged ligand have also been synthesised by the Bertrand group, with the later two shown to be catalysts for the ring-opening polymerization of heterocycles.[31] Furthermore, tantalum hydrazido complexes have also been synthesised and studied by Bercaw and co-workers.[32]

Using a synthesis based on that by the Seth group,[33] the desired diamine is prepared in two straightforward steps by reaction of 2-fluoronitrophenol and diamine **22** in the presence of $CaCO_3$, followed by reduction of nitro groups with H_2 using a Pd/C catalyst (Scheme 8). The cyclisation step was screened briefly for the best conditions, including solvent (CH_2Cl_2, MeOH, EtOH, IPA, $CHCl_3$, toluene), temperature (-20 °C to 100 °C), acid (TFA, *p*-toluenesulfonic acid, HCl and $BF_3{\cdot}OEt_2$) and base (KOH, NEt_3) with the best results using TFA and KOH in methanol at room temperature; this resulted in the formation of $H_2L^{(NH)NMe}$ as a yellow powder in low yield (10 %) (Scheme 8).

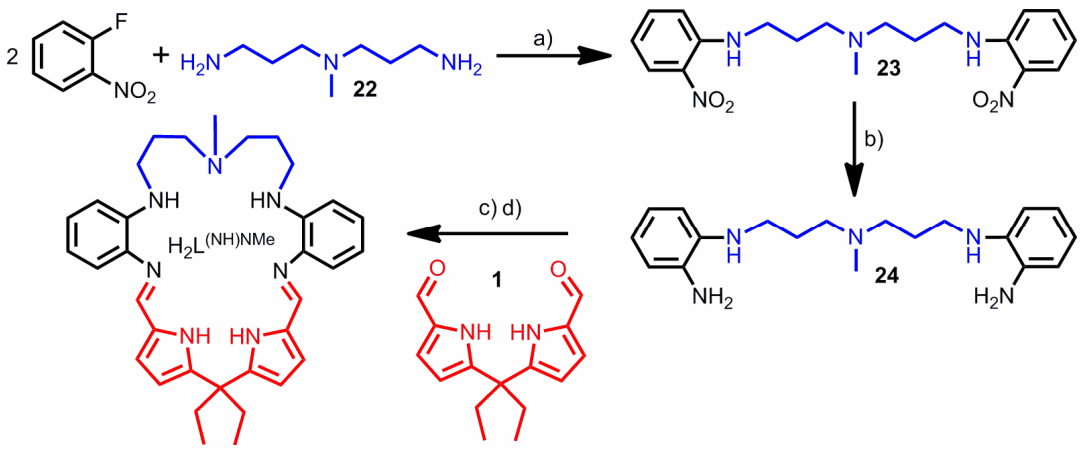

Scheme 8: Synthesis of $H_2L^{(NH)NMe}$ a) $CaCO_3$, CH_2Cl_2 b) H_2 Pd/C c) 2.1 TFA, MeOH d) KOH, MeOH

Interestingly, the inclusion of arene-amine, rather than arene-ether connectors enabled the use of Brønsted acids, rather than Lewis acids, in the cyclisation step. Addition of a slight excess of TFA to a mixture of diamine **22** and dialdehyde **1** causes a colour change from light orange to a deep red. However, despite a seemingly clean formation of the TFA-salt of the macrocycle by ^{1}H NMR spectroscopy, deprotonation to the free-base macrocycle requires further investigation. Addition of NEt_3 or KOH to the TFA-salt of the macrocycle results in a colour change from red to yellow with the precipitation of copious amounts of a bright yellow solid; however, the ^{1}H NMR spectrum of this precipitate indicates the formation of several products. Removal of solvent from the filtrate however, indicates clean formation of the desired macrocyclic product, albeit in poor yield. Further investigation into the base-addition step would undoubtedly increase the yield of clean macrocycle formed.

The ^{1}H NMR spectrum of $H_2L^{(NH)NMe}$ (Figure 22) indicates its successful formation with a resonance attributed to an imine proton at 8.19 ppm. Four aromatic backbone multiplets are present at 7.07, 6.92, 6.65 and 6.61 ppm with the pyrrolic doublets at 6.60 and 6.14 ppm. The resonance at 4.89 ppm is attributed to the amine/alkyl backbone-NH. Only one environment is observed for the amine/alkyl backbone protons at 3.22, 2.50 and 1.84 ppm and *meso*-ethyl groups at 2.23 (CH_2) and 0.88 ppm (CH_3). The single ethyl-environment is mirrored in the ^{13}C{^{1}H} NMR spectrum which shows resonances at 28.37 and 8.23 ppm for the ethyl CH_2 and CH_3 protons, respectively.

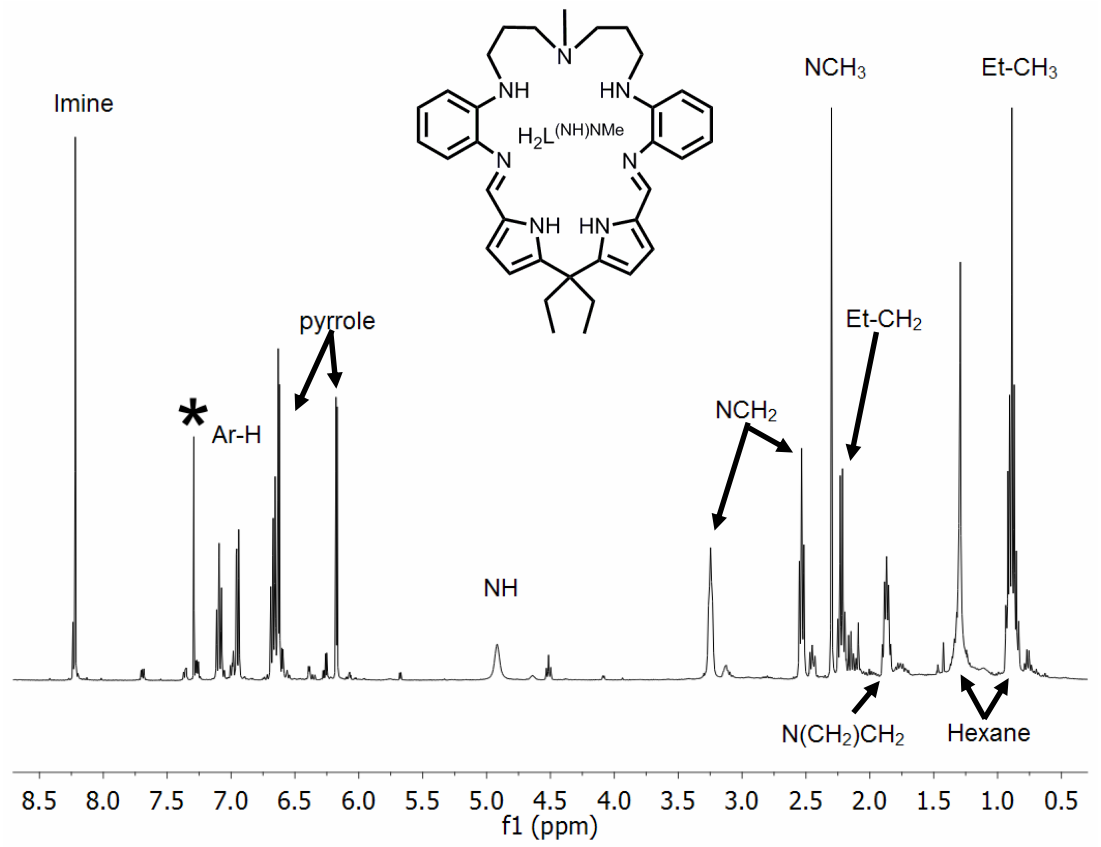

Figure 22: ^{1}H NMR spectra ($CDCl_3$) of $H_2L^{(NH)NMe}$. '*' denotes residual protio solvent

The IR spectrum displays NH stretches at 3444 and 3306 cm^{-1} with an imine absorbance at 1614 cm^{-1}. The formulation is supported by microanalysis and also in the EI mass spectrum with a parent ion seen at 549 amu. However, lower intensity peaks are also present at 547 and 545 amu, which correspond to an intramolecularly-cyclised product which will be explained below.

Crystallisation of the macrocycle was attempted by slow diffusion of diethylether into a CH_2Cl_2/MeOH solution of $H_2L^{(NH)NMe}$, and resulted in crystals suitable for single crystal X-ray diffraction (Table 5, Figure 23); this structure shows that the macrocycle is capable of intramolecular cyclisation reactions. Three crystallographically independent macrocycles were present in the asymmetric unit, but due to their similarity only one will be discussed.

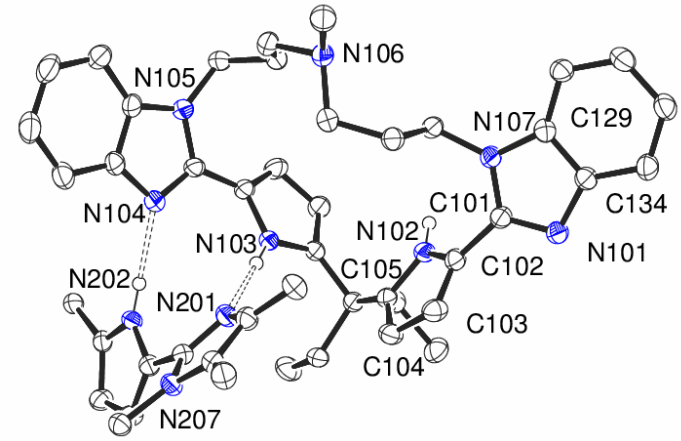

Figure 23: X-ray crystal structure of cyclised $H_2L^{(NH)NMe}$. For clarity, all hydrogen atoms except those on N102, N103 and N202 are omitted and displacement ellipsoids are drawn at 50% probability. Only part of a second macrocycle, interacting through intermolecular hydrogen bonding of benzimidazole/pyrrole units is shown. The asymmetric unit contains three crystallographically independent macrocycles, only one is shown

Table 5: Selected bond lengths (Å) and angles (°) of cyclised $H_2L^{(NH)NMe}$

N101-C101	1.3244(19)	C103-C104	1.418(2)
C101-N107	1.3731(19)	C104-C105	1.371(2)
N107-C129	1.3814(19)	C105-N102	1.3736(19)
C129-C134	1.403(2)	N102-C102	1.3795(19)
C134-N101	1.392(2)	N103-N201	2.930
N101-C101-N107	113.06(13)	N104-N202	2.916
C102-C103	1.365(2)		

The amine NH of the flexible backbone has clearly attacked the imine double bond to form a benzimidazole at each end of the macrocycle. This type of reactivity is known,[34] with intermediates undergoing air-oxidation (Scheme 9). Similar reactions are also promoted by light[35] and by addition of base.[36]

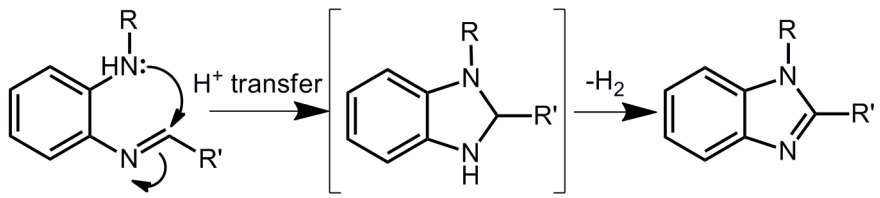

Scheme 9: General reaction scheme for formation of benzimidazoles by attack on an imine-carbon

Assignment of the benzimidazole group is confirmed by studying bond lengths and angles with the C=N double bond (N101-C101 = 1.3244(19) Å) shorter than the other C-N bonds in the five-membered ring (1.3731(19)–1.392(2) Å). Also, the bridging carbon adopts an angle of N101-C101-N107 113.06(13) °, which is similar to other benzimidazole structures (C=N 1.299(9)–1.343(3) Å, C-N 1.358(6)–1.412(2) Å, N-C-N 110.9(6)–132.4(2) °).[37] The benzimidazole is completely planar, with each benzimidazole C=N and adjacent pyrrolic NH H-bonded to a benzimidazole C=N and pyrrolic NH of an adjacent macrocycle (N103···N201 2.930 Å, N104···N202 2.916 Å).

Thus the ions seen in the mass spectrum at two and four mass units less than the parent peak can be attributed to the mono- and bis-benzimidazole macrocyclic products, though it is unclear if these compounds are formed during the synthesis of the macrocycle or under mass spectrometry conditions. Removal of all solvents from $H_2L^{(NH)NMe}$, once initially formed, by prolonged drying on high vacuum lines and storage, as a precaution, under a glove-box nitrogen atmosphere leads to no decomposition through intramolecular reactions as observed by ^{1}H NMR spectroscopy. Further investigation is needed into the exact cause of and prevention of these intramolecular reactions.

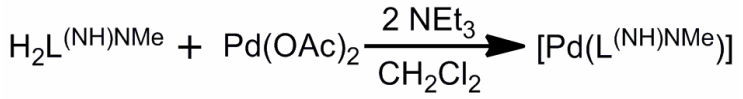

Equation 8

In order to probe if it is possible for this new macrocycle to form wedge-shaped complexes, the Pd(II) complex was synthesised. Reaction of the macrocycle with palladium acetate in CH_2Cl_2 in the presence of NEt_3 resulted in [Pd($L^{(NH)NMe}$)] a yellow solid (Equation 8). The ^{1}H NMR spectrum (Figure 24) shows the disappearance of the pyrrolic NH resonance and a shifting of the imine singlet from 8.19 to 7.61 ppm, indicating successful metallation. As seen with previously described asymmetric pacman complexes, two distinct environments are observed for the *meso*-ethyl and amine/alkyl backbone protons. The amine/alkyl backbone protons are observed as multiplets, some overlapping, at 3.03 (2H), 2.72 (2H), 2.51–2.38 (4H), and 1.86–1.77 ppm (4H) with only one environment seen in the ^{13}C{^{1}H} NMR spectrum (52.95, 41.90 and 25.17 ppm); this indicates that the protons are found in two different environments, *endo*- and *exo*- to the cleft. Dissimilar *meso*-ethyl protons are seen at 2.17 and 2.07 ppm (CH_2) and 0.53 and

0.50 ppm (CH_3), and are mirrored in the $^{13}C\{^1H\}$ NMR spectrum at 38.89 and 36.81 pm (CH_2) and 9.91 and 9.75 ppm (CH_3). Once formed, the complex is stable to decomposition, with the ^1H NMR spectrum unchanging after days left exposed to air.

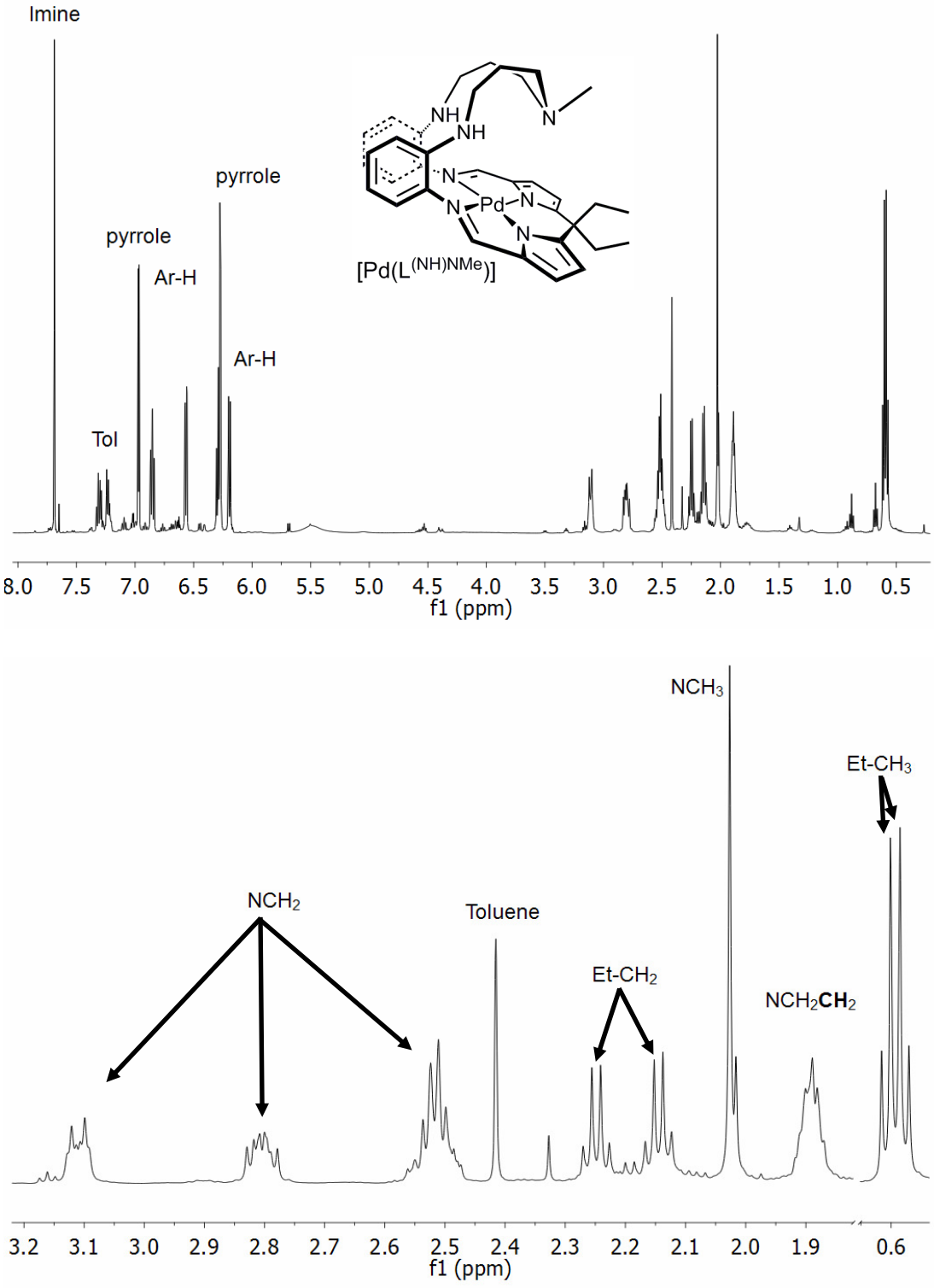

Figure 24: ^1H NMR spectra ($CDCl_3$) of [Pd($L^{(NH)NMe}$)] (top) and showing selected alkyl regions only (bottom) (Tol = toluene)

Metallation is also supported by the IR spectrum which shows only one NH stretch at 3354 cm^{-1}, rather than the two seen in the free ligand, and a shifting of the imine absorbance from 1614 to 1591 cm^{-1}. The formulation is supported by microanalysis with the EI mass spectrum displaying a parent ion at 653 amu. Crystals of [Pd($L^{(NH)NMe}$)] suitable for single crystal X-ray diffraction were grown from a saturated hexane solution (Figure 25, Table 6).

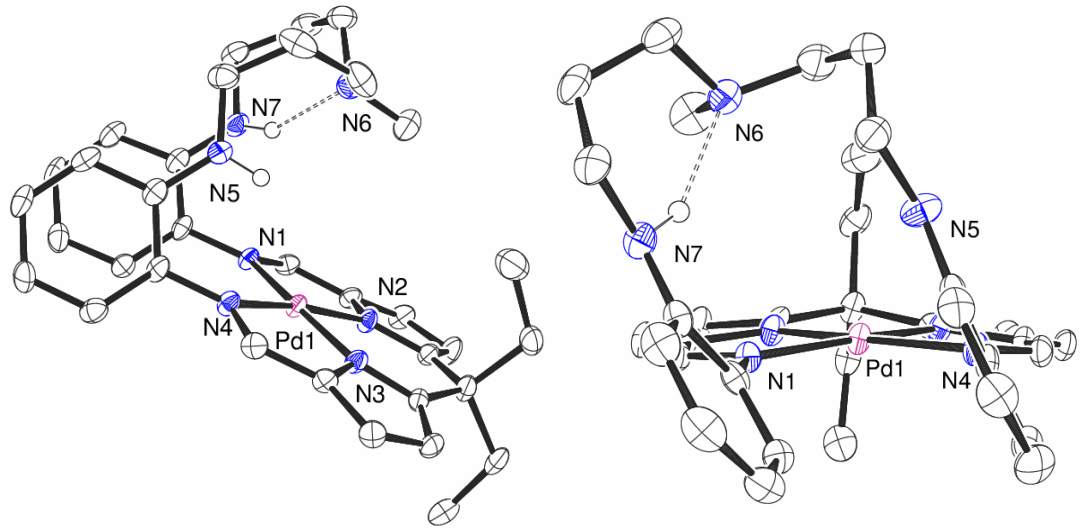

Figure 25: X-ray crystal structure of [Pd($L^{(NH)NMe}$)]. For clarity, all hydrogen atoms are omitted and displacement ellipsoids are drawn at 50% probability

Table 6: Selected bond lengths (Å) and angles (°) of [Pd($L^{(NH)NMe}$)]

Pd-N1	2.078(2)	N1-Pd-N4	110.99(8)
Pd-N2	1.9369(19)	N1-Pd-N2	80.60(8)
Pd-N3	1.936(2)	N2-Pd-N3	88.14(8)
Pd-N4	2.076(2)	N3-Pd-N4	80.17(8)
Pd···N5	3.456	Pd···N_4	0.046
Pd···N6	4.385	Σ ∠ Pd	359.9
Pd···N7	4.495	Twist Φ	33.80/25.03
N5···N6	3.625	Dihedral α	11.85
N7···N6	2.841		

The complex adopts a wedge-shaped pacman conformation as expected from the solution NMR data. The palladium resides in a distorted square planar environment

sitting within the N_4-plane (Σ Pd ∠ 359.9 °, N_4···Pd 0.046 Å). The Pd-N_{im} bond lengths (2.076(2)/2.078(2) Å) are marginally shorter than other asymmetric macrocycle-palladium complexes (Pd-N_{im} 2.078(2)–2.096(2) Å) with Pd-N_{py} distances (1.9369(19)/1.936(2) Å) within other asymmetric-palladium complexes (Pd-N_{py} 1.934(2)–1.945(2) Å). All Pd-N distances also within symmetric macrocycle palladium distances (Pd-N_{im} 2.043(7)–2.096(2) Å, Pd-N_{py} 1.928(4)–1.947(4) Å).[7-9] An intermolecular hydrogen bond is seen between the amine/alkyl backbone (N6···N7 2.841 Å) creating a Pd···N6 separation of 4.385 Å, *ca*. 1.2 Å shorter than that of [Pd(L^{NMes})] and [Pd(L^{FNMe})] (5.543 and 5.610 Å respectively) and comparable to that of the "closed mouth" [Pd(L^{NMe})] structure (4.356 Å, see Chapter 2). This hydrogen bonding interaction appears to pre-organise the amine/alkyl backbone towards further metal binding.

$$H_2L^{(NH)NMe} + 3\ KH \xrightarrow[THF]{} [K_2(L^{(NH)Me})] \xrightarrow[THF]{CoCl_2} [Co(L^{(NH)Me})] + 2\ KCl$$

Equation 9

Though only attempted on a small scale, the deprotonation of the pyrrolic protons by KH followed by addition to cobalt dichloride results in a colour change from red to dark red (Equation 9). The EI mass spectrum of the resulting red solid shows a parent ion at 606 amu due to [Co($L^{(NH)NMe}$)], though more work is required to confirm this result. Further research into the metallation reactions of this macrocycle with other metals is also needed. Furthermore, this ligand possesses the potential to bind two different metal centres to yield heterobimetallic complexes that could be a promising area of future research (Scheme 10).

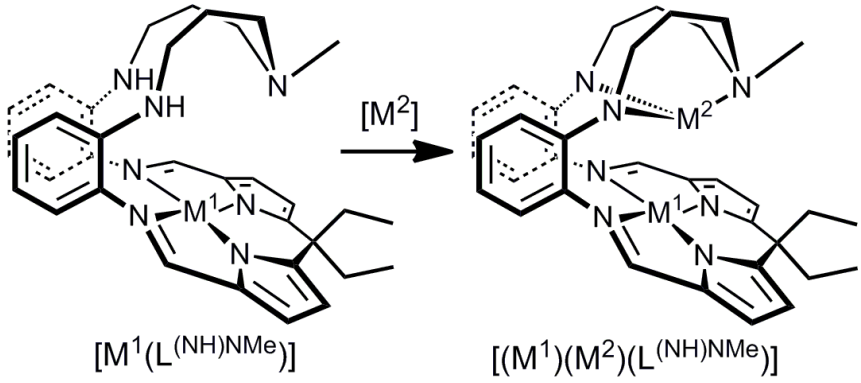

Scheme 10: The macrocycle $H_2L^{(NH)NMe}$ has the potential to bind two different metals

3.6 Conclusion

A further four new asymmetric macrocycles, capable of folding to a pacman conformation upon metallation have been synthesised and characterised.

Modification of the asymmetric macrocycles H_2L^{NMe} and H_2L^{P} is possible by altering the dialdehyde used in the cyclisation step. Introduction of the large, bulky fluorenyl group yielded H_2L^{FP} and H_2L^{FNMe} which were fully characterised. The synthesis of these ligands occurs in a higher yield giving purer products than their ethyl counterparts; however, due to poor solubility the yields arising from subsequent metallation reactions are less than that of L^{P} and L^{NMe}. The complexes $[Pd(L^{FP})]$, $[Pd(L^{FNMe})]$, $[K_2(L^{FP})]$, $[K_2(L^{FNMe})]$, $[Mg(L^{FP})]$, $[Mg(L^{FNMe})]$, $[Co(L^{FP})]$ and $[Co(L^{FNMe})]$ were synthesised and characterised, with the cobalt complexes undergoing air-oxidation to form new Co(III) complexes. The electrochemistry of the cobalt(II) complexes $[Co(L^{P})]$, $[Co(L^{NMe})]$, $[Co(L^{FP})]$ and $[Co(L^{FNMe})]$ was investigated and it was found that the introduction of the fluorenyl group introduced two ligand-based features as well as shifting the Co(II)/Co(III) couple by *ca*. -0.4 V relative to *meso*-ethyl substituted complexes. Furthermore, the substituent on the amine-dichloride macrocycle precursor can be altered to incorporate a large, bulky mesityl group, giving H_2L^{NMes} upon cyclisation, and the complexes $[Pd(L^{NMes})]$ and $[Co(L^{NMes})]$ were also synthesised and characterised. Though more work on modified macrocycles with groups such as urea or NH appended macrocycles is needed, a sixth asymmetric macrocycle, $H_2L^{(NH)NMe}$, was synthesised and characterised, as was its Pd complex $[Pd(L^{(NH)NMe})]$. This macrocycle shows future potential for the synthesis of heterobimetallic complexes.

3.7 References

† Miss Berengere Escuyer: A first year "Brevet de technicien supérieur" (BTS) student studying at the National School of Chemistry, Physics and Biology (Ecole Nationale de Chimie, Physique et Biologie), Paris, France. She worked on L^{FP} and L^{FNMe} ligands and complexes for a two month period in summer 2010 under the supervision of James W. Leeland and Dr. Jason B. Love.

‡ Mr. Colin Finn: A chemistry BSc final year project student at the University of Edinburgh. He worked on the L^{NMes} ligand and complexes in the 2009/2010 academic year under the supervision of James W. Leeland and Dr. Jason B. Love. As of September 2010, he is studying for a PhD under the supervision of Dr Jason B. Love. All results involving L^{NMes} were gained whilst Mr. Finn was a project student with the exception of the solid-state structure of [Co(L^{NMes})]. This was grown whilst a PhD student and is included in this thesis with the permission of Mr. Colin Finn and Dr. Jason B. Love.

[1] J. P. Collman, P. Denisevich, Y. Konai, M. Marrocco, C. Koval, F. C. Anson, *J. Am. Chem. Soc.* **1980**, *102*, 6027.

[2] J. P. Collman, P. S. Wagenknecht, J. E. Hutchison, *Angew. Chem., Int. Ed. Engl.* **1994**, *33*, 1537; R. Guilard, M. A. Lopez, A. Tabard, P. Richard, C. Lecomte, S. Brandes, J. E. Hutchison, J. P. Collman, *J. Am. Chem. Soc.* **1992**, *114*, 9877; J. P. Collman, J. E. Hutchison, M. A. Lopez, A. Tabard, R. Guilard, W. K. Seok, J. A. Ibers, M. L'Her, *J. Am. Chem. Soc.* **1992**, *114*, 9869; C. K. Chang, I. Abdalmuhdi, *Angew. Chem., Int. Ed. Engl.* **1984**, *23*, 164; C. K. Chang, I. Abdalmuhdi, *J. Org. Chem.* **1983**, *48*, 5388; C. J. Chang, Y. Deng, S.-M. Peng, G.-H. Lee, C.-Y. Yeh, D. G. Nocera, *Inorg. Chem.* **2002**, *41*, 3008; C. J. Chang, Y. Deng, A. F. Heyduk, C. K. Chang, D. G. Nocera, *Inorg. Chem.* **2000**, *39*, 959; C. J. Chang, E. A. Baker, B. J. Pistorio, Y. Deng, Z.-H. Loh, S. E. Miller, S. D. Carpenter, D. G. Nocera, *Inorg. Chem.* **2002**, *41*, 3102; Y. Deng, C. J. Chang, D. G. Nocera, *J. Am. Chem. Soc.* **1999**, *122*, 410.

[3] J. Rosenthal, D. G. Nocera, *Acc. Chem. Res.* **2007**, *40*, 543.

[4] R. McGuire Jr, D. K. Dogutan, T. S. Teets, J. Suntivich, Y. Shao-Horn, D. G. Nocera, *Chem. Sci.* **2010**, *1*, 411.

[5] C.-Y. Yeh, C. J. Chang, D. G. Nocera, *J. Am. Chem. Soc.* **2001**, *123*, 1513.

[6] J. W. Leeland, A. M. Z. Slawin, J. B. Love, *Organometallics* **2010**, *29*, 714.

[7] G. Givaja, M. Volpe, J. W. Leeland, M. A. Edwards, T. K. Young, S. B. Darby, S. D. Reid, A. J. Blake, C. Wilson, J. Wolowska, E. J. L. McInnes, M. Schröder, J. B. Love, *Chem., Eur., J.* **2007**, *13*, 3707.

[8] E. Askarizadeh, A. M. J. Devoille, D. M. Boghaei, A. M. Z. Slawin, J. B. Love, *Inorg. Chem.* **2009**, *48*, 7491.

[9] G. Givaja, A. J. Blake, C. Wilson, M. Schroder, J. B. Love, *Chem. Commun.* **2003**, 2508.

[10] E. Askarizadeh, S. B. Yaghoob, D. M. Boghaei, A. M. Z. Slawin, J. B. Love, *Chem. Commun.* **2010**, *46*, 710.

[11] J. P. Collman, L. Fu, P. C. Herrmann, X. Zhang, *Science* **1997**, *275*, 949; J. P. Collman, N. K. Devaraj, R. A. Decreau, Y. Yang, Y.-L. Yan, W. Ebina, T. A. Eberspacher, C. E. D. Chidsey, *Science* **2007**, *315*, 1565.

[12] M. Volpe, H. Hartnett, J. W. Leeland, K. Wills, M. Ogunshun, B. J. Duncombe, C. Wilson, A. J. Blake, J. McMaster, J. B. Love, *Inorg. Chem.* **2009**, *48*, 5195.

[13] C. J. Chang, Z.-H. Loh, C. Shi, F. C. Anson, D. G. Nocera, *J. Am. Chem. Soc.* **2004**, *126*, 10013; Y. Le Mest, C. Inisan, A. Laouenan, M. L'Her, J. Talarmin, M. El Khalifa, J.-Y. Saillard, *J. Am. Chem. Soc.* **1997**, *119*, 6095.

[14] A. J. Downard, A. M. Bond, A. J. Clayton, L. R. Hanton, D. A. McMorran, *Inorg. Chem.* **1996**, *35*, 7684.
[15] O. S. M. Nasman, R. M. Baraka, A. A. Khaldi, I. E. Nahhal, S. P. Varkey, M. Shakir, *Trans. Met. Chem.* **1997**, *22*, 273.
[16] W. Lijinsky, H. W. Taylor, *J. Cancer Res. Clin. Oncol* **1979**, *94*, 131.
[17] G. R. Pettit, D. S. Blonda, R. A. Upham, *Can. J. Chem.* **1965**, *43*, 1798.
[18] F. D. Popp, H. Swarz, *J. Org. Chem.* **1961**, *26*, 4764.
[19] F. D. Popp, D. W. Alwani, *Can. J. Chem.* **1964**, *42*, 1506.
[20] R. N. Salvatore, F. Chu, A. S. Nagle, E. A. Kapxhiu, R. M. Cross, K. W. Jung, *Tetrahedron* **2002**, *58*, 3329.
[21] E. Chapoteau, B. P. Czech, A. Kumar, W. Zazulak, *J. Incl. Phenom. Macro.* **1993**, *16*, 367; E. Graf, M. W. Hosseini, R. Ruppert, *Tetrahedron Lett.* **1994**, *35*, 7779.
[22] J. Jurczak, R. Ostaszewski, *Tetrahedron Lett.* **1988**, *29*, 959.
[23] M. W. Glenny, L. G. A. van de Water, J. M. Vere, A. J. Blake, C. Wilson, W. L. Driessen, J. Reedijk, M. Schröder, *Polyhedron* **2006**, *25*, 599.
[24] X. Shen, H. Liu, Y. Li, S. Liu, *Macromolecules* **2008**, *41*, 2421.
[25] J. M. Veauthier, W.-S. Cho, V. M. Lynch, J. L. Sessler, *Inorg. Chem.* **2004**, *43*, 1220.
[26] H. C. S. Clark, F. G. N. Cloke, P. B. Hitchcock, J. B. Love, A. P. Wainwright, *J. Organomet. Chem.* **1995**, *501*, 333; F. G. N. Cloke, P. B. Hitchcock, J. B. Love, *J. Chem. Soc., Dalton Trans.* **1995**, 25.
[27] T. A. Lowes, B. D. Ward, R. A. Whannel, S. R. Dubberley, P. Mountford, *Chem. Commun.* **2005**, 113.
[28] B. D. Ward, S. R. Dubberley, A. Maisse-Francois, L. H. Gade, P. Mountford, *J. Chem. Soc., Dalton Trans.* **2002**, 4649.
[29] P.-J. Tiong, A. D. Schofield, J. D. Selby, A. Nova, E. Clot, P. Mountford, *Chem. Commun.* **2010**, *46*, 85; J. D. Selby, C. D. Manley, M. Feliz, A. D. Schwarz, E. Clot, P. Mountford, *Chem. Commun.* **2007**, 4937; A. D. Schofield, A. Nova, J. D. Selby, C. D. Manley, A. D. Schwarz, E. Clot, P. Mountford, *J. Am. Chem. Soc.* **2010**, *132*, 10484; A. D. Schofield, A. Nova, J. D. Selby, A. D. Schwarz, E. Clot, P. Mountford, *Chem., Eur., J.* **2011**, *17*, 265.
[30] J.-L. Fauré, H. Gornitzka, R. Réau, D. Stalke, G. Bertrand, *Eur. J. Inorg. Chem.* **1999**, *1999*, 2295.
[31] N. Emig, H. Nguyen, H. Krautscheid, R. Reau, J.-B. Cazaux, G. Bertrand, *Organometallics* **1998**, *17*, 3599.
[32] I. A. Tonks, J. E. Bercaw, *Inorg. Chem.* **2010**, *49*, 4648.
[33] P. P. Seth, E. A. Jefferson, L. M. Risen, S. A. Osgood, *Bioorg. Med. Chem. Lett.* **2003**, *13*, 1669.
[34] S. Lin, L. Yang, *Tetrahedron Lett.* **2005**, *46*, 4315; H. Chikashita, S. Nishida, M. Miyazaki, Y. Morita, K. Itoh, *Bull. Chem. Soc. Jpn.* **1987**, *60*, 737.
[35] K. H. Grellmann, E. Tauer, *Tetrahedron Lett.* **1967**, *8*, 1909.
[36] A. S. Kiselyov, *Tetrahedron Lett.* **1999**, *40*, 4119.
[37] C. Foces-Foces, F. Hernández Cano, M. Martínez-Ripoll, R. Faure, C. Roussel, R. M. Claramunt, C. López, D. Sanz, J. Elguero, *Tetrahedron: Asymmetry* **1990**, *1*, 65; V. N. Baumer, A. A. Karasev, Z. A. Sizova, *Acta Crystallogr., Sect. E* **2003**, *59*, o54; L.-P. Zhang, Y.-Y. Liu, Z.-F. Jia, G.-H. Wei, *Acta Crystallogr., Sect. E* **2008**, *64*, o143; N. C. Fletcher, D. Abeln, A. von Zelewsky, *J. Org. Chem.* **1997**, *62*, 8577; P. Molina, M. Alajarín, C. López-Leonardo, I. Madrid, C. Foces-Foces, F. H. Cano, *Tetrahedron* **1989**, *45*, 1823.

Chapter 4: Complexes of Symmetric Ligand H_4L^{Et}

4.1 Introduction

As discussed in Chapter 1, nature often employs metals, often two or more held closely together, to carry out transformations which have proven challenging to recreate in a laboratory environment. The transformation of atmospheric nitrogen to higher end products or the interconversion of water and dioxygen are but two examples. The design of tailor-made ligands which bind multiple metal centres with well-defined architectures with the aim to perform such transformations is a very active area of research. One such example is the aforementioned cofacial "pacman" diporphyrins, followed by the development of catalytically efficient, first and second generation single pillared porphyrins. Porphyrins however, are generally challenging to synthesise. The development of the "H_4L" macrocycle by the Love and Sessler groups opened the door to a pacman-based system in which the addition of metal substrates to the ligand cause spontaneous folding into a wedge-shape, reminiscent of pacman-porphyrins. The facile synthesis, high yield and versatility towards modification hold many advantages over their diporphyrin counterparts though further work is needed to fully understand and tailor reactivity.

4.2 Symmetric Ligand H_4L^{Et}

4.2.1 Synthesis of H_4L^{Et}

To further aid the study of the complexes of H_4L, a modified ligand with increased solubility in common solvents was sought, whilst retaining the facile, high yielding synthesis of its predecessors. The addition of solubilising methyl substituents at the 3, 4 positions of the aryl backbone combined with *meso*-diethyl substituents, instead of the standard dimethyl, was targeted. A synthesis reminiscent of previously reported ligands[1, 2] was found by members of the Love group and subsequently fine-tuned (Scheme 1). The dialdehyde, 5,5'-diformyldiethyl-2,2'-dipyrromethane **1**, straightforwardly synthesised in two steps from pyrrole and 3-pentanone[1], was reacted with 3,4-dimethyl-1,2-diaminobenzene in the presence of *para*-toluenesulfonic acid in methanol to give the [2+2] condensation product H_8L^{Et}·4TsOH as a bright orange solid. Treatment of a suspension of the acid-salt in methanol with excess triethylamine yielded H_4L^{Et} as a bright yellow solid in good yield after workup.[2]

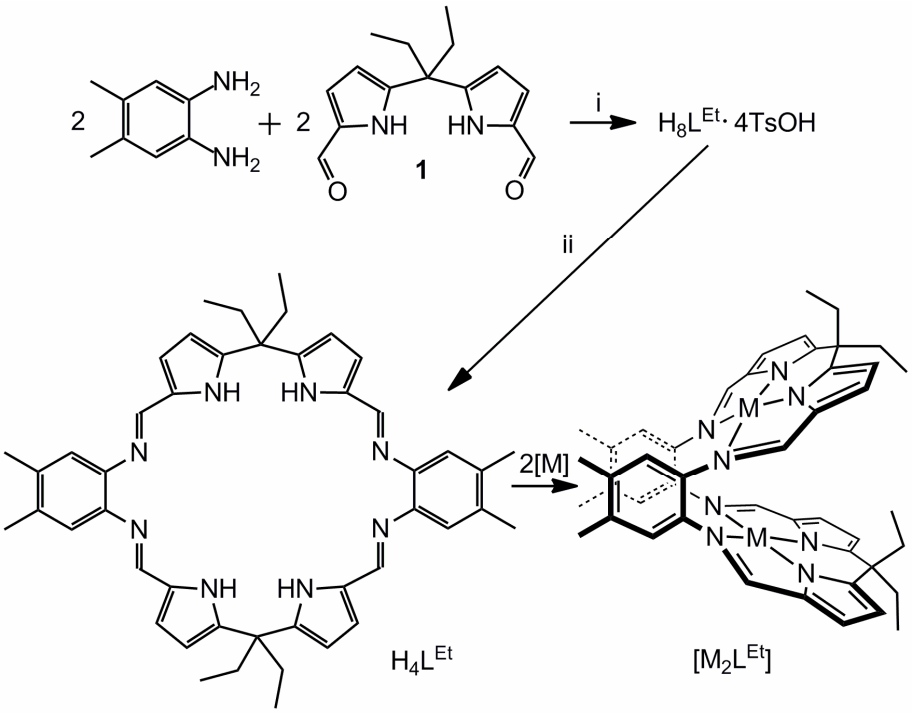

Scheme 1: Synthesis of H_4L^{Et} i) 2.2 TsOH, MeOH ii) NEt_3, MeOH

The resultant H_4L^{Et} macrocycle was thus obtained in a high yielding, facile synthesis giving solely the [2+2] cyclic product with two N_4 donor pockets which, upon metallation forms the desired complexes that adopt the desired pacman geometry similar to those of H_4L. The EI mass spectrum of H_4L^{Et}, up to *m/z* = 2000, shows an ion at *m/z* = 717 with appropriate isotopic pattern for the parent macrocycle H_4L^{Et}, with no higher or lower order condensation products. Crystals suitable for X-ray diffraction were grown from a saturated toluene solution (Figure 1, Table 1).

The macrocycle adopts a non-linear, bowl-shaped conformation around two hydrogen bonded waters of crystallisation and is similar to previous reported structures of closely related ligands.[3] The macrocycle is folded at the *meso*-carbon and demonstrates an ability to behave as an H-bond donor, through the pyrrole NH protons (HN···OH_2 *ca.* 3.01 Å), as well as an H-bond acceptor through the imine nitrogens (N···OH_2, *ca.* 3.01 Å). The water molecule (O1) is bound *exo*- to the cleft by imine N4 and pyrrole HN3 with the remaining water molecule (O2) bound *endo*-to the cleft by imine N1 and pyrrole HN2.

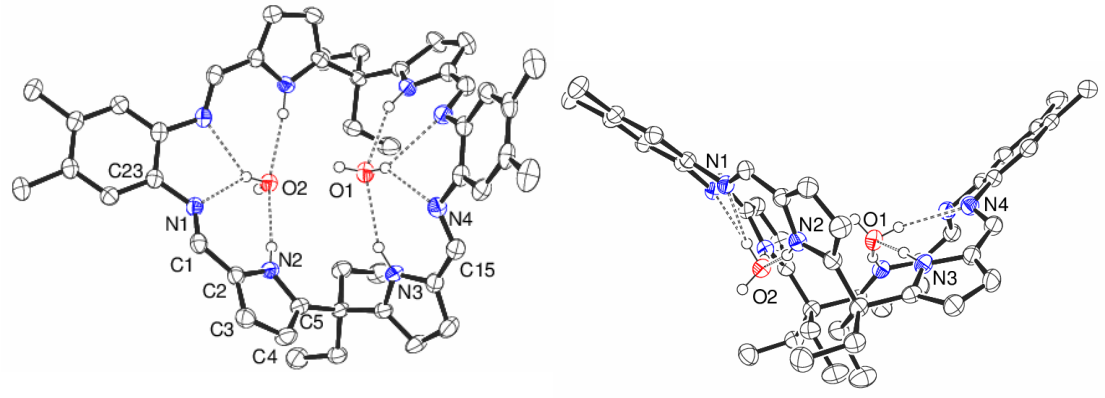

Figure 1: X-ray crystal structure of H_4L^{Et}. For clarity, all hydrogen atoms, except those on N2 N3, O1 and O2, are omitted and displacement ellipsoids are drawn at 50% probability. H-atoms on O1 and O2 were found from the difference map and refined with restraints

Table 1: Selected bond lengths (Å) and angles (º) of H_4L^{Et}

$C=N_{im}$	1.284(3)/1.286(3)	C4-C5	1.379(3)
$N_{py}\cdots O_{H2O}$	2.976/3.044	C5-N2	1.359(3)
$N_{im}\cdots O_{H2O}$	2.972/3.057	C2-N2	1.380(3)
C1-C2	1.423(3)	C1-N1-C23	120.5(2)
C2-C3	1.380(3)	Dihedral α	104.65
C3-C4	1.397(4)		

Once extensively dried under vacuum at high temperatures (120 °C), the ^{1}H NMR spectrum of H_4L^{Et} displays the pyrrolic NH resonance at 9.02 ppm. Given the symmetry of the macrocycle, the ^{1}H spectrum shows one imine (8.06 ppm), one arene-backbone (6.81 ppm), two pyrrolic CH doublets (6.41 and 6.06 ppm), one aryl-CH_3 (2.21 ppm), and crucially, one ethyl-CH_2 quartet and one ethyl-CH_3 triplet at 1.99 and 0.68 ppm respectively. This shows the *meso*-ethyl groups are all equivalent and thus the macrocycle is flexible in solution. The importance of this fact is demonstrated upon complexation by metal centres (Scheme 1). Should the macrocycle form a wedge-shaped pacman conformation upon complexation of two identical metal centres to form pacman-$[M_2(L^{Et})]$, the previously equivalent *meso*-ethyl groups (red) exist in two different environments, *endo*- and *exo*-to the cleft (red and blue) and thus the NMR spectrum will display two separate resonances for these ethyl groups. Thus, in this case,

the presence of two distinct ethyl resonances in the NMR spectrum is indicative of a pacman-shaped complex in solution.

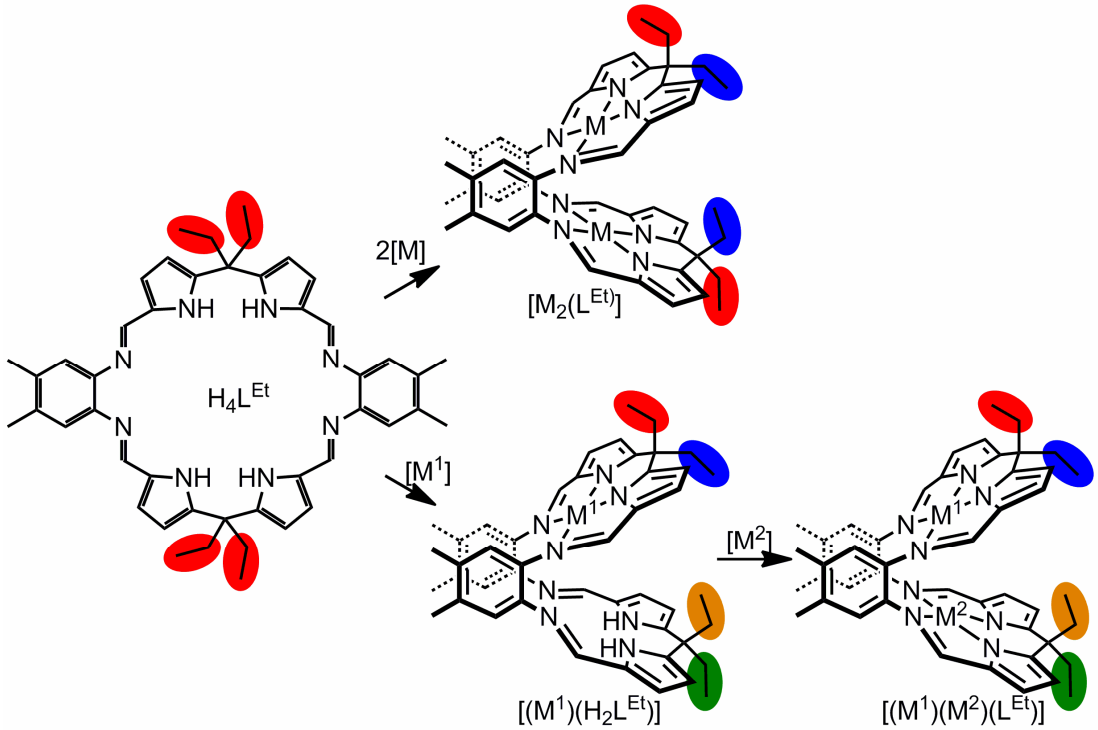

Scheme 2: Desymmetrisation of the *meso*-ethyl groups upon complexation to give homo-bimetallic pacman-$[M_2(L^{Et})]$, monometallic pacman $[(M^1)(H_2L^{Et})]$ and hetero-bimetallic pacman $[(M^1)(M^2)(L^{Et})]$

Further to this, complexation of just one metal centre to the ligand, while retaining a pacman geometry, to form $[(M^1)(H_2L^{Et})]$, or two different metals to form $[(M^1)(M^2)(L^{Et})]$ would display four ethyl environments. Resonances would be seen for substituents *endo*- and *exo*- to the cleft in the M^1 environment and also *endo*- and *exo*- to the cleft in the opposing compartment.

Thus with this in mind, and with the previous successes of related ligands,[3-6] new complexes of H_4L^{Et} were sought.

4.3 Monometallic and Heterobimetallic Complexes of H_4L^{Et}

Though complexes of the form $[Co_2(L)]$ have been shown to activate dioxygen to form bridging peroxo $[Co_2(O_2)(pyr)_2(L)]$, superoxo $[Co_2(O_2)(pyr)_2(L)][OH]$ and hydroxo $[Co_2(OH)(pyr)_2(L)]$ complexes, the reaction rates of oxygen reduction when catalysed by these complexes are slow and with limited overall catalytic turnover.[4] This is thought to be due to the formation of a highly stable μ-OH complex, removing it from the catalytic

cycle, and is a problem also observed with related single-pillared diporphyrin complexes.[2, 3] The use of the single-pillared 'hangman' porphyrins has in part overcome these problems by removal of the second metal centre thus preventing μ-O(H) formation whilst also gaining secondary coordination sphere control *via* the "hanging" group.[2, 4]

With this in mind, a route to monometallic transition metal complexes of L^{Et} was sought. A monometallic species of the form [M(H_2L)] (Scheme 3) would both prevent μ-O(H) formation due to the absence of a second metal as well as allowing for possible secondary coordination sphere control through the pyrrolic NHs of the opposing compartment. Furthermore, different metals could be introduced into the vacant N_4-donor pocket to fine-tune any reactivity.

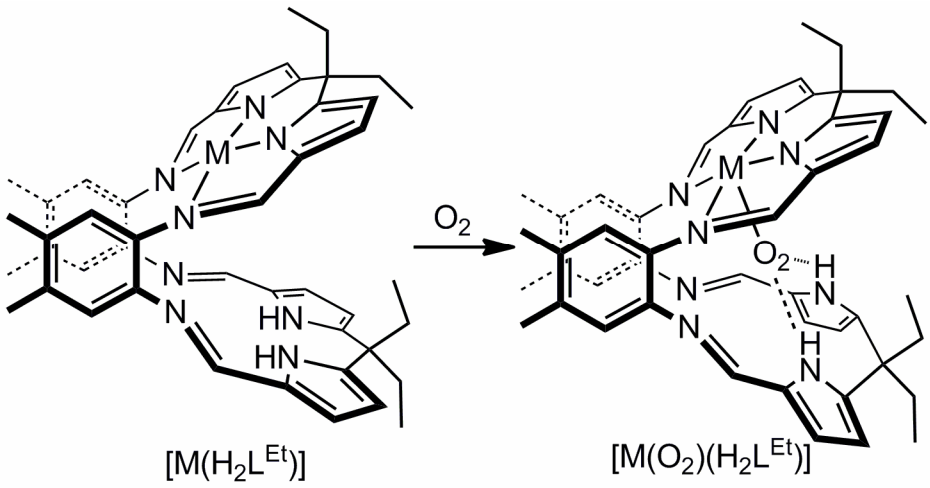

Scheme 3: Target complex showing desired reactivity (M = transition metal)

As mentioned in Chapter 1, reactions of ligands of the type H_4L with one equivalent of metal reagents such as $Pd(OAc)_2$ or $Co(OAc)_2$ were found to result in the formation of complex mixtures of free ligand, mono-metallated and doubly-metallated products. However, the synthesis of monometallic uranyl complexes of ligands closely related to L^{Et} have been synthesised by reaction of H_4L with one equivalent of $[(UO_2)(THF)(N\{SiMe_3\}_2)_2]$ to give $[(UO_2)(THF)(H_2L)]$ whilst retaining the distinctive pacman conformation.[5] This has resulted in a rich vein of chemistry geared towards the reductive functionalisation of the $[UO_2]^{2+}$ substituent.[6] The successful synthesis of mono-metallated uranyl compounds is attributed to the steric bulk of the linear $[UO_2]^{2+}$ group which hinders the complexation of a second uranyl. Thus a metal which could retain a trans-arrangement of ligands to disfavour coordination of a second metal was sought. Complexes of tin-alkyls are known in which the alkyl

groups are *trans* to each other[7] although a *cis*-arrangement of ligands is also possible.[8] With this in mind, the steric bulk of the potentially linear Me-Sn-Me group was chosen as a possible route into the target monometallic complexes.

4.3.1 Synthesis of $[SnMe_2(H_2L^{Et})]$

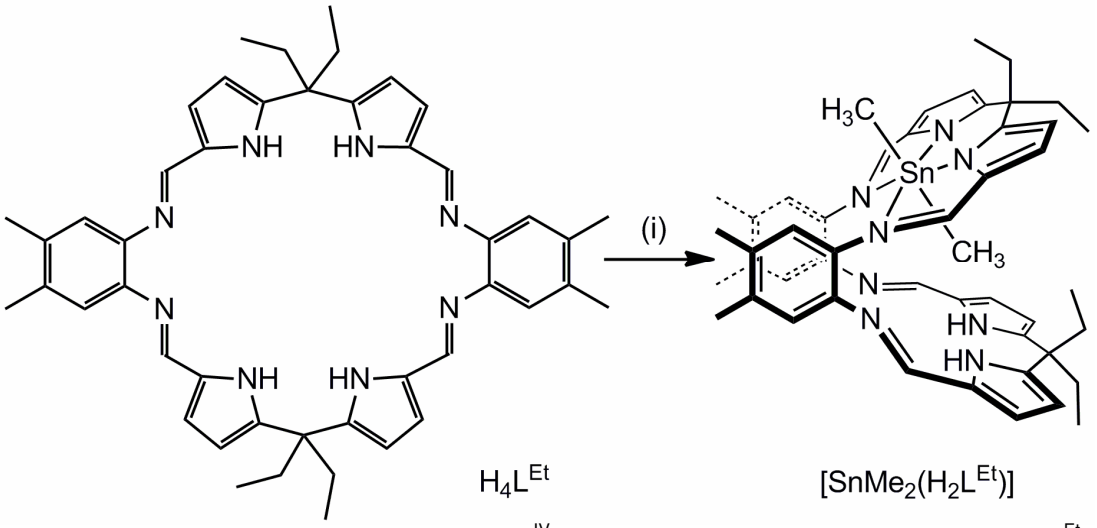

Scheme 4: Formation of a mono-metallic Sn^{IV} complex of the Schiff base calixpyrrole H_4L^{Et}. (i) Me_2SnCl_2, DABCO, Toluene, 73 %

The dehydrohalogenation reaction of the ligand H_4L^{Et} with one equivalent of Me_2SnCl_2 in the presence of DABCO results in the formation of monometallic, dialkyl $[SnMe_2(H_2L^{Et})]$ in good yield (Scheme 4). Though attempts to grow crystals suitable for single crystal X-ray diffraction were unsuccessful, the solution state structure could be identified through ^1H and $^{13}C\{^1H\}$ NMR spectroscopy.

The ^1H NMR spectra of $[SnMe_2(H_2L^{Et})]$ (Figure 2) shows the desymmetrisation of the ligand, with one metallated and one free N_4 pocket. An N-H resonance at 9.29 ppm integrating to 2H as well as two imine resonances at 8.00 and 7.87 ppm is noted along with two aromatic singlets and four pyrrolic CH doublets. Furthermore, the alkyl region (Figure 2) shows four resonances for each of the *endo*- and *exo*-ethyl-CH_2 and -CH_3 groups.

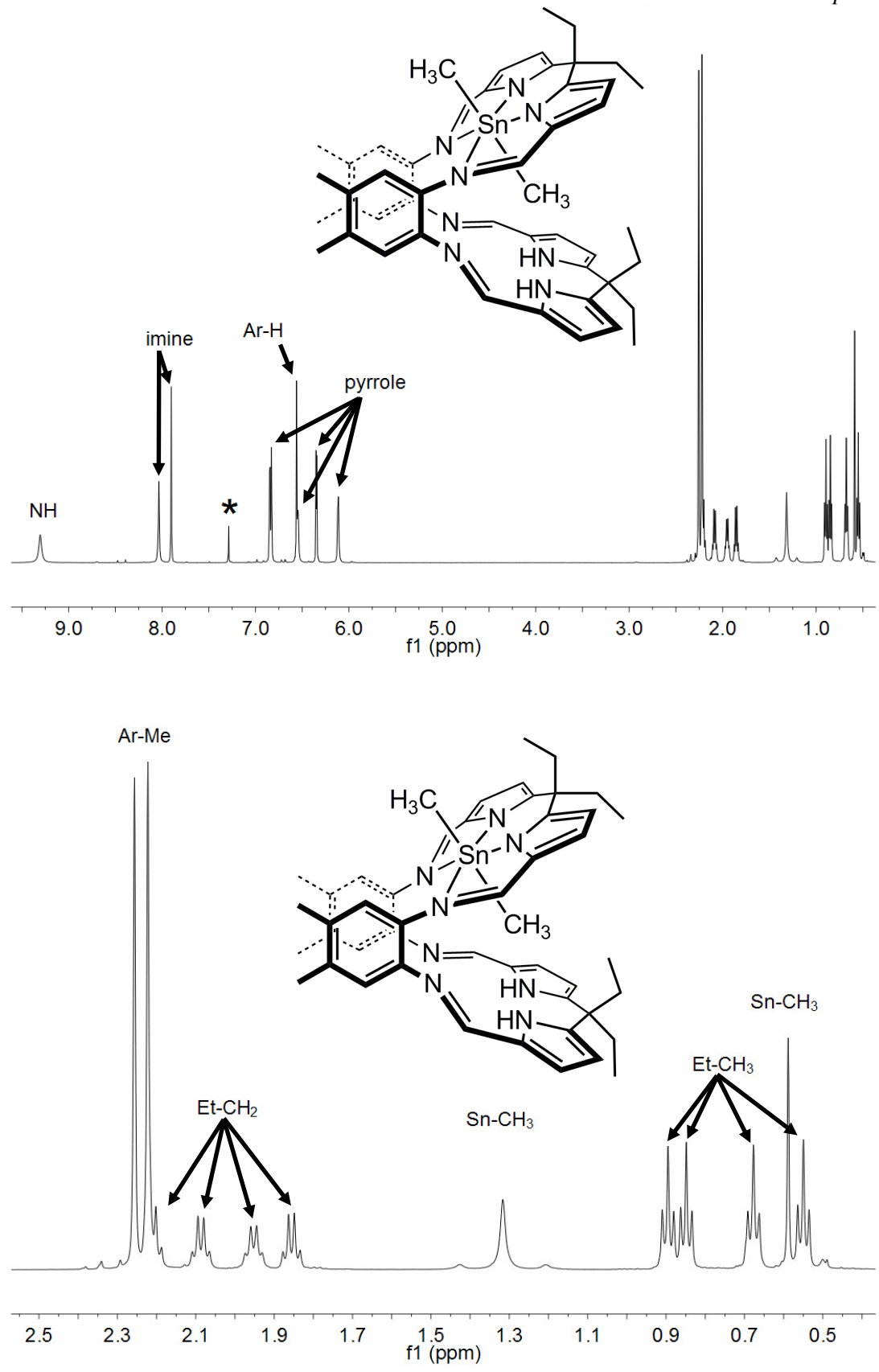

Figure 2: ^{1}H NMR spectra (C_6D_6) of [$SnMe_2(H_2L^{Et})$] (top) and showing aliphatic region only (bottom)

The two tin-methyl groups are also in very different environments, with clear Sn-Me resonances, complete with Sn satellites, at 1.28 and 0.55 ppm. Analysis of the Sn-Me coupling constants ($^2J_{SnMe}$ = 100.5 Hz) using Lockhart and Manders' empirical correlation[9] indicate an Me-Sn-Me angle of 163.4 °. ^{1}H-^{1}H nOe experiments were used to fully assign the methyl groups with a clear interaction between the resonances at 0.55 ppm (Sn-CH_3) and 9.0 ppm (pyrrole-NH) and no interaction associated with the methyl resonance at 1.3 ppm confirming the resonance at 0.55 ppm to be within the macrocyclic cleft. The successful synthesis is also supported by the EI mass spectrum which displays a molecular ion at *m/z* = 864 and by the IR spectrum which shows the presence of an NH stretch at 3441 cm^{-1}. The metallation of L^{Et} with tin was also attempted using the bulky tin(IV) alkyls Bu_2SnCl_2 and Ph_2SnCl_2 in the presence of DABCO. Unfortunately, only unidentifiable mixtures were seen in the ^{1}H NMR spectra of these reactions.

4.3.2 Synthesis of [$SnMe_2Zn(THF)L^{Et}$] and [$SnMe_2Fe(THF)L^{Et}$]

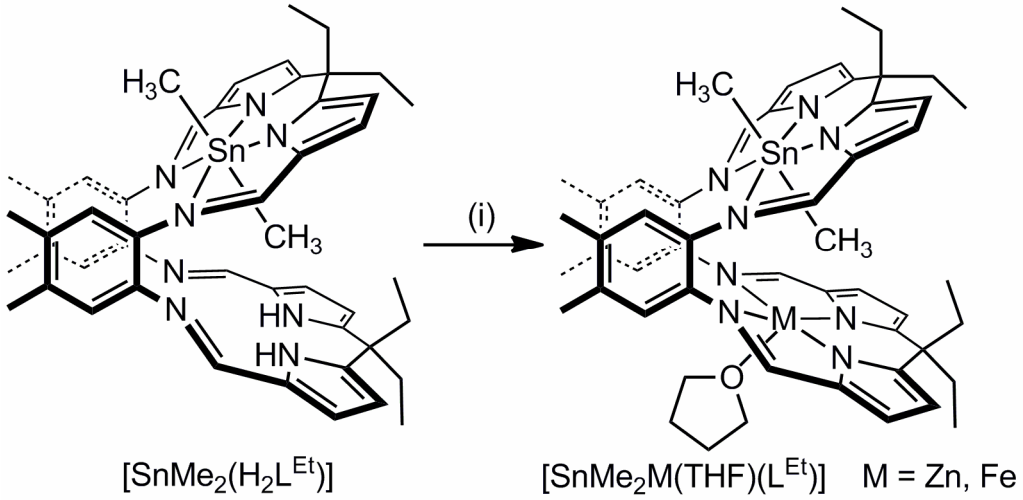

Scheme 5: Formation of hetero-bimetallic Sn-Zn or Sn-Fe complexes of L^{Et}
(i) [$M(THF)_n(N\{SiMe_3\}_2)_2$], THF (M = Zn, n = 0, 80 %; M = Fe, n = 1, 48 %)

As with the aforementioned complex [$(UO_2)(THF)(H_2L)$], the vacant N_4-donor compartment allows for the complexation of a second metal. As such, transamination reactions of [$SnMe_2(H_2L^{Et})$] with either [$Zn(N\{SiMe_3\}_2)_2$] or [$Fe(THF)(N\{SiMe_3\}_2)_2$] were carried out and were found to result in the heterobimetallic complexes [$SnMe_2Zn(THF)(L^{Et})$] or [$SnMe_2Fe(THF)(L^{Et})$] in good yield (Scheme 5). Though the ^{1}H NMR spectrum resonances of [$SnMe_2Fe(THF)(L^{Et})$] are paramagnetically shifted and broadened, analysis of the number and integral values of the resonances are consistent with the adoption of a pacman geometry in solution. This is further supported by the

analogous zinc complex [$SnMe_2Zn(THF)(L^{Et})$]. The ^1H NMR spectra of [$SnMe_2Zn(THF)(L^{Et})$] shows the absence of any NH resonances, which is also supported by the IR spectrum, and again shows two different N_4-donor pockets with the distinctive four separate triplets, three overlapping at 2.20 to 2.00 ppm, with a fourth at 1.90 ppm and four separate quartets 0.97, 0.90, 0.80 and 0.49 ppm for the fully desymmtreised *meso*-ethyl groups, as seen for [$SnMe_2(H_2L^{Et})$]. Two distinct Sn-Me resonances are observed at 1.13 and 0.06 ppm with the Sn-Me coupling constants corresponding to a calculated solution state Me-Sn-Me angle of 150.5 °,[9] a compression of 12.9 ° relative to [$SnMe_2(H_2L^{Et})$]. These solution state observations are also true in the solid state. X-ray quality crystals of both [$SnMe_2Zn(THF)(L^{Et})$] and [$SnMe_2Fe(THF)(L^{Et})$] were grown from a saturated C_6D_6 solution and by slow hexane diffusion into a THF solution respectively and the structures determined (Figure 3, Table 2). Due to the similarity of these two structures only the tin-zinc complex will be discussed.

The tin cation sits in a distorted octahedral environment of one N_4-donor pocket with a *trans*-Me-Sn-Me angle of 150.06(16) °, similar to that calculated for the solution state (150.5 °) and so indicating that a very similar structure exists in both the solution and solid state. Crystallographic data of six-coordinate dialkyltin substituents stabilised by nitrogen donor ligands are rare.[10, 11] There are few examples of tin(IV) porphyrin complexes[10] with none containing simple alkyl groups such as methyl groups as well as few salen-ligand complexes, though there are some examples dimethyltin salen complexes.[12, 13] Though the Sn1-N1(pyrrole) bond length (2.153(2) Å) is comparable to that of Sn^{IV} porphyrin complexes (*ca*. 2.07–2.37 Å),[10] the Sn1-N2 (imine) bond lengths of 2.534(2) Å are appreciably longer than those reported for Sn-salen complexes of *ca*. 2.24–2.29 Å.[13] This is attributed to both the bent nature of the Me-Sn-Me as well as the ability of the aryl hinges of the ligand to splay away from each other, causing elongated Sn1-N2(imine) lengths and an increased N2-Sn1-N2' bond angle (132.39(11) °). This feature is also seen in the uranyl complex [$(UO_2)(THF)(H_2L)$] in which, again, the aryl backbone splays away to accommodate a THF molecule bound equatorially to the uranium.[5]

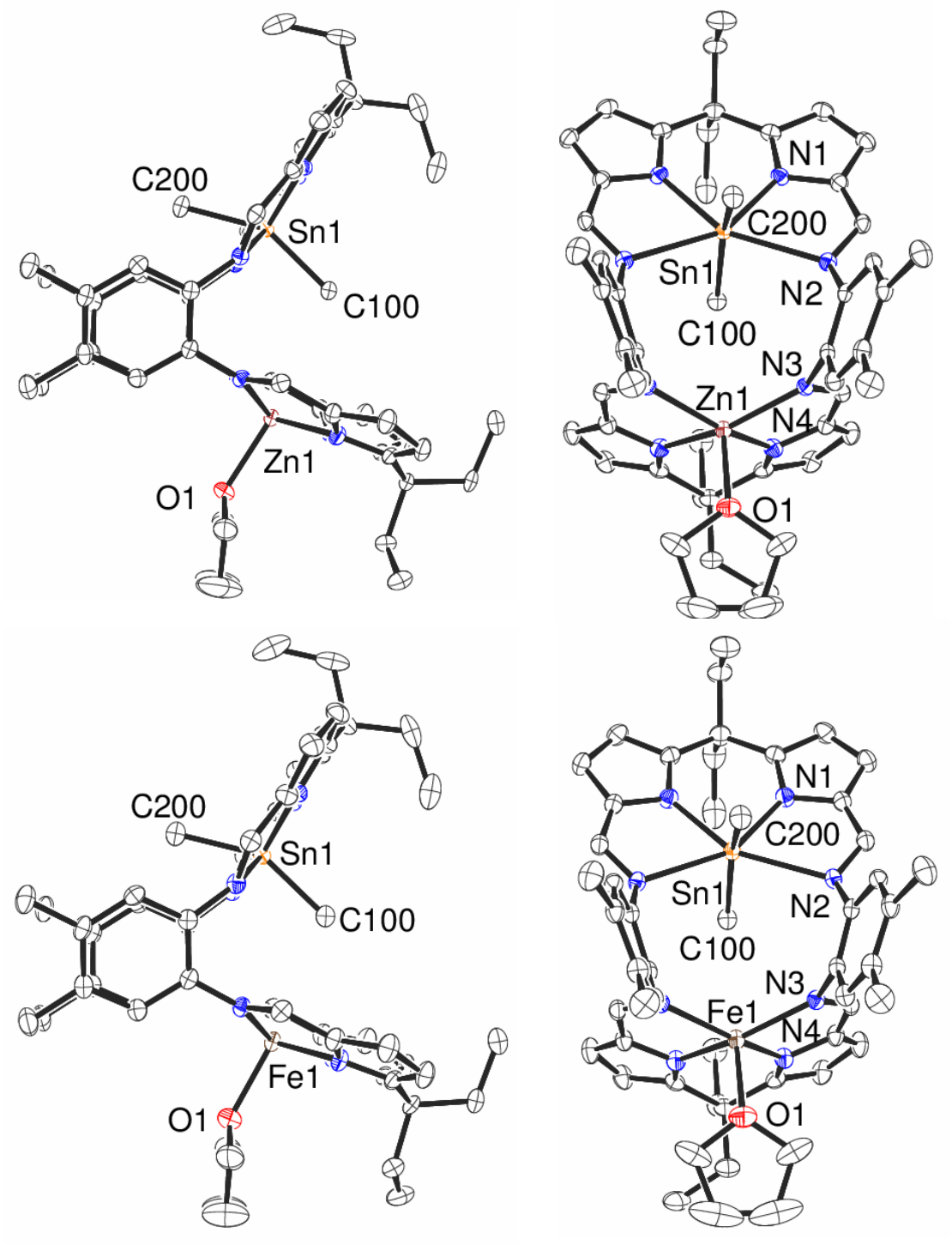

Figure 3: X-ray crystal structure of [$SnMe_2Zn(THF)(L^{Et})$] (top) and [$SnMe_2Fe(THF)(L^{Et})$] (bottom). For clarity, all hydrogen atoms are omitted and displacement ellipsoids are drawn at 50% probability

Table 2: Selected bond lengths (Å) and angles (º) of $[SnMe_2Zn(THF)(L^{Et})]$ and $[SnMe_2Fe(THF)(L^{Et})]$

	$[SnMe_2Zn(THF)(L^{Et})]$ M = Zn	$[SnMe_2Fe(THF)(L^{Et})]$ M = Fe
Sn1-C100	2.118(4)	2.113(3)
Sn1-C200	2.127(4)	2.127(3)
C100-Sn1-C200	150.06(16)	149.76(14)
Sn1-N1	2.153(2)	2.1433(19)
Sn1-N2	2.534(2)	2.5367(19)
Sn1···N_4	0.129	0.129
C100···M1	3.369	3.265
M1-N3	2.177(2)	2.1703(19)
M1-N4	2.048(2)	2.0599(19)
M1···N_4	0.432	0.375
Sn1···M1	4.559	4.483
'Bite' angle θ	72.29	71.89
Dihedral angle α	43.37	41.84

In the second N_4 donor compartment, the zinc cation is bound in a square-based pyramidal geometry with a coordinating THF molecule providing axial donation. The zinc sits 0.432 Å exogenous to the N_4-plane (for comparison the tin sits 0.129 Å endogenous to the N_4-plane) resulting in the imine-pyrrole units folding around the *meso*-carbon by some 38.19 ° (15.44 ° for the Sn compartment). The Zn-N_{py} bond lengths of 2.048(2) Å are comparable to those in zinc porphyrins (*ca*. 2.0–2.1 Å)[12] though the zinc-imine bond (2.177(2) Å) is long in comparison to salen-based zinc complexes (*ca*. 2.00–2.16 Å)[14] due to the splaying of the aryl backbone. To incorporate both metals as well as the *endo*-methyl, the pacman structure has distorted significantly compared to homo-bimetallic complexes $[(M)_2(L)]$ (M = transition metal). The "bite angle" of 72.29 ° and M···M separation (4.559 Å) is considerably more than for homo-bimetallic complexes (44.8–65.8 ° and 3.15–4.12 Å).[3] This difference is due to the distortion of the $SnMe_2$-containing N_4-plane folding away from the cleft at the N2/N2'

position by 19.83 °. The steric clash of the *exo*-methyl with the aryl hinge resulting from this distortion, coupled with the compression of the Me-Sn-Me angle forces the aryl backbone to contort away from co-planarity, as is normally seen, to avoid a steric clash, thus creating a V-shape of dihedral angle 43.37 °.

4.3.4 Study of $[SnMe_2(H_2L^{Et})]$, $[SnMe_2Zn(THF)L^{Et}]$ and $[SnMe_2Fe(THF)L^{Et}]$ reactivity.

The introduction of metals to the vacant N_4-donor pocket of $[(UO_2)(THF)(H_2L)]$ led to the unprecedented reactions of $[UO_2]^{2+}$.[5, 6] With this in mind, it was hoped that the proximity of the lower N_4-donor pocket could cause one of the methyl groups bound to the tin to be activated toward insertion of a small molecule such as H_2, CO or CO_2.

The three fully characterised Sn^{IV} complexes, $[SnMe_2(H_2L^{Et})]$, $[SnMe_2Zn(THF)(L^{Et})]$ and $[SnMe_2Fe(THF)(L^{Et})]$ were screened for reactivity toward H_2, CO and CO_2. NMR-tube scale C_6D_6/H_8-THF solutions were freeze-pump-thaw-degassed three times in Teflon-tapped NMR tubes before exposure to the required gas. Reactions were heated to 80 °C and monitored by ^1H NMR spectroscopy at various times. Unfortunately, no reactions were observed in all cases.

The abstraction of one of the methyl groups to form a tin alkyl cation was also investigated. Unfortunately, the reaction between $[SnMe_2Zn(THF)(L^{Et})]$ and $B(C_6F_5)_3$ yielded an unidentifiable mixture of products by ^1H NMR spectroscopy.

4.3.5 Attempted synthesis of $[M(H_2L^{Et})]$ *via* $[SnMe_2(H_2L^{Et})]$

$$[SnMe_2(H_2L^{Et})] + MX_y \longrightarrow [MX_{(y-2)}(H_2L^{Et})] + Me_2SnX_2$$

$$MX_y = FeBr_2,\ CoCl_2,\ PdCl_2(MeCN)_2$$

Equation 1

It was envisaged that the "$SnMe_2$" unit could be substituted in transmetallation reactions with other transition metal halides such as $FeBr_2$, $CoCl_2$ or $PdCl_2$ (Equation 1). Reactions between $[SnMe_2(H_2L^{Et})]$ and these metal salts were attempted under a variety of experimental conditions but unfortunately all reactions resulted in unidentifiable mixtures of products.

4.3.6 Synthesis of mono-metallic calcium complex $[Ca(THF)_2(H_2L^{Et})]$

After the success of using the bulky, trans-directed $SnMe_2$ group to synthesise mono- and hetero-bimetallic complexes of H_4L^{Et}, it was thought that calcium, with its

large ionic radius of 99 pm could also be a candidate to form a monometallic complex of L^{Et} that could act subsequently as a transmetallating agent.

The reaction of one equivalent of $[Ca(N\{SiMe_3\}_2)_2(THF)_2]$ with H_4L^{Et} at -80 °C in THF and allowing the reaction to warm to room temperature gives $[Ca(THF)_2(H_2L^{Et})]$ in good yield (87 %) after workup. X-ray quality crystals (twinned) were grown from a saturated THF solution (Figure 4, Table 3).

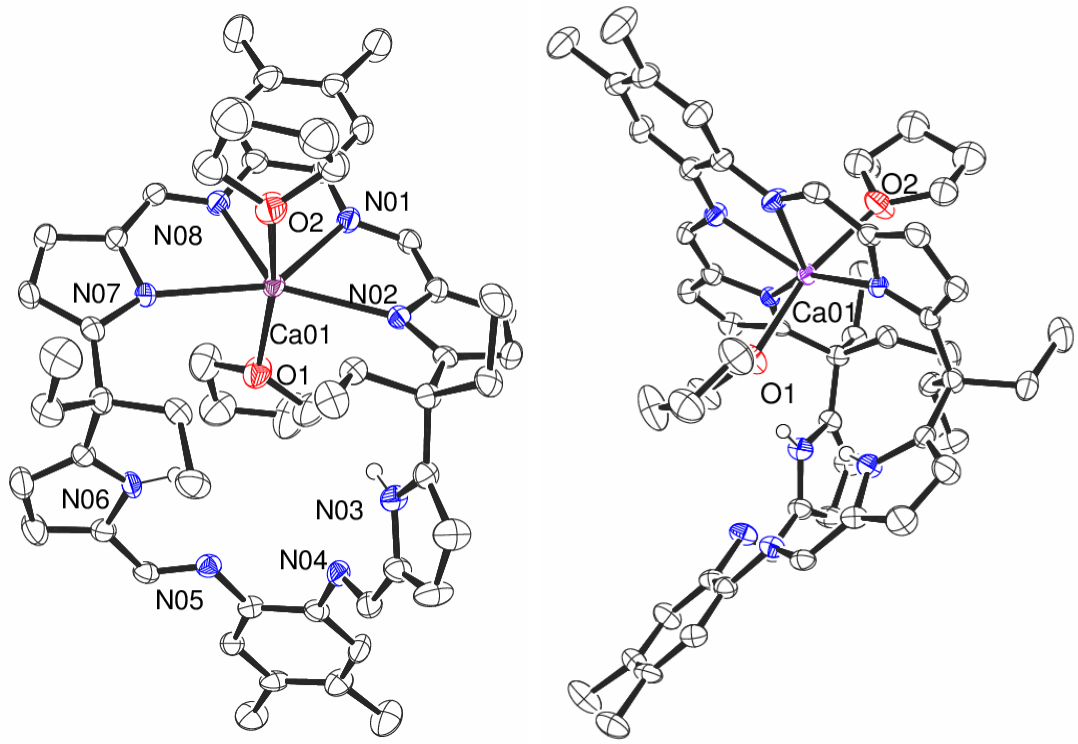

Figure 4: X-ray crystal structure of $[Ca(THF)_2(H_2L^{Et})]$. For clarity, all hydrogen atoms, except those on N03 and N06 are omitted and displacement ellipsoids are drawn at 50% probability

Table 3: Selected bond lengths (Å) and angles (º) of $[Ca(THF)_2(H_2L^{Et})]$

Ca01-N01/N08	2.420(3)/2.438(3)	O1-Ca01-O2	166.78(12)
Ca01-N07/N02	2.543(3)/2.509(3)	Ca01···N_4	0.006
Ca01-O1/O2	2.370(3)/2.344(3)	Dihedral α	88.14
N01-Ca01-N08	65.33(11)	Σ ∠ Ca01	360.09
N02-Ca01-N07	155.43(10)		

In the solid state structure of $[Ca(THF)_2(H_2L^{Et})]$, the overall geometry is clearly bowl-shaped and not "pacman" with the large size of Ca favouring coordination to a

different N_4 donor set than usual. The calcium ion is bound in a distorted octahedral geometry by two imine nitrogens, both attached to the same aryl-backbone, two non-adjacent pyrrolic nitrogens and two THF donors. Structures of calcium-containing porphyrin complexes are very rare, with only two examples in the literature.[15] However, the Ca-N_{py} distances (*ca.* 2.5 Å) are similar to the few published structures that contain Ca-N_{py} bonds (2.589(10)–2.384(6) Å).[32, 33] The calcium sits directly in the N_4 plane (Ca···N_4 0.006 Å) which contrasts greatly to the porphyrin structures (Ca···N_4 1.577(5)–1.657(5) Å), and is related to the small size of the porphyrin cavity and the high degree of flexibility present in the H_2L^{Et} macrocycle, especially when in a bowl-shaped conformation. This conformation also results in a very large N_{im}-Ca-N_{im} bond angle of 155.43(10) °. The Ca-N_{im} distances of 2.420(3) and 2.438(3) Å are also of a similar length to the two reported structures of calcium salen complexes[18, 19] and related compounds (2.402(3)–2.518(3) Å).[16] The *endo*-axial THF (O1) is bound at an angle of 94.61 ° to the N_4 plane, presumably due to steric interactions with the vacant N_4H_2 compartment, with standard Ca-O_{THF} distances of *ca.* 2.36 Å.[33, 35, 37]

The bowl-shaped conformation is similar to some previously reported homobimetallic complexes of closely-related ligands.[28-31]

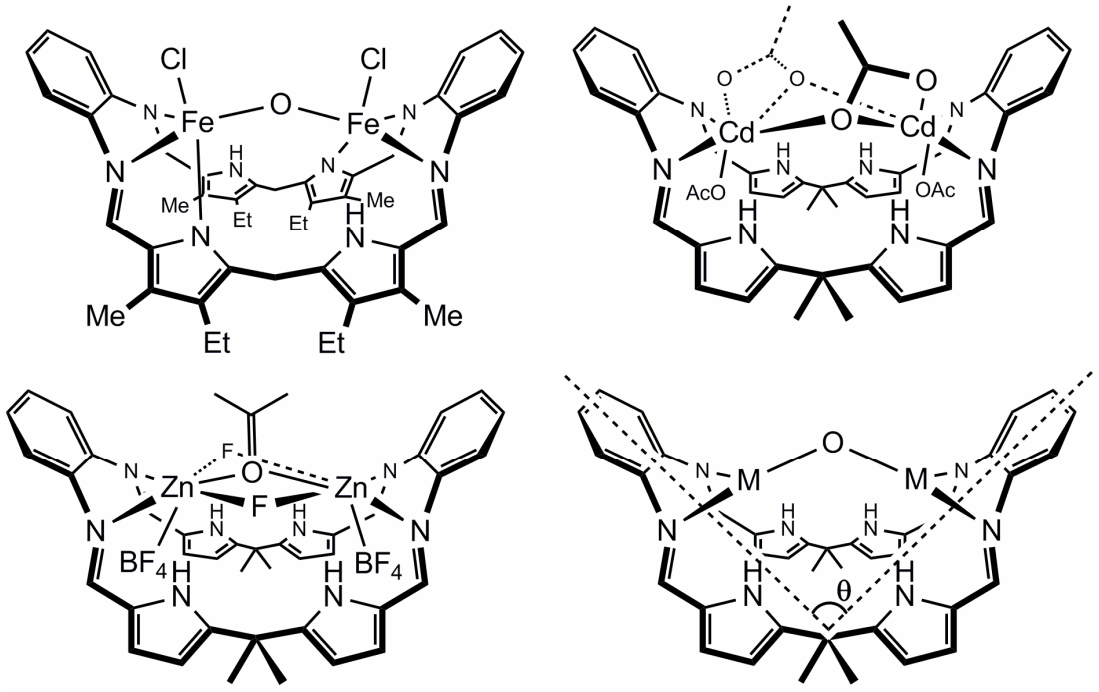

Figure 5: Selected "bowl-shaped" complexes of L. a) $[(FeCl)_2(\mu\text{-}O)(L)]$[17], b) $[(CdOAc)_2(\mu OAc)_2(L)]$[18], c) $[(ZnBF_4)(\mu\text{-}C_3H_6O)(\mu F)_2(L)]$[19], d) diagram showing the angle of the arene backbones (dihedral angle) 'α'

The structure of the calcium complex is much more open with the dihedral angle (88.14 °) being noticeably larger than the aforementioned complexes (41.09–81.43 °). However only in the bis-iron structure published by Sessler and co-workers (Figure 5-a) are any of the pyrrolic nitrogens bound directly to the metal. Bowl-shaped complexes have synthesised by reactions of the HCl salt of the ligand with $Fe_2(mesitylene)_4$[17] or by addition of metal acetates (Ni or Cd)[28, 30] or metal tetrafluoroborates (Zn or Cd)[30, 31] to the ligand.

To confirm if the proposed conformation is retained in solution, the ^1H and $^{13}C\{^1H\}$ NMR spectra were studied. Both pacman and bowl-shaped monometallic complexes (Figure 6) would show resonances corresponding to two imines, four pyrrolic CHs and two aryl-CHs. The solution state structure can only be confirmed by studying the low frequency region, specifically the *meso*-ethyl groups.

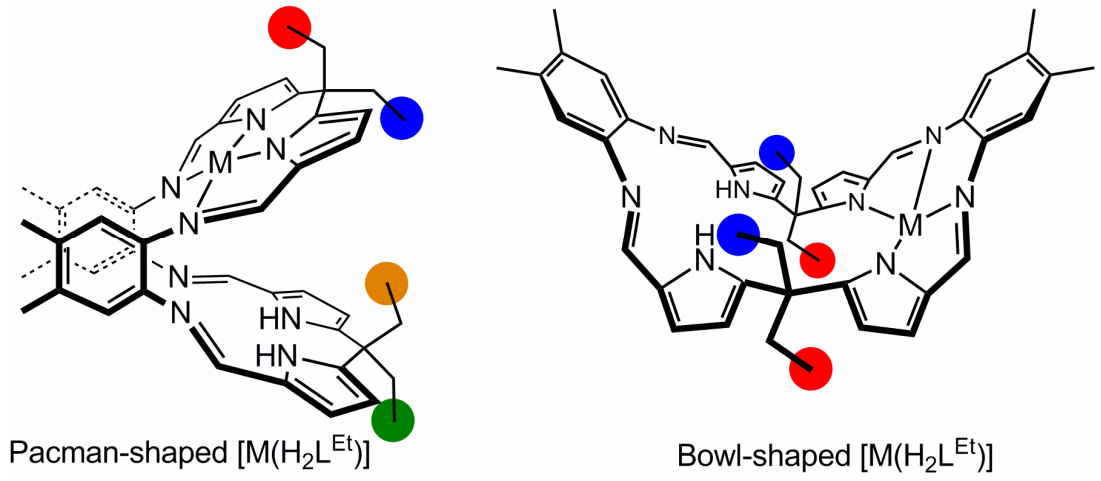

Figure 6: Pacman and bowl-shaped complexes of $[M(H_2L^{Et})]$ highlighting the *meso*-ethyl-CH_3

If pacman-shaped, four ethyl resonances will be seen (similar to $[SnMe_2(H_2L^{Et})]$), whereas if a bowl-shaped structure, two ethyl resonances will be seen (Figure 6). However, a bowl-shaped conformation would be expected to have an increased flexibility about the *meso*-carbon thus potentially causing the ethyl groups to become equivalent. Further to this, a pacman-shaped complex would display two quaternary $^{13}C\{^1H\}$ resonances corresponding to two *meso*-carbons in different environments, whereas a bowl-shaped conformation would show only one resonance. The high frequency region of the ^1H NMR spectrum shows the expected desymmetrisation of the ligand, with two imine resonances at 8.37 and 7.88 ppm, two arene-H resonances at 7.08 and 6.69 ppm and four pyrrolic C-H resonances (7.17, 6.57, 6.48 and 6.36 ppm). In the

low-frequency region two resonances corresponding to two Ar-CH_3 resonances (2.10 and 2.03 ppm) as well as resonances corresponding to two bound THF molecules are found. Importantly only one, broad singlet resonance is observed corresponding to *meso*-ethyl-CH_3 (0.96–0.86 ppm), with a broad multiplet (2.59–2.16 ppm) corresponding to the ethyl-CH_2 fragments. This behaviour is also seen in the ^{1}H NMR spectra of previously-reported diamagnetic bowl-shaped complexes. The diamagnetic bowl-shaped complexes (Zn and Cd, Figure 5) show one resonance for the *meso*-groups, with the bowl-shaped zinc complex displaying broad resonances, attributed to a slow exchange process between conformational states.[15, 16] Furthermore, the $^{13}C\{^1H\}$ spectrum of $[Ca(THF)_2(H_2L^{Et})]$ shows only one *meso*-quaternary resonance (45.93 ppm) thus confirming that the bowl-shaped conformation is retained in solution, with the broadness of the ethyl resonances indicating a degree of flexibility about the *meso*-carbon on the NMR timescale.

4.3.7 Reactions involving $[Ca(THF)_2(H_2L^{Et})]$

$$[Ca(THF)_2(H_2L^{Et})] + MX_y \longrightarrow [MX_{(y-2)}(H_2L^{Et})] + CaX_2$$

MX_y = $FeBr_2$, $CoCl_2$, $PdCl_2(MeCN)_2$, $ZnCl_2$, $MnCl_2$, $RuCl_2(MeCN)_2$, YCl_3, $FeBr_3$, $TiCl_3(THF)_3$, $VCl_3(THF)_3$

Equation 2

It was envisaged that $[Ca(THF)_2(H_2L^{Et})]$ could be used for salt-elimination reactions with one equivalent of metal halide to yield a host of monometallic complexes (Equation 2). Unfortunately, these reactions led to either an unidentifiable mixture of products or the formation of homobimetallic complexes and an equivalent of free ligand. It is thought that the initial coordination of the first metal *via* a salt-elimination reaction pre-organises the vacant N_4-donor pocket, so increasing its reactivity towards a second metal.

4.4 Homobimetallic complexes $[M_2(L^{Et})]$

Since the inception of the ligand set H_4L by the Love and Sessler groups, homo-bimetallic pacman complexes of various metals have been synthesised and studied including Pd, Mn, Ni,[3, 20], Fe,[17] Cu,[3, 21] Ti, V,[22] and Co[4, 23]. To further the understanding of these complexes, further homo-bimetallic complexes of L^{Et} were sought.

4.4.1 Synthesis of $[Co_2(L^{Et})]$ and $[Co_2(O_2)(L^{Et})]$

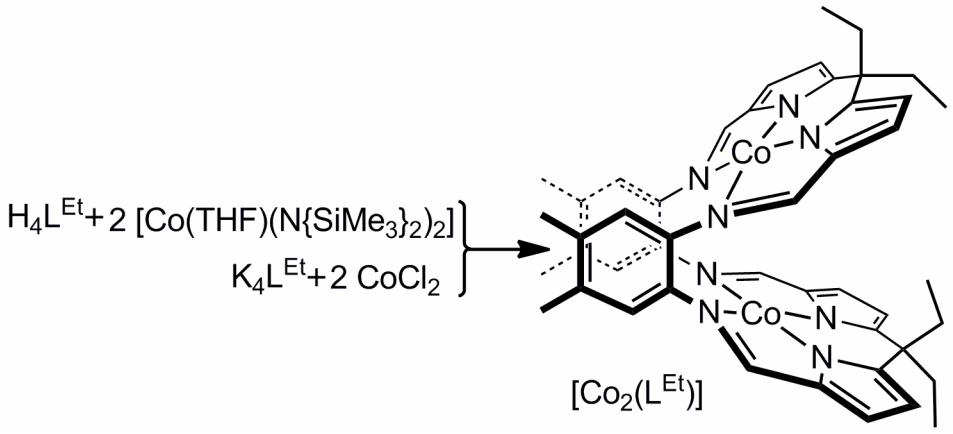

Scheme 6: Synthesis of $[Co_2(L^{Et})]$

Whilst attempting to synthesise a mono-cobalt complex, the bis-cobalt product was instead isolated, after which the prep involving related macrocycles was modified and $[Co_2(L^{Et})]$ synthesised specifically. Binuclear cobalt complexes of L^{Et} were synthesised by two different methods; a protonolysis reaction of H_4L^{Et} with two equivalents of $[Co(THF)(N\{SiMe_3\}_2)_2]$ in THF or alternatively by the reaction of *in-situ* generated K_4L^{Et} and $CoCl_2$ (Scheme 6). The resonances in the ^1H NMR spectrum of $[Co_2(L^{Et})]$ are paramagnetically shifted and broadened, though the number of and integral values of the resonances are consistent with a pacman-shaped complex (Figure 7).

Synthesis is also supported by elemental analysis with the EI mass spectrum showing a peak at 830 amu, consistent with $[Co_2(L^{Et})]$. The IR spectrum shows the disappearance of NH stretches at *ca.* 3200 cm^{-1} and a shifting of the imine absorbance from 1620 to 1555 cm^{-1}. Single crystal X-ray diffraction quality crystals were grown by slow diffusion of hexane into a THF solution of $[Co_2(L^{Et})]$ (Figure 8, Table 4).

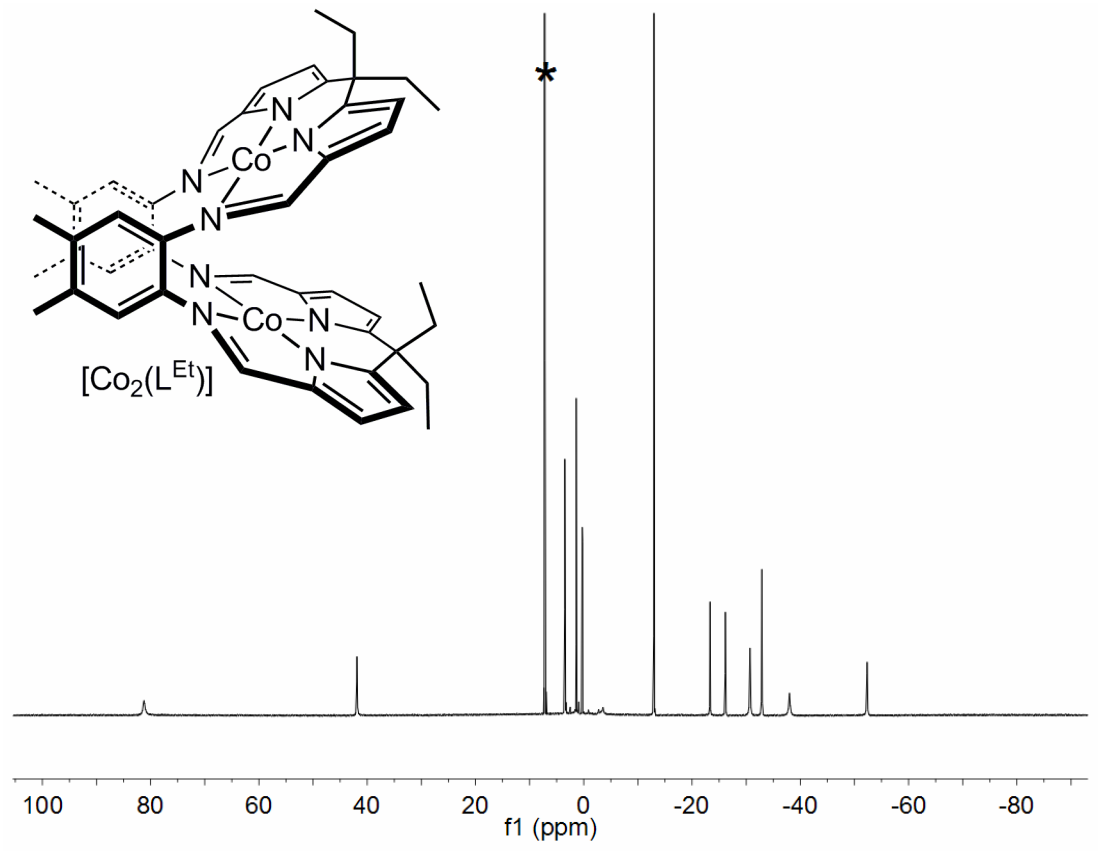

Figure 7: ^{1}H NMR spectra (C_6D_6) of [Co_2L^{Et}] '*' denotes residual protio solvent.

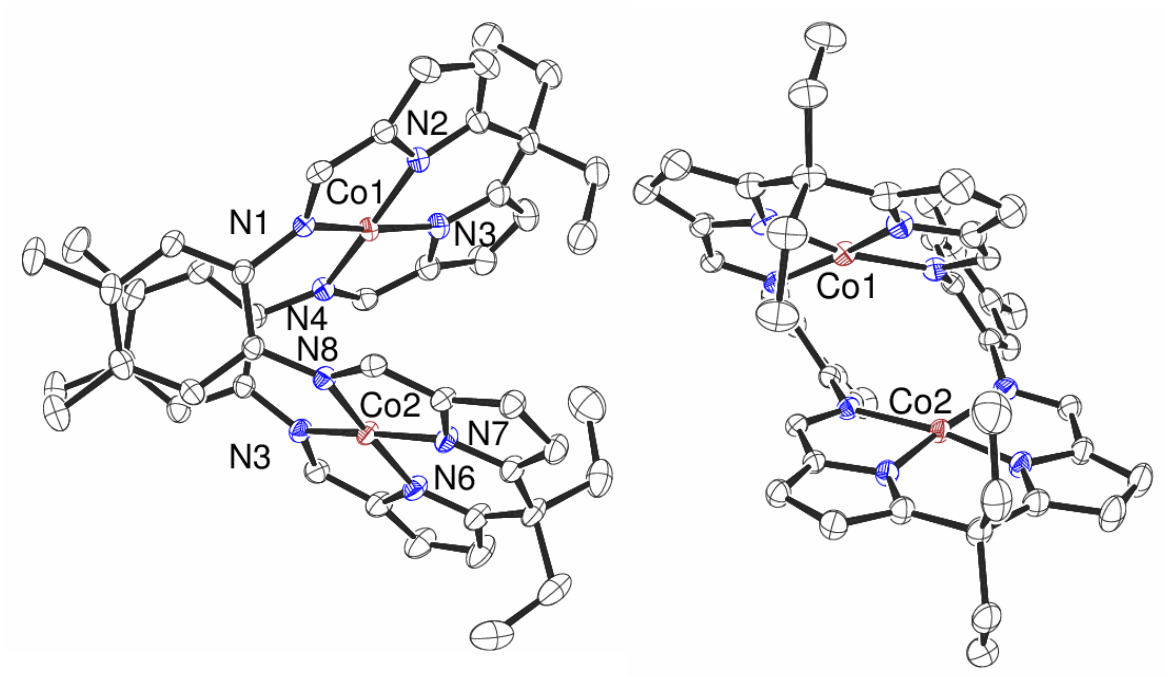

Figure 8: X-ray crystal structure of [Co_2L^{Et}]. For clarity, all hydrogen atoms are omitted and displacement ellipsoids are drawn at 50% probability

Table 4: Selected average bond lengths (Å) and angles (º) of $[Co_2(L^{Et})]$

$Co\text{-}N_{im}$	1.946	Twist Φ	33.49/30.04
$Co\text{-}N_{py}$	1.843	Bite angle θ	58.47
Co···Co	3.862	Dihedral α	12.54
$Co\cdots N_4$	0.019	Σ ∠ Co	360.3

The general structure of $[Co_2(L^{Et})]$ is comparable to that of dicobalt complexes of related ligands.[4, 23] The cobalt lies within the N_4 plane, with the Co^{II} in a square planar environment with standard $Co\text{-}N_{py}$ (*ca.* 1.843 Å) and $Co\text{-}N_{im}$ (*ca.* 1.946 Å) bond lengths.[4, 23]

Exposure of a $[Co_2(L^{Et})]$ to air resulted in an immediate change in colour from red to deep red/brown. The ^1H NMR spectrum of this material shows resonances only in the diamagnetic region that correspond to a pacman-shaped binuclear Co^{III} complex (Figure 9).

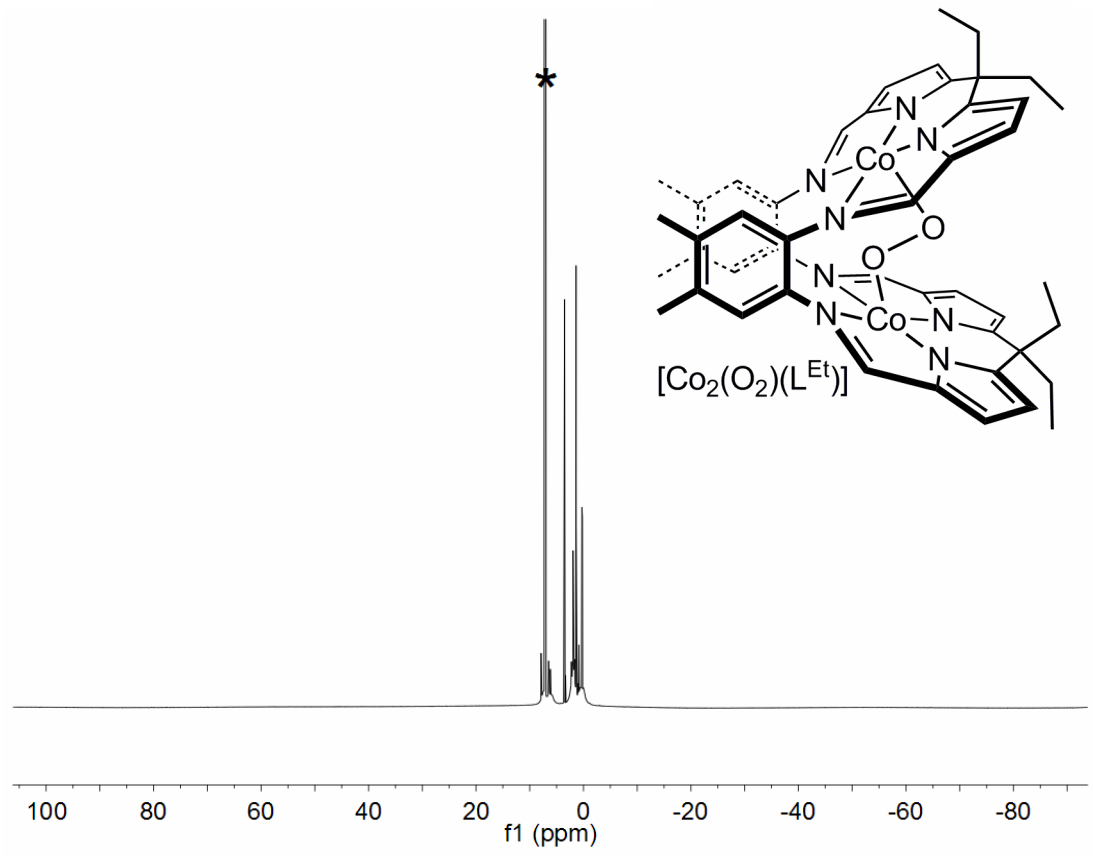

Figure 9: ^1H NMR spectra (C_6D_6) of $[Co_2(O_2)L^{Et}]$ showing no paramagnetically shifted resonances. '*' denotes residual protio solvent

The EPR spectra of $[Co_2(O_2)(L^{Et})]$ in air saturated THF were silent in both the fluid and frozen (140 K) solution, which is indicative of the presence of only peroxo-bridged Co^{III}-O_2-Co^{III} complex. The ESI mass spectrum was dominated by a mono-protonated, single oxygen containing species at 847 amu, resulting from the loss of one O, and fragments thereof which was also observed in the mass spectra of related ligands. A study of biscobalt complexes of related ligands showed low temperature mass spectrometry was required to observed a dioxygen containing complex[4] though this was not carried out with $[Co_2(O_2)(L^{Et})]$. Crystals suitable for single crystal X-ray diffraction were grown from an air saturated solution of $[Co_2(L^{Et})]$ with a few drops of pyridine (Figure 10, Table 5).

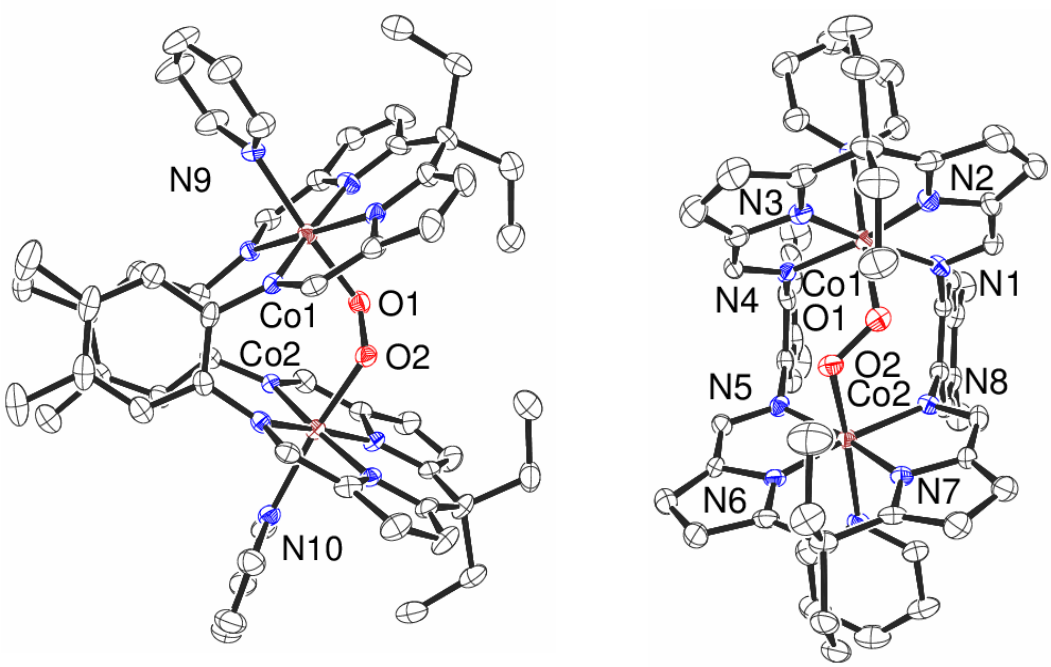

Figure 10: X-ray crystal structure of $[Co_2(pyr)_2(O_2)(L^{Et})]$. For clarity, all hydrogen atoms are omitted and displacement ellipsoids are drawn at 50% probability

Table 5: Selected average bond lengths (Å) and angles (º) of $[Co_2(pyr)_2(O_2)(L^{Et})]$

Co-N_{im}	1.979	Dihedral α	6.05
Co-N_{py}	1.864	Σ ∠ Co	360.05
Co···Co	4.089	O1-O2	1.335(4)
Co···N_4	0.020	Co-O	1.927
Twist Φ	5.41/2.93	Co-N_{pyr}	2.122
Bite θ	61.83	Co1-O1-O2	117.3(2)

The Co^{III} of $[Co_2(O_2)(pyr)_2(L^{Et})]$ resides in a distorted octahedral environment with standard Co-N_{py} (*ca*. 1.864 Å) and Co-N_{im} bond lengths (*ca*. 1.979 Å).[4, 23] The incorporation of the O_2 widens the mouth and so increases the Co···Co distance by 0.227 Å relative to $[Co_2(L^{Et})]$. This is accompanied with a straightening of the aryl-backbone to almost perpendicular to the N_4-plane (Φ *ca*. 4 °) and an increase in bite angle of 3.4 ° all of which is in-line with that observed with related ligand cobalt complexes.[4, 23] The peroxo ligand binds to the two cobalt centres in a Pauling mode with the O-O distance of 1.335(4) Å. This distance is shorter than for the related ligands (1.361(3)–1.382(14) Å)[4] and is very short in comparison to the bulk of published peroxo-bridged dicobalt structures (1.353(11)–1.496(3) Å).[24] The bond length is more comparable to that of superoxo bridged dicobalt species (1.325(3)–1.336(17) Å)[25] though the lack of any counterion does confirm the Co^{III}-O_2-Co^{III} peroxo-bridged structure. The complex $[Co_2(L^{Et})]$ is yet to be investigated for any catalytic activity towards dioxygen.

4.4.2 Synthesis of $[Mg_2(THF)_2(L^{Et})]$ and $[Mg_4(OH)_4(\mu\text{-}OH)_4(H_4L^{Et})_2]$

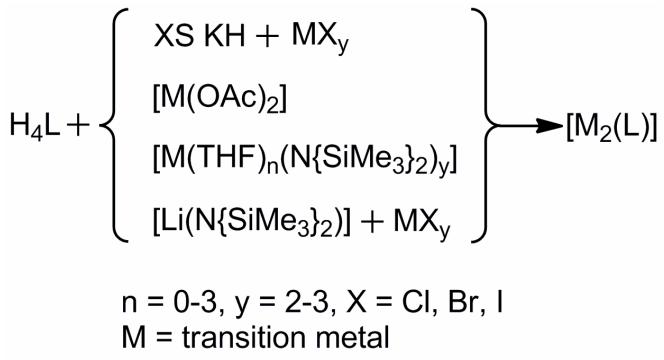

Scheme 7: Different routes into $[M_2(L)]$

Current routes to form $[M_2(L)]$ complexes include: (i) reaction with metal acetates in the presence of a base; (ii) transamination reactions with transition metal silylamides; (iii) salt elimination reactions between $K_4(L)$ or $Li_4(L)$ and metal halides (Scheme 7).[3, 4] New routes into complexes may open up the possibility of forming complexes with new metals, increasing the yield or ease of synthesis of known compounds or even open the window to forming monometallic or heterobimetallic complexes of L.

Addition of a solution of two equivalents of dibutylmagnesium to a solution of H_4L^{Et} in THF at -80 °C caused a slight change in colour from yellow/orange to orange. Warming to room temperature followed by removal of the volatiles under vacuum produced $[Mg_2(THF)_2(L^{Et})]$ in good yield (85 %).[26] The EI mass spectrum shows a peak

consistent with the molecular ion at *m/z* = 760, and the ^{1}H NMR spectrum (Figure 11) shows the disappearance of the NH resonance, as well as the shifting of the imine resonance from 8.26 to 7.71 ppm. The IR spectrum also confirms the loss of the NH stretch and the shifting of the imine stretch from 1680 to 1604 cm^{-1}. The ^{1}H NMR spectrum also supports a pacman geometry in solution with two distinct environments representing the *endo*- and *exo-meso*-ethyl substituents with two Et-CH_2 quartets at 2.15 and 2.06 ppm as well as overlapping triplets for Et-CH_3 from 1.13 to 1.05 ppm. Resonances for bound THF molecules integrate to two molecules of THF per macrocycle. The same product was also formed by the reaction of two equivalents of $[Mg(N\{SiMe_3\}_2)_2(THF)_2]$ with H_4L^{Et} in THF.

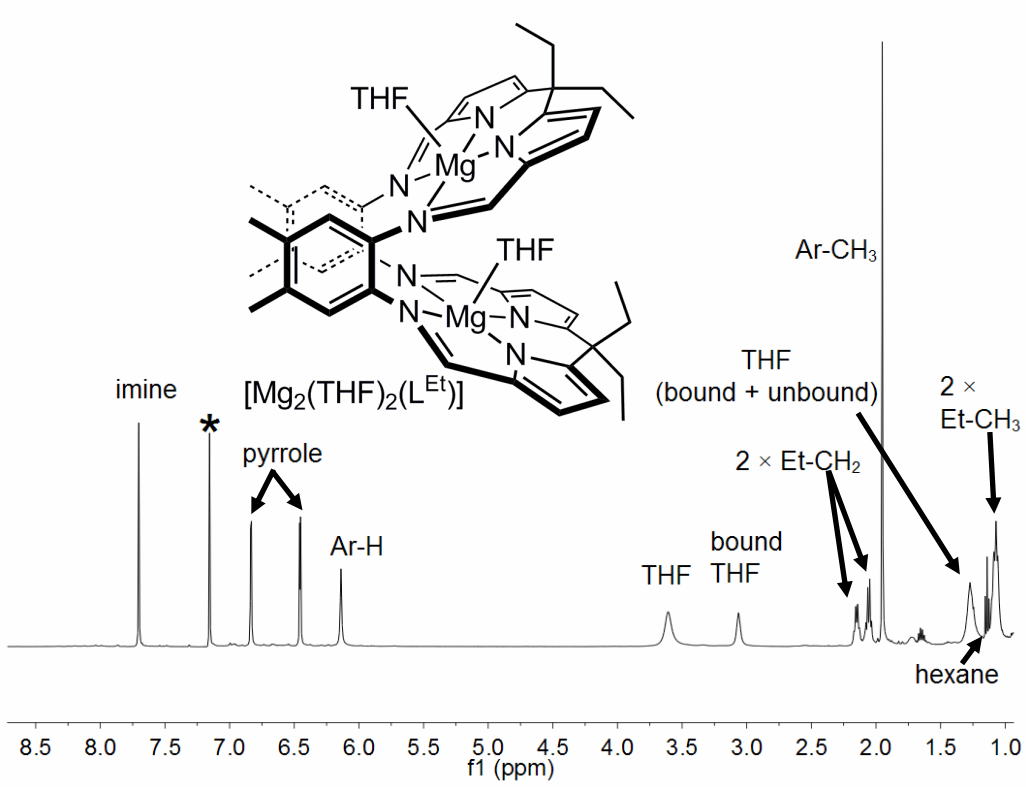

Figure 11: ^{1}H NMR spectra (C_6D_6) of $[Mg_2(THF)_2(L^{Et})]$. '*' denotes residual protio solvent.

Crystals of $[Mg_2(THF)_2(L^{Et})]$ suitable for single crystal X-ray diffraction analysis were grown from a saturated toluene solution (Figure 12, Table 6). An overall pacman geometry is observed in the solid state with each magnesium sitting in a distorted square-based pyramidal environment, bound by a THF molecule and four nitrogen donors (two imine, two pyrrolic). One magnesium lies *exo*-to the cleft, 0.571 Å from the distorted N_4-plane, bound to an exogenous THF, the other lies within the cleft 0.562 Å from the N_4-plane, also bound to a THF found within the cleft. This results in the

imine-pyrrole units folding around the *meso*-carbon by 43.6/53.4 °, a larger distortion than observed for the similarly bound 5-coordinte zinc cation in [$SnMe_2Zn(THF)(L^{Et})$] of 38.19 °.[2] The *endo*-/*exo*-solvent conformation is also observed with other complexes such as bis-cobalt complexes with *exo*- and *endo*-bound pyridine[23] and is the cause of a rather large bite-angle of 69.95 ° compared to other symmetric homobimetallic complexes of L (44.8–64.8 °).[1, 3, 17]

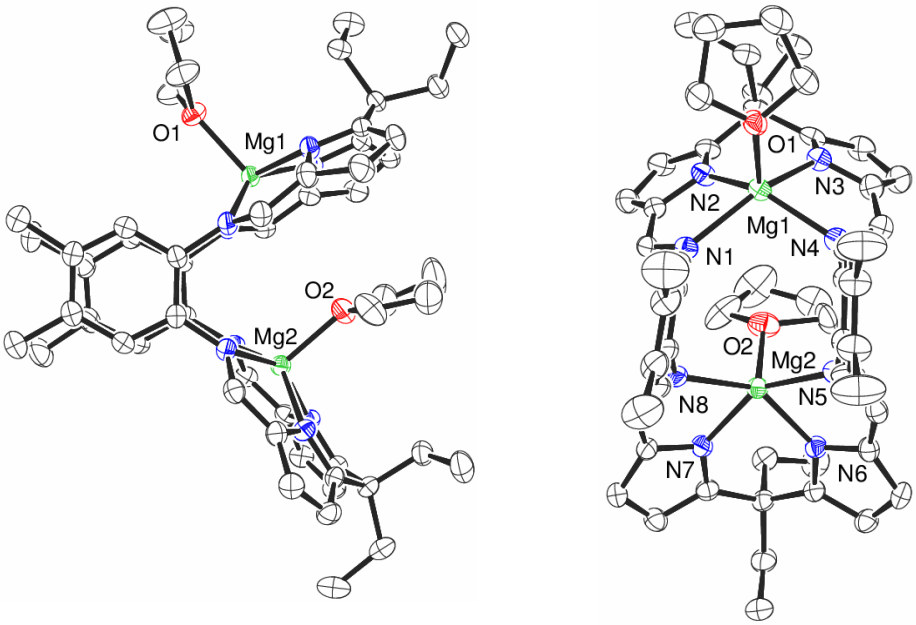

Figure 12: X-ray crystal structure of [$Mg_2(THF)_2(L^{Et})$]. For clarity, all hydrogen atoms are omitted and displacement ellipsoids are drawn at 50% probability

Table 6: Selected bond lengths (Å) and angles (°) of [$Mg_2(THF)_2(L^{Et})$]

Mg-N_{im}	2.131(2)–2.249(2)	N_{im}-Mg-N_{py}	77.74(7)–78.63(7)
Mg-N_{py}	2.0267(17)–2.0779(18)	N_{py}-Mg-N_{py}	82.20(8)/80.17(7)
Mg-O_{THF}	2.0434(15)/2.0267(17)	Σ ∠ Mg	343.11/343.93
Mg···Mg	4.650	Bite θ	69.95
Mg1···N_4	0.571	Twist Φ	7.75/3.16
Mg2···N_4	0.562	Dihedral α	11.00
N_{im}-Mg-N_{im}	103.71(7)/107.89(7)		

The ligand is much less twisted (Φ = 7.75/3.16 °) than many homobimetallic complexes of this ligand type, though within reported values (0.3–34.2 °).[1, 3, 17, 23] The Mg-N_{im} bond lengths (2.131(2)–2.249(2) Å) are comparable to salen-based magnesium complexes (2.137(2)–2.236(7) Å)[27] and other imine ligands (2.0882(16)–2.296(4) Å).[30] Mg-N_{py} distances (2.0267(17)–2.0779(18) Å) are shorter than that of porphyrin complexes (2.064(2)–2.110(5) Å)[28] but within that of other Mg-pyrrole complexes (2.006(2)–2.194(9) Å).[32] The Mg-O_{THF} distances of 2.0434(15) and 2.0267(17) Å are also within reported values (1.993(2)–2.236(8) Å)[29]

A similar reaction using Et_2O as the solvent yields the doubly-solvated product $[Mg_2(Et_2O)_2(L^{Et})]$ by ^{1}H NMR spectroscopy, though longer reaction times are needed (16 h compared to 3 h in THF). Furthermore, addition of pyridine to $[Mg_2(THF)_2L^{Et}]$ results in the pyridine adduct $[Mg_2(pyr)_2(L^{Et})]$ in quantitative yield. It was envisaged that these binuclear magnesium pacman complexes could be used as a route into new mononuclear, homo- and hetero-binuclear complexes of L^{Et}. Unfortunately reactions with metal halides gave unidentifiable mixtures of products by ^{1}H NMR spectroscopy.

A different set of crystals suitable for single crystal X-ray diffraction were grown by slow hexane diffusion into a benzene solution of $[Mg_2(THF)_2(L^{Et})]$. However, these proved to be an interesting magnesium hydroxide cubane decomposition product, $[Mg_4(OH)_4(\mu\text{-}OH)_4(H_4L^{Et})_2]$ that is formed due to a reaction with adventitious water (Figure 13, Figure 14 and Table 7).

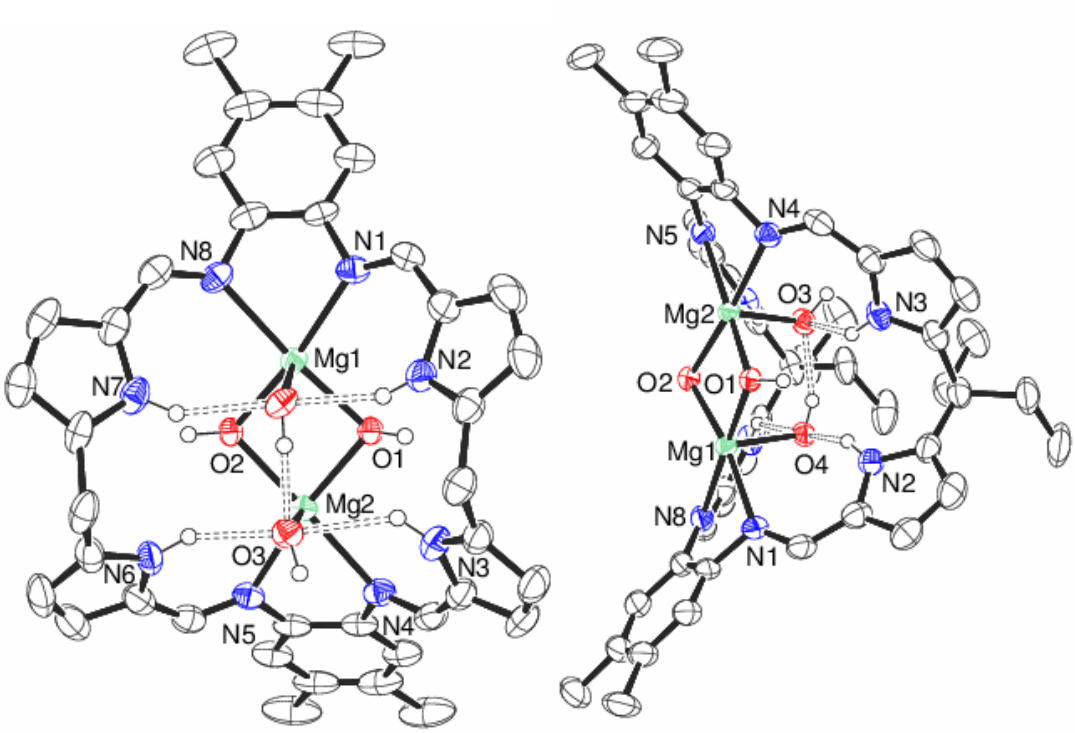

Figure 13: X-ray crystal structure of $[Mg_4(OH)_4(\mu\text{-}OH)_4(H_4L^{Et})_2]$ showing the asymmetric unit only. Hydrogen-bonds shown as dotted lines. For clarity, all hydrogen atoms except those on N2, N3, N6, N7 and O1-4, which were located from the difference map and refined with restraints are omitted, furthermore also for clarity the left figure has the *meso*-ethyl groups removed. Displacement ellipsoids are drawn at 50% probability

The full symmetry-generated structure consists of two fully protonated ligands (H_4L^{Et}) that encapsulate a $Mg_4(OH)_4$ cubane, with a further four terminal-OH units in a "tennis-ball" topology (Figure 14), similar to that seen by Rebek and co-workers on assembly of C-shaped glycoluril into capsules.[30] Capsules are also briefly discussed later in this section. This is the first example where magnesium atoms present in the cubane are bound and encapsulated by only two ligands. The ligands adopt a bowl-shaped conformation and lie perpendicular to each other with the terminal hydroxy groups displaying hydrogen bonding between each other and to the pyrrolic NHs.

Table 7: Selected bond lengths (Å) and angles (º) of $[Mg_4(OH)_4(\mu\text{-}OH)_4(H_4L^{Et})_2]$. Mean values in square brackets [ ]

Mg-N_{im}	2.195(2)–2.264(3) [2.229]	N_{im}-Mg-μO'	91.73(8)–97.65(8) [94.81]
Mg···N_{py}	3.445–3.587 [3.515]	μO-Mg-μO	78.98(8)–84.60(8) [81.64]
Mg-μO	2.049(2)–2.095(2) [2.070]	Mg-μO-Mg (N_4-plane)	94.00(8)–94.06(8) [94.03]
μO-H	0.835(17)–0.869(17) [0.852]	Mg-μO'-Mg'	97.74(8)–100.94(8) [98.86]
Mg-μO-H	111–128 [120]	Mg···Mg	3.040–3.204 [3.130]
Mg-$O_{terminal}$	2.020(2)–2.065(2) [2.0425]	O3···O4	2.605
Mg-$O_{terminal}$-H	111(2)–118(2) [115]	μO···μO	2.641–2.793 [2.705]
$O_{terminal}$-H	0.805(18)–0.836(17) [0.821]	N_{py}···$O_{terminal}$	2.735–2.986[2.836]
N_{im}-Mg-N_{im}	73.36(9)–73.53(9) [73.445]	N_{py}···μO	3.204–3.270 [3.228]
N_{im}-Mg-μO (N_4-plane)	98.01(9)–103.79(9) [100.86]	Mg··· $N_2(\mu O)_2$-plane	0.078/0.108

Each magnesium atom is bound in a pseudo-octahedral fashion by two imine nitrogens, one terminal hydroxide and three bridging hydroxides. The magnesium sits out of the intra-$N_2(\mu O)_2$-plane by *ca.* 0.09 Å with Mg-N_{im} bonds (2.195(2)–2.264(3) Å) comparable to those of the pacman $[Mg_2(THF)_2(L^{Et})]$ complex (2.131(2)–2.249(2) Å) as well as salen-based complexes (2.137(2)–2.236(7) Å)[27] and other imine ligands (2.0882(16)–2.296(4) Å).[31] The Mg-μO bond distances of 2.049(2)–2.095(2) Å are within the range of published magnesium-cubane structures (2.032(3)–2.146(6) Å)[32-34] as are the Mg···Mg distances (3.040–3.204 Å, literature 2.979–3.398 Å).[35, 36] The Mg-μO distances are marginally shorter bridging between ligands (2.049(2)–2.0579(19) Å) than in the N_4-plane (2.0593(19)-2.095(2) Å) with the N_{im}-Mg-μO angle also larger in the N_4-plane (98.01(9)–103.79(9) °) than to the symmetry-generated μO' (91.73(8)–97.65(8) °).

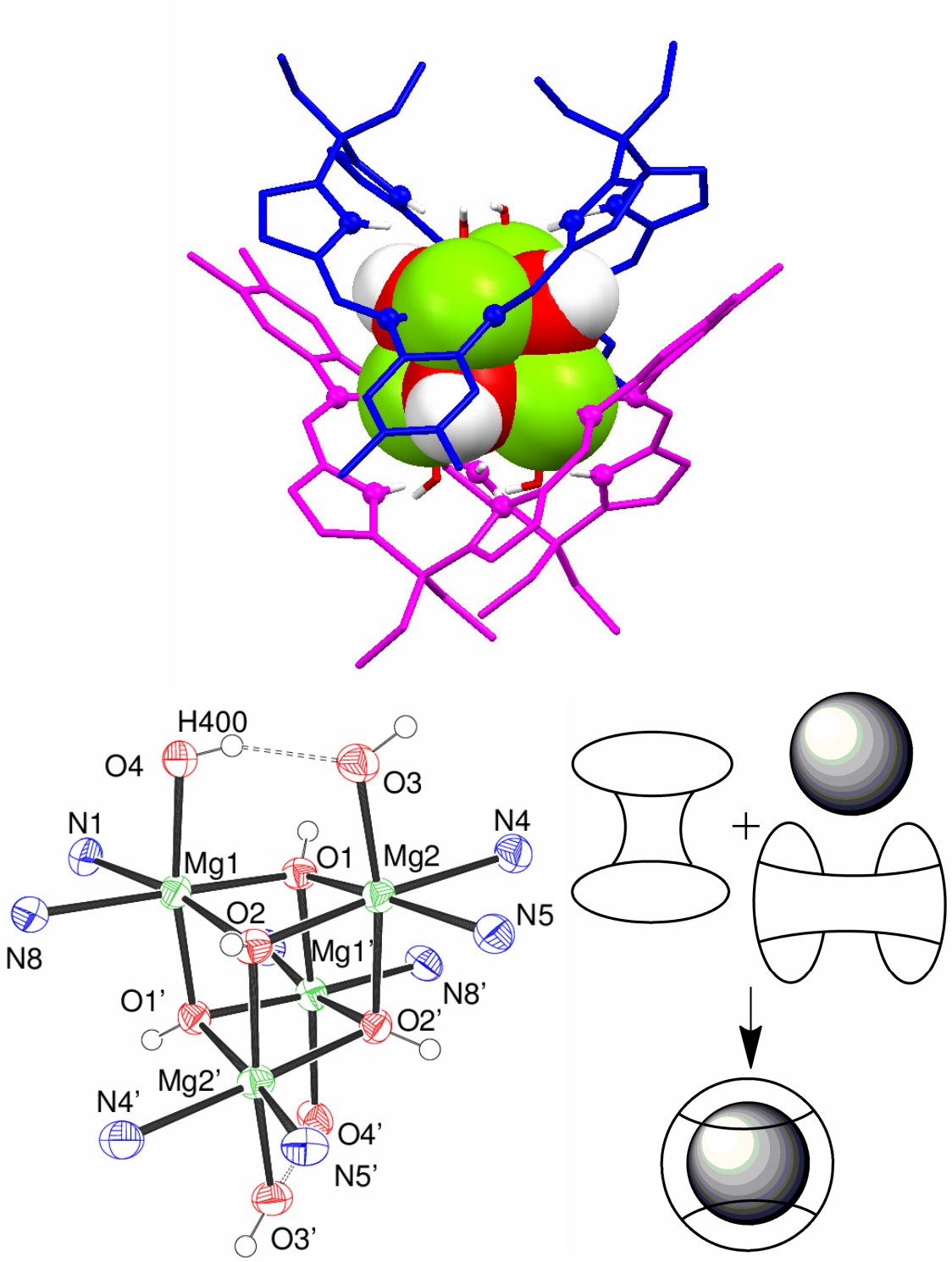

Figure 14: X-ray crystal structures of $[Mg_4(OH)_4(\mu\text{-}OH)_4(H_4L^{Et})_2]$ showing symmetry-generated full structure with two ligands (blue and pink) with space-filled cubane (top) and the cubane centre only (bottom left), labels denoted with a dash "'" are symmetry generated. For clarity, all hydrogen atoms except for hydrogen atoms on O1-4, which were found from the difference map and refined with restraints are omitted and displacement ellipsoids are drawn at 50% probability. Rebek and co-workers' "tennis ball" topology for encapsulation[37] (bottom right)

Surprisingly a search of the chemical literature yielded no structurally-characterised Mg hydroxide compounds containing a terminal Mg-OH ligand and so the structure is also unique in that respect with bond distances Mg-$O_{terminal}$ 2.020(2)–2.065(2) Å, $O_{terminal}$-H 0.805(18)–0.836(17) Å. The hydrogen of the terminal-OH group, O4, is hydrogen bonded to the other terminal hydroxo, O3, with a O3···O4 distance of *ca* 2.7 Å. The terminal hydroxides are further stabilised by an H-bonding interaction between the pyrrolic NH and terminal hydroxide (HN···$O_{terminal}$ *ca*. 2.8 Å). Furthermore, structures in which a discrete magnesium cubane with hydroxides, as oppose to alkoxides, at all vertices, are unknown. The hydrogens of the bridging hydroxides were found from the difference map and refined with restraints. The hydrogens of the μ_3-O(H) are orientated away from the cubane core, to the area of least steric bulk, in a distorted tetrahedral fashion (mean Mg-μO-H = 120 °, μO-H = 0.835(17)–0.869(17) Å). A structure containing two face-sharing cubanes published by Brumaghim and co-workers (Figure 15) contains a μ_4-OH at two corners in the face-sharing plane.[35] Mg-μ_4-O(H) distances which range from 2.122(3) to 2.238(3) Å are considerably longer than in the L^{Et} complex (2.049(2)–2.095(2) Å).

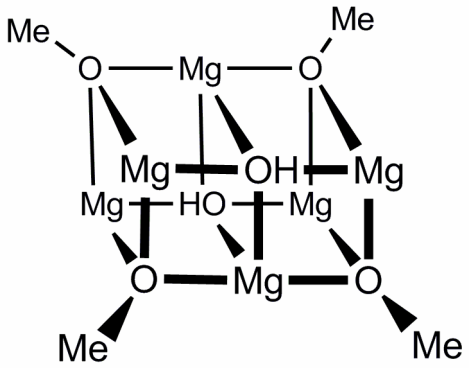

Figure 15: Face-sharing cubane core showing μ_4-OH by Brumaghin and co-workers

There are generally few published structures containing an Mg-μ-OH-Mg group, but despite this, the Mg-μOH bond distances (2.049(2)–2.095(2) Å) are within the μ_3-OH (2.0030 (16)–2.1208(15) Å)[38, 39] and μ_2-OH (1.951(6)–2.093(2) Å)[40] bond lengths reported for the closely related structures of a series of alkaline earth metal tetranuclear aryloxide hydroxides reported by Teng and co-workers[39] (Figure 16, a))

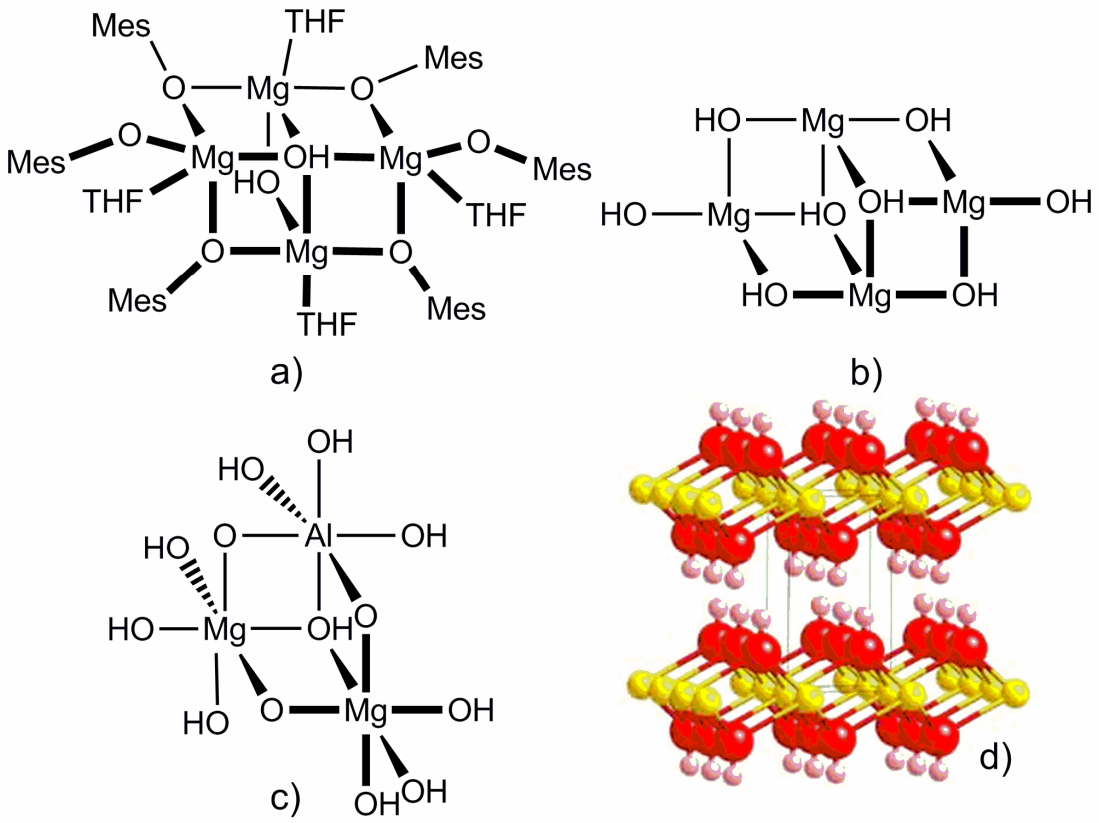

Figure 16: a) Structure reported by Teng and co-workers[39] b) $[Mg(OH)_2]_4$ core used for DFT calculations by the Sato group.[41] c) core used for DFT calculations by Wei and co-workers[42] d) Brucite (red = oxygen, yellow = magnesium, pink = hydrogen)[43]

Closely-related, naturally-occurring materials such as brucite, which incorporate infinite $[Mg(OH)_4]$ sheets, or layered double hydroxides such as hydrotalcite $(Mg_6Al_2(CO_3)(OH)_{16}{\cdot}4(H_2O)$ have also been investigated. Wei and co-workers probed the stability of Al-Mg layered double hydroxides (LDHs) by DFT.[42] DFT calculations have also been used to model mono-magnesium-hydroxy clusters by Sato and co-workers as a means to study solid state structures containing infinite Mg-O(H) sheets which can be found in nature such as in brucite (Figure 16).[41, 44] The bond lengths resulting from these calculations, as well as those for brucite itself, are remarkably close to the structure reported here (Table 8).

Table 8: Average bond lengths (Å) of $[Mg_4(OH)_4(\mu\text{-}OH)_4(H_4L^{Et})_2]$, brucite and $[Mg(OH)_2]_4$ and of LDHs. *DFT calculated structure

	$[Mg(OH_2)]_4$ (DFT)[41]	LDHs[42]*	Brucite[41, 44]	$[Mg_4(OH)_4(\mu\text{-}OH)_4(H_4L^{Et})_2]$
Mg···Mg	3.000*	3.046–3.142 3.139–3.150*	3.142	3.130
Mg-μO	2.020*	1.974–2.123 2.191–2.202*	2.102	2.070
μO···μO	2.650*	–	2.787	2.705

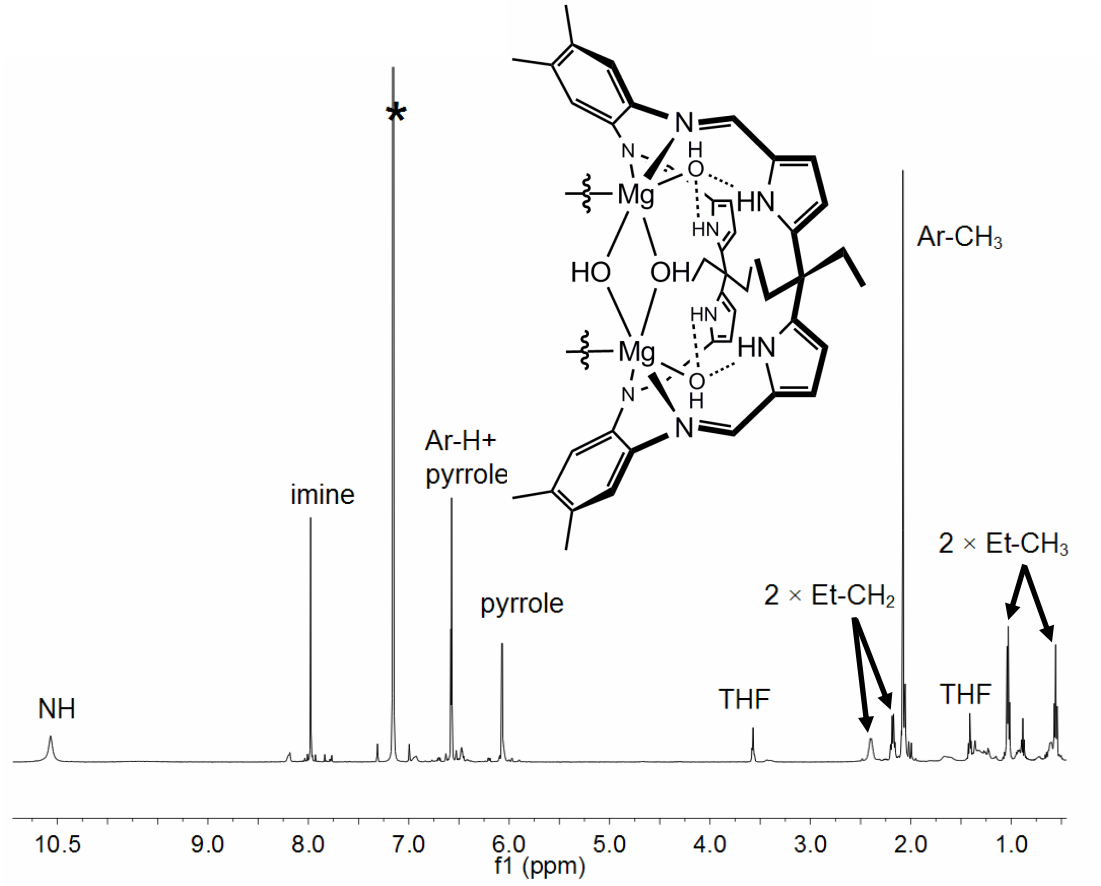

Figure 17: ^1H NMR spectra (C_6D_6) of $[Mg_4(OH)_4(\mu\text{-}OH)_4(H_4L^{Et})_2]$. '*' denotes residual protio solvent

A solution state cubane structure is also supported by ^1H and $^{13}C\{^1H\}$ NMR spectroscopy. The ^1H NMR spectrum of $[Mg_4(OH)_4(\mu\text{-}OH)_4(H_4L^{Et})_2]$ (Figure 17) shows the appearance of the pyrrolic NH appears at 10.57 ppm, shifted from 9.89 ppm in the free ligand, and is consistent with hydrogen bonding. This resonance at 10.57 ppm has an integral value of 16H and so is thought to result from the overlapping of

pyrrolic-NH and OH resonances. The imine resonance has shifted from 7.71 ppm in the pacman complex to 7.98 ppm in the cubane. Two environments are observed for the *meso*-ethyl groups with resonances at 2.40 and 2.18 ppm (CH_2) and 1.03 and 0.56 ppm (CH_3) and are reflected in the $^{13}C\{^1H\}$ NMR spectrum with resonances at 26.36 and 25.38 ppm (CH_2) and 8.49 and 7.92 ppm (CH_3). Only a small amount of residual unbound THF is present at 3.56 and 1.39 ppm. The dissimilarity of the ethyl groups implies a rigid bowl shaped structure for the ligand in solution with ethyl groups *endo*- and *exo*- to the cleft and thus the cubane structure is maintained in the solution state. The IR spectrum also supports cubane formation with absorptions seen at 3440 and 3280 cm^{-1} that are consistent with O-H and N-H stretches.

It was also found bulk isolation of $[Mg_4(OH)_4(\mu\text{-}OH)_4(H_4L^{Et})_2]$ was possible by intentional hydrolysis of $[Mg_2(THF)_2(L^{Et})]$.‡[26] Addition of 4.7 equivalents of water to a solution of $[Mg_2(THF)_2(L^{Et})]$ in benzene resulted in the precipitation of the above magnesium cubane as a bright yellow solid in 45 % yield, the ^1H NMR spectrum of which was identical to that of crystalline $[Mg_4(OH)_4(\mu\text{-}OH)_4(H_4L^{Et})_2]$. Furthermore, ESI mass spectrometry showed the parent peak plus a proton at 1665 amu with microanalytical data confirming the elemental make up. Exposure of a solution of $[Mg_4(OH)_4(\mu\text{-}OH)_4(H_4L^{Et})_2]$ to air resulted in the slow decomposition to the free macrocycle H_4L^{Et} with 25 % decomposition over 48 h as observed by ^1H NMR spectroscopy, however, solid $[Mg_4(OH)_4(\mu\text{-}OH)_4(H_4L^{Et})_2]$ is stable indefinitely.

Further investigation is required to determine whether this product could be synthesised by a more direct route, such as a reaction of H_4L^{Et} with two equivalents of $Mg(OH)_2$ or $Mg(OMe)_2$, or whether transition metal cubanes/clusters could be synthesised.[17]

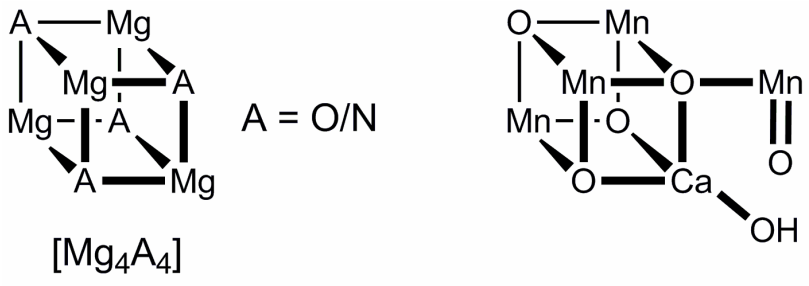

Figure 18: (Left) General structure of the core of a magnesium cubane. (Right) Cubane core of photosystem II

Opposing corners of magnesium cubanes can be occupied by μ_3-N-amines,[45] or more commonly by μ_3-O-alk-oxy substituents, on the remaining verticies (Figure 18). The magnesium atoms can be bound in an octahedral[34, 35, 46] or tetrahedral fashion,[32, 47] depending on the ligands used. Though there are some (16) published structures of discreet "Mg_4O_4" cubanes, a search of chemical literature indicates $[Mg_4(OH)_4(\mu\text{-}OH)_4(H_4L^{Et})_2]$ is the first example using nitrogen donors to stabilise a magnesium, or any group II metal, $[M_4O_4]$ core-cubane structure. There are however many examples of transition metal cubanes stabilised with imine-nitrogen, and other nitrogen donors.[48-50] Transition metal and mixed metal cubanes are currently targets for single-molecule-magnets[48, 49, 51] as well as being of biological interest due to the Ca-Mn cubane core in photosystem II (Figure 18)[52] or the Fe_4S_4 cubanes involved in biological electron transport.[53] Sessler and co-workers have eluded to the synthesis of $Mn^{II/IV}$-μ-oxo clusters using closely-related ligands though these results are yet to be published.[17]

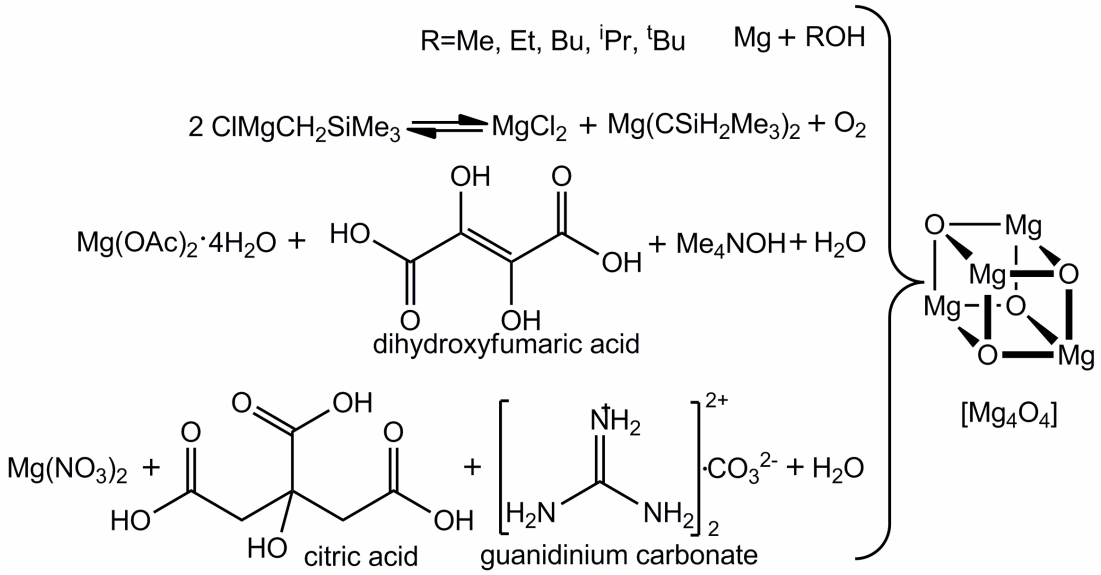

Figure 19: Selected methods towards the formation of $[MgO_4]$ cubanes

Discrete magnesium cubanes have mainly been synthesised by the crystallisation of a variety of magnesium alkoxides,[33-35, 54, 55] including through CO_2 insertion into a solution of magnesium alkoxides[36] and also from decomposition of $ClMgCH_2SiMe_3$ with O_2 *via* a Schlenk equilibrium product.[32] By far the most facile method was discovered by the Robson group by aqueous reactions of magnesium acetate with dihydroxyfumaric acid,[56] or magnesium nitrate with citric acid and guanidinium

carbonate (Figure 19).[48] These latter two routes are can also be applied to a variety of M^{2+} ions such as Mn, Fe, Co, Ni, and Zn.

Discrete magnesium cubanes have recently been synthesised for the study of solid state materials such as thin-layer magnesium oxide layers and nanoparticles.[47, 55, 57]

Encapsulation of discreet molecules is an active area of research, with encapsulated molecules often behaving differently when isolated from the bulk, with normally unstable intermediates being stabilised or host molecules being forced into unusual conformations by existing in rigid cavities.[58-60] Examples include captivands, such as calixarenes and cucurbiturils, also hemicarcerands were used by Cram and co-workers to stabilise cyclobutadiene (Figure 20).[59-61] Encapsulation is being studied for its applications in the study of biological phenomenon as well as drug delivery.[62] Self-assembled molecular containers have also been synthesised using methods such as metal-ligand interactions[63] or hydrophobic interactions.[64] H-bonds were employed in ligands by the Rebek group, forming the aforementioned "tennis-ball" topology to encapsulate guests such as methane (Figure 14, Figure 20).[37, 65]

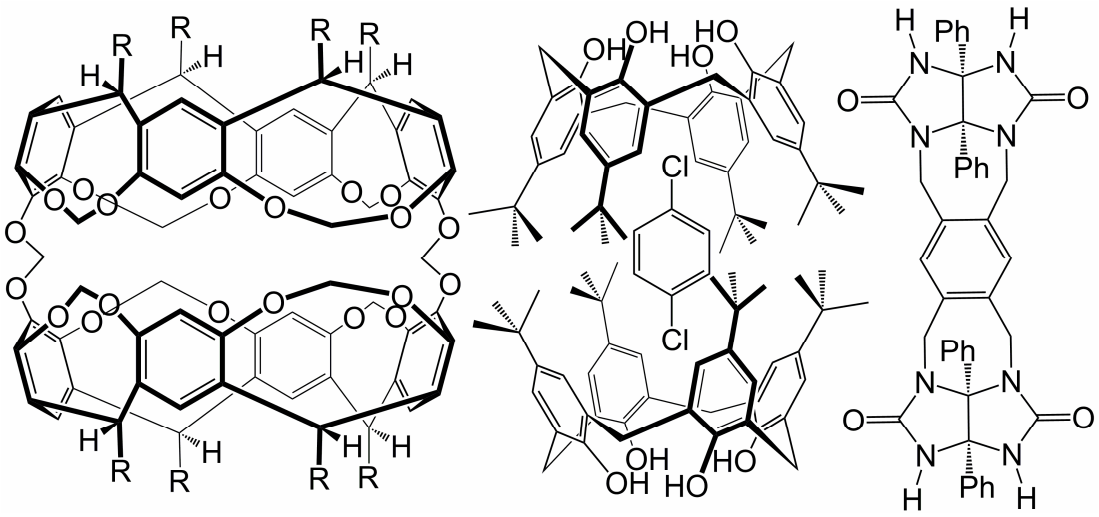

Figure 20: Hemicarcerand capsule used by Crab and co-workers to stabilise cyclobutadiene[59] (R = CH_2CH_2Ph, left). Two calix[4]arene ligands encapsulate a 1,4-dichlorobenzene[60] (middle). Rebek and co-workers found two ligands used H-bonds to encapsulate a methane *via* a "tennis ball" topology[37] (right, also see Figure 14)

4.4.3 Attempted synthesis of $[(NbCl)_2(L^{Et})]$

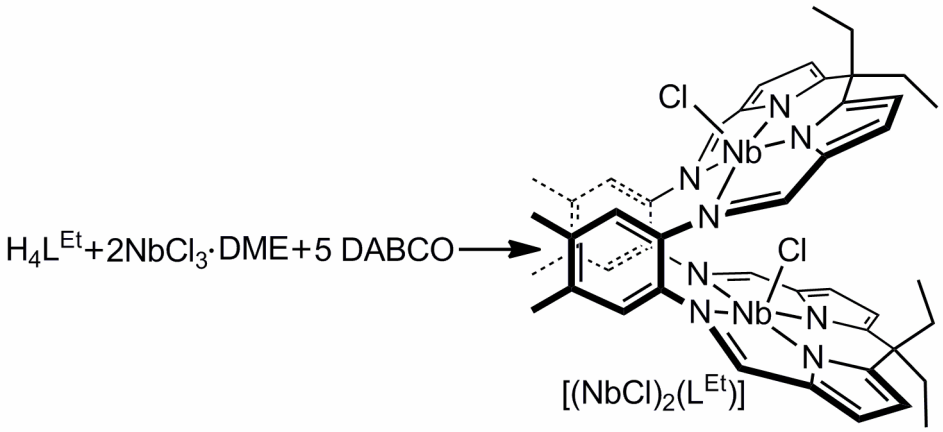

Scheme 8: Attempted synthesis of $[(NbCl)_2(L^{Et})]$

In work carried out at the Tokyo Institute of Technology under the supervision of Prof. Hiroyuki Kawaguchi†, the reaction of the free ligand with two equivalents of $NbCl_3(DME)$, in either THF or toluene, in the presence of DABCO leads to an immediate colour change from yellow to dark brown. Filtration followed by removal of volatiles under vacuum resulted in isolation of a dark brown solid. The ^1H NMR spectrum of this solid is silent, showing only residual solvent resonances. The IR spectrum showed the disappearance of the NH stretch and the shifting of the imine stretch from 1680 to 1579 cm^{-1} and indicates that metallation had occurred. The mass spectrum (EI) showed a peak at *m/z* = 966.3 corresponding to the molecular ion for $[(NbCl_2)(L^{Et})]$. However further analysis is needed to fully characterise this complex.

There are many examples of niobium complexes that bind and activate dinitrogen.[66-70] Floriani and co-workers showed that reduction of a niobium(V) calix[4]arene complex to niobium(III), followed by exposure to N_2 resulted in the binding of N_2 in a bridged mode between two Nb(calixarene) entities (Figure 21, left).[70] The Kawaguchi group also found that reduction of a niobium complex of a tripodal ligand with hydrogen formed a tetrahydride complex that cleaved N_2 (Figure 21, right).[68] As such, dinitrogen activation is achieved in both of these cases by reduction of two niobium centres in the presence of N_2.[68-70]

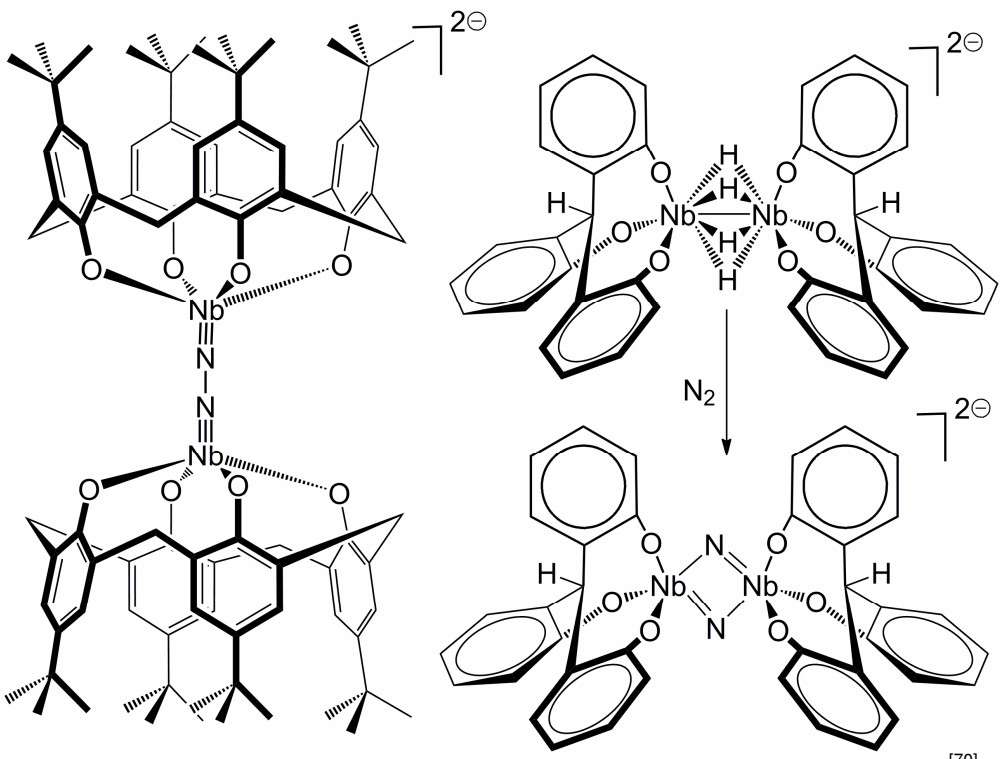

Figure 21: Examples of niobium complex dinitrogen activation by the Floriani group[70] (left) and Kawaguchi group[67] (right)

Thus reduction of $[(NbCl)_2(L^{Et})]$ was attempted under an N_2 atmosphere in the hope of binding and perhaps cleaving N_2 (Scheme 9)

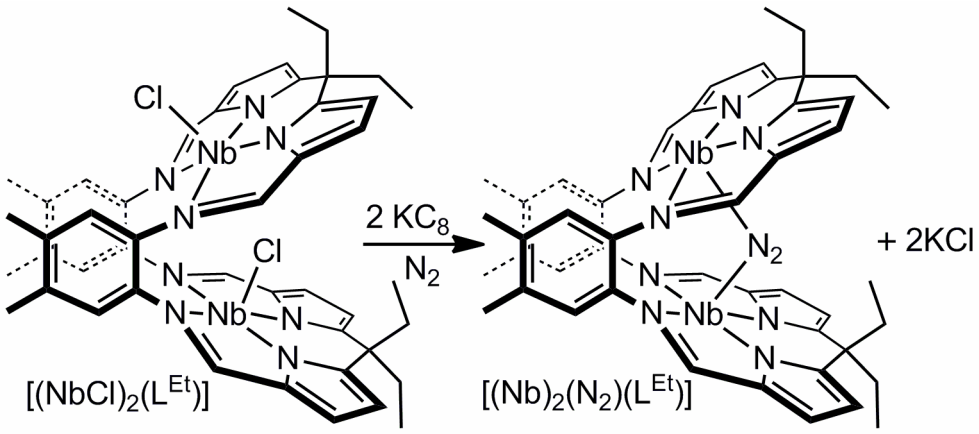

Scheme 9: Attempted activation of N_2 with $[(NbCl)_2(L^{Et})]$

The addition of a THF solution of $[(NbCl)_2(L^{Et})]$ to a suspension of two equivalents of KC_8 results in the precipitation of solid black graphite. Filtration followed by removal of volatiles gave a brown solid which was silent in the ^1H NMR spectrum. No obvious IR absorption corresponding to an N_2 stretch was observed, which is expected if a symmetric N_2 complex has been formed, and unfortunately attempts to

crystallise the product have been unsuccessful. Further work is needed to characterise all of these niobium complexes.

4.5 Conclusions

The Schiff-base pyrrole macrocycle, H_4L^{Et}, has been synthesised in a straightforward, three-step synthesis in good yield and has been characterised fully. Reaction of H_4L^{Et} with Me_2SnCl_2 resulted in the formation of the first pacman-shaped, non-f-element-based, mono-metallic complex of the H_4L range of ligands, $[SnMe_2(H_2L^{Et})]$, in good yield. Further, reactions have led to rare examples of structurally-characterised, six-coordinate heterobimteallic dialkyltin(IV) complexes of L in the form of $[SnMe_2Zn(THF)(H_2L^{Et})]$ and $[SnMe_2Fe(THF)(H_2L^{Et})]$. These are also the first non-f-element-based heterobimetallic complexes of L. All the Sn^{IV} complexes were shown to maintain a pacman geometry in solution. Unfortunately no further reactivity towards small molecules such as H_2, CO or CO_2 was observed nor could the tin cation be successfully exchanged for a transition metal.

The reaction of H_4L^{Et} with $[Ca(N\{SiMe_3\}_2)_2(THF)_2]$ results in the formation of mono-metallated $[Ca(THF)_2(H_2L^{Et})]$ in high yield. Analysis showed this complex is bowl-shaped, rather than pacman-shaped, in both solution and the solid state, with the complex showing a degree of flexibility in solution. The complex was structurally-characterised with bond lengths and angles being similar to those reported in the few cases of porphyrin and salen-based calcium complexes. Unfortunately, attempts at salt-elimination reactions to substitute the calcium cation with that of a transition metal yielded only mixtures of products including doubly-metallated complexes and free ligand.

A fourth binuclear-cobalt complex in the $[Co_2(L)]$ series was produced and was shown to react with dioxygen resulting in the bridged peroxo complex $[Co_2(O_2)(py)_2(L^{Et})]$; both complexes were characterised fully and are closely related to those of previously published versions.

A novel binuclear magnesium complex $[Mg_2(THF)_2(L^{Et})]$ was synthesised in good yield by reaction with $[Mg(^nBu)_2]$ and characterised. The diethylether and pyridine analogues were also synthesised, either by carrying out the reaction in Et_2O or by addition of pyridine. Though $[Mg_2(THF)_2(L^{Et})]$ was characterised structurally, it was found to decompose by reaction with water, resulting in the formation of a rare example

of an encapsulated magnesium cubane. The core of the complex is the first known discrete magnesium cubane containing μ_3-hydroxides as well as the first example of a structurally-characterised, terminal magnesium hydroxide. These terminal hydroxides are further stabilised by hydrogen bonding between both each other and the ligand pyrrolic-NHs. Further investigation is needed to determine whether encapsulation of cubanes of other metals can be achieved.

Though some analysis does point towards the successful synthesis of new binuclear-niobium complexes of L^{Et}, further work is needed to fully characterise and study their reactivity.

4.6 References

† Funded by the Japanese Society for the Promotion of Science (JSPS) summer program, two months were spent at the Tokyo Institute of Technology under the supervision of Prof. Hiroyuki Kawaguchi during summer 2009. Work on niobium chemistry was undertaken in Japan.

‡ Work on the bulk isolations of $[Mg_4(OH)_4(\mu\text{-}OH)_4(H_4L^{Et})_2]$ was undertaken with the help of Mr John Hart, a PhD student working under the supervision of Dr. Jason B. Love at the University of Edinburgh.

[1] E. Askarizadeh, A. M. J. Devoille, D. M. Boghaei, A. M. Z. Slawin, J. B. Love, *Inorg. Chem.* **2009**, *48*, 7491.

[2] J. W. Leeland, A. M. Z. Slawin, J. B. Love, *Organometallics* **2010**, *29*, 714.

[3] G. Givaja, M. Volpe, J. W. Leeland, M. A. Edwards, T. K. Young, S. B. Darby, S. D. Reid, A. J. Blake, C. Wilson, J. Wolowska, E. J. L. McInnes, M. Schröder, J. B. Love, *Chem. Eur. J.* **2007**, *13*, 3707.

[4] M. Volpe, H. Hartnett, J. W. Leeland, K. Wills, M. Ogunshun, B. J. Duncombe, C. Wilson, A. J. Blake, J. McMaster, J. B. Love, *Inorg. Chem.* **2009**, *48*, 5195.

[5] P. L. Arnold, A. J. Blake, C. Wilson, J. B. Love, *Inorg. Chem.* **2004**, *43*, 8206.

[6] P. L. Arnold, D. Patel, C. Wilson, J. B. Love, *Nature* **2008**, *451*, 315.

[7] M. Carcelli, G. Corazzari, S. Ianelli, G. Pelizzi, C. Solinas, *Inorg. Chim. Acta* **2003**, *353*, 310; R. Luna-Garcia, B. M. Damian-Murillo, V. Barba, H. Hopfl, H. I. Beltran, L. S. Zamudio-Rivera, *Chem. Commun.* **2005**, 5527.

[8] L. Annunziata, D. Pappalardo, C. Tedesco, C. Pellecchia, *Organometallics* **2005**, *24*, 1947.

[9] T. P. Lockhart, W. F. Manders, *Inorg. Chem.* **1986**, *25*, 892.

[10] I. Noda, S. Kato, M. Mizuta, N. Yasuoka, N. Kasai, *Angew. Chem., Int. Ed. Engl.* **1979**, *18*, 83; J. Chen, L. K. Woo, *Inorg. Chem.* **1998**, *37*, 3269; D. Y. Dawson, J. C. Sangalang, J. Arnold, *J. Am. Chem. Soc.* **1996**, *118*, 6082.

[11] A. Wirth, O. Moers, A. Blaschette, P. G. Jones, *Z. Anorg. Allg. Chem.* **2000**, *626*, 529; E. J. Gabe, L. Prasad, Y. Le Page, F. E. Smith, *Acta Crystallogr., Sect. B.* **1982**, *38*, 256; L. Prasad, E. J. Gabe, Y. Le Page, F. E. Smith, *Acta Crystallogr., Sect. A: Cryst. Phys., Diffr., Theor. Crystallogr.* **1981**, *37*, C222; D. Cunningham, K. Gilligan, M. Hannon, C. Kelly, P. McArdle, A. O'Malley, *Organometallics* **2004**, *23*, 984; J. Bravo, M. B. Cordero, J. S. Casas, M. V. Castaño, A. Sánchez, J. Sordo, *J. Organomet. Chem.* **1996**, *513*, 63; J. Halfpenny, *Acta Crystallogr., Sect. C.* **1995**, *51*, 2044.

[12] D. K. Dey, M. K. Saha, M. K. Das, N. Bhartiya, R. K. Bansal, G. Rosair, S. Mitra, *Polyhedron* **1999**, *18*, 2687; S.-G. Teoh, G.-Y. Yeap, C.-C. Loh, L.-W. Foong, S.-B. Teo, H.-K. Fun, *Polyhedron* **1997**, *16*, 2213.

[13] M. Calligaris, G. Nardin, L. Randaccio, *J. Chem. Soc., Dalton Trans.* **1972**, 2003; D. K. Dey, M. K. Das, H. Noth, *Z. Naturforsch., B: Chem. Sci.* **1999**, *54*.

[14] A. L. Singer, D. A. Atwood, *Inorg. Chim. Acta* **1998**, *277*, 157; A. W. Kleij, M. Kuil, M. Lutz, D. M. Tooke, A. L. Spek, P. C. J. Kamer, P. W. N. M. van Leeuwen, J. N. H. Reek, *Inorg. Chim. Acta* **2006**, *359*, 1807; W.-K. Wong, X. Yang, R. A. Jones, J. H. Rivers, V. Lynch, W.-K. Lo, D. Xiao, M. M. Oye, A. L. Holmes, *Inorg. Chem.* **2006**, *45*, 4340.

[15] L. Bonomo, M.-L. Lehaire, E. Solari, R. Scopelliti, C. Floriani, *Angew. Chem., Int. Ed. Engl.* **2001**, *40*, 771.

[16] Y. Sarazin, R. H. Howard, D. L. Hughes, S. M. Humphrey, M. Bochmann, *Dalton Trans.* **2006**, 340.

[17] J. M. Veauthier, W.-S. Cho, V. M. Lynch, J. L. Sessler, *Inorg. Chem.* **2004**, *43*, 1220.

[18] G. Givaja, A. J. Blake, C. Wilson, M. Schroder, J. B. Love, *Chem. Commun.* **2005**, 4423.

[19] E. Tomat, L. Cuesta, V. M. Lynch, J. L. Sessler, *Inorg. Chem.* **2007**, *46*, 6224.

[20] G. Givaja, A. J. Blake, C. Wilson, M. Schroder, J. B. Love, *Chem. Commun.* **2003**, 2508.

[21] J. M. Veauthier, E. Tomat, V. M. Lynch, J. L. Sessler, U. Mirsaidov, J. T. Markert, *Inorg. Chem.* **2005**, *44*, 6736.

[22] M. Volpe, S. D. Reid, A. J. Blake, C. Wilson, J. B. Love, *Inorg. Chim. Acta* **2007**, *360*, 273.

[23] G. Givaja, M. Volpe, M. A. Edwards, A. J. Blake, C. Wilson, M. Schröder, J. B. Love, *Angew. Chem., Int. Ed. Engl.* **2007**, *46*, 584.

[24] S. E. McMullen, K. S. Hagen, *Acta Crystallographica Section E* **2002**, *58*, m141; K. Hegetschweiler, O. Maas, A. Zimmer, Rodney J. Geue, Alan M. Sargeson, J. Harmer, A. Schweiger, I. Buder, G. Schwitzgebel, V. Reiland, W. Frank, *Eur. J. Inorg. Chem.* **2003**, *2003*, 1340; U. Thewalt, R. E. Marsh, *Inorg. Chem.* **1972**, *11*, 351.

[25] S. Schmidt, Frank W. Heinemann, A. Grohmann, *Eur. J. Inorg. Chem.* **2000**, *2000*, 1657; D. D. Dexter, C. N. Sutherby, M. W. Grieb, R. C. Beaumont, *Inorg. Chim. Acta* **1984**, *86*, 19.

[26] J. W. Leeland, F. White, J. B. Love, *J. Am. Chem. Soc.* **2011**, Accepted.

[27] A. Shafir, D. Fiedler, J. Arnold, *Journal of the Chemical Society, Dalton Transactions* **2002**, 555; A. Erxleben, D. Schumacher, *Eur. J. Inorg. Chem.* **2001**, *2001*, 3039.

[28] R. Bonnett, M. B. Hursthouse, K. M. A. Malik, B. Mateen, *J. Chem. Soc., Perkin Trans. 2* **1977**, 2072; K. M. Barkigia, L. D. Spaulding, J. Fajer, *Inorg. Chem.* **1983**, *22*, 349.

[29] H. Gritzo, F. Schaper, H.-H. Brintzinger, *Acta Crystallogr., Sect. E.* **2004**, *60*, m1108; D. Seebach, J. Hansen, P. Seiler, J. M. Gromek, *J. Organomet. Chem.* **1985**, *285*, 1.

[30] R. Wyler, J. de Mendoza, J. Rebek, *Angew. Chem., Int. Ed. Engl.* **1993**, *32*, 1699.

[31] H. Khanmohammadi, S. Amani, H. Lang, T. Rüeffer, *Inorg. Chim. Acta* **2007**, *360*, 579; P. J. Bailey, D. Lorono-Gonzalez, S. Parsons, *Chem. Commun.* **2003**, 1426.

[32] C. A. Moreno, D. L. Hughes, M. Bochmann, *Polyhedron* **2007**, *26*, 2523.

[33] Z. Janas, L. B. Jerzykiewicz, P. Sobota, J. Utko, *New J. Chem.* **1999**, *23*, 185.

[34] G. S. Nichol, W. Clegg, *Inorg. Chim. Acta* **2006**, *359*, 3474.

[35] R. Sathyamurthy, J. Brumaghim, D. VanDerveer, *J. Chem. Cryst.* **2007**, *37*, 109.

[36] V. Cumaran Arunasalam, I. Baxter, J. A. Darr, S. R. Drake, M. B. Hursthouse, K. M. Abdul Malik, D. M. P. Mingos, *Polyhedron* **1998**, *17*, 641.

[37] N. Branda, R. Wyler, J. Rebek, Jr., *Science* **1994**, *263*, 1267.
[38] J. K. Vohs, L. E. Downs, J. Stasalovich, M. Barfield, G. H. Robinson, *Journal of Cluster Science* **2002**, *13*, 601; A. Armstrong, T. Chivers, H. M. Tuononen, M. Parvez, *Inorg. Chem.* **2005**, *44*, 5778; Q. Wu, Y. Zhang, S. Wang, *Journal of Cluster Science* **2000**, *11*, 253.
[39] W. Teng, M. Guino-o, J. Hitzbleck, U. Englich, K. Ruhlandt-Senge, *Inorg. Chem.* **2006**, *45*, 9531.
[40] J. Guo, J.-S. Lee, M.-C. Foo, K.-C. Lau, H.-W. Xi, K. H. Lim, C.-W. So, *Organometallics* **2010**, *29*, 939; L. F. Sanchez-Barba, D. L. Hughes, S. M. Humphrey, M. Bochmann, *Organometallics* **2006**, *25*, 1012; P. Ghosh, G. Parkin, *Inorg. Chem.* **1996**, *35*, 1429.
[41] H. Sato, A. Morita, K. Ono, H. Nakano, N. Wakabayashi, A. Yamagishi, *Langmuir* **2003**, *19*, 7120.
[42] H. Yan, M. Wei, J. Ma, F. Li, D. G. Evans, X. Duan, *J. Phys. Chem. A* **2009**, *113*, 6133.
[43] M. Westerhausen, S. Schneiderbauer, Alexander N. Kneifel, Y. Söltl, P. Mayer, H. Nöth, Z. Zhong, Pieter J. Dijkstra, J. Feijen, *Eur. J. Inorg. Chem.* **2003**, *2003*, 3432.
[44] P. Baranek, A. Lichanot, R. Orlando, R. Dovesi, *Chem. Phys. Lett.* **2001**, *340*, 362.
[45] J. A. Rood, B. C. Noll, K. W. Henderson, *Inorg. Chem.* **2007**, *46*, 7259; J. A. Rood, S. E. Hinman, B. C. Noll, K. W. Henderson, *Eur. J. Inorg. Chem.* **2008**, *2008*, 3935.
[46] L. B. Jerzykiewicz, J. Utko, P. Sobota, *Acta Crystallographica Section C* **1997**, *53*, 1393; V. G. Kessler, S. Gohil, M. Kritikos, O. N. Korsak, E. E. Knyazeva, I. F. Moskovskaya, B. V. Romanovsky, *Polyhedron* **2001**, *20*, 915.
[47] S. Heitz, Y. Aksu, C. Merschjann, M. Driess, *Chem. Mater.*, *22*, 1376.
[48] T. A. Hudson, K. J. Berry, B. Moubaraki, K. S. Murray, R. Robson, *Inorg. Chem.* **2006**, *45*, 3549.
[49] N. Lopez, T. E. Vos, A. M. Arif, W. W. Shum, J. C. Noveron, J. S. Miller, *Inorg. Chem.* **2006**, *45*, 4325; A. J. Atkins, A. J. Blake, M. Schroder, *J. Chem. Soc., Chem. Commun.* **1993**, 1662.
[50] S. Brooker, V. McKee, T. Metcalfe, *Inorg. Chim. Acta* **1996**, *246*, 171.
[51] I. Mirebeau, M. Hennion, H. Casalta, H. Andres, H. U. Gudel, A. V. Irodova, A. Caneschi, *Phys. Rev. Lett.* **1999**, *83*, 628.
[52] K. N. Ferreira, T. M. Iverson, K. Maghlaoui, J. Barber, S. Iwata, *Science* **2004**, *303*, 1831.
[53] I. Dance, *Inorg. Chem.* **2011**, *50*, 178; P. Venkateswara Rao, R. H. Holm, *Chem. Rev.* **2003**, *104*, 527.
[54] H. Thoms, M. Epple, H. Viebrock, A. Reller, *J. Mater. Chem.* **1995**, *5*, 589; Z. A. Starikova, A. I. Yanovsky, E. P. Turevskaya, N. Y. Turova, *Polyhedron* **1997**, *16*, 967.
[55] M. M. Sung, C. G. Kim, J. Kim, Y. Kim, *Chem. Mater.* **2002**, *14*, 826.
[56] B. F. Abrahams, T. A. Hudson, R. Robson, *J. Am. Chem. Soc.* **2004**, *126*, 8624.
[57] J. M. Zeng, H. Wang, S. X. Shang, Z. Wang, M. Wang, *J. Cryst. Growth* **1996**, *169*, 474.
[58] D. J. Cram, *Science* **1983**, *219*, 1177.
[59] D. J. Cram, M. E. Tanner, R. Thomas, *Angew. Chem., Int. Ed. Engl.* **1991**, *30*, 1024.
[60] K. A. Udachin, G. D. Enright, E. B. Brouwer, J. A. Ripmeester, *J. Supramol. Chem.* **2001**, *1*, 97.
[61] P. Cintas, *J. Inclusion Phenom. Macro. Chem.* **1994**, *17*, 205; Y.-M. Jeon, J. Kim, D. Whang, K. Kim, *J. Am. Chem. Soc.* **1996**, *118*, 9790.
[62] J. E. Betancourt, C. Subramani, J. L. Serrano-Velez, E. Rosa-Molinar, V. M. Rotello, J. M. Rivera, *Chem. Commun.* **2010**, *46*, 8537; D. A. Uhlenheuer, K. Petkau, L. Brunsveld, *Chem. Soc. Rev.* **2010**, *39*, 2817; L. M. Greig, D. Philp, *Chem. Soc. Rev.* **2001**, *30*, 287.

[63] S. R. Seidel, P. J. Stang, *Acc. Chem. Res.* **2002**, *35*, 972.
[64] C. L. D. Gibb, B. C. Gibb, *J. Am. Chem. Soc.* **2004**, *126*, 11408.
[65] J. Rebek, *Angew. Chem., Int. Ed. Engl.* **2005**, *44*, 2068.
[66] D. R. Gray, C. H. Brubaker, *J. Chem. Soc. D: Chem. Commun.* **1969**, 1239.
[67] H. Kawaguchi, T. Matsuo, *Angew. Chem., Int. Ed. Engl.* **2002**, *41*, 2792.
[68] F. Akagi, T. Matsuo, H. Kawaguchi, *Angew. Chem., Int. Ed. Engl.* **2007**, *46*, 8778.
[69] P. Berno, S. Gambarotta, *Organometallics* **1995**, *14*, 2159.
[70] A. Zanotti-Gerosa, E. Solari, L. Giannini, C. Floriani, A. Chiesi-Villa, C. Rizzoli, *J. Am. Chem. Soc.* **1998**, *120*, 437.

Chapter 5: Conclusions

It is known that secondary coordination sphere interactions can be used to promote and/or manipulate the activation of small molecules bound within a well defined environment.

Following the successes of the commonly bis-metallated pacman-ligand set H_4L, a new series of straightforwardly modified asymmetric Schiff-base pacman macrocycles were designed and synthesised with secondary coordination sphere control in mind.

Desymmetrisation of the H_4L-type ligand was realised by the [1+1] condensation of a diamine containing either a polyether or ether/amine linkage with a *meso*-ethyl substituted dialdehyde in good yield. The asymmetric macrocycles H_2L^P and H_2L^{NMe} contain one neutral and one potentially dianionic binding pocket and were shown to adopt the desired pacman geometry in both the solid and solution state upon complexation and a series of transition metal complexes synthesised and characterised.

Both the L^P and L^{NMe} ligands were observed to be capable of secondary coordination sphere interactions by the inclusion of a H-bonded water molecule within the cleft of certain complexes. Further investigation however is needed to shed light on the products formed by the reactions of vanadium and titanium complexes with reducing agents such as KC_8 which lead to dramatic colour changes. Furthermore, an unforeseen application to the area of supramolecular chemistry was found as the crystallisation of $[Co(OH_2)(OH)(L^P)]\cdot H_2O$ resulting in crenallated cyclic hexamers, which are linked through hydrogen-bonded interactions and which stack to form large columns. This opens the door to the possibility of designing macrocycles and complexes which promote the spontaneous formation of supramolecular pacman structures to tailor potential catalytic activity.

The presence of small quantities of [2+2] condensation products was confirmed by the crystallisation of $[M_2(L^{P(2+2)})]$, (M = Fe, Mn) and $[Co_2(L^{NMe(2+2)})]$, which form helicate structures in the solid state. The cores of these structures are reminiscent of imine-pyrrole chelates published by the Love group which also form helicates upon metallation. Therefore this area could be furthered by the joining of two or more of such chelating units by flexible strapping units. The targeted syntheses of the [2+2]

condensation products as well as the further purification of all asymmetric macrocycles are also potential areas for further work.

Modification of the macrocycles was possible by the alteration of either the arene-backbone-linker or the dialdehyde used in the cyclisation step.

This was demonstrated by the use of a bulky fluorenyl-appended dialdehyde to form the macrocycles H_2L^{FP} and H_2L^{FNMe} and by introduction of a large mesityl group to the amine/ether linker to give H_2L^{NMes}. Complexes of all of these macrocycles were shown to again adopt a pacman geometry upon metallation.

The introduction of the fluorenyl substituent had a large effect on the electrochemistry, as investigated by cyclic voltammetry. The palladium and cobalt complex of $L^{FP/FNMe}$ displayed two ligand-based features not observed in their ethyl counterparts $L^{P/NMe}$.

The synthesis and characterisation of H_2L^{NMes} yielded the possibly of further fine-tuning of complex reactivity by the introduction of alternative groups to the amine linker. Although the synthesis of urea- or H-appended linkers was not realised, there is scope of successful product forming utilising as yet untried methods. The synthesis of a urea macrocycle is desirable with regards to secondary coordination sphere control whereas an NH-appended macrocycle would introduce new routes into various N-substituents.

A final asymmetric macrocycle, $H_2L^{(NH)NMe}$, which employs secondary-amine, rather than ether, linkages was prepared. This macrocycle holds potential for the formation of heterobimetallic complexes due to the similarity to complexes published by both the Cloke and Mountford groups. Though the macrocycle and the pacman-palladium complex $[Pd(L^{(NH)NMe})]$ were synthesised and characterised, the free macrocycle is capable of intramolecular cyclisation to form benzimidazoles and so further work is needed to disfavour this unwanted reactivity. Despite this, the ease of macrocyclic formation combined with the potential for further modification *via* either the alteration of the central-N or the secondary-amine linkers gives scope for further investigation.

Unfortunately the introduction of a second metal centre to any asymmetric macrocycle is yet to be realised, though avenues for this are far from exhausted and thus any further work is needed towards this end, especially with the amine-appended

macrocycles. Furthermore, work is needed with regards to the activity of all complexes towards small molecules.

The symmetric Schiff-base pyrrole macrocycle, H_4L^{Et}, was also synthesised in a straightforward synthesis in good yield and mono- and heterobi-metallic complexes synthesised by reactions with Me_2SnCl_2 and metal silyl-amides. These rare examples of tin(IV)alkyl complexes again adopted pacman geometries. Unfortunately no further reactivity towards small molecules such as H_2, CO or CO_2 was observed, and further investigation is required to exchange the tin for a transition metal.

The synthesis of an unusual, monometallated bowl-shaped Ca complex was also realised. However, with attempts at substitution of a transition metal cation for the calcium cation resulted in a mixture of products including free ligand and homo-bimetallic complexes, this route into monometallic complexs of L^{Et} was abandoned.

The homo-bimetallic magnesium, cobalt and niobium complexes of L^{Et} were also synthesised. The cobalt complexes were shown to have similar reactivity to closely related, previously published versions where as further work is needed to elucidate the structure of the niobium complex due to a lack of crystal structure data. A new potential application of the H_4L-type macrocycles was unearthed with the synthesis of a magnesium cubane encapsulated by two macrocycles. Encapsulations of cubanes of other metals, such as manganese, or by other bridging groups, such as alkoxy groups, again requires further investigation as does the synthesis of such systems by alternative routes.

In summary, the design of six asymmetric macrocycles, H_2L^{P}, H_2L^{NMe}, H_2L^{FP}, H_2L^{FNMe}, H_2L^{NMes} and $H_2L^{(NH)NMe}$ have been realised with all ligands displaying a folded pacman geometry in both the solid and solution state upon metallation and are capable of secondary coordination sphere interactions. Avenues of further investigation include further ligand modification, including the deliberate synthesis of [2+2] condensation products, ligand purification, complex reactivity towards small molecules and formation of supramolecular structures as well as the synthesis of complexes of other metals. A new application of the H_4L ligand set towards encapsulation of cubane structures is also a potential area for future investigations.

Chapter 6: Experimental details and characterising data

6.1 General methods and instrumentation

All manipulations involving transition metals were carried out using standard Schlenk line or drybox techniques under an atmosphere of dinitrogen unless stated otherwise. Dry solvents (THF, toluene, CH_2Cl_2, and hexane) were purified by passage through Vacuum Atmospheres solvent drying towers and stored over activated 4 Å molecular sieves. Deuterated solvents were dried (C_6D_6 and C_5D_5N over potassium, $CDCl_3$ was stirred over activated alumina), trap to trap vacuum distilled, and freeze-pump-thaw degassed three times prior to use.

^1H NMR spectra were recorded at 298 K, unless otherwise stated on Bruker DPX 250, DPX 360, AVA 400, DMX 500, AVA 500, AVA 600 or JEOL ECX 400 spectrometers at operating frequencies of 250.13, 360.13, 399.90, 500.13, 500.12, 599.81 and 391.79 MHz respectively. $^{13}C\{^1H\}$ spectra were recorded on the same spectrometers at operating frequencies of 62.90, 90.55, 100.55, 125.76, 125.76, 150.82 and 98.51 MHz respectively. Two dimensional ^1H-^1H and ^{13}C-^1H correlation experiments were used, when necessary, to confirm ^1H and ^{13}C assignments. All NMR spectra were referenced internally to residual protio solvent (^1H) or solvent ($^{13}C\{^1H\}$) resonances and are reported relative to tetramethylsilane (δ = 0 ppm). Chemical shifts are quoted in δ (ppm) and coupling constants in Hertz.

Mass spectra were recorded by Mr Alan Taylor of the mass spectrometry service of Edinburgh University's Department of Chemistry; Electrospray mass spectra were recorded using a Thermo LCQ instrument, EI mass spectra and high resolution mass spectra were recorded using a Mat 900 XP instrument. Electrospray mass spectra for $[Co(OH_2)(OH)(L^P)]\cdot H_2O$ were acquired by Dr. Logan McKay at the University of Edinburgh on a SolariX FT-ICR mass spectrometer equipped with a 12T superconducting magnet (Bruker Daltronics) and an ESI source (Agilent). Dry gas flow was set at 4.0L/min and nebulising gas set at 2.0L/min. Dry gas temperature was kept at 150 °C. Instrument control was achieved using SolariX control v1.5.0 build 42.8 software (Bruker Daltronics). Time of flight was 1.0 ms and ions were accumulated for 0.06 s and detected between *m/z* = 245.73 and 3000, yielding a 2 Mword time-domain

transient. Each spectrum was the sum of 30 acquisitions. Cryospray mass spectra were collected by Jennifer Mathieson (Cronin group) of the University of Glasgow using a Q-trap, time-of-flight MS (MicrOTOF-Q MS) instrument supplied by Bruker Daltonics Ltd and a cryospray source, also supplied by Bruker Ltd., under the conditions specified below. The detector was a time-of-flight, microchannel plate detector, and all data were processed using the Bruker Daltonics Data Analysis 4.0 software, while simulated isotope patterns were investigated using Bruker Isotope Pattern software. The following parameters were consistent for all CSI-MS scans given below. The calibration solution used was Agilent ES tuning mix solution, Recorder No. G2421A, enabling calibration between *m/z* = -100 and *m/z* = 3000. This solution was diluted 60:1 with 1:1 acetonitrile:methanol mixture. Samples were introduced into the MS *via* direct injection at 180 μL/h having been diluted to 10^{-5} M in acetonitrile. The liquid nitrogen gas used for the cryospray nebuliser gas was set to -40 °C and the drying nitrogen gas set to -20 °C. The ion polarity for all MS scans recorded was positive, with the voltage of the capillary tip set at 4500 V, end plate offset at -500 V, funnel 1RF at 400 Vpp, funnel 2 RF at 400 Vpp, ion energy set to 5.0 eV, the collision energy at 9.0 eV and the collision cell RF at 3500 Vpp. Elemental analyses were carried out at by Mr Stephen Boyer at London Metropolitan University. IR data were collected on a Jasco FT/IR 410 spectrometer.

EPR spectra were obtained on an X-band Bruker ER200D-SCR spectrometer connected to a Datalink 486DX PC with EPR Acquisition System, version 2.42 software. A Bruker ER4111 VT unit was used for temperature control

Cyclic voltammagrams were obtained using an Autolab ECO CHEMIE PGSTAT 12 using tetrabutylammonium tetrafluoroborate electrolyte (0.2 M) and complex (1 mmol) in dry THF under N_2. A platinum working electrode with a silver wire reference electrode and either a platinum wire or platinum foil counter electrode were used for the measurements and values referenced against ferrocene (Fc/Fc^+ $E_{1/2}$ = 0 V).

Single-crystal X-ray diffraction data were collected on one of four machines:

At 100 K using an Oxford Cryosystems low temperature device attached to an Oxford Diffraction SuperNova dual wavelength diffractometer equipped with an Atlas CCD detector and operating mirror monochromated Cu*K*α radiation mode (λ = 1.54184 Å).

At 150 K using an Oxford Cryosystems low temperature device attached to an Oxford Diffraction Xcalibur Eos diffractometer equipped with an Eos detector and operating graphite monochromated Mo*K*α radiation (λ = 0.71073Å).

At 150 K on a Bruker SMART APEX diffractometer equipped with a CCD area detector using graphite monochromated Mo*K*α radiation (λ = 0.71073 Å).

Graphite monochromated Mo*K*α radiation (λ = 0.71073 Å) at 150 K on a Rigaku MM007 diffractometer equipped with a high brilliance Saturn 70 CCD detector.

The structures were solved using the WINGX suite of programs by direct methods and refined using full-matrix least square refinement on $|F^2|$ using SHELXTL-97.[1] Unless otherwise stated, all non-hydrogen atoms were refined with anisotropic displacement parameters while hydrogen atoms were placed at calculated position and included as part of a riding model. When stated, if modelling of disordered solvent was unsuccessful the SQUEEZE routine of PLATON was used.[2]

X-ray crystallography tables and X-ray crystallographic information files can be found in Appendix CD-2 and CD-3 respectively.

Syntheses of $[Ca(THF)_2(N\{SiMe_3\}_2)_2]$,[3] $[Fe(THF)(N\{SiMe_3\}_2)_2]$,[4] $[Zn(N\{SiMe_3\}_2)_2]$,[5] $[Mg(THF)_2(N\{SiMe_3\}_2)_2]$,[6] $[Co(THF)(N\{SiMe_3\}_2)_2]$,[7] $VCl_3(THF)_3$ and $TiCl_3(THF)_3$,[8] 5,5'-diformyldiethyl-2,2'dipyrromethane **1** and 9,9-Bis(5-formylpyrrole-2-yl)fluorene **9**,[9] 2,2'-dichloro-N-methyldiethylamine **4**,[10] tetraethylene glycol bis(o-nitrophenyl ether) $\mathbf{5^P}$,[11] dichloro-N-BOC-diethylamine **17**[12] and amide-diamine $\mathbf{11^{amideNH}}$[13] were carried out as described in the literature. Pyrrole was distilled under reduced pressure prior to use, and all other chemicals were used as purchased.

6.2 Synthetic procedures as described in Chapter 2

6.2.1 N-methyl-2,2'-bis(o-nitrophenoxy)diethylamine, 5^{NMe}

In a modification of the syntheses of related compounds,[11, 14] 2-nitrophenol (16.70 g, 0.12 mol), K_2CO_3 (16.59 g, 0.12 mol) and DMF (60 mL) were stirred at 100 °C for 1 h. To this, amine-dichloride **4** (9.40 g, 60 mmol) in DMF (20 mL) was added and the resulting red mixture stirred at 120 °C overnight. The mixture was poured into water (*ca*. 500 mL), extracted with chloroform (*ca*. 250 mL) and washed repeatedly with water to remove DMF. The crude product was purified by gradient column chromatography on

silica using 1:1 to 5:1 ethylacetate hexanes eluent, giving **5^{NMe}** as a thick, light yellow oil which solidifies upon cooling to -20 °C (10.2 g, 28.2 mmol, 47 %). ^{1}H NMR (500.12 MHz, $CDCl_3$): δ 7.80 (dd, *J* = 8.1, 1.7 Hz, 2H, Ar-H), 7.54–7.47 (m, 2H, Ar-H), 7.11 (dd, *J* = 8.6, 0.6 Hz, 2H, Ar-H), 7.02–6.97 (m, 2H, Ar-H), 4.21 (t, *J* = 5.4 Hz, 4H, OCH_2), 3.00 (t, *J* = 5.4 Hz, 4H, NCH_2), 2.49 (s, 3H, NCH_3); ^{13}C NMR (125.76 MHz, $CDCl_3$): δ 152.39 (s, quaternary, Ar), 139.95 (s, quaternary, Ar), 134.33 (s, CH, Ar-H), 125.65 (s, CH, Ar-H), 120.41 (s, CH, Ar-H), 114.70 (s, CH, Ar-H), 68.69 (s, CH_2, O-CH_2), 56.31 (s, CH_2, N-CH_2), 44.16 (s, CH_3, N-CH_3); HRMS (ESI): *m/z* = 362.36901 $[M^+H]^+$; IR (neat, KBr): ν 1609 (NO_2), 1343 cm^{-1} (NO_2).

6.2.2 N-methyl-2,2'-bis(o-aminophenoxy) diethylamine, 6^{NMe}

5^{NMe} (1.52 g, 4.2 mmol) was treated with EtOH (50 mL), THF (50 mL) and 10 % Pd/C (0.1 g) and stirred at room temperature overnight under a H_2 atmosphere. The catalyst was removed by filtration and solvents removed by rotary evaporator. The product was then dissolved in CH_2Cl_2 (50 mL) extracted into 0.5% HCl (50 mL), then extracted into fresh CH_2Cl_2 (50 mL) by addition of a saturated aqueous $NaHCO_3$ solution until the aqueous layer was basic. The CH_2Cl_2 layer was separated, dried over $MgSO_4$ and the solvent removed by rotary evaporation to give **6^{NMe}** as a yellow oil (1.20 g, 3.98 mmol, 95 %). ^{1}H NMR (500.12 MHz, $CDCl_3$): δ 6.81 (m, 4H, Ar-H), 6.71 (m, 4H, Ar-H), 4.13 (t, 4H, *J* = 5.6 Hz, O/N-CH_2), 3.90 (br, s, 4H, NH_2), 2.95 (t, 4H, *J* = 5.6Hz, O/N-CH_2), 2.46 (s, 3H, NCH_3); ^{13}C{^{1}H} NMR (125.76 MHz, $CDCl_3$): δ 146.5 (s, quaternary), 137.1 (s, quaternary), 12.18 (s, CH, Ar-CH), 118.4 (s, CH, Ar-CH), 115.3 (s, CH, Ar-CH), 112.8 (s, CH, Ar-CH), 67.0 (s, CH_2, O/N-CH_2), 57.0 (s, CH_2, O/N-CH_2), 43.2 (s, CH_3, N-CH_3); HRMS (ESI): *m/z* = 302.182766 $[M^+H]^+$; IR (KBr): ν 3444 (N-H), 3365 cm^{-1} (N-H).

6.2.3 Tetraethylene glycol bis(o-aminophenyl ether), 6^{P}

This compound was synthesised by a modification of literature proceedure.[15] The dinitro compound **5^{P}** (1.75 g, 4.01 mmol) was treated with EtOH (50 mL) and THF (50 mL) with 10 % Pd/C (0.12 g) and stirred at room temperature overnight under an H_2 atmosphere. Work-up as per **6^{NMe}** gave **6^{P}** as a yellow oil (1.45 g, 3.85 mmol, 96 %). NMR analysis agrees with that previously published.[15]

6.2.4 Synthesis of H_2L^{NMe}

To a solution of dialdehyde **1** (1.498 g, 5.8 mmol) and diamine **6^{NMe}** (1.75 g, 5.8 mmol), 2.1 eq of $BF_3{\cdot}OEt_2$ (1.6 mL, 12.2 mmol) was added dropwise. The resulting

mixture was stirred at room temperature for 4 h, during which a yellow precipitate was obtained. The solvent was decanted and the solid washed with EtOH (3 × 20 mL). The BF_3 salt was dissolved in CH_2Cl_2 (*ca*. 50 mL) and treated with 7 M NH_3 in MeOH (2.1 mL) causing BF_3NH_3 to precipitate. The mixture was filtered and the filtrate evaporated *in-vacuo* to give crude H_2L^{NMe} as a yellow powder. This was dissolved in dry THF (50 mL) and filtered to remove further BF_3NH_3 and the filtrate evaporated giving H_2L^{NMe} as a yellow solid (1.73 g, 3.30 mmol, 57 %). ^{1}H NMR (250.13 MHz, $CDCl_3$): δ 8.69 (br, s, 2H, pyrrole NH), 8.03 (s, 2H, imine), 7.00 (m, 2H, Ar-H), 6.88 (m, 4H, Ar-H), 6.82 (d, 2H, *J* = 7.9 Hz, Ar-H), 6.51 (d, 2H, *J* = 3.5 Hz, pyrrole), 6.19 (d, *J* = 3.5 Hz, pyrrole), 4.00 (m, 4H, O/N-CH_2), 2.86 (m, 4H, O/N-CH_2), 2.37 (s, 3H, N-CH_3), 1.99 (q, 4H, *J* = 7.4 Hz, Et-CH_2), 0.69 (t, 6H, *J* = 7.5 Hz, Et-CH_3); ^{13}C{^{1}H} NMR (62.90 MHz, $CDCl_3$): δ 150.5 (s, CH, Ar-H), 149.7 (s, quaternary), 141.6 (s, quaternary), 140.7 (s, quaternary), 129.7 (s, quaternary), 124.6 (s, CH, Ar-H), 120.7 (s, CH, Ar-H), 120.0 (s, CH, Ar-H), 115.5 (s, CH, pyrrole), 112.6 (s, CH, Ar-H), 108.2 (s, CH, pyrrole), 67.3 (s, CH_2, O/N-CH_2), 56.1 (s, CH_2, O/N-CH_2), 42.9 (s, quaternary), 41.8 (s, CH_3, N-CH_3), 27.3 (s, CH_2, Et-CH_2), 7.0 (s, CH_3, Et-CH_3); MS(EI): *m/z* = 523.2 (M^+, 10 %), 440.2 ([M^+–$(CH_2)_4$NMe]$^+$, 100 %), 411.1 ([M^+–$(CH_2)_4$NMe–Et]$^+$, 100 %); Analysis. Found: C, 73.26; H, 7.08; N, 13.41; $C_{32}H_{37}N_5O_2$ requires: C, 73.39; H, 7.12; N, 13.37 %; IR (nujol, KBr): ν 3187 (N-H), 1618 (C=N), 1498 cm^{-1} (C=C).

6.2.5 Synthesis of H_2L^P

To a solution of dialdehyde **1** (1.291 g, 5.0 mmol) and diamine $\mathbf{6^P}$ (1.88 g, 5.0 mmol) in EtOH (150 mL), $BF_3{\cdot}OEt_2$ (1.4 mL, 11 mmol) was added dropwise and then allowed to stir at room temperature for 2 h, during which a red oil formed. The solvent was decanted and the oil washed with EtOH (2 × 20 mL). The oil was dissolved in CH_2Cl_2 (70 mL) and treated with 7 M NH_3 in MeOH (1 mL) causing BH_3NH_3 to precipitate. The solids were filtered and the filtrate evaporated to dryness to yield a fluffy orange solid. Dry THF (20 mL) was added, the mixture filtered from any remaining BF_3NH_3 and the filtrate evaporated giving H_2L^P as a yellow orange solid (1.21 g, 2.02 mmol, 40 %). ^{1}H NMR (399.90 MHz, C_6D_6): δ 9.44 (s, 2H, pyrrole NH), 8.24 (s, 2H, imine), 7.03 (dd, *J* = 7.6, 1.6 Hz, 2H, Ar-H), 6.96 (td, *J* = 7.8, 1.7 Hz, 2H, Ar-H), 6.86 (td, *J* = 7.5, 1.3 Hz, 2H, Ar-H), 6.68 (dd, *J* = 8.0, 1.1 Hz, 2H, Ar-H), 6.55 (d, *J* = 3.6 Hz, 2H, pyrrole), 6.05 (d, *J* = 3.7 Hz, 2H, pyrrole), 3.79–3.74 (m, 4H, OCH_2), 3.62–3.57 (m, 4H, OCH_2), 3.53–3.46 (m, 8H, OCH_2), 1.67 (q, *J* = 7.3 Hz, 4H, Et-CH_2), 0.59 (t, *J* = 7.3

Hz, 6H, Et-CH_3); $^{13}C\{^1H\}$ NMR (100.55 MHz, C_6D_6): δ 152.3 (s, CH), 151.0 (s, CH), 142.9 (s, quaternary), 141.8 (s, quaternary), 131.5 (s, quaternary), 125.7 (s, CH, Ar-H), 121.9 (s, CH, Ar-H), 121.8 (s, CH, Ar-H), 116.2 (s, quaternary), 114.3 (s, CH, pyrrole), 108.0 (s, CH, pyrrole), 71.5 (s, CH_2, OCH_2), 71.0 (s, CH_2, OCH_2), 69.8 (s, CH_2, OCH_2), 69.7 (s, CH_2, OCH_2), 44.3 (s, quaternary), 29.1 (s, CH_2, Et-CH_2), 8.5 (s, CH_3, Et-CH_3); MS(EI): *m/z* = 598.3 (M^+, 12 %), 569.2 ([M^+–Et]$^+$, 100 %); Analysis. Found: C, 70.08; H, 6.94; N, 9.20. $C_{35}H_{42}N_4O_5$ requires: C, 70.21; H, 7.07; N, 9.36 %; IR (nujol, KBr): ν 3244 (N-H), 1617 (C=N), 1496 cm^{-1} (C=C).

6.2.6 Synthesis of [Pd(L^{NMe})]

A mixture of H_2L^{NMe} (0.500 g, 0.954 mmol) and $Pd(OAc)_2$ (0.214 g, 0.954 mmol) in toluene (*ca*. 30 mL) was stirred for 30 mins. The resulting red/brown mixture was treated with NEt_3 (0.30 mL). The reaction was stirred overnight, filtered and solvents removed under vacuum. The product was extracted into hexane (3 × 20 mL) to give pure [Pd(L^{NMe})] as a yellow solid (0.44 g, 0.70 mmol, 73 %). Crystals suitable for X-ray crystallography were grown from a saturated hexane solution. ^1H NMR (391.79 MHz, $CDCl_3$): δ 7.54 (s, 2H, imine), 6.92 (d, 2H, *J* = 3.9 Hz, pyrrole), 6.87 (m, 2H, Ar-H), 6.75 (d, *J* = 7.7 Hz, Ar-H), 6.47 (m, 4H, Ar-H), 6.20 (d, *J* = 3.6 Hz, pyrrole), 4.06 (m, 2H, O/N-CH_2), 3.60 (m, 2H, O/N-CH_2), 3.02 (m, 2H, O/N-CH_2), 2.85 (m, 2H, O/N-CH_2), 2.43 (s, 3H, N-CH_3), 2.16 (q, 2H, *J* = 7.4 Hz, Et-CH_2), 2.07 (q, 2H, *J* = 7.2 Hz, Et-CH_2), 0.56 (t, 3H, *J* = 7.1 Hz, Et-CH_2), 0.53 (t, 3H, *J* = 7.5 Hz, Et-CH_2); $^{13}C\{^1H\}$ NMR (98.51 MHz): δ 160.0 (s, CH, imine), 151.2 (s, quaternary), 148.6 (s, quaternary), 138.8 (s, quaternary), 136.5 (s, quaternary), 125.9 (s, CH, Ar-H), 124.1 (s, CH, Ar-H), 120.5 (s, CH, Ar-H), 118.7 (s, CH, Ar-H), 112.7 (s, CH, pyrrole), 107.4 (s, CH, pyrrole), 68.0 (s, CH_2, O/N-CH_2), 55.2 (s, CH_2, O/N-CH_2), 53.7 (s, quaternary), 46.5 (s, CH_2, Et-CH_2), 38.7 (s, CH_3, N-CH_3), 37.0 (s, CH_2, Et-CH_2), 10.0 (s, CH_3, Et-CH_3), 9.7 (s, CH_3, Et-CH_3); MS(EI): *m/z* = 627.1 (M^+, 9 %), 598.0 ([M^+–Et]$^+$, 100 %). Analysis. Found: C, 61.20; H, 5.66; N, 11.07. $C_{32}H_{35}N_5O_2Pd$ requires: C, 61.19; H, 5.62; N, 11.15 %; IR (nujol, KBr): ν 1562 (C=N), 1496 cm^{-1} (C=C)

6.2.7 Synthesis of [Pd(L^P)]

A mixture of H_2L^P (0.100 g, 0.167 mmol) and $Pd(OAc)_2$ (37.5 mg, 0.167 mmol) in toluene (*ca*. 10 mL) was stirred for 30 mins. The resulting red/brown mixture was treated with NEt_3 (56 µl). The reaction was stirred overnight, filtered and solvents removed under vacuum. The product was extracted into hexane (3 × 10 mL) to give pure

[Pd(L^P)] as a yellow solid (79 mg, 0.112 mmol, 67 %). ^{1}H NMR (391.79 MHz, $CDCl_3$): δ 7.55 (s, 2H, imine), 6.83 (d, 2H, *J* = 4.0 Hz, pyrrole), 6.78 (m, 4H, Ar-H), 6.71 (m, 2H, Ar-H), 6.38 (m, 2H, Ar-H), 6.34 (m, 2H, Ar-H), 6.11 (d, 2H, *J* = 4.0 Hz, pyrrole), 4.05 (m, 2H, OCH_2), 3.83–3.32 (m, 14H, OCH_2), 2.05 (q, 2H, *J* = 7.2 Hz, Et-CH_2), 2.01 (q, 2H, *J* = 7.3 Hz, Et-CH_2), 0.45 (t, 3H, *J* = 7.1 Hz, Et-CH_3), 0.42 (t, 3H, *J* = 7.3 Hz, Et-CH_3); ^{13}C{^{1}H} NMR (98.51 MHz, $CDCl_3$): δ 160.0 (s, CH, imine), 151.2 (s, quaternary), 148.5 (s, quaternary), 138.0 (s, quaternary), 136.7 (s, quaternary), 125.9 (s, CH, Ar-H), 124.3 (s, CH, Ar-H), 120.4 (s, CH, Ar-H), 118.7 (s, CH, Ar-H), 111.1 (s, CH, pyrrole), 107.3 (s, CH, pyrrole), 71.0 (s, CH_2, OCH_2), 70.5 (s, CH_2, OCH_2), 69.6 (s, CH_2, OCH_2), 68.2 (s, CH_2, OCH_2), 53.8 (s, quaternary), 38.3 (s, CH_2, Et-CH_2), 37.6 (s, CH_2, Et-CH_2), 9.9 (s, CH_3, Et-CH_3); MS(EI): *m/z* = 702.1 (M^+, 4 %), 673.0 ([M^+–Et]$^+$, 100 %); Analysis. Found: C, 59.94; H, 5.69; N, 8.00; $C_{35}H_{40}N_4O_5Pd$ requires: C, 59.79; H, 5.73; N, 7.97 %; IR (nujol, KBr): ν 1557 (C=N), 1496 cm^{-1} (C=C).

6.2.8 Synthesis of [$K_2(L^{NMe})$]

A mixture of H_2L^{NMe} (0.21g, 0.40 mmol) and excess KH (48 mg, 1.2 mmol) was treated with THF (8 mL). Gas evolved immediately, and the mixture stirred for 3 h at room temperature giving a red solution from which [$K_2(L^{NMe})$] as an orange solid (0.23 g, 0.38 mmol, 96 %) precipitated on addition of hexane (15 mL). ^{1}H NMR (399.90 MHz, C_6D_6/H_8-THF): δ 8.31 (s, 2H, imine), 7.29–7.23 (m, 2H, Ar-H), 7.20–7.04 (m, 6H, Ar-H), 6.81 (d, *J* = 3.0 Hz, 2H, pyrrole), 6.40 (d, *J* = 3.1 Hz, 2H, pyrrole), 4.35–4.27 (m, 4H, O/N-CH_2), 3.03 (s, 4H, O/N-CH_2), 2.59 (s, 3H, N-CH_3), 1.10 (t, *J* = 7.3 Hz, 3H, Et-CH_3) [Et-CH_2 resonance masked by suppressed THF]; ^{13}C{^{1}H} NMR (100.55 MHz, C_6D_6/H_8-THF): δ 159.68 (s, quaternary), 154.71 (s, quaternary), 152.35 (s, CH, imine), 146.33 (s, quaternary), 138.30 (s, quaternary), 122.34 (s, CH, Ar-H), 121.98 (s, CH, Ar-H), 119.21 (s, CH, Ar-H), 118.55 (s, CH, Ar-H), 113.76 (s, CH, pyrrole), 108.23 (s, CH, pyrrole), 65.82 (s, CH_2, O/N-CH_2), 56.95 (s, CH_2, O/N-CH_2), 47.69 (s, quaternary), 45.05 (s, CH_3, NCH_3), 30.98 (s, CH_2, Et-CH_2), 9.65 (s, CH_3, Et-CH_3); MS(EI): *m/z* = 599.3 ($M^{+\cdot}$, 4%), 570 ([M^+–Et]$^+$, 50 %), 561.2 ([M^+–K]$^+$, 15 %), 532.3 ([M^+–K–Et]$^+$, 100%); Analysis. Found: C, 63.97; H, 6.01; N, 11.59; $C_{32}H_{35}K_2N_5O_2$ requires: C, 64.07; H, 5.88; N, 11.68 %; IR (nujol, KBr): ν 1565 (C=N), 1499 cm^{-1} (C=C).

6.2.9 Synthesis of [$K_2(L^P)$]

A mixture of H_2L^P (0.15g, 0.25 mmol) and excess KH (26 mg, 0.66 mol) was treated with THF (5 mL). Gas evolved immediately, and the mixture stirred for 3 h at

room temperature giving a red solution from which [$K_2(L^P)$] as an orange solid (0.16 g, 0.24 mmol, 95 %) precipitated on addition of hexane (10 mL). Crystals suitable for X-ray crystallography of [$K_2(L^P)$] were grown by hexane diffusion in to a THF solution of [$K_2(L^P)$]. ^{1}H NMR (399.90 MHz, C_6D_6/H_8-THF): δ 8.35 (s, 2H, imine), 7.39 (d, *J* = 7.4 Hz, 2H, Ar-H), 7.17–7.01 (m, 6H, Ar-H), 6.83 (d, *J* = 3.1 Hz, 2H, pyrrole), 6.39 (d, *J* = 3.1 Hz, 2H, pyrrole), 4.31 (s, 4H, OCH_2), 2.52 (q, *J* = 7.2 Hz, 4H, Et-CH_2), 1.06 (t, *J* = 7.3 Hz, 6H, Et-CH_3) [NB Other OCH_2 resonances masked by suppressed THF]; $^{13}C\{^1H\}$ NMR (100.55 MHz, C_6D_6/H_8-THF): δ 161.67 (s, quaternary), 152.92 (s, quaternary), 152.06 (s, CH, imine), 145.21 (s, quaternary), 138.98 (s, quaternary), 122.34 (s, CH, Ar-H), 121.77 (s, CH, Ar-H), 120.30 (s, CH, Ar-H), 116.94 (s, CH, Ar-H), 113.01 (s, CH, pyrrole), 108.19 (s, CH, pyrrole), 72.05 (s, CH_2, OCH_2), 66.53 (s, CH_2, OCH_2), 65.83 (s, CH_2, OCH_2), 65.75 (s, CH_2, OCH_2), 48.40 (s, quaternary), 29.05 (s, CH_2, Et-CH_2), 9.14 (s, CH_3, Et-CH_3); MS(EI): *m/z* = 674.3 (M^+, 75 %), 646.1 ([M^+–Et]$^+$, 100 %, 607.2 ([M^+–K–Et]$^+$, 78 %); Analysis. Found:. C, 62.18; H, 5.87; N, 8.18; $C_{35}H_{40}K_2N_4O_5$ requires: C, 62.29; H, 5.97; N, 8.30 %; IR (nujol, KBr): ν 1557 (C=N), 1502 cm^{-1} (C=C).

6.2.10 Synthesis of [Co(L^P)]

A mixture of H_2L^P (0.150 g, 0.25 mmol) and excess KH (30 mg, 0.75 mmol) was treated with THF (15 mL). Gas evolved immediately, and, once effervescence had ceased, the mixture was filtered onto a stirring suspension of $CoCl_2$ (33 mg, 0.25 mmol) in THF (10 mL) at -80 °C. A rapid colour change from red to very dark red was observed and the reaction warmed to room temperature and left to stir overnight, after which it was filtered and solvents removed under vacuum giving [Co(L^P)] as a red solid (0.112g, 0.171 mmol, 68%). Crystals suitable for X-ray crystallography of [Co(L^P)] were grown by hexane diffusion in to a THF solution of [Co(L^P)]. ^{1}H NMR (399.90 MHz, C_6D_6): δ 68.76 (s, 2H), 41.32 (s, 2H), 10.87 (s, 2H), 3.60 (s, 2H), -0.20 (s, 2H), -0.49 (s, 2H), -0.98 (s, 2H), -2.64 (s, 2H), -3.41 (s, 2H), -5.71 (s, 2H), -6.26 (s, 2H), -11.63 (s, 2H), -12.44 (s, 2H), -18.87 (s, 2H), -20.44 (s, 2H), -25.74 (s, 2H), -28.00 (s, 3H), -29.42 (s, 3H), -39.68 (s, 2H); MS(EI): *m/z* = 655.1 (M^+, 56 %), 627.1 ([M^+–Et]$^+$, 100 %); Analysis. Found: C, 63.95; H, 6.08; N, 8.49; $C_{35}H_{40}N_4O_5Co$ requires: C, 64.12; H, 6.15; N, 8.55 %; IR (nujol, KBr): ν 1562 (C=N), 1496 cm^{-1} (C=C).

6.2.11 Synthesis of $[Co(OH_2)(OH)(L^P)]\cdot H_2O$

A solution of $[Co(L^P)]$ (0.102 g, 0.156 mmol) in air saturated benzene (*ca.* 5 mL) was left to stand exposed to air for one week, resulting in the formation of $[Co(OH_2)(OH)(L^P)]\cdot H_2O$ as a brown precipitate (80 %, 88 mg, 0.125 mmol). Red crystals of $[Co(OH_2)(OH)(L^P)]\cdot H_2O$ were grown from slow diffusion of hexane into an air-saturated benzene solution of $[Co(L^P)]$. ^{1}H NMR (500.12 MHz, C_6D_6): δ 7.50 (s, 2H, imine), 7.47 (dd, *J* = 7.6, 1.4 Hz, 3H, Ar-H), 7.29 (d, *J* = 3.9 Hz, 2H, pyrrole), 6.82 (td, *J* = 8.0, 1.6 Hz, 2H, Ar-H), 6.57 (d, *J* = 3.9 Hz, 2H, pyrrole), 6.53 (td, *J* = 7.6, 0.8 Hz, 2H, Ar-H), 6.11 (d, *J* = 7.4 Hz, 2H, Ar-H), 3.38–3.26 (m, 6H, OCH_2), 3.17–3.11 (m, 2H, OCH_2), 3.01–2.91 (m, 4H, OCH_2), 2.89–2.83 (m, 4H, OCH_2), 2.38 (q, *J* = 7.3 Hz, 3H, Et-CH_2), 2.35 (q, *J* = 7.3 Hz, 4H, Et-CH_2), 0.71 (t, *J* = 7.0 Hz, 3H, Et-CH_3), 0.68 (t, *J* = 7.1 Hz, 3H, Et-CH_3); $^{13}C\{^1H\}$ NMR (125.76 MHz, C_6D_6): δ 162.53 (s, CH, imine), 152.41 (s, quaternary), 150.90 (s, quaternary), 140.25 (s, quaternary), 139.11 (s, quaternary), 128.23 (s, CH, Ar), 125.41 (s, CH, Ar), 121.62 (s, CH, Ar), 120.36 (s, CH, pyrrole), 110.82 (s, CH, Ar), 109.39 (s, CH, pyrrole), 70.06 (s,CH_2, OCH_2), 70.04 (s, CH_2,OCH_2), 68.66 (s, CH_2, OCH_2), 67.95 (s, CH_2, OCH_2), 51.08 (s, quaternary), 38.79 (s, CH_2, Et-CH_2), 38.35 (s, CH_2, Et-CH_2), 10.30 (s, CH_3, Et-CH_3), 9.98 (s, CH_3, Et-CH_3); Analysis. Found: C, 59.27; H, 6.32; N, 7.96; $C_{35}H_{45}N_4O_8Co$ requires: C, 59.32; H, 6.40; N, 7.91%; MS(ESI): *m/z* = 655 ($[Co(L^P)]^+$, 100 %), 625 ($[[Co(L^P)]–2Me]^+$, 75 %), 687 ($[[Co(L^P)]+OMe]^+$, 6 %), 679($[[Co(L^P)]+Na]^+$, 10 %), 695 ($[[Co(L^P)]+K]^+$, 10 %), 1310 ($[2 \times [Co(L^P)]]^+$, 5 %), 1355 ($[2 \times [Co(L^P)]+2Na]^+$, 5 %); MS(cyrospray in PhMe/CH_3CN): *m/z* = 2018.7 $[(C_{35}H_{40}CoN_4O_5)_3(OH)_2(H_2O)]$; IR (nujol, KBr): ν 3468 (O-H), 3413 (O-H), 1571 (C=N), 1507 cm^{-1} (C=C).

6.2.12 Synthesis of $[Co(OH_2)(I)(L^P)]$

$[Co(L^P)]$ (0.11g, 0.17 mmol) and $LiI\cdot 3H_2O$ (32 mg, 0.17 mmol) were dissolved in THF (10 mL) and left to stand overnight resulting in precipitation of $[Co(OH_2)(I)(L^P)]$ as a deep red solid which was isolated by filtration (95 mg, 0.119 mmol, 70 %). X-ray quality crystals were grown from slow hexane diffusion into the THF solution. ^{1}H NMR (399.90 MHz, C_6D_6/H_8-THF): δ 8.04 (s, 2H, imine), 7.90–7.83 (m, 2H, Ar-H), 7.63 (d, *J* = 4.3 Hz, 2H, pyrrole), 7.39–7.33 (m, 2H, Ar-H), 6.96 (d, *J* = 7.7 Hz, 2H, Ar-H), 6.75 (d, *J* = 4.2 Hz, 2H, pyrrole), 6.61–6.54 (m, 2H, Ar-H), 2.71–2.62 (m, 2H, Et-CH_2), 2.60–2.50 (m, 2H, Et-CH_2), 1.15 (q, *J* = 7.1 Hz, 3H, Et-CH_3), 1.05 (q, *J* = 6.8 Hz, 3H, Et-CH_3) [due to solvent suppression experiment, the 4 × OCH_2 cannot be seem as it is

underneath the THF resonance at *ca*. 3.5ppm]; $^{13}C\{^{1}H\}$ NMR (125.76 MHz, $CDCl_3$): δ 164.99 (s, CH, imine), 154.15 (s, quaternary), 151.43 (s, quaternary), 140.03 (s, quaternary), 139.81 (s, quaternary), 127.66 (s, CH, Ar-H), 126.33 (s, CH, Ar-H), 122.26 (s, CH, Ar-H), 121.55 (s, CH, Ar-H), 112.00 (s, CH, pyrrole), 111.63 (s, CH, pyrrole), 70.42 (s, CH_2, OCH_2), 70.05 (s, CH_2, OCH_2), 69.16 (s, CH_2, OCH_2), 68.50 (s, CH_2, OCH_2), 51.17 (s, quaternary), 38.88 (s, CH_2, Et-CH_2), 37.40 (s, CH_2, Et-CH_2), 10.50 (s, CH_3, Et-CH_3), 10.35 (s, CH_3, Et-CH_3); MS(EI): *m/z* = 781.1 ($[M^+–H_2O]^+$, 7 %), 752.0 ($[M^+–H_2O–Et]^+$, 17 %), 655.1 ($[M^+–H_2O–I]^+$, 27 %), 627.1 ($[M^+–H_2O–I–Et]^+$, 100 %); Analysis. Found: C, 52.43; H, 5.20; N, 6.92; $C_{35}H_{42}CoIN_4O_6$ requires: C, 52.51; H, 5.29; N, 7.00 %; IR (KBr): ν 3424 (br, O-H), 3242 (sh, O-H), 1569 (C=N), 1500 cm^{-1} (C=C).

6.2.13 Synthesis of [Co(L^{NMe})]

A mixture of H_2L^{NMe} (0.231 g, 0.441 mmol) and excess KH (53 mg, 1.32 mmol) was treated with THF (15 mL). Gas evolved immediately, and, once effervescence had ceased, the mixture was filtered onto a stirring suspension of $CoCl_2$ (57 mg, 0.44 mmol) in THF (10 mL) at -80 °C. A rapid colour change from red to very dark red was observed and the reaction warmed to room temperature and left to stir overnight after which it was filtered and solvents removed under vacuum giving [Co(L^{NMe})] as a red solid (0.153g, 0.265 mmol, 60%). Crystals of [Co_2($L^{NMe(2+2)}$)] were grown by hexane diffusion into a THF solution of [Co(L^{NMe})]. ^{1}H NMR (399.90 MHz, C_6D_6): δ 72.01 (s, 2H), 44.51 (s, 2H), 24.34 (s, 2H), -3.77 (s, 2H), -4.74 (s, 3H), -10.07 (s, 2H), -11.35 (s, 2H), -13.40 (s, 3H), -20.44 (s, 2H), -21.78 (s, 5H, (3H + 2H), -24.23 (s, 2H), -28.29 – -34.00 (m, 6H (3 × 2H)), -43.33 (s, 2H); MS(EI): *m/z* = 580.2 (M^+, 40 %), 551.2 ($[M^+–Et]^+$, 100%); Analysis. Found: C, 66.13; H, 5.98; N, 12.10; $C_{32}H_{35}CoN_5O_2$ requires: C, 66.20; H, 6.08; N, 12.06 %; IR (nujol, KBr): ν 1565 (C=N), 1500 cm^{-1} (C=C).

6.2.14 Synthesis of [Co(OH_2)(Cl)(L^{NMe})]

A solution of [Co(L^{NMe})] (50 mg, 0.086 mmol) and KCl (8 mg, 0.11 mmol) in air saturated THF (2 mL) was left to stand for 1 week resulting in crystals [Co(OH_2)(Cl)(L^{NMe})].

6.2.15 Potential Synthesis of [Co(OH_2)(OH)(L^{NMe})]

A solution of [Co(L^{NMe})] (0.250 g, 0.431 mmol) in air saturated THF (10 mL) was left exposed to air for one week resulting in a deep red solution. Removal of solvent gave [Co(OH_2)(OH)(L^{NMe})] as a red solid. The ^{1}H NMR spectrum (C_6D_6) shows

resonances in the diamagnetic region but isolation of a pure single compound was not possible. IR (nujol, KBr): ν 3403 (O-H), 3230 (O-H), 1562 (C=N), 1498 cm^{-1} (C=C).

6.2.16 Synthesis of [(VCl)(L^P)]

A mixture of H_2L^P (0.40 g, 0.67 mmol) and excess KH (80 mg, 2 mmol) was treated with THF (30 mL). Gas evolved immediately, and, once effervescence had ceased, the mixture was filtered onto a stirring suspension of $VCl_3{\cdot}(THF)_3$ (0.251g, 0.67 mmol) in THF (10 mL) at -80 °C. A rapid colour change from red to very dark red was observed and the reaction was warmed to room temperature and left to stir for 2 h. The mixture was filtered through Celite, the Celite washed with THF (3 × 5 mL) and solvents removed under vacuum giving [(VCl)(L^P)] as a red solid (0.28 g, 0.41 mmol, 61 %). Crystals of [(VCl)(OH_2)(L^P)] suitable for X-ray crystallography were grown by hexane diffusion into a THF solution of [(VCl)(L^P)]. MS(EI): *m/z* = 683.5 (M^+, 4 %, 634.1 ([M^+–Cl–Me]$^+$, 100 %); Analysis. Found: C, 61.39; H, 5.99; N, 8.15; $C_{35}H_{40}ClN_4O_5V$ requires: C, 61.54; H, 5.90; N, 8.20 %; IR (nujol, KBr): ν 1566 (C=N), 1507 cm^{-1} (C=C).

6.2.17 Synthesis of [(VCl)(L^{NMe})]

A mixture of H_2L^{NMe} (0.497 g, 0.949 mmol) and excess KH (0.114 g, 2.85 mmol) was treated with THF (30 mL). Gas evolved immediately, and, once effervescence had ceased, the mixture was filtered onto a stirring suspension of $VCl_3{\cdot}(THF)_3$ (0.355 g, 0.949 mmol) in THF (10 mL) at -80 °C. A rapid colour change from red to deep red was observed and the reaction was warmed to room temperature and left to stir for 2 h. The mixture was filtered through Celite, the Celite washed with THF (3 × 5 mL) and solvents removed under vacuum giving [(VCl)(L^{NMe})] as a red solid (0.31 g, 0.51 mmol, 54 %). MS(EI): *m/z* = 607.1 (M^+, 5 %), 588.2 ([M^+–Cl+O]$^+$, 100 %), 572.2 ([M^+–Cl]$^+$, 85 %); Analysis. Found: C, 63.30; H, 5.96; N, 11.42; $C_{32}H_{35}ClN_5O_2V$ requires: C, 63.21; H, 5.80; N, 11.52 %; IR (nujol, KBr): ν 1564 (C=N), 1500 cm^{-1} (C=C).

6.2.18 Synthesis of [(TiCl)(L^P)]

A mixture of H_2L^P (0.438 g, 0.732 mmol) and excess KH (90 mg, 2.2 mmol) was treated with THF (30 mL). Gas evolved immediately, and, once effervescence had ceased, the mixture was filtered onto a stirring suspension of $TiCl_3{\cdot}(THF)_3$ (0.271 g, 0.732 mmol) in THF (10 mL) at -80 °C. A rapid colour change from red to dark brown was observed and the reaction was warmed to room temperature and left to stir for 2 h.

The mixture was filtered through Celite, the Celite was washed with THF (3 × 5 mL) and solvents removed under vacuum giving [(TiCl)(L^P)] as a brown solid (0.22 g, 0.30 mmol, 45 %). Crystals of [(TCl)(L^P)] suitable for X-ray crystallography were grown by hexane diffusion into a THF solution of [(TiCl)(L^P)]. MS(EI): *m/z* = 679.2 (M^+, 35 %), 631.2 ([M^+–Cl–Me]$^+$, 100 %), 616.2 ([M^+–Et–Cl]$^+$, 40 %); Analysis. Found: C, 61.70; H, 6.05; N, 8.16; $C_{35}H_{40}ClN_4O_5Ti$ requires: C, 61.82; H, 5.93; N, 8.24 %; IR (nujol, KBr): ν 1579 (C=N), 1520 cm^{-1} (C=C).

6.2.19 Synthesis of [(TiCl)(L^{NMe})]

A mixture of H_2L^{NMe} (0.499 g, 0.952 mmol) and excess KH (92 mg, 2.3 mmol) was treated with THF (30 mL). Gas evolved immediately, and, once effervescence had ceased, the mixture was filtered onto a stirring suspension of $TiCl_3$·$(THF)_3$ (0.353 g, 0.952 mmol) in THF (10 mL) at -80 °C. A rapid colour change from red to dark brown was observed and the reaction was warmed to room temperature and left to stir for 2 h. The mixture was filtered through Celite, the Celite was washed with THF (3 × 5 mL) and solvents removed under vacuum giving [(TiCl)(L^{NMe})] as a brown solid (0.29 g, 0.48 mmol, 50 %). MS(EI): *m/z* = 604.3 ($M^{+\cdot}$, 15 %), 585.2 ([M^+–2Me]$^+$, 50 %), 556.2 ([M^+–Me–Cl]$^+$, 100%); Analysis. Found: C, 63.48; H, 5.78; N, 11.52; $C_{32}H_{35}ClN_5O_2Ti$ requires: C, 63.53; H, 5.83; N, 11.58 %; IR (nujol, KBr): ν 1574 (C=N), 1500 cm^{-1} (C=C).

6.2.20 Reaction of [(VCl)(L^P)] with KC_8 or Na(Hg)

A solution of [(VCl)(L^P)] (0.102 g, 0.149 mmol) in THF (10 mL) was added dropwise to a stirring suspension of KC_8 (40 mg, 0.30 mmol) in THF (5 mL) at -80 °C and allowed to warm to room temperature resulting in a deep green solution. Filtering through Celite and removal of solvent gave a deep green solid [V(L^P)]K (31 mg, 0.045 mmol, 30 %). Analysis. Found: C, 61.15; H, 6.00; N, 8.08; $C_{35}H_{40}N_4O_5VK$ requires: C, 61.21; H, 5.87; N, 8.16 %. IR (nujol, KBr) ν : 1552 (C=N), 1494 cm^{-1} (C=C).

Alternative method: A mixture of [(VCl)(L^P)] (0.151 g, 0.221 mmol) in THF (10 mL) and 5 % Na(Hg) (0.20 g, 0.441 mmol) was stirred at room temperature overnight, during which the colour changed from red to deep green. The mixture was allowed to settle, cooled to -80 °C the solution decanted and solvents removed under vacuum. The IR spectrum agreeded with that above.

6.2.21 Reaction of [(VCl)(L^{NMe})] with KC_8

To a stirring suspension of KC_8 (44.5 mg, 0.33 mmol) at -80 °C was added a solution of [(VCl)(L^{NMe})] (0.100 g, 0.17 mmol). The solution was allowed to warm to room temperature during which the soltion turned from red/brown to a deep green solution which was isolated by filtration through Celite and solvent removed under vacuum to give [(V^{II})(L^{NMe})] as a green solid (40 mg, 0.068 mmol, 40 %) IR (nujol, KBr): ν 1555 (C=N), 1495 cm^{-1} (C=C).

6.2.22 Reaction of [(TiCl)(L^{P})] with KC_8

To a stirring suspension of KC_8 (48 mg, 0.356 mmol) at -80 °C was added a solution of [(TiCl)(L^{P})] (0.121 g, 0.178 mmol) in THF (5 mL). The solution was allowed to warm to room temperature during which it turned from red/brown to a deep red colour. The solution was filtered through Celite and solvent removed under vacuum to give [(Ti^{II})(L^{P})] as a deep red solid (39 mg, 0.061 mmol, 34 %) IR (nujol, KBr): ν 1565 (C=N), 1501 cm^{-1} (C=C).

6.2.23 Reaction of [(TiCl)(L^{NMe})] with KC_8

To a stirring suspension of KC_8 (72 mg, 0.529 mmol) at -80 °C was added a solution of [(TiCl)(L^{NMe})] (0.160 g, 0.264 mmol) in THF (5 mL). The solution was allowed to warm to room temperature during which it turned from red/brown to a deep red colour. The solution was filtered through Celite and solvent removed under vacuum to give [(Ti^{II})(L^{NMe})] as a deep red solid (57 mg, 0.100 mmol, 38 %). IR (nujol, KBr): ν 1560 (C=N), 1495 cm^{-1} (C=C).

6.2.24 Synthesis of [Mg(L^{P})]

A 1 M solution of $Mg^{n}Bu_2$ in heptane (1 mL, 1.0 mmol) was added dropwise to a stirring solution of H_2L^{P} (0.600 g, 1.0 mmol) in THF (10 mL) at -80 °C. The solution was allowed to warm to room temperature and stirred for 3 h during which a colour changed from yellow/orange to a dichroic bright yellow solution was observed, after which the solvent volume was reduced under vacuum and [Mg(L^{P})] precipitated with hexane (5 mL) giving [Mg(L^{P})] as a yellow solid (0.590 g, 0.95 mmol, 95 %). ^{1}H NMR (500.12 MHz, C_6D_6): δ 8.23 (s, 2H, imine), 7.16–7.15 (m, 2H, pyrrole), 6.92–6.83 (m, 6H, 3 × Ar-H), 6.65 (d, *J* = 3.5 Hz, 2H, pyrrole), 6.63–6.60 (m, 2H, Ar-H), 3.78–3.71 (m, 2H, OCH_2), 3.71–3.64 (m, 2H, OCH_2), 3.44 (d, *J* = 12.3 Hz, 2H, OCH_2), 3.37–3.29 (m, 4H, 2 × O-CH_2), 3.21–3.13 (m, 2H, O-CH_2), 3.07 (dd, *J* = 11.1, 1.7 Hz,

2H, OCH_2), 2.94–2.85 (m, 2H, OCH_2), 2.38 (q, J = 7.3 Hz, 2H, Et-CH_2), 2.12 (q, J = 7.3 Hz, 2H, Et-CH_2), 1.16 (t, J = 7.2 Hz, 3H, Et-CH_3), 0.89 (t, J = 7.4 Hz, 3H, Et-CH_3); $^{13}C\{^1H\}$ NMR (125.76 MHz, C_6D_6): δ 156.98 (s, quaternary), 156.58 (s, CH, imine), 151.62 (s, quaternary), 143.54 (s, quaternary), 136.48 (s, quaternary), 123.59 (s, CH, Ar-H), 122.92 (s, CH, Ar-H), 122.43 (s, CH, Ar-H), 120.03 (s, CH, pyrrole), 116.75 (s, CH, Ar-H), 111.67 (s, CH, pyrrole), 71.04 (s, CH_2, OCH_2), 70.72 (s, CH_2, OCH_2), 70.63 (s, CH_2, OCH_2), 70.24 (s, CH_2, OCH_2), 48.55 (s, quaternary), 41.47 (s, CH_2, Et-CH_2), 34.33 (s, CH_2, Et-CH_2), 11.48 (s, CH_3, Et-CH_3), 10.52 (s, CH_3, Et-CH_3). MS(EI): *m/z* = 621.2 (M^+, 8%), 592.1 ($[M^+–Et]^+$, 100 %); Analysis. Found: C, 67.64; H, 6.37; N, 8.93; $C_{35}H_{40}N_4O_5Mg$ requires: C, 67.69; H, 6.49; N, 9.02 %; IR (nujol, KBr): ν 1564 (C=N), 1506 cm^{-1} (C=C).

6.2.25 Synthesis of [Mg(L^{NMe})]

A 1 M solution of Mg^nBu_2 in heptane (1.2 mL, 1.2 mmol) was added dropwise to a stirring solution of H_2L^{NMe} (0.628 g, 1.2 mmol) in THF (10 mL) at -80 °C. The solution was allowed to warm to room temperature and stirred for 3 h, during which the colour changed from yellow/orange to a dichroic bright yellow solution, after which the solvent volume was reduced under vacuum and [Mg(L^{NMe})] precipitated with hexane (5 mL) giving [Mg(L^{NMe})] as a yellow solid (0.609 g, 0.112 mmol, 93 %). ^1H NMR (500.12 MHz, C_6D_6): δ 8.20 (s, 2H, imine), 7.13 (d, J = 3.5 Hz, 2H, pyrrole), 6.90–6.83 (m, 4H, 2 × Ar-H), 6.67 (d, J = 4.5 Hz, 2H, Ar-H), 6.60 (d, J = 3.5 Hz, 2H, pyrrole), 6.52 (d, J = 8.1 Hz, 2H, Ar-H), 3.61–3.53 (m, 2H, O/N-CH_2), 3.03 (s, 2H, O/N-CH_2), 2.46–2.38 (m, 2H, O/N-CH_2), 2.31–2.21 (m, 4H, 2 × Et-CH_2), 2.06 (s, 3H, N-CH_3), 2.09–2.00 (m, 2H, O/N-CH_2), 0.97–0.89 (m, 3H, Et-CH_3), 0.89–0.80 (m, 3H, Et-CH_3); $^{13}C\{^1H\}$ NMR (125.76 MHz, C_6D_6): δ 158.57 (s, CH, imine), 157.27 (s, quaternary), 152.38 (s, quaternary), 142.13 (s, quaternary), 134.95 (s, quaternary), 123.55 (s, CH, Ar), 122.36 (s, CH, Ar), 120.97 (s, CH, Ar), 120.33 (s, CH, pyrrole), 114.58 (s, Ar-H), 110.96 (s, CH, pyrrole), 57.47 (s, quaternary), 55.48 (s, CH_2, O/N-CH_2), 48.83 (s, CH_2, O/N-CH_2), 45.60 (s, CH_3, N-CH_3), 38.67 (s, CH_2, Et-CH_2), 38.03 (s, CH_2, Et-CH_2), 10.48 (s, CH_3, Et-CH_3), 10.19 (s, CH_3, Et-CH_3); MS(EI): 584.3 ($[M^+$+K$]^+$, 10 %), 551.2 ($[M^+$+Li$]^+$, 50 %), 503 ($[M^+–Et–Me]^+$, 100 %); Analysis. Found: C, 70.31; H, 6.53; N, 12.87; $C_{32}H_{35}MgN_5O_2$ requires: C, 70.40; H, 6.46; N, 12.83 %; IR (nujol, KBr): ν 1569 (C=N), 1490 cm^{-1} (C=C)

6.2.26 Attempted synthesis of [M(L^P)] and [M(L^{NMe})] via Mg salts

An example using $CoCl_2$ and H_2L^P: A suspension of $CoCl_2$ (10 mg, 0.077 mmol) in THF (5 mL) was added a solution of [Mg(L^P)] (48 mg, 0.083 mmol) in THF (5 mL) at -80 °C. An instant colour change from yellow to deep red was observed. The mixture was allowed to warm to room temperature and stirred for 3 h. After filtration, the solvent was removed under vacuum giving a red solid (20 mg). ^{1}H NMR (C_6D_6) analysis showed a mixture of products.

6.2.27 Synthesis of [Fe(L^{NMe})]

A mixture of H_2L^{NMe} (0.374 g, 0.714 mmol) and excess KH (86 mg, 2.14 mmol) was treated with THF (10 mL). Gas evolved immediately, and, once effervescence had ceased, the mixture was filtered onto a stirring suspension of $FeBr_2{\cdot}THF_2$ (0.257 mg, 0.714 mmol) in THF (5 mL) at -80 °C. A colour change from orange to deep red was observed upon warming to room temperature, the reaction was then stirred overnight after which it was filtered and solvents removed under vacuum giving [Fe(L^{NMe})] as a red solid (0.235 g, 0.407 mmol, 57 %). ^{1}H NMR (399.90 MHz, C_6D_6): δ 26.88 (s, 2H), 19.33 (s, 2H), 9.56 (s, 2H), 9.02 (s, 2H), 7.83 (s, 2H), 7.16 (s, 2H), 5.36 (m, 3H), 3.55–3.45 (m, 3H), 3.35–3.22 (m, 3H), 2.14–2.05 (m, 2H), 0.40 (s, 2H), 0.29 (s, 2H), -5.21 (s, 2H), -9.46 (s, 2H), -13.02 (s, 2H), -16.36 (s, 2H); MS(EI): *m/z* = 577.2 (M^+, 30 %), 548.2 ($[M^+–Et]^+$, 40 %); Analysis. Found: C, 66.41; H, 6.03; N, 12.06; $C_{32}H_{35}FeN_5O_2$ requires: C, 66.55; H, 6.11; N, 12.13 %; IR (nujol, KBr): ν 1555 (C=N), 1502 cm^{-1} (C=C).

6.2.28 Synthesis of [Fe(L^P)]

A mixture of H_2L^P (0.387 g, 0.646 mmol) and excess KH (78 mg, 1.94 mmol) was treated with THF (10 mL). Gas evolved immediately, and, once effervescence had ceased, the mixture was filtered onto a stirring suspension of $FeBr_2.THF_2$ (0.232 mg, 0.646 mmol) in THF (5 mL) at -80 °C. A colour change from orange to deep red was observed. The reaction was warmed to room temperature and left to stir overnight after which it was filtered and solvents removed from the filtrate under vacuum giving [Fe(L^P)] as a red solid (0.262 g, 0.40 mmol, 62 %). Crystals of [Fe_2($L^{P(2+2)}$)] were grown by hexane diffusion into a THF solution of [Fe(L^P)]. ^{1}H NMR (399.90 MHz, C_6D_6): δ 36.66 (s, 2H), 35.21 (s, 2H), 30.55 (s, 2H), 24.58 (s, 2H), 23.84 (s, 2H), 12.12 (s, 2H), 9.91 (s, 2H), 9.20 (s, 2H), 1.41–1.16 (m, 4H), 0.99–0.71 (m, 3H), -2.41 (s, 3H), -4.72 (s,

2H), -6.81 (s, 2H), -10.81 (s, 4H), -11.89 (s, 2H), -14.72 (s, 4H). MS(EI): *m/z* = 652.2 (M^+, 100%), 624.2 ($[M^+–Et]^+$, 89%); IR (nujol, KBr) : ν 1559 (C=N), 1507 cm^{-1}(C=C).

6.2.29 Synthesis of [Mn(L^{NMe})]

A mixture of H_2L^{NMe} (0.507 g, 0.968 mmol) and excess KH (0.116 g, 2.9 mmol) was treated with THF (15 mL). Gas evolved immediately, and, once effervescence had ceased, the mixture was filtered onto a stirring suspension of $MnCl_2$ (0.122 mg, 0.968 mmol) in THF (10 mL) at -80 °C. A rapid colour change from red to very dark red was observed and the reaction warmed to room temperature and left to stir overnight after which it was filtered and solvents removed under vacuum giving [Mn(L^{NMe})] as a red solid (0.223 g, 0.387 mmol, 40 %). MS(EI) *m/z* = 577.1 (M^+, 20 %), 489.1 ($[M^+–(O_2(CH_2)_4NMe)]^+$, 100 %); Analysis. Found: C, 66.55; H, 6.22; N, 12.04; $C_{32}H_{35}N_5O_2Mn$ requires: C, 66.66; H, 6.12; N, 12.15 %; IR (nujol, KBr): ν 1566 (C=N), 1507 cm^{-1} (C=C).

6.2.30 Synthesis of [Mn(L^P)]

A mixture of H_2L^P (0.412 g, 0.688 mmol) and excess KH (83 Mg, 2.1 mmol) was treated with THF (15 mL). Gas evolved immediately, and, once effervescence had ceased, the mixture was filtered onto a stirring suspension of $MnCl_2$ (86.5 mg, 0.688 mmol) in THF (10 mL) at -80 °C. A rapid colour change from red to very dark red was observed and the reaction warmed to room temperature and left to stir overnight after which it was filtered and solvents removed under vacuum giving [Mn(L^P)] as a red solid (0.282 g, 0.433 mmol, 63 %). Crystals of [$Mn_2(L^{P(2+2)})$] were grown by hexane diffusion into a THF solution of [Mn(L^P)]. MS(EI): *m/z* = 651.2 (M^+, 20 %), 622.1 ($[M^+–Et]^+$, 100 %); Analysis. Found: C, 64.40; H, 6.27; N, 8.48; $C_{35}H_{40}MnN_4O_5$ requires: C, 64.51; H, 6.19; N, 8.60 %; IR (nujol, KBr): ν 1562 (C=N), 1507 cm^{-1}(C=C).

6.3 Experimental from Chapter 3

6.3.1 Synthesis of H_2L^{FP}

To a suspension of dialdehyde **9** (0.982 g, 2.79 mmol) and diamine $\mathbf{6^P}$ (1.05 g, 2.79 mmol) in EtOH (150 mL) was added dropwise $BF_3{\cdot}OEt_2$ (0.73 mL, 5.86 mmol) and allowed to stir at 40 °C overnight, under N_2, during which a yellow precipitate formed. The solvent was decanted and the yellow solid washed with EtOH (3 × 20 mL). The solid was dissolved in CH_2Cl_2 (70 mL) and treated with 7 M NH_3 in MeOH (1 mL) causing BH_3NH_3 to precipitate. The solids were filtered and the filtrate evaporated to

dryness to yield a fluffy yellow solid. Dry THF (20 mL) was added, the mixture filtered away from any remaining BF_3NH_3 and the filtrate evaporated giving H_2L^{FP} as a yellow solid (1.26 g, 1.82 mmol, 65 %). ^{1}H NMR (399.90 MHz, $CDCl_3$): δ 9.52 (br, s, 2H, NH), 8.17 (s, 2H, imine), 7.81 (d, *J* = 7.2 Hz, 2H, Ar-H), 7.75 (d, *J* = 7.5 Hz, 2H, Ar-H), 7.45 (td, *J* = 7.5, 1.1 Hz, 2H, Ar-H), 7.38 (td, *J* = 7.5, 1.2 Hz, 2H, Ar-H), 7.15–7.08 (m, 2H, Ar-H), 7.01–6.93 (m, 4H, 2 × Ar-H), 6.89 (dd, *J* = 8.9, 0.9 Hz, 2H, Ar-H), 6.57 (d, *J* = 3.7 Hz, 2H, pyrrole), 6.08 (d, *J* = 3.7 Hz, 2H, pyrrole), 4.18–4.14 (m, 4H, CH_2), 3.92–3.87 (m, 4H, CH_2), 3.80–3.76 (m, 4H, CH_2), 3.64–3.59 (m, 4H, CH_2); $^{13}C\{^1H\}$ NMR (125.76 MHz, $CDCl_3$): δ 151.89 (s, quaternary), 150.19 (s, CH, imine), 147.99 (s, quaternary), 141.67 (s, quaternary), 140.04 (s, quaternary), 138.83 (s, quaternary), 131.56 (s, quaternary), 128.66 (s, CH, Ar-H), 128.28 (s, CH, Ar-H), 126.13 (s, CH, Ar-H), 125.86 (s, CH, Ar-H), 121.65 (s, CH, Ar-H), 120.74 (s, CH, Ar-H), 119.97 (s, CH, Ar-H), 117.18 (s, CH, Ar-H), 112.77 (s, CH, pyrrole), 110.26 (s, CH, pyrrole), 71.65 (s, CH_2, OCH_2), 70.84 (s, CH_2, OCH_2), 69.72 (s, CH_2, OCH_2), 69.21 (s, CH_2, OCH_2), 58.59 (s, quaternary); MS(EI): 692.2 (M^+, 100%), 545.3 ([M^+–fluorenyl]$^+$, 30 %); Analysis. Found: C, 74.42; H, 5.96; N, 7.94; $C_{43}H_{40}N_4O_5$ requires: C, 74.55; H, 5.82; N, 8.09 %; IR (nujol, KBr): ν 3211 (N-H), 1620 (C=N), 1492 cm^{-1}(C=C).

6.3.2 Synthesis of H_2L^{FNMe}

To a suspension of dialdehyde **9** (1.213 g, 3.44 mmol) and diamine $\mathbf{6}^{NMe}$ (1.04 g, 3.44 mmol) in EtOH (150 mL) was added dropwise $BF_3{\cdot}OEt_2$ (0.91 mL, 7.22 mmol) and allowed to stir at room temperature overnight, under N_2, during which a yellow precipitate formed. The solvent was decanted and the yellow solid washed with EtOH (3 × 20 mL). The solid was dissolved in CH_2Cl_2 (70 mL) and treated with 7 M NH_3 in MeOH (1.2 mL) causing BH_3NH_3 to precipitate. The solids were filtered and the filtrate evaporated to dryness to yield a fluffy yellow solid. Dry THF (20 mL) was added, the mixture filtered from any remaining BF_3NH_3 and the filtrate evaporated giving H_2L^{FNMe} as a yellow solid (1.49 g, 2.41 mmol, 70 %). ^{1}H NMR (500.12 MHz,$CDCl_3$): δ 9.50 (br, s, 2H, NH), 8.16 (s, 2H, imine), 7.93 (d, *J* = 7.3 Hz, 2H, Ar-H), 7.81 (d, *J* = 7.3 Hz, 2H, Ar-H), 7.44 (td, *J* = 7.4, 1.1 Hz, 2H, Ar-H), 7.38 (td, *J* = 7.4, 1.3 Hz, 2H, Ar-H), 7.34 (td, *J* = 7.6, 1.8 Hz, 2H, Ar-H), 7.01 (m, 4H, Ar-H), 6.51 (d, *J* = 3.8 Hz, 2H, pyrrole CH), 5.83 (d, 3.8 Hz, 2H, pyrrole CH), 4.22 (m, 4H, CH_2), 3.08 (m, 4H, CH_2), 2.64 (s, 3H, N-CH_3); $^{13}C\{^1H\}$ NMR (125.76 MHz, $CDCl_3$): δ 151.10 (s, CH, imine), 150.99 (s, quaternary), 147.42 (s, quaternary), 146.44 (s, quaternary), 142.40 (s, quaternary),

139.80 (s, quaternary), 132.01 (s, quaternary), 128.38 (s, CH, Ar-H), 127.96 (s, CH, Ar-H), 125.90 (s, CH, Ar-H), 125.38 (s, CH, Ar-H), 121.75 (s, CH, Ar-H), 120.91 (s, CH, Ar-H), 120.60 (s, CH, Ar-H), 116.70 (s, CH, Ar-H), 113.57 (s, CH, pyrrole), 109.66 (s, CH, pyrrole), 68.42(s, CH_2, O/N-CH_2), 66.99 (s, CH_2, O/N-CH_2), 55.91 (s, quaternary), 43.21 (s, CH_3, NCH_3); MS(EI): 617.2 (M^+, 20 %), 534.2 ([M^+–(C_4H_8NMe)]$^+$, 100 %); Analysis. Found: C, 77.64; H, 5.59; N, 11.28; $C_{40}H_{35}N_5O_2$ requires: C, 77.77; H, 5.71; N, 11.34 %; IR (nujol, KBr): ν 3197 (N-H), 1621 (C=N), 1502 cm^{-1} (C=C).

6.3.3 Synthesis of [Pd(L^{FP})]

A solution of H_2L^{FP} (0.200 g, 0.289 mmol) and $Pd(OAc)_2$ (65 mg, 0.289 mmol) in CH_2Cl_2 (10 mL) was stirred for 30 mins, giving a deep red solution. To this, 2.1 eq of NEt_3 (0.09 mL, 0.61 mmol) was added dropwise and the solution stirred overnight. The solvent was removed under vacuum, the product extracted into hexane giving [Pd(L^{FP})] as a yellow solid (81 mg, 0.101 mmol, 35 %). ^{1}H NMR (399.90 MHz, $CDCl_3$): δ 7.78 (dd, *J* = 7.8, 1.7 Hz, 2H, Ar-H), 7.63 (s, 2H, imine), 7.42–7.33 (m, 2H, Ar-H), 7.31 (d, *J* = 7.4 Hz, 2H, Ar-H), 7.16 (dt, *J* = 7.8, 1.7 Hz, 2H, Ar-H), 6.89 (dt, *J* = 7.8, 1.6 Hz, 2H, Ar-H), 6.82 (dd, *J* = 7.7, 1.6 Hz, 2H, Ar-H), 6.63 (d, *J* = 3.9 Hz, 2H, pyrrole), 6.52–6.44 (m, 4H, Ar-H), 5.43 (d, *J* = 3.9 Hz, 2H, pyrrole), 4.24–4.14 (m, 2H, CH_2), 3.96–3.87 (m, 4H, CH_2), 3.77–3.67 (m, 6H CH_2), 3.64–3.58 (m, 2H CH_2), 3.54–3.47 (m, 2H CH_2); $^{13}C\{^1H\}$ NMR (125.76 MHz, $CDCl_3$): δ 160.63 (s, CH, imine), 151.34 (s, quaternary), 150.55 (s, quaternary), 149.83 (s, quaternary), 145.92 (s, quaternary), 140.93 (s, quaternary), 140.37 (s, quaternary), 137.78 (s, quaternary), 137.73 (s, quaternary), 128.31 (s, CH, Ar-H), 128.01 (s, CH, Ar-H), 127.90 (s, CH, Ar-H), 127.55 (s, CH, Ar-H), 126.30 (s, CH, Ar-H), 125.51 (s, CH, Ar-H), 124.67 (s, CH, Ar-H), 124.16 (s, CH, Ar-H), 120.49 (s, CH, Ar-H), 120.30 (s, CH, Ar-H), 120.13 (s, CH, Ar-H), 118.51 (s, CH, Ar-H), 111.39 (s, CH, pyrrole), 108.59 (s, CH, pyrrole), 71.29 (s, CH_2, OCH_2), 70.59 (s, CH_2, OCH_2), 69.68 (s, CH_2, OCH_2), 68.23 (s, CH_2, OCH_2), 61.56 (s, quaternary); MS(EI): *m/z* = 796.2 (M^+, 100%); Analysis. Found:. C, 64.73; H, 6.37; N, 6.94; $C_{43}H_{38}N_4O_5Pd$ requires: C, 64.78; H, 4.80; N, 7.03 %; IR (nujol, KBr): ν 1552 (C=N), 1496 cm^{-1} (C=C).

6.3.4 Synthesis of [Pd(L^{FNMe})]

A solution of H_2L^{FNMe} (0.213 g, 0.345 mmol) and $Pd(OAc)_2$ (81 mg, 0.345 mmol) in CH_2Cl_2 (10 mL) was stirred for 30 mins, giving a deep red solution. To this, 2.1 eq of NEt_3 (1.1 mL, 0.796 mmol) was added dropwise and the solution stirred overnight. The solvent was removed under vacuum, the product extracted into hexane

giving [Pd(L^{FNMe})] as a yellow solid (0.104 g, 0.145 mmol, 42 %). ^{1}H NMR (500.12 MHz, $CDCl_3$): δ 7.82 (t, *J* = 7.0 Hz, 2H, Ar-H), 7.57 (s, 2H, imine), 7.46–7.35 (m, 4H, Ar-H), 7.29–7.23 (m, 2H, Ar-H), 6.96 (td, *J* = 7.9, 1.6 Hz, 2H, Ar-H), 6.83 (dd, *J* = 7.9, 1.6 Hz, 2H, Ar-H), 6.68 (d, *J* = 3.9 Hz, 2H, pyrrole), 6.58–6.53 (m, 4H, Ar-H), 5.48 (d, *J* = 3.9 Hz, 2H, pyrrole), 4.28–4.22 (m, 2H, CH_2), 3.89–3.82 (m, 2H, CH_2), 3.39–3.31 (m, 2H, CH_2), 3.31–3.24 (m, 2H, CH_2), 2.66 (s, 3H, N-CH_3); ^{13}C{^{1}H} NMR (125.76 MHz, $CDCl_3$): δ 160.55 (s, CH, imine), 150.38 (s, quaternary), 149.93 (s, quaternary), 149.72 (s, quaternary), 146.02 (s, quaternary), 140.63 (s, quaternary), 140.41 (s, quaternary), 138.14 (s, quaternary), 137.43 (s, quaternary), 128.17 (s, CH, Ar-H), 128.09 (s, CH, Ar-H), 127.73 (s, CH, Ar-H), 127.57 (s, CH, Ar-H), 126.35 (s, CH, Ar-H), 125.15 (s, CH, Ar-H), 124.93 (s, CH, Ar-H), 123.98 (s, CH, Ar-H) , 120.78 (s, CH, Ar-H), 120.13 (s, CH, Ar-H), 120.07 (s, CH, Ar-H), 118.65 (s, CH, Ar-H), 112.35 (s, CH, pyrrole), 108.61 (s, CH, pyrrole), 65.85 (s, CH_2, O/N-CH_2), 61.44 (s, quaternary), 54.41 (s, CH_2, O/N-CH_2), 45.40 (s, CH_3, NCH_3); MS(EI): *m/z* = 721.1 (M^+, 87 %), 638.0 ([M^+–$O(CH_2)_2N(CH_3)(CH_2)_2O$]$^+$, 100 %); Analysis. Found: C, 66.67; H, 4.62; N, 9.71; $C_{40}H_{33}N_5O_2Pd$ requires: C, 66.53; H, 4.61; N, 9.70 %; IR (nujol, KBr): ν 1562 (C=N), 1504 cm^{-1} (C=C).

6.3.5 Synthesis of [$K_2(L^{FP})$]

A mixture of H_2L^{FP} (50 mg, 0.072 mmol) and excess KH (9 mg, 0.22 mmol) was treated with THF (2 mL). Gas evolved immediately, and the mixture stirred for 5 h at room temperature giving a red solution after which the solution was filtered and precipitated by addition of hexane (15 mL) to give [$K_2(L^{FP})$] as a red powder (52 mg, 0.068 mmol, 94 %). ^{1}H NMR (399.90 MHz, C_6D_6/H_8-THF): δ 8.42 (s, 2H, imine), 8.31 (d, *J* = 7.1 Hz, 2H, Ar-H), 8.00 (d, *J* = 7.1 Hz, 2H, Ar-H), 7.57–7.47 (m, 6H, Ar-H), 7.45 (d, *J* = 7.2 Hz, 2H, Ar-H), 7.28 (d, *J* = 3.5 Hz, 2H, Ar-H), 7.23–7.18 (m, 2H, Ar-H), 6.75 (d, *J* = 3.1 Hz, 2H, pyrrole), 6.03 (d, *J* = 3.0 Hz, 2H, pyrrole) [OCH_2 not seen due to THF suppression]; ^{13}C{^{1}H} NMR (125.76 MHz, C_6D_6/H_8-THF): δ 154.28 (s, quaternary), 152.90 (s, quaternary), 152.47 (s, CH, imine), 145.10 (s, quaternary), 141.00 (s, quaternary), 139.70 (s, quaternary), 128.19 (s, CH, Ar-H), 126.27 (s, CH, Ar-H), 125.91 (s, CH, Ar-H), 122.42 (s, CH, Ar-H), 122.22 (s, CH, Ar-H), 119.67 (s, CH, Ar-H), 119.19 (s, CH, Ar-H), 117.14 (s, CH, Ar-H), 113.30 (s, CH, pyrrole), 108.83 (s, CH, pyrrole), 69.96 (s, CH_2, OCH_2), 66.82 (s, CH_2, OCH_2), 65.83 (s, CH_2, OCH_2), 65.41

(s, CH_2, OCH_2); MS(EI): *m/z* = 768.1 ($M^{+\cdot}$, 55 %), 730.2 ($[M^+-K]^+$, 100%); IR (nujol, KBr): ν 1563 (C=N), 1499 cm^{-1} (C=C).

6.3.6 Synthesis of $[K_2(L^{FNMe})]$

A mixture of H_2L^{FNMe} (52 mg, 0.084 mmol) and excess KH (10 mg, 0.25 mmol) was treated with THF (2 mL). Gas evolved immediately, and the mixture stirred for 5 h at room temperature giving a red solution after which the solution was filtered and precipitated by addition of hexane (15 mL) to give $[K_2(L^{FNMe})]$ as a red powder (52 mg, 0.075 mmol, 89 %). ^{1}H NMR (399.90 MHz, C_6D_6/H_8-THF): δ 8.01 (s, 2H, imine), 7.71 (d, *J* = 7.4 Hz, 2H, Ar-H), 7.64 (d, *J* = 7.4 Hz, 2H, Ar-H), 7.15 (t, *J* = 7.3 Hz, 2H, Ar-H), 7.07 (t, *J* = 7.3 Hz, 2H, Ar-H), 6.99–6.93 (m, 2H, Ar-H), 6.87–6.82 (m, 2H, Ar-H), 6.82–6.74 (m, 4H, Ar-H), 6.31 (d, *J* = 3.1 Hz, 2H, pyrrole), 5.45 (d, *J* = 3.1 Hz, 2H, pyrrole), 4.03–3.96 (m, 4H, CH_2), 2.75–2.67 (m, 4H, CH_2) [NCH_3 not seen due to THF suppression]; $^{13}C\{^1H\}$ NMR (125.76 MHz, C_6D_6/H_8-THF): δ 155.20 (s, quaternary), 154.75 (s, CH, imine), 154.21 (s, quaternary), 151.91 (s, quaternary), 145.83 (s, quaternary), 140.62 (s, quaternary), 138.73 (s, quaternary), 127.07 (s, CH, Ar-H), 125.96 (s, CH, Ar-H), 125.70 (s, CH, Ar-H), 122.31 (s, CH, Ar-H), 121.67 (s, CH, Ar-H), 119.01 (s, CH, Ar-H), 118.97 (s, CH, Ar-H), 118.30 (s, CH, pyrrole), 113.52 (s, CH, Ar-H), 108.40 (s, CH, pyrrole), 66.84 (s, CH_2, O/N-CH_2), 64.35 (s, quaternary), 56.46 (s, CH_2, O/N-CH_2), 44.79 (s, CH_3, NCH_3); MS(EI): *m/z* = 693.1 ($M^{+\cdot}$, 10 %), 655.2 ($[M^+–K]^+$, 100%); Analysis. Found: C, 69.23; H, 4.68; N, 9.97; $C_{40}H_{33}K_2N_5O_2$ requires: C, 69.23; H, 4.79; N, 10.09 %; IR (nujol, KBr): ν 1565 (C=N), 1510 cm^{-1} (C=C).

6.3.7 Synthesis of $[Mg(L^{FP})]$

A 0.5 M solution of $Mg(^nBu)_2$ in heptane (0.48 mL, 0.244 mmol) was added dropwise to a stirring solution of H_2L^{FP} (0.169 g, 0.244 mmol) in THF (5 mL) at -80 °C. The solution was allowed to warm to room temperature and stirred for 3 h after which the solvent volume was reduced under vacuum and $[Mg(L^{FP})]$ precipitated with hexane (5 mL) giving $[Mg(L^{FP})]$ as a yellow solid (0.166 g, 0.232 mmol, 95 %). ^{1}H NMR (500.12 MHz, C_6D_6): δ 8.23 (d, *J* = 8.1 Hz, 1H, Ar^F-H), 8.21 (s, 2H, imine), 7.80 (d, *J* = 6.9 Hz, 1H, Ar^F-H), 7.67 (d, *J* = 7.5 Hz, 1H, Ar^F-H), 7.58 (d, *J* = 6.8 Hz, 1H, Ar^F-H), 7.46 (d, *J* = 7.5 Hz, 1H, Ar^F-H), 7.41–7.33 (m, 2H, Ar^F-H), 7.12 (t, *J* = 7.1 Hz, 1H, Ar^F-H), 7.01–6.98 (m, 2H, Ar-H), 6.97–6.93 (m, 4H, Ar-H), 6.81 (d, *J* = 3.5 Hz, 2H, pyrrole), 6.70–6.67 (m, 2H, Ar-H), 5.97 (d, *J* = 3.4 Hz, 2H, pyrrole), 3.44–3.14 (m, 14H, OCH_2), 2.77 (t, *J* = 9.7 Hz, 2H, OCH_2); $^{13}C\{^1H\}$ NMR (125.76 MHz, C_6D_6): δ 156.58 (s,

CH, imine), 155.20 (s, quaternary), 153.65 (s, quaternary), 152.61 (s, quaternary), 151.52 (s, quaternary), 143.36 (s, quaternary), 142.34 (s, quaternary), 138.67 (s, quaternary), 136.84 (s, quaternary), 127.27 (s, CH, Ar-H), 127.24 (s, CH, Ar-H), 126.95 (s, CH, Ar-H), 126.53 (s, CH, Ar-H), 126.00 (s, CH, Ar-H), 124.59 (s, CH, Ar-H), 123.53 (s, CH, Ar-H), 122.55 (s, CH, Ar-H), 122.30 (s, CH, Ar-H), 120.06 (s, CH, Ar-H), 119.96 (s, CH, Ar-H), 119.75 (s, CH, pyrrole), 116.63 (s, CH, Ar-H), 111.51 (s, CH, pyrrole), 71.15 (s, CH_2, OCH_2), 70.34 (s, CH_2, OCH_2), 70.26 (s, CH_2, OCH_2), 69.94 (s, CH_2, OCH_2), 59.66 (s, quaternary); MS(EI): *m/z* = 714.2 ($M^{+\cdot}$, 100 %); IR (nujol, KBr): ν 1567 (C=N), 1482 cm^{-1} (C=C).

6.3.8 Synthesis of [Mg(L^{FNMe})]

A 0.5 M solution of $Mg(^nBu)_2$ in heptane (0.67 mL, 0.336 mmol) was added dropwise to a stirring solution of H_2L^{FNMe} (0.207 g, 0.336 mmol) in THF (5 mL) at -80 °C. The solution was allowed to warm to room temperature and stirred for 3 h after which the solvent volume was reduced under vacuum and [Mg(L^{FNMe})] precipitated with hexane (5 mL) giving [Mg(L^{FNMe})] as a yellow solid (0.200 g, 0.312 mmol, 93 %). ^{1}H NMR (500.12 MHz, C_6D_6): δ 8.22 (s, 2H, imine), 7.70 (br, s, 2H, Ar-H), 7.47 (d, *J* = 7.4 Hz, 2H, Ar-H), 7.32–6.99 (m, 8H, Ar-H), 6.90–6.84 (m, 2H, Ar-H), 6.79 (d, *J* = 3.5 Hz, 2H, pyrrole), 6.69–6.65 (m, 4H, Ar-H), 6.47 (d, *J* = 8.1 Hz, 2H, Ar-H), 5.97 (d, *J* = 3.5 Hz, 2H, pyrrole), 3.56 (br, s, 2H, CH_2), 3.14 (br, s, 2H, CH_2), 2.45 (br, s, *J* = 21.3 Hz, 2H, CH_2), 2.13 (br, s, 2H, CH_2), 1.94 (s, 3H, N-CH_3); $^{13}C\{^1H\}$ NMR (125.76 MHz, C_6D_6): δ 159.57 (s, CH, imine), 153.82 (s, quaternary), 151.94 (s, quaternary), 141.55 (s, quaternary), 136.12 (s, quaternary), 128.19 (s, quaternary), 127.98 (s, quaternary), 127.79 (s, quaternary), 127.60 (s, quaternary), 126.86 (s, CH, Ar-H),126.82 (s, CH, Ar-H), 126.78 (s, CH, Ar-H), 126.60 (s, CH, Ar-H), 126.41 (s, CH, Ar-H), 124.69 (s, CH, Ar-H), 123.91 (s, CH, Ar-H), 122.69 (s, CH, Ar-H), 120.71 (s, CH, Ar-H), 120.11 (s, CH, Ar-H), 119.91 (s, CH, Ar-H), 119.76 (s, CH, pyrrole), 113.77 (s, CH, Ar-H), 112.19 (s, CH, pyrrole), 67.44 (s, CH_2, OCH_2), 59.34 (s, quaternary), 54.79 (s, CH_2, NCH_2), 45.00 (s, CH_3, NCH_3); MS(EI): *m/z* = 639.1 (M^+, 15 %), 626.2 ([M^+–Me]$^+$, 100 %). IR (nujol, KBr): ν 1557 (C=N), 1496 cm^{-1} (C=C).

6.3.9 Synthesis of [Co(L^{FP})]

A mixture of H_2L^{FP} (0.215 g, 0.310 mmol) and excess KH (37 mg, 0.931 mmol) was treated with THF (5 mL). Gas evolved immediately, and, once effervescence had ceased, the mixture was filtered onto a stirring suspension of $CoCl_2$ (40 mg, 0.310 mmol)

in THF (5 mL) at -80 °C. A rapid colour change from red to very dark red was observed and the reaction warmed to room temperature and left to stir overnight after which it was filtered and solvents removed under vacuum giving [Co(L^{FP})] as a red solid (45 mg, 0.060 mmol, 19 %). ^{1}H NMR (399.90 MHz, C_6D_6): δ 60.04 (s, 2H), 35.53 (s, 2H), 12.83 (s, 2H), 4.65 (s, 2H), 3.21 (s, 1H), 2.88 (t, *J* = 7.3 Hz, 1H), 2.76 (d, *J* = 8.1 Hz, 1H), 2.51 (d, *J* = 8.0 Hz, 1H), 1.35 (s, 2H), 1.20 (s, 4H), 0.60 (s, 2H), -1.17 (d, *J* = 6.3 Hz, 1H), -1.43 (s, 1H), -1.57 (s, 1H), -2.86 (s, 2H), -3.72 (s, 2H), -5.35 (s, 2H), -9.22 (s, 2H), -12.00 (s, 2H), -18.74 (s, 2H), -22.85 (s, 1H), -37.06 (s, 2H); MS(EI): *m/z* = 749.2 (M^+, 100%); IR (nujol, KBr): ν 1562 (C=N), 1502 cm^{-1} (C=C).

6.3.10 Possible synthesis of [Co(OH_2)(OH)(L^{FP})]

A solution of [Co(L^{FP})] (0.201 g, 0.268 mmol) in air saturated THF (8 mL) was left to stand exposed to air overnight during which a brown/red precipitate formed. This was isolated by filtration and dried under vacuum giving [Co(OH_2)(OH)(L^{FP})] as a red/brown solid (0.179 g, 0.228 mmol, 85 %). ^{1}H NMR (399.90 MHz, C_6D_6): δ 7.78–7.71 (m, *J* = 5.8 Hz, 2H, Ar-H), 7.53–7.45 (m, 1H, Ar-H), 7.43 (s, 2H, imine), 7.40–7.31 (m, *J* = 6.2 Hz, 2H, Ar-H), 7.28–7.21 (m, 2H, Ar-H), 7.12–7.05 (m, 3H, Ar-H), 6.93–6.82 (m, 4H, pyrrole + Ar-H), 6.58–6.50 (m, 2H, Ar-H), 6.25–6.18 (m, 2H, Ar-H), 6.01 (s, 2H, pyrrole), 3.48–2.72 (m, 16H, OCH_2); ^{13}C{^{1}H} NMR (125.76 MHz, C_6D_6): δ 162.88 (s, CH, imine), 151.20 (s, quaternary), 149.43 (s, quaternary), 139.94 (s, quaternary), 133.38 (s, quaternary), 128.61 (s, quaternary), 125.72 (s, quaternary), 125.47 (s, quaternary) 121.77 (s, CH), 121.63 (s, CH, Ar-H), 121.28 (s, CH, Ar-H), 120.84 (s, CH, Ar-H), 120.52 (s, CH, Ar-H), 120.19 (s, quaternary), 119.64 (s, CH, Ar-H), 118.76 (s, CH, Ar-H), 117.53 (s, CH, Ar-H), 117.28 (s, CH, Ar-H), 115.07 (s, CH, Ar-H), 111.57 (s, CH, Ar-H), 111.45 (s, CH, pyrrole), 107.93 (s, CH, Ar-H), 106.27 (s, CH, pyrrole), 73.00 (s, CH_2, OCH_2), 70.36 (s, CH_2, OCH_2), 70.12 (s, CH_2, OCH_2), 68.64 (s, CH_2, OCH_2) 57.53 (s, quaternary); Analysis. Found: C, 65.90.; H, 5.34; N, 7.11; $C_{43}H_{41}CoN_4O_7$ requires: C, 65.81; H, 5.27; N, 7.14 %; IR (KBr): ν 3409 (O-H), 3232 (O-H), 1564 (C=N), 1500 cm^{-1} (C=C).

6.3.11 Synthesis of [Co(L^{FNMe})]

A mixture of H_2L^{FNMe} (0.195 g, 0.316 mmol) and excess KH (38 mg, 0.95 mmol) was treated with THF (5 mL). Gas evolved immediately, and, once effervescence had ceased, the mixture was filtered onto a stirring suspension of $CoCl_2$ (41 mg, 0.316 mmol) in THF (5 mL) at -80 °C. A rapid colour change from red to very dark red was observed

and the reaction warmed to room temperature and left to stir overnight after which it was filtered and solvents removed under vacuum giving [Co(L^{FNMe})] as a red solid (50 mg, 0.074 mmol, 23 %). ^{1}H NMR (399.90 MHz, H_8-THF/C_6D_6): δ 44.61 (s, 2H), 26.05 (s, 2H), 11.49 (s, 1H), 9.71 (s, 1H), 7.79 (s, 2H), 6.68 (s, 2H), 5.89 (s, 2H), 5.61 (s, 1H), 4.30 (s, 2H), 0.83 (s, 1H), -0.84 (s, 3H), -1.77–-2.50 (m, 2 × 1H), -3.26 (s, 1H), -5.15 (s, 2H), -6.29 (s, 2H), -6.89 (s, 2H), -8.66 (s, 2H), -14.07 (s, 1H), -17.19 (s, 2H). MS(EI): *m/z* = 674.3 (M^+, 100 %); Analysis. Found: C, 71.18; H, 4.84; N, 10.29; $C_{40}H_{33}CoN_5O_2$ requires: C, 71.21; H, 4.93; N, 10.38 %; IR (nujol, KBr): ν 1560 (C=N), 1495 cm^{-1} (C=C).

6.3.12 Possible synthesis of [Co(OH_2)(OH)(L^{FNMe})]

A solution of [Co(L^{FNMe})] (0.154 g, 0.228 mmol) in air saturated THF (10 mL) was left to stand exposed to air overnight during which a brown/red precipitate formed. This was isolated by filtration and dried under vacuum giving [Co(OH_2)(OH)(L^{FNMe})] as a red/brown solid (0.130 g, 0.183 mmol, 80 %). The ^{1}H NMR spectrum (H_8-THF/C_6D_6) of this highly insoluble compound showed resonances in the diamagnetic region though a mixture of products were present. A pure compound could not be isolated. IR (nujol, KBr): ν 3403 (O-H), 3230 (O-H), 1562 (C=N), 1498 cm^{-1} (C=C).

6.3.13 Attempted synthesis of tetranitro compounds 10^{NMe} and 10^{P}

2,6-dinitro-*p*-cresol (0.202 g, 1.02 mmol), K_2CO_3 (0.141 g, 1.02 mmol) and dichloride **2** (0.1 mL, 0.506 mmol) or **4** (80 mg, 0.506 mmol) in DMF (20 mL) was stirred at 120 °C for 4 d, with the mixture sonicated for 30 mins twice daily. The mixture was poured into water, extracted with $CHCl_3$ (2 × 20 mL), washed with water (3 × 50 mL), dried over $MgSO_4$, filtered and solvent removed by rotary evaporation to give an orange-yellow solid. The ^{1}H NMR spectrum showed multiple products including large amounts of unreacted starting materials.

6.3.14 Attempted synthesis of $H_2L^{amideNH}$

An example procedure: A stirring solution of amide-diamine $\mathbf{11}^{amideNH}$ (0.251 g, 0.879 mmol) and dialdehyde **1** (0.277 g, 0.879 mmol) in methanol (20 mL) was treated dropwise with TFA (0.36 mL, 1.93 mmol) and the mixture stirred for 4 h during which the colour changed from light red to a slightly darker red. Treatment with NEt_3 until a basic pH was achieved caused a lightening of the colour after which solvent was removed by rotary evaportaion giving a red oil. The ^{1}H NMR spectrum showed a mixture of products. Reactions were attempted using 2 or 5 eq of $BF_3{\cdot}OEt_2$, TFA or

p-toluenesulfonic acid, at -20 °C, room temperature and 75 °C with either NEt_3 or KOH. Template reactions were attempted by addition of one or two eq of $Ni(OAc)_2$, $Cu(OAc)_2$, $Zn(OAc)_2$ and $Co(OAc)_2$ to mixtures of **11**$^{\mathbf{amideNH}}$ and **1** in MeOH and stirred overnight. Any precipitate was isolated by filtration and solvents removed under vacuum. Analysis by ^{1}H NMR spectroscopy or EI mass spectrometry indicated the desired product was not present.

6.3.15 Synthesis of amide-diamine compound, 11$^{\mathbf{amideNMe}}$

A solution of 2-aminobenzoic acid (20.571 g, 150 mmol) and bis(3-aminopropyl)amine (9.67 mL, 60 mmol) in ethanol (250 mL) was stirred at 100 °C for 3 d. After this the solvent was removed and the product recrystallised from a EtOH 50:50 $CHCl_3$ mixture at -20 °C giving **11**$^{\mathbf{amideNMe}}$ as a yellow solid in 76 % yield (15.1g, 46.1 mmol). ^{1}H NMR (500.12 MHz, MeOD): δ 7.81 (dd, *J* = 7.9 Hz, 1.6, 2H, Ar-H), 7.17–7.11 (m, 2H, Ar-H), 6.72 (dd, *J* = 8.1 Hz, 1.0, 2H, Ar-H), 6.63–6.57 (m, 2H, Ar-H), 2.96 (t, *J* = 7.2 Hz, 4H, NCH_2), 2.49 (t, *J* = 7.0 Hz, 4H, NCH_2), 2.23 (s, 3H, NCH_3), 1.82 (p, *J* = 7.0 Hz, 4H, NCH_2CH_2); ^{13}C{^{1}H} NMR (125.76 MHz, MeOD): δ 176.07 (s, quaternary), 150.83 (s, quaternary), 132.59 (s, CH, Ar-H), 132.52 (s, CH, Ar-H), 120.53 (s, quaternary), 117.79 (s, CH, Ar-H), 117.17 (s, CH, Ar-H), 56.02 (s, CH_2, NCH_2), 41.64 (s, CH_3, NCH_3), 39.59 (s, CH_2, NCH_2), 25.50 (s, CH_2, NCH_2CH_2); MS(EI): 384.3 ($[M^+ + H]^+$, 15 %), 368.3 ($[M^+ – Me]^+$, 100%); IR (KBr): ν 3460 (N-H), 3336 (N-H), 3286 (N-H), 1664 cm^{-1} (C=O).

6.3.16 Attempted synthesis of $H_2L^{\mathbf{amideNMe}}$

An example procedure: A stirring solution of diamine **11**$^{\mathbf{amideNMe}}$ (0.250 g, 0.763 mmol) and dialdehyde **1** (0.240 g, 0.763 mmol) in ethanol (20 mL) was treated dropwise with TFA (0.30 mL, 1.60 mmol) and the mixture stirred for 4 h during which the colour changed from light red to a slightly darker red. Treatment with NEt_3 until a basic pH was achieved caused a lightening of the colour after which solvent was removed by rotary evaportaion giving a red oil. The ^{1}H NMR spectrum showed a mixture of products. Reactions were attempted using 2 or 5 eq of $BF_3{\cdot}OEt_2$, TFA or *p*-toluenesulfonic acid, at -20 °C, room temperature and 75 °C with either NEt_3 or KOH. Template reactions were attempted by addition of one or two eq of $Ni(OAc)_2$, $Cu(OAc)_2$, $Zn(OAc)_2$ and $Co(OAc)_2$ to mixtures of **11**$^{\mathbf{amideNMe}}$ and **1** in MeOH and stirred overnight. Any precipitate was isolated by filtration and solvents removed under vacuum. Analysis by

^{1}H NMR spectroscopy or EI mass spectrometry indicated the desired product was not present.

6.3.17 Attempted synthesis of urea-dinitro compound, 13

In a synthesis based on work by Lijinsky and Taylor[16] bis-(2-chloroethyl)-amine hydrochloride **3** (0.986 g, 5.52 mmol) was stirred with KOH (0.306 g, 5.52 mmol) in water (0.22 mL), toluene (3 mL) and petroleum ether (3 mL). After stirring for 1 h, the organic layer was separated, the aqueous layer washed with toluene (2 × 2 mL) and dried over $MgSO_4$ and filtered. To this, phenylisocyanate (0.6 mL, 5.52 mmol) was added dropwise, after which the mixture was heated to reflux for 1 h after which solvent was removed under vacuum. The crude yellow solid was washed with toluene to give what was thought to be the urea-dichloride **12** in good yield (1.00 g, 3.86 mmol) (NB: the desired product was not successfully synthesised). This "urea-dichloride" (0.101 g, 0.384 mmol) was mixed with 2-nitrophenol (0.107 g, 0.769 mmol) and K_2CO_3 (0.106 g, 0.769 mmol) in DMF (1 mL) and stirred at 120 °C overnight. The mixture was then poured into water, extracted with $CHCl_3$ (2 × 20 mL), washed with water (4 × 20 mL), dried over $MgSO_4$, filtered and the solvent removed by rotary evaporation. The product was recrystalised from a 1:1 mixture of $CHCl_3$:hexane at -20 °C. The product formed was not the desired product but a mono-nitrophenol-imidazolidinone **15**. ^{1}H NMR (360.13 MHz, $CDCl_3$): δ 8.11 (dd, *J* = 8.5, 1.7 Hz, 1H ,Ar-H), 8.01 (s, 1H, Ar-H), 7.87 (dd, *J* = 8.1, 1.7 Hz, 1H, Ar-H), 7.62–7.56 (m, 1H, Ar-H), 7.56–7.51 (m, 3H, Ar-H), 7.36–7.30 (m, 2H, Ar-H), 4.29 (t, *J* = 4.7 Hz, 2H, CH_2), 3.85–3.78 (m, 4H, CH_2), 3.77 (t, *J* = 7.8 Hz, 2H, CH_2); MS(ESI): *m/z* = 327.1 (M^+ (imidazolidinone), 100 %).

6.3.18 Attempted synthesis of amine-dinitro compound, 16 or 17

16; Direct reaction method: A mixture of bis-(2-chloroethyl)-amine hydrochloride **3** (0.251 g, 1.41 mmol), K_2CO_3 (0.391 g, 2.81 mol) and 2-nitrophenol (0.391 g, 2.81 mmol) in DMF (10 mL) was stirred at 120 °C overnight. The mixture was poured into water, extracted with $CHCl_3$ (2 × 20 mL), washed with water (3 × 50 mL), dried over $MgSO_4$, filtered and solvent removed by rotary evaporation. The ^{1}H NMR spectrum showed that multiple products has formed.

17; *Via* Boc protected amine: A mixture of dichloro-N-Boc-diethylamine (0.680 g, 2.81 mmol), 2-nitrophenol (0.782 g, 0.562 mmol) and Cs_2CO_3 (1.836 g, 5.64 mmol) in

dry DMF (30 mL) was heated to 80 °C and stirred overnight. Workup was performed as above and the ^{1}H NMR spectrum showed that multiple products had formed.

6.3.19 Synthesis of N,N-bis(2-hydroxyethyl)-2,4,6-trimethylaniline, 18

This compound was synthesised by modification of a related method.[17] A 20% NaOH in water solution (60 mL) was added dropwise to a stirring solution of 2,4,6-trimethylaniline (17.5 g, 0.13 mol) and 2-chloroethanol (23.5 g, 0.29 mol) in a sealed ampoule. The reaction was stirred for 4 d at 120 °C. After cooling to room temperature the organic layer was collected and the aqueous layer extracted with EtOAc (5 × 30 mL). The organic layers were combined, dried over $MgSO_4$ and solvent removed by rotary evaporation. The organic product was purified by vacuum distillation with the desired product obtained between 145 and 155 °C at 3 × 10^{-2} mbar in a yield of 30 % (8.6 g, 38.7 mmol). ^{1}H NMR (500.12 MHz, $CDCl_3$): δ 6.91 (s, 2H, Ar-H), 4.43 (s, 2H, OH), 3.65 (t, *J* = 5.0 Hz, 4H, O/N-CH_2), 3.25 (t, *J* = 5.0 Hz, 4H, O/N-CH_2), 2.38 (s, 6H, Ar-CH_3), 2.29 (s, 3H, Ar-CH_3); ^{13}C NMR (125.76 MHz, $CDCl_3$): δ 146.2 (s, quaternary), 137.8 (s, quaternary), 137.1 (s, quaternary), 135.6 (s, quaternary), 129.9 (s, CH, Ar-H), 62.3 (s, CH_2, O/N-CH_2), 58.5 (s, CH_2, O/N-CH_2), 20.8 (s, CH_3, Ar-CH_3), 19.0 (s, CH_3, Ar-CH_3); MS(EI): *m/z* = 223.1 (M^+, 5%), 192.1 ($[M^+–2Me]^+$, 100%) 148.1 ($[M^+–2(CH_2OH)–CH_3]^+$, 50%); Analysis. Found: C, 69.83; H, 9.36; N, 6.19; $C_{13}H_{22}NO_2$ requires: C, 69.92; H, 9.48; N, 6.27 %; IR (KBr, nujol): ν 3251cm^{-1} (OH).

6.3.20 Synthesis of N,N-bis(2-chloroethyl)-2,4,6-trimethylaniline, 19

Synthesised by a modification of a related method,[17] 2-hydroxyethyl-2,4,6-trimethylaniline **18** (8.6 g, 38.7mmol) was placed in an ampoule under a flow of nitrogen and cooled to -60 °C. Neat $POCl_3$ (7.8 mL, 85 mmol) was added dropwise with stirring. The ampoule was sealed and the reaction mixture heated at 110 °C for 2.5 h before being allowed to cool to room temperature and extracted with EtOAc (3 × 50 mL). The organic layer was washed with water until the washings themselves became neutral. The organic layers were dried over $MgSO_4$ and solvent removed by rotary evaporation giving **19** in 76 % yield (7.7 g, 0.03 mol). ^{1}H NMR (500.12 MHz, $CDCl_3$): δ 7.30 (s, 2H, Ar-H), 3.54 (t, *J* = 5.0 Hz, 4H, O/N-CH_2), 3.43 (t, *J* = 5.0 Hz, 4H, O/N-CH_2), 2.23 (s, 6H, Ar-CH_3), 2.30 (s, 3H, Ar-CH_3); ^{13}C{^{1}H} NMR (125.76 MHz, $CDCl_3$): δ 143.7 (s, quaternary), 137.2 (s, quaternary), 135.7 (s, quaternary), 129.3 (s, CH, Ar-H), 57.8 (s, CH_2, O/N-CH_2), 42.8 (s, CH_2, O/N-CH_2), 21.0

(s, CH_3, Ar-CH_3), 18.4 (s, CH_3, Ar-CH_3); MS(EI): *m/z* = 259.1 (M^+, 5%), 210.1 ($[M^+–CH_2Cl]^+$, 100%), 146.1 ($[M^+–2(CH_2Cl)]^+$, 23%).

6.3.21 Synthesis of N-mesityl-2,2'-bis(*o*-nitrophenoxy)diethylamine, 20

In a modification of the syntheses of related compounds,[11, 14] dichloride **19** (7.733 g, 0.03 mol) was added to a mixture of 2-nitrophenol (11.2 g, 0.036 mol) and K_2CO_3 (11.28 g, 0.082 mol) in DMF (25 mL). The reaction was refluxed for 2 d until a red brown colour persisted and then allowed to cool to room temperature. The reaction mixture was poured onto water (100 mL) and extracted with chloroform (3 × 50 mL). The product was reduced to a minimum volume by rotary evaporation and purified by column chromatography on alumina with hexane/EtOAc (1:2) eluent. Rf = 0.86, Yield = 81% (11.2 g, 0.0242 mol). ^{1}H NMR (500.12 MHz, $CDCl_3$): δ 7.84 (m, 2H, Ar-H), 7.53 (t, *J* = 7.9 Hz, 2H, Ar- H), 7.09 (d, *J* = 8.5 Hz, 2H Ar-H), 7.02 (m, 2H, Ar-H), 6.87 (s, 2H, Ar-H), 4.11 (t, J =5.0 Hz, 4H, CH_2), 3.64 (t, *J* = 5.5 Hz, 4H, CH_2), 2.27 (s, 6H, Ar-CH_3), 2.26 (s, 3H, Ar-CH_3); ^{13}C{^{1}H} NMR (125.76 MHz, $CDCl_3$): δ 171.2 (s, quaternary),152.3 (s, quaternary), 139.7 (s, quaternary), 135.4 (s, quaternary), 137.8 (s, quaternary), 143.8 (s, quaternary), 134.2 (s, CH, Ar-H), 129.7 (s, CH, Ar-H), 125.6 (s, CH, Ar-H), 129.7 (s, CH, Ar-H), 114.2 (s, CH, Ar-H), 69.0 (s, CH_2, O/N-CH_2), 54.0 (s, CH_2, O/N-CH_2), 20.87 (s, CH_3, Ar-CH_3), 18.7 (s, CH_3, Ar-CH_3); MS(EI): *m/z* = 465.1 (M^+, 3 %) 195.1 ($[M^+–C_7H_6NO_3]^+$, 100 %) 148.1 ($[M^+–2(C_7H_6NO_3)]^+$, 8 %); Analysis. Found: C, 64.43; H, 5.93 N, 9.04 %; $C_{23}H_{27}N_3O_6$ requires C, 64.50; H, 5.85; N, 9.03 %.

6.3.22 Synthesis of N-mesityl-2,2'-bis(o-aminophenoxy)diethylamine, 21

The dinitro compound **20** (5.04 g, 0.011 mol) was reduced by H_2 and 10 % Pd/C (0.25 g) in an ethanol (90 mL) and THF (90 mL) mixture. The solution was reacted under an atmosphere of H_2 for 2 d, the catalyst was removed by filtration under reduced pressure and the product washed with ethanol (3 × 50 mL). The solvent was removed by rotary evaporation and **21** obtained in a yield of 98 %. (4.30 g, 0.012 mol). ^{1}H NMR (500.12 MHz, $CDCl_3$): δ 7.28 (s, 4H, NH_2), 6.89 (s, 2H, Ar-H), 6.81 (m, 2H, Ar-H), 6.73 (m, 6H, Ar-H), 4.06 (t, *J* = 5.8 Hz, 4H, CH_2), 3.61 (t, *J* = 5.8 Hz, 4H, CH_2), 2.35 (s, 6H, Ar-CH_3), 2.28 (s, 3H, Ar-CH_3); ^{13}C{^{1}H} NMR (125.76 MHz, $CDCl_3$): δ 146.5 (s, quaternary), 145.0 (s, quaternary), 137.5 (s, quaternary), 136.2 (s, quaternary), 135.1 (s, quaternary), 129.7 (s, quaternary), 121.2 (s, CH, Ar-H), 118.3 (s, CH, Ar-H), 115.1 (s, CH, Ar-H), 111.15 (s, CH, Ar-H), 67.9 (s, CH_2), 54.6 (s, CH_2), 20.82 (s, CH_3, Ar-CH_3),

19.1 (s, CH_3, Ar-CH_3); MS(EI): *m/z* = 406.2 (M^+, 2 %), 297.2 ($[M^+–C_7H_6NO_3]^+$, 64 %), 192.1 ($[M^+–2(C_7H_6NO_3)]^+$,100 %); Analysis. Found: C, 74.34; H, 7.16; N, 10.36 %; $C_{23}H_{29}N_3O_2$ requires: 74.04; H, 7.70; N, 10.36 %; IR (KBr, nujol): ν 3466 (N-H), 3367 cm^{-1} (N-H).

6.3.23 Synthesis of H_2L^{NMes}

A mixture of dialdehyde **1** (2.13 g, 8.234 mmol) and diamine **21** (3.34 g, 8.234 mmol) were combined in absolute ethanol (200 mL) and gently warmed, purging with nitrogen, until complete dissolution. BF_3·OEt (1 mL) was added dropwise, a colour change was observed from red to yellow. The solution was stirred for 4 h, during whch a yellow precipitate formed. The solid was isolated by filtration then dissolved in CH_2Cl_2 (*ca*. 100 mL) and a 7 M NH_3 solution in MeOH (11 mL) added drop wise. The solid was isolated by filtration and dried under reduced pressure to obtain a yellow product in a yield of 77% (3.98 g, 6.331 mmol). ^{1}H NMR (599.81 MHz, $CDCl_3$): δ 8.84 (s, 2H, NH), 8.12 (s, 2H, imine), 7.03–6.98 (m, 2H, Ar-H), 6.93–6.90 (m, 4H, 2 × Ar-H), 6.80 (s, 2H, Mes-H), 6.75 (d, *J* = 8.1 Hz, 2H, Ar-H), 6.61 (d, *J* = 3.6 Hz, 2H, pyrrole), 6.29 (d, *J* = 3.6 Hz, 2H, pyrrole), 3.84 (t, *J* = 5.4 Hz, 4H, O-CH_2), 3.52 (t, *J* = 5.4 Hz, 4H, N-CH_2), 2.22 (s, 3H, *p*-Mes-CH_3), 2.20 (s, 6H, 2 × *o*-Mes-CH_3), 2.06 (q, *J* = 7.4 Hz, 4H, Et-CH_2), 0.82 (t, *J* = 7.3 Hz, 6H, Et-CH_3); $^{13}C\{^1H\}$ NMR (150.82 MHz, $CDCl_3$): δ 153.81 (s, CH, imine), 153.63 (s, quaternary), 145.81 (s, quaternary), 145.20 (s, quaternary), 144.12 (s, quaternary), 140.29 (s, quaternary), 137.07 (s, quaternary), 133.41 (s, quaternary), 132.13 (s, CH, Mes-H), 128.19 (s, CH, Ar-H), 124.37 (s, CH, Ar-H), 123.51 (s, CH, Ar-H), 119.13 (s, CH, pyrrole-H), 117.43 (s, CH, Ar-H), 111.92 (s, CH, pyrrole-H), 72.09 (s, CH_2, NCH_2), 56.29 (s, CH_2, OCH_2), 46.70 (s, quaternary), 31.68 (s, CH_2, Et-CH_2), 22.39 (s, CH_3, Mes-CH_3), 21.59 (s, CH_3, Mes-CH_3), 10.93 (s, CH_3, Et-CH_3); MS(EI): *m/z* = 627.3 (M^+, 8%), 408.3 ($[M^+–C_{13}H_{19}NO_2$-2$(CH_3)]^+$, 100%); Analysis. Found: 76.57; H, 7.16 N; 11.17 %; $C_{40}H_{45}N_5O_2$ requires: C, 76.52; H, 7.22; N, 11.16 %; IR (KBr, nujol): ν 3437 (N-H), 1624 (C=N), 1499 cm^{-1} (C=C).

6.3.24 Synthesis of [Pd(L^{NMes})]

A solution of H_2L^{NMes} (0.20 g, 3.20 mmol) and $Pd(OAc)_2$ (0.072 g, 3.20 mmol) in dry toluene (20 mL) was stirred for 1 h. NEt_3 (0.032 g, 0.023 mL) was added dropwise and the reaction stirred for 2 d. The solvent was removed under reduced pressure, the product extracted into hexane (100 mL) and solvent removed under vacuum to obtain a yellow solid in a yield of 68 % (0.15 g, 0.22 mol). ^{1}H NMR (500.12 MHz, $CDCl_3$): δ

7.54 (s, 2H, imine), 6.96 (d, *J* = 3.9 Hz, 2H, pyrrole), 6.93–6.89 (m, 2H, Ar-H), 6.84 (s, 1H, Mes-H), 6.79 (dd, *J* = 7.7 Hz, 2H, Ar-H), 6.78 (s, 1H, Mes-H), 6.51–6.45 (m, 4H, 2 × Ar-H), 6.21 (d, *J* = 3.9 Hz, 2H, pyrrole), 4.09–4.02 (m, 2H, N/OCH$_2$), 3.77–3.69 (m, 4H, N/OCH$_2$), 3.22–3.14 (m, 2H, N/OCH$_2$), 2.23 (s, 3H, Mes-CH$_3$), 2.20 (s, 3H, Mes-CH$_3$), 2.17 (q, *J* = 7.1 Hz, 2H, Et-CH$_3$), 2.10 (s, 3H, Mes-CH$_3$), 2.07 (q, *J* = 7.1 Hz, 2H, Et-CH$_2$), 0.58 (t, *J* = 7.2 Hz, 3H, Et-CH$_3$), 0.51 (t, *J* = 7.2 Hz, 3H, Et-CH$_3$); ^{13}C{^{1}H} NMR (125.76 MHz, $CDCl_3$): δ 159.90 (s, CH, imine), 151.27 (s, quaternary), 148.53 (s, quaternary), 147.61 (s, quaternary), 138.31 (s, quaternary), 136.95 (s, quaternary), 136.35 (s, quaternary), 136.34 (s, quaternary), 134.83 (s, quaternary), 130.29 (s, CH, Ar-H), 128.76 (s, CH, Ar-H), 125.87 (s, CH, Ar-H), 123.88 (s, CH, Ar-H), 120.21 (s, CH, Ar-H), 118.65 (s, CH, Ar-H), 111.97 (s, CH, Ar-H), 107.24 (s, CH, Ar-H), 69.94 (s, CH$_2$, O/N-CH$_2$), 53.76 (s, quaternary), 53.51 (s, CH$_2$, O/N-CH$_2$), 38.90 (s, CH$_2$, Et-CH$_2$), 36.74 (s, CH$_2$, Et-CH$_2$), 20.71 (s, CH$_3$, Ar-CH$_3$), 19.14 (s, CH$_3$, Ar-CH$_3$), 18.80 (s, CH$_3$, Ar-CH$_3$), 9.93 (s, CH$_3$, Et-CH$_3$), 9.46 (s, CH$_3$, Et-CH$_3$); MS(EI): *m/z* = 731.2 (M^+, 3%), 702.1 ([M^+–2(CH$_3$)]$^+$, 100%); Analysis. Found: 65.54; H, 5.97; N, 9.50; $C_{40}H_{43}N_5O_2Pd$ requires: C, 65.61; H, 5.92; N, 9.56 %; IR (KBr, nujol): ν 1560 (C=N), 1497 cm^{-1} (C=C).

6.3.25 Synthesis of [Co(L^{NMes})]

H_2L^{NMes} (0.19 g, 0.298 mmol) was combined with KH (0.070 g, 1.78 mmol) and THF (20 mL). Gas evolved immediately, and, once effervescence had ceased, the mixture was filtered onto a stirring suspension of $CoCl_2$ (0.039g, 0.298 mmol) and stirred at room temperature for 16 h. Filtration followed by solvent removal under reduced pressure gave [Co(L^{NMes})] as a red solid. (0.153 g, 2.23 mmol, 75 %). ^{1}H NMR (599.81 MHz, C_6D_6): δ 73.63 (2H), 45.37 (2H), 3.68 (3H), 2.19 (2H), 1.53 (2H), 0.44 (3H), -0.12 (3H), -3.38 (2H), -3.92 (2H), -5.41 (2H), -5.73 (2H), -8.35 (2H), -9.09 (2H), -14.21 (2H), -14.75 (2H), -20.19 (1H), -22.78 (1H), -30.16 (3H), -33.01 (3H), -42.96 (2H); Analysis. Found: C, 70.00; H, 6.21; N, 10.15; $C_{40}H_{43}N_5O_2Co$ requires: C, 70.16; H, 6.33; N, 10.23 %; MS(EI): *m/z* = 684.2(M^+, 41%); IR (KBr, nujol): ν 1558 (C=N), 1499 cm^{-1} (C=C).

6.3.26 Synthesis of 3,3'-bis(o-nitroanilino) N-methyl dipropylamine, 23

In a modification of reported procedures,[18] a mixture of 2-fluoronitrophenol (20 mL, 0.19 mol), 0.9 eq of 3,3'-diamino-N-methyldipropylamine **22** (27.5 mL, 0.17 mol) and $CaCO_3$ (40 g, 0.4 mol) in CH_2Cl_2 (*ca*. 250 mL) was stirred at room temperature overnight. The resulting orange mixture was filtered and solvents removed under

reduced pressure to give crude **23**. This was purified by gradient column chromatography on silica 2% MeOH/CH_2Cl_2 to 5% MeOH/CH_2Cl_2 giving pure **23** as a thick bright orange oil. (11.0 g, 28.4 mmol, 30 %). ^{1}H NMR (500.12 MHz, $CDCl_3$): δ 8.31 (br, s, 2H, NH), 8.12 (dd, 2H, *J* = 8.6, 1.6 Hz, aryl), 7.37 (m, 2H, aryl), 6.80 (dd, 2H, *J* = 8.7, 0.9 Hz, aryl), 6.58 (m, 2H, aryl), 3.36 (m, 4H, NCH_2), 2.52 (t, 4H, *J* = 6.6 Hz, NCH_2), 2.29 (s, 3H, NCH_3), 1.89 (m, 4H, NCH_2CH_2); ^{13}C{^{1}H} NMR (125.76 MHz): δ 145.6 (s, quaternary), 136.2 (s, CH, Ar-H), 131.8 (s, quaternary), 126.9 (s, CH, Ar-H), 115.0 (s, CH, Ar-H), 113.7 (s, CH, Ar-H), 55.8 (s, CH_2, NCH_2), 42.0 (s, CH_3, NCH_3), 41.7 (s, CH_2, NCH_2), 26.3 (s, CH_2, NCH_2CH_2); HRMS(ESI): 388.19760 ($[M^+ + H]^+$); IR (KBr): ν 3380 (N-H), 1616 (NO_2), 1351 cm^{-1} (NO_2).

6.3.27 Synthesis of 3,3'-bis(*o*-aminoanilino) N-methyl dipropylamine, 24

A mixture of **23** (1.0 g, 2.58 mmol) and 10 % Pd/C (0.05 g) in EtOH (100 mL) was stirred at room temperature overnight under a H_2 atmosphere. The catalyst was removed by filtration and solvents removed by rotary evaporator to give the crude product as a purple solid. Stirring in Et_2O (75 mL) for 3 h gave pure **24** as a white solid which was isolated by filtration (0.828 g, 2.53 mmol, 98 %). ^{1}H NMR (500.12 MHz, $CDCl_3$): δ 6.82 (m, 2H, aryl), 6.72–6.62 (m, 6H, aryl), 4.04 (br, s, 2H, NH), 3.34 (br, s, 4H, NH_2), 3.20 (t, 4H, *J* = 6.6Hz, NCH_2), 2.53 (t, 4H, *J* = 6.8Hz, NCH_2), 2.31 (s, 3H, N-CH_3), 1.88 (m, 4H, N CH_2CH_2); ^{13}C{^{1}H} NMR (125.76 MHz): δ 138.0 (s, quaternary), 134.2 (s, quaternary), 120.6 (s, CH, Ar-H), 118.3 (s, CH, Ar-H), 116.2 (s, CH, Ar-H), 111.5 (s, CH, Ar-H), 56.7 (s, CH_2, NCH_2), 43.3 (s, CH_2, NCH_2), 42.2 (s, CH_3, NCH_3), 26.8 (s, CH_2, N CH_2CH_2); MS(ESI): *m/z* = 327.24 (M^+, 100 %), 592.1 ($[M^+ – PhNH_2]^+$, 15 %); Analysis. Found: C, 69.78; H, 9.02; N, 21.28; $C_{19}H_{29}N_5$ requires: C, 69.69; H, 8.93; N, 21.39 %; IR (KBr): ν 3390 (N-H), 3350 (N-H), 3291 cm^{-1} (N-H).

6.3.28 Synthesis of $H_2L^{(NH)NMe}$

A stirring solution of diamine **24** (2.0 g, 5.31 mmol) and dialdehyde **1** (1.37 g, 5.31 mmol) in MeOH (100 mL) was treated with 2.1 eq of TFA (0.86 mL), turning the solution deep red. After 3 h, 2.5 eq of KOH (0.74 g, 13.3 mmol) in MeOH (20 mL) was added causing a yellow precipitate to form. The mixture was filtered, the filtrate isolated and the solvent removed by rotary evaporation giving $H_2L^{(NH)NMe}$ as a yellow solid (0.291 g, 5.30 mmol, 10%). ^{1}H NMR (399.90 MHz, $CDCl_3$): δ 8.85 (br, s, 2H, pyrrole-NH), 8.19 (s, 2H, imine), 7.09–7.04 (m, 2H, Ar-H), 6.92 (dd, *J* = 7.7, 1.3 Hz, 2H, Ar-H), 6.65 (d, *J* = 7.5 Hz, 2H, Ar-H), 6.61 (d, *J* = 7.7 Hz, 2H, Ar-H), 6.60 (d, *J* = 3.8

Hz, 2H, pyrrole), 6.14 (d, *J* = 3.7 Hz, 2H, pyrrole), 4.89 (br, s, 2H, NH), 3.22 (s, 4H, NCH_2), 2.50 (t, *J* = 7.1 Hz, 4H, NCH_2), 2.28 (s, 3H, NCH_3), 2.23 (q, *J* = 7.3 Hz, 4H, Et-CH_2), 1.88–1.79 (m, 4H, N CH_2CH_2), 0.88 (t, *J* = 7.3 Hz, 6H, Et-CH_3); $^{13}C\{^1H\}$ NMR (125.76 MHz, $CDCl_3$): δ 147.46 (s, CH, imine), 143.20 (s, quaternary), 138.05 (s, quaternary), 134.22 (s, quaternary), 130.72 (s, quaternary), 126.98 (s, CH, Ar-H), 120.62 (s, CH, Ar-H), 118.29 (s, CH, Ar-H), 116.20 (s, CH, Ar-H), 111.61 (s, CH, pyrrole), 110.25 (s, CH, pyrrole), 56.67 (s, CH_2, NCH_2), 54.44 (s, CH_2, NCH_2), 43.98 (s, CH_2, NCH_2CH_2), 43.33 (s, quaternary), 43.18 (s, CH_3, NCH_3), 28.37 (s, CH_2, Et-CH_2), 8.23 (s, CH_3, Et-CH_3); MS(EI): 549.3 (M^+, 40%), 545.7 (bicyclic M^+, 30%), 537.3 ($[M^+–Me]^+$, 40%), 518.3 ($[M^+–2Me]^+$, 100 %); Analysis. Found: C, 74.15; H, 7.92; N, 17.64; $C_{34}H_{43}N_7$ requires: C, 74.28; H, 7.88; N, 17.83 %; IR (nujol, KBr): ν 3444 (N-H), 3306 (N-H), 1614 (C=N), 1511 cm^{-1}(C=C).

6.3.29 Synthesis of Bicyclic $H_2L^{(NH)NMe}$

$H_2L^{(NH)NMe}$ (50 mg, 0.091mmol) was dissolved in a mixture of MeOH (2 mL) and CH_2Cl_2 (2 mL), layered with Et_2O (3 mL) and left to stand for 3 d yielding crystals of the bicyclic product. ^1H NMR (500.12 MHz, $CDCl_3$): δ 9.04 (br, s, 2H, pyrrole NH), 7.65 (m, 2H, aryl), 7.21 (m, 4H, aryl), 6.46 (m, 2H, pyrrole), 6.23 (m, 2H, pyrrole), 4.39 (m, 4H, NCH_2), 2.20 (q, 4H, *J* = 7.3Hz, Et-CH_2), 1.67 (m, 11H, NCH_2+NCH_2CH_2+NCH_3), 0.82 (t, 6H, *J* = 7.3Hz, Et-CH_3); $^{13}C\{^1H\}$ NMR (125.76 MHz): δ 147.9 (s, quaternary), 140.5 (s, quaternary), 135.0 (s, quaternary), 122.5 (s, CH, Ar-H), 122.4 (s, CH, Ar-H), 119.2 (s, CH, Ar-H), 110.4 (s, CH, pyrrole), 109.9 (s, CH, Ar-H), 107.0 (s, CH, pyrrole), 55.48 (s, CH_2, NCH_2), 43.10 (s, quaternary), 42.49 (s, CH_2, NCH_2), 39.81 (s, CH_3, NCH_3), 26.43 (s, CH_2, Et-CH_3), 26.25 (s, CH_2, NCH_2CH_2), 7.98 (s, CH_2, Et-CH_3).

6.3.30 Synthesis of [Pd($L^{(NH)NMe}$)]

A solution of $H_2L^{(NH)NMe}$ (0.208 g, 0.378 mmol) and $Pd(OAc)_2$ (85 mg, 0.378 mmol) in CH_2Cl_2 (10 mL) was stirred for 30 mins, giving a deep red solution. To this, 2.1 eq of NEt_3 (1.1 mL, 0.796 mmol) was added dropwise and the solution stirred overnight. The solvent was removed under vacuum, toluene (2 mL) added, and the product extracted with hexane (*ca.* 15 mL) giving [Pd($L^{(NH)NMe}$)] as a yellow solid (49 mg, 0.076 mmol, 20 %). ^1H NMR (500.12 MHz, $CDCl_3$): δ 7.61 (s, 2H, imine), 6.89 (d, *J* = 3.9 Hz, 2H, pyrrole), 6.78 (td, *J* = 7.9, 1.5 Hz, 2H, Ar-H), 6.49 (dd, *J* = 7.6, 1.4 Hz, 2H, Ar-H), 6.25–6.17 (m, 4H, Ar-H + pyrrole), 6.12 (dd, *J* = 8.0, 0.7 Hz, 2H, Ar-H),

3.03 (dt, *J* = 10.4, 3.3 Hz, 2H, NCH_2), 2.77–2.68 (m, 2H, NCH_2), 2.51–2.38 (m, 4H, 2 × NCH_2), 2.17 (q, *J* = 7.2 Hz, 2H, Et-CH_2), 2.07 (q, *J* = 7.3 Hz, 2H, Et-CH_2), 1.95 (s, 3H, NCH_3), 1.86–1.77 (m, 4H, 2 × NCH_2CH_2), 0.53 (t, *J* = 7.3 Hz, 3H, Et-CH_3), 0.50 (t, *J* = 7.4 Hz, 3H, Et-CH_3); $^{13}C\{^1H\}$ NMR (125.76 MHz, $CDCl_3$): δ 160.98 (s, CH, imine), 148.65 (s, quaternary), 141.73 (s, quaternary), 136.20 (s, quaternary), 134.82 (s, quaternary), 126.55 (s, CH, imine), 125.40 (s, CH, Ar-H), 122.53 (s, CH, Ar-H), 118.79 (s, CH, Ar-H), 116.49 (s, CH, Ar-H), 109.92 (s, CH, pyrrole), 107.57 (s, CH, Ar-H), 53.99 (s, quaternary), 52.95 (s, CH_2, NCH_2), 42.66 (s, CH_3, NCH_3), 41.90 (s, CH_2, NCH_2), 38.89 (s, Et-CH_2), 36.81 (s, Et-CH_2), 25.17 (s, CH_2, NCH_2CH_2), 9.91 (s, Et-CH_3), 9.75 (s, Et-CH_3); MS(EI): *m/z* = 653.2 (M^+, 30 %), 624.1 ($[M^+–2Me]^+$, 100 %), 622.1 ($[M^+–2Me\text{-}2H]^+$, 5 %); Analysis. Found: C, 62.32; H, 6.25; N, 14.85; $C_{34}H_{41}N_7Pd$ requires: C, 62.43; H, 6.32; N, 14.99 %; IR (KBr): ν 3354 (N-H), 1591 (C=N), 1509 cm^{-1} (C=C).

6.3.31 Synthesis of [Co($L^{(NH)NMe}$)]

Addition of THF (2 mL) to a mixture of $H_2L^{(NH)NMe}$ (30 mg, 0.055 mmol) and KH (11 mg, 0.27 mmol) resulted in immediate effervescence of hydrogen. This was stirred for 3 h during which the solution turned a deep red colour. The solution was filtered onto a suspension of $CoCl_2$ (7 mg, 0.055 mmol) in THF (1 mL). The deep red mixture was stirred overnight after which the mixture was filtered and solvents removed giving [Co($L^{(NH)NMe}$)] as a red solid (15 mg, 0.025 mmol, 46 %). MS(EI): *m/z* = 606.3 (M^+, 3 %), 575.2 ($[M^+–2Me]^+$, 100 %).

6.4 Synthetic procedures as described in Chapter 4

6.4.1 Synthesis of H_4L^{Et}

A mixture of 2,4-dimethyl-1,2-diaminobenzene (21.0 g, 0.155 mol) and dialdehyde **1** (40.0 g, 0.155 mol) was warmed in MeOH (900 mL) until complete dissolution. To this solution was added a solution of $TsOH{\cdot}H_2O$ (65.0 g, 0.342 mol) in MeOH (90 mL) and the resulting deep red solution was stirred for 45 min, after which a bright orange precipitate had formed. The solids were collected on a glass frit, washed with MeOH (3 × 10 mL), and then suspended in MeOH (1000 mL). Neat NEt_3 was added dropwise until the conversion to a yellow solid was complete and the liquors strongly basic. The neutral ligand H_4L^{Et} was collected on a glass frit, washed with cold MeOH (3 × 10 mL) and hexane (3 × 10 mL) and dried under reduced pressure at 100 °C

to yield 39.0 g (70 %) of H_4L^{Et} as bright yellow solids. ^{1}H NMR (360.13 MHz, $CDCl_3$): δ 9.02 (s, 4H, NH), 8.06 (s, 4H, imine), 6.81 (s, 4H, Ar-H), 6.41 (m, 4H, pyrrole), 6.06 (m, 4H, pyrrole), 2.21 (s, 12H, Ar-Me), 1.99 (q, *J* = 7.3 Hz, 4H, Et-CH_2), 0.675 (t, *J* = 7.4 Hz, 12H, Et-CH_3); $^{13}C\{^1H\}$ NMR (90.55 MHz, $CDCl_3$): δ 148.9 (s, CH, imine), 143.3 (quaternary), 134.7 (quaternary), 131.1 (quaternary), 119.9 (s, CH, Ar-H), 116.8 (s, CH, pyrrole), 108.0 (s, CH, pyrrole), 44.0 (quaternary), 27.7 (s, CH_2, Et-CH_2), 19.8 (s, CH_3, Ar-CH_3), 8.7 (s, CH_3, Et-CH_3); MS(EI): *m/z* = 717 ($[M^+ + H]^+$, 100 %); Analysis. Found: C, 76.99; H, 7.27; N, 15.56; $C_{46}H_{52}N_8$ requires: C, 77.06; H, 7.31; N, 15.63 %; IR (nujol, KBr): ν 3303 (N-H), 1680 (C=N), 1552 cm^{-1} (C=C).

6.4.2 Synthesis of [$SnMe_2(H_2L^{Et})$]

A solution of Me_2SnCl_2 (0.220 g, 1.00 mmol) in toluene (10 mL) was added dropwise to a stirred solution of H_4L^{Et} (0.718 g, 1.00 mmol) and 1,4-diazabicyclo[2.2.2]octane, DABCO, (0.337 g, 3.00 mmol) in toluene (40 mL) at -80 °C, the solution changing colour from yellow to red. The resulting mixture was allowed to warm to room temperature and stirred for 14 h, during which a white precipitate formed. The solvents were evaporated under vacuum and the product extracted into toluene (3 × 20 mL), the filtrate evaporated and the resulting yellow powder washed with warm hexane (2 × 15 mL). Excess DABCO was removed by sublimation (100 °C, 2 × 10^{-2} mbar) to afford 0.630 g, 73 % of [$SnMe_2(H_2L^{Et})$] as a light yellow powder. ^{1}H NMR (360.13 MHz, $CDCl_3$): δ 9.29 (br, s, 2H, pyrrole NH), 8.00 (s, 2H, imine), 7.87 (s, 2H, imine), 6.81 (d, 2H, *J* = 3.5 Hz, pyrrole), 6.80 (s, 2H, Ar-H), 6.53 (s, 2H, Ar-H), 6.51 (d, 2H, *J* = 3.9 Hz, pyrrole), 6.31 (d, 2H, *J* = 3.5 Hz, pyrrole), 6.08 (d, 2H, *J* = 3.9 Hz, pyrrole), 2.22 (s, 6H, Ar-CH_3), 2.19 (s, 6H, Ar-CH_3), 2.18 (q, 2H, *J* = 7.0 Hz, Et-CH_2), 2.05 (q, 2H, *J* = 7.5 Hz, Et-CH_2), 1.92 (q, 2H, *J* = 7.5 Hz, Et-CH_2), 1.82 (q, 2H, *J* = 7.0 Hz, Et-CH_2), 1.28 (s, 3H, J_{SnCH3} = 92 Hz, Sn-CH_3), 0.86 (t, 3H, *J* = 7.5 Hz, Et-CH_3), 0.81 (t, 3H, *J* = 7.01 Hz, Et-CH_3), 0.65 (t, 3H, *J* = 7.01 Hz, Et-CH_3), 0.55 (s, 3H, J_{SnCH3} = 109 Hz, Sn-CH_3), 0.52 (t, 3H, *J* = 7.5 Hz, Et-CH_3); $^{13}C\{^1H\}$ NMR (90.55 MHz, CDCl3): δ 153.3 (s, CH imine), 150.7 (s, quaternary), 149.3 (s, CH, imine), 141.8 (s, quaternary), 140.0 (s, quaternary), 133.1 (s, quaternary), 132.7 (s, quaternary), 129.7 (s, quaternary), 128.0 (s, quaternary), 127.2 (s, quaternary), 123.1 (s, CH, Ar-H), 120.3 (s, CH, Ar-H), 118.0 (s, CH, pyrrole), 115.8 (s, CH, pyrrole), 108.7 (s, CH, pyrrole), 107.0 (s, CH, pyrrole), 76.2 (s, CH, pyrrole), 46.3 (s, quaternary), 43.9 (s, quaternary), 41.7 (s, CH_2, Et-CH_2), 34.3 (s, CH_2, Et-CH_2), 30.2 (s, CH_2, Et-CH_2), 30.0

(s, CH_2, Et-CH_2), 18.2 (s, CH_3, Ar-CH_3), 18.1 (s, CH_3, Ar-CH_3), 9.0 (s, CH_3, Et-CH_3), 8.8 (s, CH_3, Sn-CH_3), 8.6 (s, CH_3, Et-CH_3), 7.9 (s, CH_3, Et-CH_3), 7.8 (s, CH_3, Et-CH_3), 5.1 (s, CH_3, Sn-CH_3); due to the low solubility of this compound, no $^1J_{SnC}$ information could be gained; MS(EI): *m/z* = 864.4 (M^+, 6 %), 849.4 ($[M^+\text{-Me}]^+$, 4 %), 835.4 ($[M^+\text{–Et}]^+$, 100 %); Analysis. Found: C, 66.15; H, 6.90; N, 12.87. $C_{48}H_{56}N_8Sn$ requires: C, 66.75; H, 6.54; N, 12.97 %; IR (nujol, KBr): ν 3441 (N-H), 1608 (C=N), 1598 cm^{-1} (C=C).

6.4.3 Attempted synthesis of [$SnPh_2(H_2L^{Et})$] and [$SnBu_2(H_2L^{Et})$]

The syntheses were carried out in a similar manner to that described above with; Ph_2SnCl_2 (48 mg, 0.140 mmol), H_4L^{Et} (0.100 g, 0.140 mmol) and DABCO (31 mg, 0.420 mmol), in either THF (5 mL) or toluene (5 mL), to give 50 mg of yellow solid or; Bu_2SnCl_2 (43 mg, 0.140 mmol), H_4L^{Et} (0.100 g, 0.140 mmol) and DABCO (31 mg, 0.420 mmol), in either THF (5 mL) or toluene (5 mL) to give 40 mg of yellow solid. The ^{1}H NMR spectra of all reactions showed unidentifiable mixtures of products.

6.4.4 Synthesis of [$SnMe_2Zn(THF)(L^{Et})$]

A solution of [$Zn\{N(SiCH_3)_2\}_2$] (0.054 g, 0.014 mmol) in THF (10 mL) was added dropwise to a stirred solution of [$SnMe_2(H_2L^{Et})$] (0.12 g, 0.14 mmol) in THF (10 mL) at -80 °C. The resulting yellow solution was allowed to warm to room temperature and stirred for 16 h. The solvents were removed under reduced pressure to generate 0.11 g, 80 % of [$SnMe_2Zn(THF)(L^{Et})$] as a yellow powder. ^{1}H NMR (360.13 MHz, C_6D_6): δ 7.86 (s, 2H, imine), 7.54 (s, 2H, imine), 6.94 (d, 2H, *J* = 3.6 Hz, pyrrole), 6.90 (s, 2H, Ar-H), 6.77 (d, 2H, *J* = 3.6 Hz, pyrrole), 6.47 (d, 2H, pyrrole, *J* = 3.6 Hz), 6.38 (d, 2H, *J* = 3.9 Hz, pyrrole), 6.20 (s, 2H, Ar-H), 3.75 (t, 4H, THF-CH_2) 2.22–2.20 (m, 12H, 3 × Et-CH_2 + Ar-CH_3), 1.90 (q, 2H, *J* = 7.3 Hz, Et-CH_2), 1.73 (s, 6H, Ar-CH_3), 1.39 (m, 4H, THF-CH_2), 1.13 (s, 3H, J_{SnCH3} = 91.1 Hz, Sn-CH_3), 0.97 (t, 3H, *J* = 7.3 Hz, Et-CH_3), 0.90 (t, 3H, *J* = 6.9 Hz, Et-CH_3), 0.80 (t, 3H, *J* = 7.3 Hz, Et-CH_3), 0.49 (t, 3H, *J* = 6.9 Hz, Et-CH_3), 0.06 (s, 3H, J_{SnCH3} = 96.1 Hz, Sn-CH_3); $^{13}C\{^1H\}$ (90.55 MHz, $CDCl_3$): δ 161.74 (s, CH, imine), 156.70 (s, CH, imine), 153.61 (s, quaternary), 150.73 (s, CH), 146.31 (s, quaternary), 141.30 (s, quaternary), 134.53 (s, quaternary), 133.54 (s, quaternary), 133.13 (s, quaternary), 132.44 (s, quaternary), 127.81 (quaternary), 125.33 (s, CH, Ar-H), 125.53 (s, CH, Ar-H), 120.19 (s, CH, pyrrole), 119.90 (s, CH, pyrrole), 112.54 (s, CH, pyrrole), 111.05 (s, CH, pyrrole), 68.79 (s, CH_2, THF), 48.81 (s, quaternary), 47.39 (s, quaternary), 41.25 (s, CH_2, Et-CH_2), 39.46 (s, CH_2, Et-CH_2), 39.14

(s, CH_2, Et-CH_2), 31.75 (s, CH_2, Et-CH_2), 25.69 (s, CH_2, THF), 19.51 (s, CH_3, Ar-CH_3), 18.87 (s, CH_3, Ar-CH_3), 14.72 (s, CH_3, Sn-CH_3), 11.21 (s, CH_3, Et-CH_3), 10.55 (s, CH_3, Et-CH_3), 10.32 (s, CH_3, Et-CH_3), 10.25 (s, CH_3, Et-CH_3), 10.22 (s, CH_3, Sn-CH_3); due to the low solubility of this compound, no $^1J_{SnC}$ information could be gained. MS(EI): *m/z* = 912 ($[M^+–Me]^+$, 100 %), 897 ($[M^+–Et]^+$, 21 %) , 868 ($[M^+–2Et]^+$, 27 %) 836 ($[M^+–Zn–2Et]^+$, 70 %); Analysis. Found: C, 62.59; H, 6.24; N, 11.16. $C_{52}H_{62}N_8OSnZn$ requires: C, 62.50; H, 6.25; N, 11.21 %; IR (nujol, KBr): ν 1591 (C=N), 1568 cm^{-1} (C=C).

6.4.5 Synthesis of [$SnMe_2Fe(THF)(L^{Et})$]

A solution of [$Fe(THF)\{N(SiMe_3)_2\}_2$] (0.10 g, 0.23 mmol) in THF (10 mL) was added dropwise to a stirred solution of [$SnMe_2(H_2L^{Et})$] (0.20 g, 0.23 mmol) in THF (20 mL) at -80 °C. The resulting red solution was allowed to warm to room temperature and stirred for 16 h, after which the solvents was evaporated under vacuum to yield 0.064 g, 0.065 mmol, 48 % of [$SnMe_2Fe(THF)(L^{Et})$] as a brown powder. ^{1}H NMR (500.13 MHz, C_6D_6/H_8-THF): δ 101.26 (s, 2H), 58.36 (s, 2H), 50.31 (s, 2H), 45.85 (s, 2H), 44.00 (s, 2H), 27.24 (s, 2H), 22.17 (s, 4H), 12.32 (s, 2H), 8.75 (s, 6H), 7.09 (s, 6H), 5.31 (s, 3H), 2.09 (s, 4H), 1.20 (s, 2H), 0.80 (s, 3H), 0.12 (s, 3H), -0.27 (s, 3H), -2.96 (s, 3H), -6.63 (s, 3H), -7.29 (s, 2H), -11.58 (s, 2H); MS(EI): *m/z* = 904 ($[M^+–Me]^+$, 100%), 860 ($[M^+–2Et]^+$, 20%); Analysis. Found: C, 63.22; H, 6.71; N, 11.37% $C_{52}H_{62}N_8OSnFe$ requires: C, 63.11; H, 6.31; Fe, 5.64; N, 11.32%; IR (nujol, KBr): ν 1587 (C=N), 1584 cm^{-1} (C=C).

6.4.6 Synthesis of [$Ca(THF)_2(H_2L^{Et})$]

A solution of [$Ca(THF)_2(N\{SiMe_3\}_2)_2$] (0.211 g, 0.418 mmol) in THF (5 mL) was added dropwise to a stirring solution of H_4L^{Et} (0.300 g, 0.418 mmol) in THF (10 mL) at -80 °C. The orange solution was allowed to warm to room temperature and stirred for 4 h after which the solvent volume was reduced and the product precipitated by addition of hexane (10 mL). This was isolated by filtration giving [$Ca(THF)_2(H_2L^{Et})$] as a yellow powder (0.327 g, 0.364 mmol, 87%). ^{1}H NMR (500.13 MHz, C_6D_6): δ 9.25 (s, 2H, NH), 8.37 (s, 2H, imine), 7.88 (s, 2H, imine), 7.12 (d, *J* = 3.8 Hz , 2H, pyrrole), 7.08 (s, 2H, Ar-H), 6.69 (s, 2H, Ar-H), 6.57 (d, *J* = 3.8 Hz, 2H, pyrrole), 6.48 (m, 2H, pyrrole), 6.36 (m, 2H, pyrrole), 3.59 (br, s, 8H, THF), 2.59–2.41 (m, 2H, Et-CH_2), 2.40–2.16 (m, 6H, Et-CH_2), 2.10 (s, 6H, Ar-CH_3), 2.03 (s, 6H, Ar-CH_3), 1.16-1.00 (m, 8H, THF), 0.96–0.86 (m, 12H, Et-CH_3); $^{13}C\{^1H\}$ NMR (125.76 MHz, C_6D_6): δ 158.04

(s, quaternary), 149.29 (s, imine), 148.62 (s, CH, imine), 145.10 (s, quaternary), 143.56 (s, quaternary), 141.99 (s, quaternary), 138.95 (s, quaternary), 133.37 (s, quaternary), 132.40 (s, quaternary), 130.73 (s, quaternary), 124.39 (s, CH, pyrrole), 120.11 (s, CH, Ar-H), 116.07 (s, CH, Ar-H), 115.72 (s, CH, pyrrole), 111.62 (s, CH, pyrrole), 107.88 (s, CH, pyrrole), 68.79 (s, CH_2, THF), 45.93 (s, quaternary), 29.77 (s, CH_2, Et-CH_2), 28.17 (s, CH_2, Et-CH_2), 19.78 (s, CH_3, Ar-CH_3), 19.43 (s, CH_3, Ar-CH_3), 8.69 (s, CH_3, Et-CH_3); Analysis. Found: C, 72.07; H, 7.49; N, 12.37; $C_{54}H_{66}CaN_8O_2$ requires: C, 72.13; H, 7.40; N, 12.46 %; MS(EI): *m/z* = 726 ($[M^+–2Me–2THF]^+$, 100 %); IR (nujol, KBr): ν 3444 (N-H), 1599 (C=N), 1560 cm^{-1} (C=C).

6.4.7 General attempted synthesis of $[M(H_2L^{Et})]$ from $[Ca(THF)_2(H_2L^{Et})]$

An example using $CoCl_2$: A suspension of $CoCl_2$ (11 mg, 0.083 mmol) in THF (5 mL) was added a solution of $[Ca(THF)_2(H_2L^{Et})]$ (75 mg, 0.083 mmol) in THF (5 mL) at -80 °C. An instant colour change from yellow to deep red was observed. The mixture was allowed to warm to room temperature and stirred for 3 h. After filtration, the solvent was removed under vacuum giving a red solid (30 mg). The ^1H NMR spectrum (C_6D_6) showed a mixture of products to be present.

6.4.8 Synthesis of $[Co_2(L^{Et})]$

A mixture of H_4L^{Et} (0.559 g, 0.780 mmol) and excess KH (0.156 mg, 3.90 mmol) was treated with THF (5 mL). Gas evolved immediately, and, once effervescence had ceased, the mixture was filtered onto a stirring suspension of $CoCl_2$ (0.202 mg, 1.56 mmol) in THF (5 mL) at -80 °C. A rapid colour change from red to very dark red was observed and the reaction warmed to room temperature and left to stir overnight after which it was filtered and solvents removed under vacuum giving $[Co_2(L^{Et})]$ as a red solid (0.518 g, 0.624 mmol, 80 %). ^1H NMR (399.90 MHz, C_6D_6): δ 81.22 (s, 4H), 41.90 (s, 4H), -13.03 (s, 12H, Ar-Me), -23.34 (s, 4H), -26.16 (s, 4H), -30.70 (s, 4H), -32.91 (s, 6H, Et-CH_3), -38.00 (s, 4H), -52.34 (s, 4H); Analysis. Found: C, 66.66; H, 5.75; N, 13.35; $C_{46}H_{48}N_8Co_2$ requires: C, 66.50; H, 5.82; N, 13.49 %; MS(EI): *m/z* = 830.2 (M^+, 50%), 801.2 ($[M^+–Et]^+$, 100 %), 772.1 ($[M^+–2Et]^+$, 50 %); IR (nujol, KBr): ν 1555 (C=N), 1506 cm^{-1} (C=C).

Alternative method: To a solution of H_4L^{Et} (0.201 g, 0.280 mmol) in THF (5 mL) was added a solution of $[Co(THF)(N\{SiMe_3\}_2)_2]$ (0.253 g, 0.561 mmol) in THF (5 mL) at -80 °C. The solution was allowed to warm to room temperature and stirred overnight. The solution was concentrated by removal of volatiles under vacuum and the product

precipitated by addition of hexane (5 mL). [$Co_2(L^{Et})$] was isolated by filtration and dried under vacuum. (0.174 g, 0.210 mmol, 75 %). Analysis agreed with above method.

6.4.9 Synthesis of [$Co_2(O_2)(L^{Et})$]

A solution of [$Co_2(L^{Et})$] (0.251 g, 0.302 mmol) in THF (5 mL) was exposed to air causing an immediate change in colour from red to dark brown. The mixture was left to stand for 1 d after which the solvent was removed under vacuum giving [$Co_2(O_2)(L^{Et})$] as a brown solid (0.247 g, 0.287 mmol, 95 %). ^{1}H NMR (399.90 MHz, C_6D_6): δ 8.20 (s, 4H), 7.39 (s, 4H), 6.88 (s, 4H), 6.48 (s, 4H), 2.57 (s, 4H, Et-CH_2), 0.74 (s, 6H, Et-CH_3), 0.48 (s, 6H, Et-CH_3). Resonances for Ar-CH_3 and a further Et-CH_2 could not be seen due to THF suppression; $^{13}C\{^1H\}$ NMR (100.55 MHz, C_6D_6/H_8-THF): δ 163.76 (s, CH, imine), 154.26 (s, quaternary), 145.33 (s, quaternary), 141.64 (s, quaternary), 133.92 (s, quaternary), 125.92 (s, CH), 120.64 (s, CH), 109.21 (s, CH), 51.50 (s, quaternary), 41.24 (s, CH_2, Et-CH_2), 35.90 (s, CH_2, Et-CH_2), 10.68 (s, CH_3, Et-CH_3), 9.66 (s, CH_3, Et-CH_3); EPR (THF) silent at both room temperature and at 140 K; Analysis. Found: C, 63.90; H, 5.67; N, 12.90; $C_{46}H_{48}N_8Co_2O_2$ requires: C, 64.04; H, 5.61; N, 12.99 %; MS(EI): 847.01 ([M^+–O+H]$^+$ or [Co_2(μ-OH)(L^{Et})]$^+$, 100 %), 789.08 ([M^+–2O–Me–Et]$^+$, 94 %); IR (KBr): ν 1562 (C=N), 1508 cm^{-1} (C=C).

6.4.10 Synthesis of [$Mg_2(THF)_2(L^{Et})$]

A 0.5 M solution of Mg(^{n}Bu)$_2$ in heptane (2.31 mL, 1.15 mmol) was added dropwise to a stirring solution of H_4L^{Et} (0.413 g, 0.576 mmol) in THF (10 mL) at -80 °C. The solution was allowed to warm to room temperature and was stirred for 3 h after which the solvent volume was reduced under vacuum and [$Mg_2(THF)_2(L^{Et})$] precipitated with hexane (15 mL) giving [$Mg_2(THF)_2(L^{Et})$] as a yellow solid (0.443 g, 0.490 mmol, 85 %). ^{1}H NMR (500.12 MHz, C_6D_6): δ 7.71 (s, 4H, imine), 6.84 (d, *J* = 3.4 Hz, 4H, pyrrole), 6.46 (d, *J* = 3.4 Hz, 4H, pyrrole), 6.14 (s, 4H, Ar-H), 3.07 (s, 8H, THF), 2.15 (q, *J* = 7.2 Hz, 4H, Et-CH_2), 2.06 (q, *J* = 7.3 Hz, 4H, Et-CH_2), 1.96 (s, 12H, Ar-Me), 1.30 (s, 8H, THF), 1.13–1.05 (m, 12H, Et-CH_3); $^{13}C\{^1H\}$ NMR (125.76 MHz, C_6D_6): δ 161.19 (s, CH, imine), 157.83 (s, quaternary), 143.02 (s, quaternary), 136.07 (s, quaternary), 132.06 (s, quaternary), 125.60 (s, CH, Ar-H), 119.32 (s, CH, py-H), 112.35 (s, CH, py-H), 69.09 (s, CH_2, THF), 48.01 (s, quaternary), 34.66 (s, CH_2, Et-CH_2), 33.33 (s, CH_2, Et-CH_2) 25.36 (s, CH_2, THF), 19.05 (s, CH_3, Ar-CH_3), 10.52 (s, CH_3, Et-CH_3), 10.34 (s, CH_3, Et-CH_3); MS(EI): *m/z* = 760.3 ($M^{+\cdot}$, 20 %), 731.2 ([M^+–2Me]$^+$, 100%); IR (nujol, KBr): ν 1604 (C=N), 1564 cm^{-1} (C=C).

Alternative method: To a solution of H_4L^{Et} (0.100 g, 0.140 mmol) in THF (5 mL) was added a solution of $[Mg(THF)_2(N\{SiMe_3\}_2)_2]$ (0.137 g, 0.280 mmol) in THF (5 mL) at -80 °C. The solution was allowed to warm to room temperature and stirred overnight. The solution was concentrated by removal of the volatiles under vacuum and the product precipitated by addition of hexane (5 mL). $[Mg_2(THF)_2(L^{Et})]$ was isolated by filtration and dried under vacuum (0.108 g, 0.12 mmol, 80 %). Analysis agreed with above method.

6.4.11 Synthesis of $[Mg_2(OEt_2)_2(L^{Et})]$

The synthesis is similar to $[Mg_2(THF)_2(L^{Et})]$, except an H_4L^{Et} suspension (0.205 g, 0.286 mmol) in Et_2O (10 mL) was used and the reaction stirred for 2 d at room temperature after which the solvent was removed by filtration and the yellow solid dried under vacuum to give $[Mg_2(OEt_2)_2(L^{Et})]$ (0.250 g, 0.274 mmol, 96 %). ^{1}H NMR (360.13 MHz, C_6D_6): δ 7.67 (s, 4H, imine), 6.83 (s, 4H, Ar-H), 6.47 (d, *J* = 2.7 Hz, 4H, pyrrole), 6.15 (s, 4H, pyrrole), 3.49 (s, 8H, Et_2O-CH_2), 2.25–2.10 (m, *J* = 7.3 Hz, 8H, Et-CH_2), 1.98 (s, 12H, Ar-CH_3), 1.22–1.10 (m, 12H, Et_2O-CH_3), 0.91–0.83 (m, 6H, Et-CH_3), 0.78 (t, *J* = 6.5 Hz, 6H, Et-CH_3).

6.4.12 Synthesis of $[Mg_2(pyr)_2(L^{Et})]$

Pyridine (10 mL) was added to $[Mg_2(THF)_2(L^{Et})]$ (0.105 g, 0.110 mmol). The resulting deep red solution was stirred at room temperature for 2 h. The solvents were removed under vacuum giving $[Mg_2(pyr)_2(L^{Et})]$ (0.100 g, 0.105 mmol) as a red solid. Yield 94 %. ^{1}H NMR (360.13 MHz, C_6D_6): δ 8.39 (s, 4H, pyr), 7.85 (s, 4H, imine), 6.84 (m, 6H, *J* = 3.6 Hz, pyr + pyrrole), 6.53 (m, 4H, pyr), 6.38 (d, 4H, *J* = 3.6 Hz, pyrrole), 6.13 (s, 4H, Ar-H), 1.82 (m, 16H, Ar-CH_3 + Et-CH_2), 1.60 (q, 4H, *J* = 7.30 Hz, Et-CH_2), 0.98 (t, 6H, *J* = 7.20 Hz, Et-CH_3), 0.77 (t, 6H, *J* = 7.24 Hz, Et-CH_3).

6.4.13 Attempted Synthesis of $[(M)(Mg)(L^{Et})]$ *via* $[Mg_2(THF)_2(L^{Et})]$

An example using $PdCl_2$: A suspension of $PdCl_2$ (16 mg, 0.088 mmol) in THF (2 mL) was added a solution of $[Mg_2(THF)_2(L^{Et})]$ (80 mg, 0.088 mmol) in THF (2 mL). An instant colour change from yellow to deep red was observed followed by precipitation of copious amounts of a red solid. After filtration, the solvent was removed under vacuum giving a red solid (10 mg). The precipitate was also dried under vacuum giving a deep red solid (80 mg). The ^{1}H NMR spectra (C_6D_6) of both the filtrate and precipitate showed a mixture of products were present.

6.4.14 Synthesis of $[Mg_4(OH)_4(\mu\text{-}OH)_4(H_4L^{Et})_2]$

Exposure of a benzene solution of $[Mg_2(THF)_2(L^{Et})]$ to some water impurity resulted in the crystalisation of $[Mg_4(OH)_4(\mu\text{-}OH)_4(H_4L^{Et})_2]$. ^{1}H NMR (500.12 MHz, C_6D_6): δ 10.57 (s, 16H, pyrrole NH + OH), 7.98 (s, 8H, imine), 6.60–6.56 (m, 16H, Ar-H + pyrrole), 6.08 (d, *J* = 3.7 Hz, 8H, pyrrole), 2.44–2.36 (m, 8H, Et-CH_2), 2.18 (d, *J* = 7.4 Hz, 8H, Et-CH_2), 2.08 (s, 24H, Ar-CH_3), 1.03 (t, *J* = 6.4 Hz, 12H, Et-CH_3), 0.56 (t, *J* = 7.2 Hz, 12H, Et-CH_3); ^{13}C{^{1}H} NMR (125.76 MHz, C_6D_6): δ 150.54 (s, CH, imine), 149.61 (s, quaternary), 141.80 (s, quaternary), 133.61 (s, quaternary), 131.68 (s, quaternary), 122.70 (s, CH, Ar-H or pyrrole), 118.35 (s, CH, Ar-H or pyrrole), 108.52 (s, CH, pyrrole), 44.00 (s, quaternary), 26.36 (s, CH_2, Et-CH_2), 25.38 (s, CH_2, Et-CH_2), 20.62 (s, CH_3, Ar-CH_3), 8.49 (s, CH_3, Et-CH_3), 7.92 (s, CH_2, Et-CH_3); IR (nujol, KBr): ν 3440 (O/N-H), 3280 (O/N-H), 1617 (C=N), 1560 cm^{-1} (C=C).

Alternative method (Note: carried out in air using 'wet' solvents): Deionised water (70 μL, 3.89 mmol, 4.7 eq) was added by microsyringe to a stirred solution of $[Mg_2(THF)_2(L^{Et})]$ (0.75 g, 0.83 mmol) in benzene (25 mL) at room temperature. The mixture was stirred for 16 h, after which the bright yellow precipitate was collected on a glass frit, washed with hexane (3 x 10 mL) and dried in air, yielding 0.31 g, 45 % of $[Mg_4(OH)_4(\mu\text{-}OH)_4(H_4L^{Et})_2]$ as a bright yellow solid. The ^{1}H NMR spectrum (C_6D_6) was identical to that detailed above for crystalline $[Mg_4(OH)_4(\mu\text{-}OH)_4(H_4L^{Et})_2]$. The filtrate and washings were combined and evaporated to dryness under vacuum to yield 0.25 g of yellow solids. The ^{1}H NMR spectrum (C_6D_6) showed this material to be a 1.0:1.5 mixture of $[Mg_4(OH)_4(\mu\text{-}OH)_4(H_4L^{Et})_2]$ and the free macrocycle H_4L^{Et}, resulting in a total yield for $[Mg_4(OH)_4(\mu\text{-}OH)_4(H_4L^{Et})_2]$ of *ca*. 64 %. Analysis. Found: C, 66.34; H, 6.83; N, 13.29 % $C_{46}H_{52}Mg_2N_8O_4$ requires: C, 66.28; H, 6.77; N, 13.44 %; MS(ESI) (+ve ion, CH_3CN/C_6H_6): *m/z* = 1665 ($[M^+{+}H]^+$, 9%), 1613 ($[M^+{+}H{-}3OH]^+$, 16%), 832 ($[\{M^+{+}H\}/2]^+$, 8%), 798 ($[\{M^+{+}H\}/2{-}2OH]^+$, 18%), 779 ($[\{M^+{+}H\}/2{-}3OH]^+$, 100%).

6.4.15 Synthesis of $[(NbCl)_2(L^{Et})]$

A stirring solution of H_4L^{Et} (0.300 g, 0.418 mmol) in THF (10 mL) was treated with a solution of $NbCl_3$·DME (0.242 g, 0.837 mmol) in THF (5 mL) at -80 °C. An immediate colour change from yellow to dark brown was observed. After allowing to warm to room temperature, a solution of DABCO (0.235 g, 2.92 mmol) in THF (5 mL) was added and the reaction stirred for 3 h. The mixture was filtered and volatiles removed under vacuum giving $[(NbCl)_2(L^{Et})]$ (0.264 g, 0.272 mmol) in 65 % yield.

MS(EI): *m/z* = 966.3 ($M^{+\cdot}$, 8 %), 897.4 ($[M^+–2Cl]^+$, 100 %); Analysis. Found: C, 56.84; H, 4.89; N, 11.62; $C_{46}H_{48}N_8Cl_2Nb_2$ requires: C, 56.98; H, 4.99; N, 11.56 %; IR (nujol, KBr): ν 1608 (C=N), 1598 cm^{-1} (C=C).

Alternative method: A mixture of H_4L^{Et} (0.100 g, 0.140 mmol) and KH (28 mg, 0.70 mmol) in THF (5 mL). Gas evolved immediately, and, once effervescence had ceased, the mixture was filtered onto a stirring suspension of $NbCl_3$·DME (81 mg, 0.280 mmol) at -80 °C causing an immediate colour change from orange to deep brown. The solution was warmed to room temperature and stirred for 2 h. Filtration followed by remove of volatiles under vaccum gave $[(NbCl)_2(L^{Et})]$ (54 mg, 0.056 mmol) in 40 % yield.

6.4.16 Attempted Synthesis of $[(Nb)_2(\mu\text{-}N_2)(L^{Et})]$

A stirring suspension of KC_8 (29 mg, 0.217 mmol) in THF (5 mL) was treated with a solution of $[(NbCl)_2(L^{Et})]$ (0.100 g, 0.103 mmol) in THF (5 mL) at -80 °C. The mixture was allowed to warm to room temperature and stirred for 2 h. The dark brown solution was filtered away from the solid black graphite and solvent removed under vacuum to give 45 mg of dark brown solid. IR (nujol, KBr): ν 1575 (C=N), 1502 cm^{-1} (C=C).

6.5 References

[1] L. J. Farrugia, *J. Appl. Crystallogr.* **1999**, *32*, 837.
[2] A. L. Spek, *Acta. Cryst.* **1990**, *A46*, C34.
[3] Y. Sarazin, R. H. Howard, D. L. Hughes, S. M. Humphrey, M. Bochmann, *Dalton Trans.* **2006**, 340.
[4] R. A. Andersen, K. Faegri, J. C. Green, A. Haaland, M. F. Lappert, W. P. Leung, K. Rypdal, *Inorg. Chem.* **1988**, *27*, 1782.
[5] H. Bürger, W. Sawodny, U. Wannagat, *J. Organomet. Chem.* **1965**, *3*, 113.
[6] D. C. Bradley, M. B. Hursthouse, A. A. Ibrahim, K. M. A. Malik, M. Motevalli, R. Möseler, H. Powell, J. D. Runnacles, A. C. Sullivan, *Polyhedron* **1990**, *9*, 2959.
[7] H. Bürger, U. Wannagat, *Monatsh. Chem., monthly* **1963**, *94*, 1007.
[8] L. E. Manzer, *Inorg. Synth.* **1982**, *21*, 135.
[9] E. Askarizadeh, A. M. J. Devoille, D. M. Boghaei, A. M. Z. Slawin, J. B. Love, *Inorg. Chem.* **2009**, *48*, 7491.
[10] C.-S. Chang, Y.-T. Lin, S.-R. Shih, C.-C. Lee, Y.-C. Lee, C.-L. Tai, S.-N. Tseng, J.-H. Chern, *J. Med. Chem.* **2005**, *48*, 3522.
[11] A. M. Skwierawska, J. F. Biernat, V. C. Kravtsov, *Tetrahedron* **2006**, *62*, 149.
[12] M. W. Glenny, L. G. A. van de Water, J. M. Vere, A. J. Blake, C. Wilson, W. L. Driessen, J. Reedijk, M. Schröder, *Polyhedron* **2006**, *25*, 599.
[13] O. S. M. Nasman, R. M. Baraka, A. A. Khaldi, I. E. Nahhal, S. P. Varkey, M. Shakir, *Transition Metal Chemistry* **1997**, *22*, 273.
[14] F. Vögtle, W. M. Müller, E. Buhleier, W. Wehner, *Chem. Ber.* **1979**, *112*, 899.
[15] H. Sieger, F. Vögtle, *Liebigs Ann. Chem.* **1980**, *1980*, 425.

[16] W. Lijinsky, H. W. Taylor, *J. Cancer Res. Clin.* **1979**, *94*, 131.
[17] X. Shen, H. Liu, Y. Li, S. Liu, *Macromolecules* **2008**, *41*, 2421.
[18] P. P. Seth, E. A. Jefferson, L. M. Risen, S. A. Osgood, *Bioorg. Med. Chem. Lett.* **2003**, *13*, 1669.